1-28-2013 12:00 AM

Simplified Tools for Performance-Based Design of Reinforced Concrete Frames Exposed to Fire

Salah El-Din F. El-Fitiany
The University of Western Ontario

Supervisor
Dr. Maged A. Youssef
The University of Western Ontario

Graduate Program in Civil and Environmental Engineering
A thesis submitted in partial fulfillment of the requirements for the degree in Doctor of Philosophy

SIMPLIFIED TOOLS FOR PERFORMANCE-BASED DESIGN OF REINFORCED CONCRETE FRAMES EXPOSED TO FIRE

(Integrated Article)

by

Salah El-Din Farouk El-Fitiany

Graduate Program in Civil and Environmental Engineering

A thesis submitted in partial fulfillment
of the requirements for the degree of
Doctor of Philosophy

The School of Graduate and Postdoctoral Studies
The University of Western Ontario
London, Ontario, Canada

Abstract

Fire safety of Reinforced Concrete (RC) buildings is an important design aspect that ensures structural integrity during fire events. As new codes are moving from prescriptive methods towards performance based design and full scale experiments and numerical simulations are expensive and time consuming. Practitioners are in need of rational design tools to assess the strength and serviceability of individual RC elements and the structure as a whole during a fire event. This thesis provides such tools for RC frames.

A previously developed sectional analysis method is extended to cover RC beams subjected to fire from three sides. An extensive parametric study is conducted to propose simple equations expressing the equivalent stress-block parameters at elevated temperatures. These equations can be utilized by designers to estimate the flexure capacity of RC beams exposed to fire.

A novel method to track the behavior of continuous RC beams during standard fire exposure is proposed and validated. The proposed method is based on separating the effects of thermal deformations and vertical loads. The effective flexural stiffness and the thermal deformations of fire-exposed RC beams are estimated using simple expressions that are developed based on a comprehensive parametric study. Designers can apply the proposed method to assess the structural fire safety of RC continuous beams.

A simple method to construct the full interaction diagram of RC columns exposed to fire is developed and validated. An existing simplified heat transfer method is extended to predict the average temperature distribution. A number of reasonable approximations are assumed to allow reaching a closed form solution for the concrete compressive forces that correspond to a specific strain distribution. The closed form solution provides formulas that engineers can use to sketch the interaction diagrams.

A practical approach to track the fire performance of RC frames during fire exposure is proposed and validated. The effective flexural and axial stiffnesses as well as unrestrained thermal deformations of heated RC sections are evaluated. Their values are used to conduct a quick assessment of the integrity of a fire exposed structure and ensure the safety of emergency response teams during fire evacuation and extinguishing.

Keywords

Concrete; Elevated temperatures; Heat transfer; Sectional analysis; Fire resistance, Stress-block parameters; Flexural stiffness; Design; Interaction diagrams; Fire performance; Frames; Thermal Restraint.

They will ask thee concerning the Spirit. Say: "The Spirit is by command of my Lord, and of knowledge ye have been vouchsafed but little."

Holy Quran, Chapter 17,

Verse 85

To my wonderful parents, Enas, Farouk, Wafaa, and Ahmed
To my beloved wife Marwa
To my beautiful daughter Laila
To my siblings Eman, Omar, and Mohamed

And,

To the martyrs of the January 25th revolution in Egypt

Co-Authorship Statement

All analytical work presented in this thesis was performed by Salah El-Fitiany. Chapters 2 and 3 of this thesis were accepted for publication in the ACI journal. Chapters 4 – 6 of this thesis will be submitted to scholarly journals as manuscripts co-authored by Salah El-Fitiany and Maged Youssef .

Acknowledgments

I am deeply thankful to Dr. Maged Ali Youssef for his supervision, guidance, and care during my research program. Dr. Youssef has devoted a lot of his time as a research advisor and mentor to me during my doctoral studies. During the past five years, we've had a meeting nearly every week even when he was travelling or on vacation. Dr. Youssef's enthusiasm and encouragement not only contributed to my technical development but also helped me in terms of personal growth.

The Natural Science and Engineering Research Council, the Government of Ontario, and the University of Western Ontario all provided me with financial support.

I'd like also to thank my late colleague, Mr. Mohamed Moftah, for sharing his knowledge and valuable references in structural fire safety with me which was really helpful to me. I gratefully acknowledge the assistance provided by Ghaly, Dessouki, Hadir, and Eltalmas for proofreading parts of this thesis prior to submission.

This dissertation would not have been possible without the support and enthusiasm of several unseen individuals who in one way or another contributed in the completion of this work. These individuals are my parents, brothers and sisters, father and mother in-law, and friends. My first daughter, Laila, was born during this work, and having her sitting on my lap and innocently looking at this thesis encouraged me a lot. My wife, Marwa, is the reason I was able to finish. We've got married during the third year of my PhD. Marwa's patience and lovely spirit were tremendous and allowed me to work on my PhD especially in the past year, thank you dear Marwa.

Table of Contents

List of Tables

List of Figures

List of Abbreviations, Symbols, and Notation

A_1	factor used in calculating internal concrete force, equals to $e^{y_1 \ z_2}$
A_2	factor used in calculating internal concrete force, equals to $e^{y_2 \ z_2}$
A_s	area of tensile steel bars
A_i	area of layer i
Agg	factor to account for the aggregate type
b	cross-section width
B_1, B_2, B_3, and B_4	constants describing concrete thermal expansion strain at elevated temperatures for different aggregate types
c	concrete cover or depth of neutral axis
C_c	internal compression force in concrete
$C_{c\ o\ (v)}$	concrete compression force at $\varepsilon_{cT} \leq (\varepsilon_{oT} + \varepsilon_{tr})$ for variable T_{avg} distribution
$C_{c\ o\ (v)}.y$	concrete moment about x axis at $\varepsilon_{cT} \leq (\varepsilon_{oT} + \varepsilon_{tr})$ for variable T_{avg} distribution
$C_{c\ u\ (v)}$	concrete compression forces at $\varepsilon_{cT} > (\varepsilon_{oT} + \varepsilon_{tr})$ for variable T_{avg} distribution
$C_{c\ u\ (v)}.y$	concrete moment about x axis at $\varepsilon_{cT} > (\varepsilon_{oT} + \varepsilon_{tr})$ for variable T_{avg} distribution
$C_{c\ o\ (c)}$	concrete compression force corresponding to $\varepsilon_{cT} \leq (\varepsilon_{oT} + \varepsilon_{tr})$ for constant T_{avg}
$C_{c\ o\ (c)}.y$	concrete moment about x axis at $\varepsilon_{cT} \leq (\varepsilon_{oT} + \varepsilon_{tr})$ for constant T_{avg}

$C_{c\,u\,(c)}$	concrete compression force corresponding to $\varepsilon_{cT} > (\varepsilon_{oT} + \varepsilon_{tr})$ for constant T_{avg}
$C_{c\,u\,(c)}.y$	concrete moment about x axis at $\varepsilon_{cT} > (\varepsilon_{oT} + \varepsilon_{tr})$ for constant T_{avg}
C_{th}	compression force in concrete due to self equilibrium under thermal strains
$C_{th\,c\,(v)}$	concrete compression force for constant ε_{st} and variable T_{avg} distribution
$C_{th\,c\,(v)}.y$	concrete moment about x axis for constant ε_{st} and variable T_{avg} distribution
$C_{th\,v\,(v)}$	concrete compression force for variable ε_{st} and T_{avg} distributions
$C_{th\,v\,(v)}.y$	concrete moment about x axis for variable ε_{st} and T_{avg} distributions
$C_{th\,c\,(c)}$	concrete compression force for constant ε_{st} and constant T_{avg}
$C_{th\,v\,(c)}.y$	concrete moment about x axis for constant ε_{st} and constant T_{avg}
d	effective depth of tensile reinforcement
EI_{eff}	effective flexural stiffness
EA_{eff}	effective axial stiffness
E_c	ambient secant modulus for concrete
E_i	modulus of elasticity of layer *i*
f'_c	compressive strength for concrete at ambient temperature
f_c	compression stress in concrete at ambient temperature
f_y	yield strength of steel bars at ambient temperature
f'_{cT}	reduced compressive strength at elevated temperatures

f_{cT}	compression stress in heated concrete
f_{yT}	reduced yield strength of reinforcing bars at elevated temperatures
f_{sT}	compression or tension stress in heated steel bars
$F_{agg.}$	factor to account for the aggregate type
$(f_{cT})_{avg}$	average concrete compressive stresses
h	cross-section height
I_g	gross sectional second moment of inertia
K_{hT}	confinement factor for concrete at elevated temperatures
L	span between the supports (mm)
M	flexural moment
M_n	nominal flexural capacity at ambient temperature
M_{th}	thermal moment
M_{nT}	reduced nominal flexural resistance during fire exposure
n	number of tensile reinforcement layers
n_w	ratio between the surface temperature and the fire temperature
n_x and n_y	ratios between the internal and surface temperatures due to heating in the x and y directions, respectively
P	axial load
P_{app}	applied concentric loads

r	length of descending branch in concrete constitutive stress-strain relationship at elevated temperatures
R	reduction factor for concrete compressive strength at elevated temperatures
t	fire duration
t^*	Equivalent fire duration assuming ISO 834 standard fire
T	temperature in degree Celsius [1 ^{o}F = 1.8 ^{o}C + 32]
T_σ	temperature produces the same average concrete strength for the layer
T_{th}	algebraic average temperature of the elements within each layer
T_{xy}	temperature rise at any point located at (x, y)
T_{avg}	algebraic average distribution along the section height
$T_{avg\,1}$	average temperature for regions affected by heating from either left or right
$T_{avg\,2}$	average temperature for regions not affected by heating from left or right
$T_{avg\,3}$	average temperature due to heating from the left and right sides simultaneously
T_f	fire temperature
$T_{f\,(\mathrm{ISO})}$	ISO 834 standard fire temperature at a modified fire duration t^*
T_i	equivalent temperature at layer i
T_s	tension force in steel assuming yielding or reinforcement
T_1, T_2, T_8, T_{64}	constants describing the reduction the concrete compressive strength at elevated temperatures for different aggregate types
V	volume fraction of aggregates

x, y	horizontal and vertical coordinates for any point within the column/beam section, origin located at bottom left of the section
y_1, y_2	boundaries of internal concrete compression force measured in y direction
y_i	distance between the center of area of layer *i* and the center of area of the cross-section.
z	boundary of fire affected regions
z_1, z_2	constants of average temperature fitting equation
z_3, z_4	constants define the linear variation of mechanical strain (ε_{cT}) in y direction
$\overline{z_3}, \overline{z_4}$	constants define the linear variation of unrestrained thermal strain ($\overline{\varepsilon_{th}}$) in y direction
Z	slope of the descending branch of the concrete constitutive stress-strain relationship
α_1 and β_1	stress-block parameters at ambient temperature
α_{1T} and β_{1T}	stress-block parameters at elevated temperatures
ε	total concrete strain at elevated temperatures
ε_{th}	unrestrained thermal strain of concrete
ε_{tr}	transient creep strain in concrete
ε_c	instantaneous stress-related strain
$\overline{\varepsilon_{th}}$	equivalent linear thermal strain
ε_i	unrestrained thermal axial strain

ε_{st}	self induced thermal strains
ε_{cT}	equivalent mechanical strain in concrete during fire exposure
ε_{sT}	equivalent mechanical strain in steel during fire exposure
ε_{o}	strain at maximum stress of unconfined concrete at ambienttemperatures
ε_{oT}	value of ε_c at peak stress f'_{cT}
ε_{uT}	ultimate/crushing concrete compressive strain at elevated temperatures
$\varepsilon_{cT\,max}$	compression strain corresponding to the flexural capacity
$\Delta\varepsilon$	difference between ε_{uT} and $(\varepsilon_{oT} + \varepsilon_{tr})$ equals to 0.02
$\Delta\varepsilon_c$	incremental centroidal axial strain
Δt	time step
ψ	total curvature
ψ_i	unrestrained thermal curvature
ψ_{cT}	mechanical curvature
$\Delta\psi$	incremental curvature
λ	axial or flexural load level or column slenderness ratio
λ_L	preloading level
ρ'	compression reinforcement ratio
ρ	tensile reinforcement ratio
Γ	compartment time factor
$\chi(\lambda)$	buckling factor

Δ_{max} maximum allowable deflection

$\left(\frac{\partial \Delta}{\partial t}\right)_{max}$ maximum allowable rate of deflection

Chapter 1

1 Introduction

Fire is a chain of exothermic chemical reactions, which release energy in the form of heat and light [1,2]. A fire needs three essential elements: a combustible material, oxygen, and a source of heat. The lack of any of these elements will stop the exothermic reaction and extinguish the fire. If fire cannot be extinguished within a reasonable amount of time, preventive and/or protective measures significantly reduce the loss of life and damage to property. Preventive, also known as active measures, includes: installation of alarm and smoke control systems and sprinkles. It can also include controlling hazardous contents and providing access for fire fighters. Protective, or passive, measures includes: ensuring adequate compartmentation, control of flammability of the structure fabric, planning fixed escape routes (egress paths), and retaining adequate structural performance during fire events. The latter is the main scope of this dissertation.

1.1 Development of Compartment Fires

Structures are required to be divided into compartments: vertically, horizontally, or a combination of the two[1]. This requirement is to limit the spread of the fire. It also allows phased evacuation of multi-storey structures to addressing critical floors first. The development of compartment fires, Fig. 1-1, can be broken down into four phases: growth, flashover, post-flashover, and the decay period [3,4].

1.1.1 Stage 1: Growth (Pre-Flashover)

In this early stage of fire development, combustion is restricted to small areas of the compartment. Therefore, temperature rise within the compartment is very small. Large number of fire incidents does not continue beyond this stage due to the lack of either sufficient fire load or air supply to allow the fire to grow beyond this stage, i.e. fuel

controlled fire. The pre-flashover stage is often ignored in the fire response calculations of civil structures.

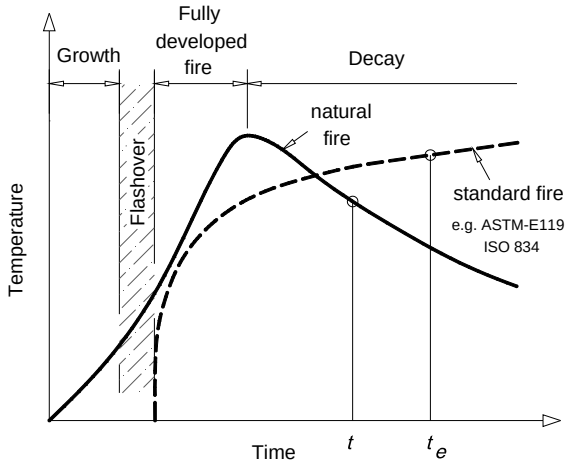

Fig. 1-1: Fire development and stages

1.1.2 Stage 2: Flashover Phenomenon

Human intervention can increase the air supply by opening a door or a window. This increase causes combustion spread over the full area of the compartment. This spread is known as “flashover”. It results in a rapid temperature fire increase and the development of the fire in a very short period.

1.1.3 Stage 3: Post-Flashover

Fire becomes fully developed in this stage and very high temperatures are reached. All combustible materials in the compartment are burnt in this stage. Structural elements are exposed to elevated temperatures. Local damage, collapse, or loss of structural integrity is likely to occur at this stage.

1.1.4 Stage 4: Decay

When the combustible materials in the room start to be fully burnt, the rate of combustion decreases and the temperature in the compartment starts decreasing.

1.2 Standard Time-Temperature Curve

As shown in Fig. 1-2, each natural fire has its own temperature-time relationship. Standard temperature-time relationships provide a basis of comparison between standard fire test and real fires for judging on the safety of a structure. The most widely used standard temperature-time relationships are: the American ASTM-E119 [2], the international ISO 834 [2], and the Eurocode Hydrocarbon. Standard fire curves, Fig. 1-2, simulate a severe fire, i.e. a fully-developed fire with no decay period.

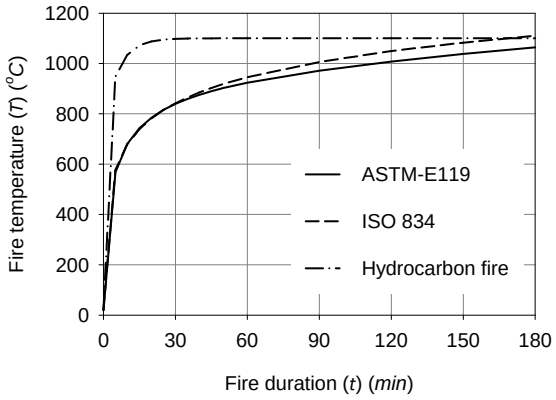

Fig. 1-2: Standard fire curves

1.3 Fire Severity

Ingberg (1928) conducted a series of compartment tests with known fire loads to evaluate the severity of each load based [1,5]. Based on these tests, it was concluded that fire severity could be characterized by the area under the temperature-time curve that is above 150 ℃ to 300 ℃ [1]. Although this method provided a basis for fire grading, it did not have a

sound theoretical justification and ignored the effect of air ventilation (Robertson and Gross, 1970) [1]. Thus, alternative approaches were proposed such as time equivalence and minimum load capacity.

1.3.1 Time Equivalence

There are two approaches to calculate the equivalent time (t_e) corresponding to a natural fire duration (t), Fig. 1-1. The first approach calculates t_e such that it results in the same maximum temperature rise of the real fire. The second approach considers equivalence based on the amount of heat input.

1.3.2 Minimum Load Capacity Concept

The equivalent time (t_e) is evaluated such that it results in the same reduction of the load bearing capacity that would occur in a complete burnout of a compartment [5].

1.4 Prescriptive Methods

Concrete structures are currently being designed for fire temperatures using prescribed methods. Engineers choose floor and wall assemblies that meet specific fire ratings using minimum cross-section dimensions and minimum clear cover to the reinforcing bars [1,4,5]. This minimum concrete cover ensures that the elevated temperature of steel reinforcement do not exceed its critical temperature, i.e. 593 ℃, at which steel loses 50% of its strength [4].

Prescriptive methods were developed based on experimental data from standard fire tests conducted on individual RC elements. Therefore, current code provisions are simplistic, prescriptive, and not realistic as they do not consider important factors such as effect of different fire scenarios, boundary conditions, load level, and failure criteria [1].

Furthermore, such methods do not account for material nonlinearity and transient creep strains which have a significant effect on the fire response of heated RC members, especially at later stages of fire exposure.

1.5 Performance-Based Fire Design

Standard fires do not consider all factors that would influence fire severity. Also, single elements are tested in isolation without considering the overall structural performance. These limitations result in uneconomic structural fire safety design. Performance-based fire design may be defined as a design approach to simulate and evaluate the performance of a structure under realistic fire loads[1]. Recent building codes, regulations, and standards are moving from prescriptive-based methods to performance-based approaches. Performance-based fire safety design has number of advantages over the prescriptive design that includes [6,7]:

• Establishing specific safety goals that the designer should achieve.

• Permitting structural engineers to design structures to meet performance criteria allowing the use of innovative design solutions.

• Allowing cost-effectiveness and flexibility in design.

• Improving the harmonization between international regulations/codes.

• providing better knowledge of the implied structural safety level which benefits insurance contractors.

• Adopting to changes in construction technology.

1.6 Spalling

Explosive spalling occurs in early stages of fire exposure due to the build-up of pore pressure during heating [1,4]. It leads to a loss of concrete cover and rapid increase in reinforcement temperature. Thus, the fire performance of the exposed element is significantly reduced. The exact mechanism of explosive spalling is still not understood and complex to predict [1,9]. High Strength Concrete (HSC) is more susceptible to explosive spalling because of its low permeability compared to Normal Strength Concrete (NSC)[10]. The thesis is focusing on NSC and thus spalling is not accounted for.

1.7 Research Objectives

As new codes are moving towards performance based design approach, engineers are in-need of simple and rational design tools to assess the structural integrity of RC buildings during fire events. To address some of the challenges faced by engineers, this thesis aims at developing simplified tools to:

1) Evaluate the flexural capacity of fire-exposed RC beams

2) Predict the fire performance of continuous RC beams

3) Predict average temperature distribution in heated concrete sections

4) Assess the flexural/axial capacity of fire-exposed RC columns

5) Predict the overall behavior of indeterminate RC frames during fire exposure

The proposed tools allow engineers to overcome the limitations of the prescriptive methods which do not account for strength degradation in concrete and steel nor thermal and transient creep strains due to fire temperature.

1.8 Outline of Thesis

This thesis is prepared in an "Integrated-Article Format" following the guidelines described in Western University-School of Postdoctoral and Graduate Studies (SPGS), General Thesis Regulations.

Chapter 2

Fire safety is a critical criterion for designing reinforced concrete (RC) structures. New codes are moving towards Performance-based design. Conducting full scale experiments and comprehensive finite element simulations are usually expensive and time consuming options for designers to achieve specific fire performance. A simplified sectional analysis methodology that tracks the axial and flexural behavior of RC square sections subjected to elevated temperatures from their four sides was previously developed and validated by the authors. In the first part of this chapter, the proposed methodology is extended to cover rectangular beams subjected to standard ASTM-E119 fire from three sides. An extensive parametric study is then conducted to study the distribution of the concrete compression stresses at different ASTM-E119 fire durations. Based on the parametric study, simple equations expressing the equivalent stress-block parameters at elevated temperatures are presented. These equations can be utilized by designers to accurately estimate the flexure capacity of simply supported and continuous beams exposed to fire temperature.

Chapter 3

Structural engineers are in need of analytical tools to evaluate the performance of Reinforced Concrete (RC) structures during fire events. Existing numerical methods require extensive knowledge of heat transfer calculations and the finite element method. This chapter proposes a rational method to track the fire performance of continuous RC beams during ASTM-E119 standard fire exposure. The proposed method utilizes a

simplified sectional analysis approach and is based on separating the effects of thermal deformations and vertical loads. The effective flexural stiffness and the thermal deformations of the beam are estimated using simple expressions that are developed based on a comprehensive parametric study.

Chapter 4

Existing analytical methods for the evaluation of fire safety of Reinforced Concrete (RC) structures require extensive knowledge of heat transfer calculations and the finite element method. With the introduction of performance based design, structural engineers need simple design tools to assess the capacity and performance of different elements during fire exposure. This chapter proposes a rational method to predict the axial capacity of RC columns exposed to fire. An existing simplified heat transfer method is first extended to predict the average temperature distribution along the section height. The corresponding distribution of the reduced concrete strength is then integrated to develop expressions to calculate the axial capacity of RC columns exposed to fire from four faces. These expressions provide emergency response teams with a tool to conduct a quick assessment of the integrity of a fire exposed structure to ensure the safety of their team.

Chapter 5

Fire safety of Reinforced Concrete (RC) columns is an important design aspect to ensure the overall integrity of structures during fire events. Currently, fire ratings of RC columns are achieved using prescriptive methods such as specifying the minimum reinforcement cover. As new codes are moving towards performance based design, practitioners are in need of rational design tools to assess the capacity of heated columns. Existing numerical methods to evaluate the axial force-moment interaction diagram have high computation demand and require knowledge of heat transfer calculations and stress analysis. This chapter proposes a practical approach to construct the interaction diagram for a RC column during fire exposure. The chapter presents the derivation for a set of formulas

that can be used to estimate the average temperature distribution within the concrete section and the corresponding internal forces. The proposed formulas are validated by comparing their predictions with the experimental and analytical results by others.

Chapter 6

Fire safety of Reinforced Concrete (RC) structures is currently satisfied through fire rating requirements. As fire codes are moving towards performance based design, structural engineers need practical tools to assess the overall behavior of a structure during exposure to fire. Existing numerical methods, which predict the fire response of RC structures, have high computation demand and require knowledge of heat transfer calculations and stress analysis. This chapter proposes a simple approach to track the fire performance of RC frames during fire exposure. The derivations of a set of formulas that can be used to estimate the average temperature distribution within a concrete section, the corresponding internal forces, the effective flexural and axial stiffnesses, and the unrestrained thermal deformations are presented. Applications of these formulas to simulate the effect of fire exposure and to predict the overall behavior of RC structures during fire events are explained. The proposed method is validated by comparing its predictions with experimental and analytical results by others.

1.9 References

1. Purkiss, J.A. 1996, "Fire Safety Engineering Design of Structures ", Butterworth-Heinemann, Oxford, 342 pp.

2. Lie, T.T. 1992, "Structural Fire Protection", ASCE Manuals and Reports on Engineering Practice, no. 78, New York, NY, 241 pp.

3. Malhotra, H.L. 1982, "Design of Fire-Resisting Structures", London: Surrey University Press, 226 pp.

4. Moftah M., 2008, “Numerical Modeling and Behaviour of Reinforced Concrete Members Under Fire Conditions”, University of Western Ontario, PhD thesis.

5. Andrew H. Buchanan, 2002, “ Structural Design for Fire Safety”, John Wiley & Sons.

6. Hadjisophocleous, George V., Benichou, Noureddine, and Tamim, Amal S., 1998, “Literature Review of Performance-Based Fire Codes and Design Environment”, J. of Fire Prot. Engr., vol. 9, no. 1, pp. 12-40.

7. Mostafaei, H., Sultan, M.A., and Bénichou, N. 2009, “Recent developments on structural fire performance engineering – a state-of-the-art report,” NRC-CNRC, 35 pages

8. Kodur, V.K.R., Wang, T.C. & Cheng, F.P. 2004, "Predicting the fire resistance behaviour of high strength concrete columns", *Cement and Concrete Composites,* vol. 26, no. 2, pp. 141-153.

9. Khoury, G.A. 2000, "Effect of fire on concrete and concrete Structure", *Progress in Structural Engineering and Materials*, vol. 2, pp. 429-447.

Chapter 2

2 Stress-Block Parameters for Reinforced Concrete Beams during Fire Events

Concrete as well as steel reinforcing bars experience significant deterioration when subjected to elevated temperatures[1]. This deterioration is accompanied by the generation of thermal and transient strains which adds to the complexity of estimating the flexural capacity of a reinforced concrete (RC) section at elevated temperatures. Currently, concrete structures are designed for fire safety using prescribed methods that are based on computational modeling and experimental investigations. These methods usually specify the minimum cross-section dimensions and clear cover to achieve specific fire ratings. As new codes are moving towards performance-based design and conducting experimental tests to satisfy different fire scenarios is expensive, different design tools are needed by design engineers[2]. One of these tools would facilitate the estimation of the flexural behavior of a RC beam at elevated temperatures.

A simplified method to track the axial and/or the flexural behavior of square column sections subjected to fire at their four sides was previously introduced by El-Fitiany and Youssef[3]. This chapter starts by extending the proposed method to be applicable to RC beams exposed to fire from three sides. The overall behavior of RC beams during fire exposure is tracked by constructing the moment-curvature relationships at different fire durations. The unrestrained simply supported beam tested by Lin et al.[4], Fig. 2-1a, is taken as an illustrative example for the proposed methodology. The tested beam has a normal strength concrete with carbonate aggregate and subjected to ASTM-E119 standard fire.

Civil engineers are familiar with using the concrete stress-block parameters in calculating the ultimate capacity of RC members at ambient temperature. These parameters convert the parabolic distribution of concrete compression stresses to an idealized rectangular stress-block. Evaluation of those parameters at elevated temperatures allows designers to easily estimate the flexural capacity of RC beams during fire exposure. The second part

of this chapter presents a parametric study to evaluate the compressive stresses distribution for different rectangular concrete cross-sections. The effect of different parameters including section dimensions, reinforcement ratio, concrete strength, fire duration, and aggregate type is evaluated.

2.1 Research Significance

The proposed simplified method extends the use of sectional analysis to be applicable at elevated temperatures. Designers are familiar with this method at ambient temperature, which allows them to use it in their fire calculations. The ultimate/nominal flexural capacity of RC beams can be evaluated at ambient temperature using equivalent stress-block parameters. No specific study was conducted to address the effect of fire temperature on such parameters. The second part of this chapter presents an extensive parametric study on the non-linear distribution of compression stresses for a number of rectangular cross-sections at different ASTM-E119 fire durations up to 2.5 hr. This chapter ends by providing simplified equations for designers to allow them to estimate the stress-block parameters at elevated temperatures.

2.2 Sectional Analysis at Ambient Temperature

At ambient temperature, RC sections are analyzed using the well-known sectional analysis approach[5]. For cases of single curvature, i.e. bending about horizontal axis, the concrete section is divided into horizontal discrete fibers. Utilizing the uniaxial stress-strain relationship for each fiber and taking into account equilibrium and kinematics, the mechanical behavior of the section is analyzed. To simplify the analysis, two variables can be assumed; incremental centroidal axial strain, $\Delta\varepsilon_{cT}$, and incremental curvature, $\Delta\psi_{cT}$. Assuming a linear strain distribution, the incremental moment and axial force are obtained using Eq. (1).

$$\begin{pmatrix} \Delta M \\ \\ \Delta P \end{pmatrix} = \begin{pmatrix} \sum_{i=1}^{n} E_i \times A_i \times y_i^2 & -\sum_{i=1}^{n} E_i \times A_i \times y_i \\ -\sum_{i=1}^{n} E_i \times A_i \times y_i & \sum_{i=1}^{n} E_i \times A_i \end{pmatrix} \times \begin{pmatrix} \Delta \psi_{cT} \\ \\ \Delta \varepsilon_{cT} \end{pmatrix} \quad (1)$$

Where E_i is the modulus of elasticity of layer i, A_i is the area of layer i, y_i is the distance between the center of area of layer i and the center of area of the cross-section.

For a given axial load, the moment-curvature behavior is obtained in two stages. In the first stage, the axial strain is increased incrementally while curvature is kept equal to zero until the required axial load is reached. In the second stage, the axial load is kept constant and the applied curvature is increased. The corresponding change in the axial strain and the moment are calculated using Eq. (1). This process is repeated until reaching the required curvature value.

2.3 Sectional Analysis at Elevated Temperatures

To apply sectional analysis at elevated temperatures, a number of modifications were proposed and validated by El-Fitiany and Youssef[3]. These modifications account for the two dimensional temperature gradient within the concrete cross section, which affects its homogeneity and increase the nonlinearity of the mechanical strain distribution. The following sections generalize the previously developed method to be applicable to rectangular sections exposed to fire temperature at a number of their sides. Beam B1, shown in Fig. 2-1, is used to illustrate the concepts. The beam was tested by Lin et. al[4] and exposed to ASTM-E119 fire at three of its faces for duration of one hour.

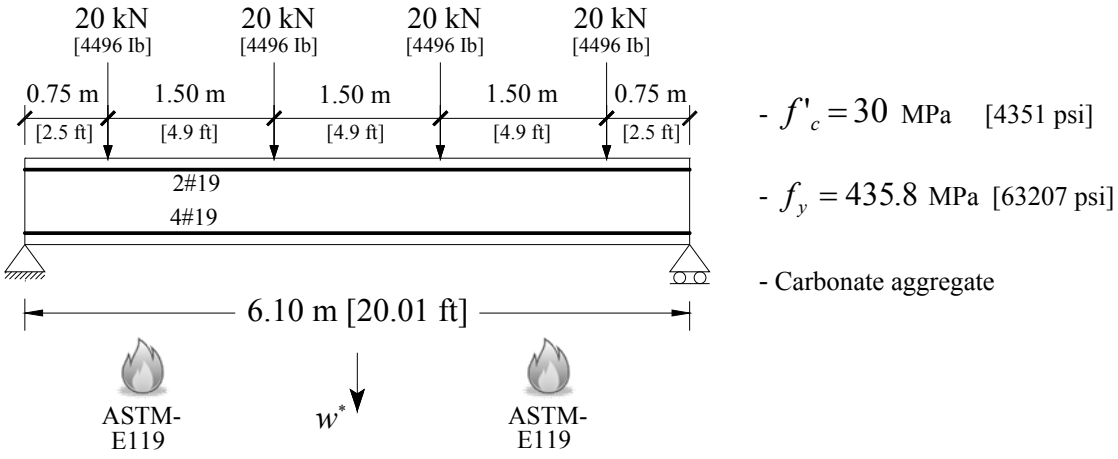

(a) Beam B1 elevation

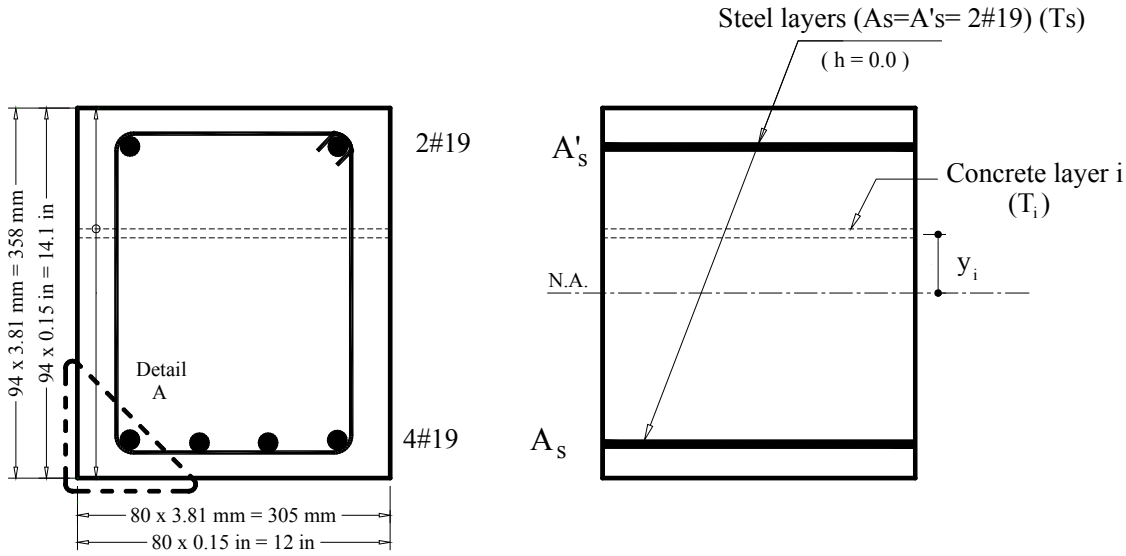

(b) Cross-section and fiber model of beam B1

Fig. 2-1-Beam B1 loading and configuration

2.3.1 Concrete and steel constitutive models

The constitutive models proposed by Youssef and Moftah[6] are adopted and their application to beam B1 is presented in the following sub-sections.

2.3.1.1 Concrete compressive strength

Hertz proposed a model[7], Eq. (2), that recognizes the variation of the concrete compressive strength (f'_{cT}) at elevated temperatures. If concrete is loaded prior to fire, f'_{cT} should be increased by 25% 7.

$$f'_{cT} = R \times f'_c \tag{2a}$$

for concrete with siliceous aggregate,

$$R = \frac{1}{1 + \frac{T}{15{,}000} + \left(\frac{T}{800}\right)^2 + \left(\frac{T}{570}\right)^8 + \left(\frac{T}{100{,}000}\right)^{64}} \tag{2b}$$

for concrete with carbonate aggregate.

$$R = \frac{1}{1 + \frac{T}{100{,}000} + \left(\frac{T}{1080}\right)^2 + \left(\frac{T}{690}\right)^8 + \left(\frac{T}{1000}\right)^{64}} \tag{2c}$$

Where R is a reduction factor, T is the temperature in degree Celsius [1 ^{o}F = 1.8 ^{o}C + 32], and f'_c is the concrete compressive strength at ambient temperature.

2.3.1.2 Fire induced strains

Total concrete strain at elevated temperatures (ε_{tot}) is composed of three terms[6]: instantaneous stress related strain (ε_{fT}), unrestrained thermal strain (ε_{th}), and transient

creep strain (ε_{tr}). The value of ε_{fT} at the peak stress (ε_{oT}) defines the stress-strain relationship during the heating stage and can be predicted using the model proposed by Terro[8], Eq. (3). Flexural RC elements have variant stress values within concrete compression zone which implies different preloading levels λ_L for each fiber.

$$\varepsilon_{oT} = (50\lambda_L^2 - 15\lambda_L + 1)\,\varepsilon_{o1} + 20(\lambda_L - 5\lambda_L^2)\,\varepsilon_{o2} + 5(10\lambda_L^2 - \lambda_L) \times 0.002 \tag{3}$$

where $\varepsilon_{o1} = 2.05\times10^{-3} + 3.08\times10^{-6}T + 6.17\times10^{-9}T^2 + 6.58\times10^{-12}T^3$

$\varepsilon_{o2} = 2.03\times10^{-3} + 1.27\times10^{-6}T + 2.17\times10^{-9}T^2 + 1.64\times10^{-12}T^3$

ε_{th} is the free thermal strain resulting from fire temperature and can be predicted using the Eurocode model[6], Eq. (4).

for concrete with siliceous aggregate,

$$\varepsilon_{th} = -1.8\times10^{-4} + 9\times10^{-6}\,(T-20) + 2.3\times10^{-11}\,(T-20)^3 \qquad \le 14\times10^{-3} \tag{4a}$$

for concrete with carbonate aggregate,

$$\varepsilon_{th} = -1.2\times10^{-4} + 6\times10^{-6}\,(T-20) + 1.4\times10^{-11}\,(T-20)^3 \qquad \le 12\times10^{-3} \tag{4b}$$

ε_{tr} is induced during the first heating cycle of loaded concrete and is considered the largest component of the total strain. Its value can be estimated using Terro's model[8].

$$\varepsilon_{tr} = \varepsilon_{0.3} \times \left(0.032 + 3.226\frac{f_c}{f'_c}\right)\frac{V_a}{0.65} \tag{5}$$

where

V_a is the volume fraction of aggregates

$\varepsilon_{0.3}$ Is the transient creep strain for initial stress of $0.3\,f'_c$, and is given by Eq. (6).

$$\varepsilon_{0.3} = 43.87\times10^{-6} - 2.73\times10^{-8}\,T - 6.35\times10^{-8}\,T^2 + 2.19\times10^{-10}\,T^3 - 2.77\times10^{-13}\,T^4 \tag{6}$$

2.3.1.3 Reinforcing steel tensile stress-strain relationship

Lie's model[1] is used to predict the reduced yield strength of reinforcing bars f_{yT}, Eq. (7).

$$f_{yT} = \left(1 + \frac{T}{900 \times \ln(T/1750)}\right) \times f_y \qquad 0 < T \le 600\ ^oC \quad [32 < T \le 1112\ ^oF] \qquad (7a)$$

$$f_{yT} = \left(\frac{340 - 0.34 \times T}{T - 240}\right) \times f_y \qquad 600 < T \le 1000\ ^oC \quad [32 < T \le 1112\ ^oF] \qquad (7b)$$

Lie et al. [1] has also proposed another model which represents a general stress-strain $(f_{sT} - \varepsilon_{sT})$ relationship of reinforcing bars at elevated temperatures, Eq. (8). The effect of creep of steel bars is found to have a minor effect on the behavior of RC sections during fire exposure[9]. Thus, it is not included in this study.

$$f_{sT} = \frac{f(T,0.001)}{0.001} \times \varepsilon_{sT} \qquad \varepsilon_{sT} \le \varepsilon_p \qquad (8a)$$

$$f_{sT} = \frac{f(T,0.001)}{0.001} \times \varepsilon_p + f(T,[\varepsilon_{sT} - \varepsilon_p + 0.001]) - f(T,0.001) \qquad \varepsilon_{sT} > \varepsilon_p \qquad (8b)$$

$$\varepsilon_p = 4 \times 10^{-6} f_y \qquad (8c)$$

$$f(T,0.001) = (50 - 0.04T) \times [1 - e^{(-30+0.03T)\sqrt{0.001}}] \times 6.9 \qquad (8d)$$

2.3.1.4 Concrete compressive stress-strain relationship

The model proposed by Youssef and Moftah[6] is adopted in this study. The model includes simplified representation of transient creep strains. The relationship between the compressive stress, f_{cT}, and the corresponding compressive strain, ε_{cT}, is given by Eq. (9).

$$f_{cT} = K_{hT} \times f'_{cT} \left[2 \times \left(\frac{\varepsilon_{cT}}{\varepsilon_{oT} + \varepsilon_{tr}} \right) - \left(\frac{\varepsilon_{cT}}{\varepsilon_{oT} + \varepsilon_{tr}} \right)^2 \right] \qquad \varepsilon_{cT} \le \varepsilon_{oT} + \varepsilon_{tr} \tag{9a}$$

$$f_{cT} = K_{hT} \times f'_{cT} \left[1 - Z\left(\varepsilon_{cT} - \varepsilon_{oT} - \varepsilon_{tr} \right) \right] \qquad \ge 0.2 \times f'_{cT} \qquad \varepsilon_{oT} \ge \varepsilon_{oT} + \varepsilon_{tr} \tag{9b}$$

where,

$$K_{hT}\ (\text{confinement factor}) = 1 + \frac{\rho_s \times f_{yT}}{f'_{cT}} \tag{9c}$$

$$\rho_s = \frac{\text{volume of transverse reinforcement}}{\text{volume of concrete core measured to their perimeter}}$$

f_{yT} is the reduced yield strength for the stirrups at elevated temperature

Z is the slope of the descending branch of the concrete stress-strain relationship and is given by Eq. (9d)

$$Z = \frac{0.5}{\frac{3 + 0.29 f'_c}{145 f'_c - 1000} \times \frac{\varepsilon_{oT}}{\varepsilon_o} - \varepsilon_{oT}} \tag{9d}$$

The ultimate compressive strain at failure is assumed to be 0.0035 in the ambient condition according to the Canadian standards CSA A23.3-04[10]. Due to the limited literature on the failure compressive strain at elevated temperature, this value is increased by the transient strain ε_{tr} as proposed by El-Fitiany and Youssef[3].

$$\varepsilon_{uT} = \varepsilon_u + \varepsilon_{tr} \quad (10)$$

2.3.2 Heat transfer model

Several methods were developed to predict the temperature distribution in a concrete section during fire exposure[1]. The Finite Difference Method (FDM) is chosen in this research because of its ability to account for irregular shapes, its accuracy, and the ease of implementation in any programming code. The boundary conditions of the FDM include the fire temperature outside the concrete. A detailed description of the FDM, in the form of prescribed equations, is given by Lie et al. [1].

For beam B1, a 45 degrees heat transfer mesh of 5.4 mm by 5.4 mm [0.21 in] square elements is generated as shown in Fig. 2-2. Based on the size of the elements, the total fire duration (t = 1 hour), is divided into time steps Δt of 4.2 seconds. Concrete's initial moisture content is assumed to be zero due to its negligible effect on the temperature predictions[1]. A heat analysis based on the FDM is then conducted and the temperatures for the steel bars were found to range from 302 ^{o}C [576 ^{o}F] to 513 ^{o}C [955 ^{o}F]. Fig. 2-3 shows a comparison between the average measured temperatures of bottom steel bars by Lin et al. [1] and the FDM predictions at different fire durations. To allow using sectional analysis, the 45 degree mesh elements are converted to horizontal square mesh elements[1,3]. The temperature at the center of each square element, Fig. 2-2b, is taken as the average temperature of the adjacent 45 degree mesh elements.

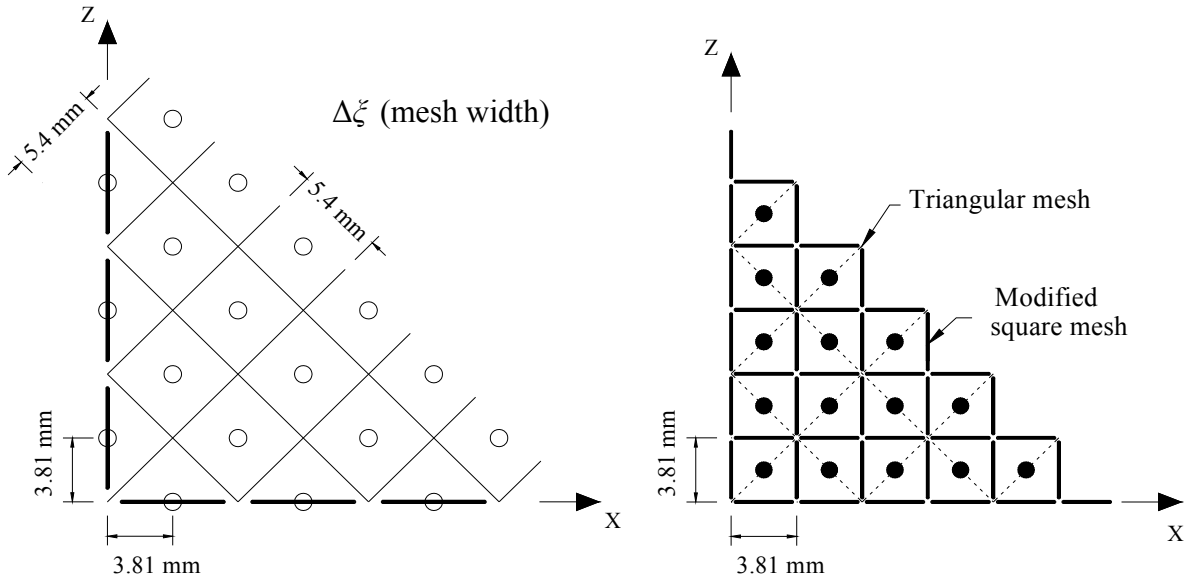

(a) Heat triangular mesh (Detail A) (b) Equivalent square mesh

Fig. 2-2-Heat Transfer mesh of beam B1

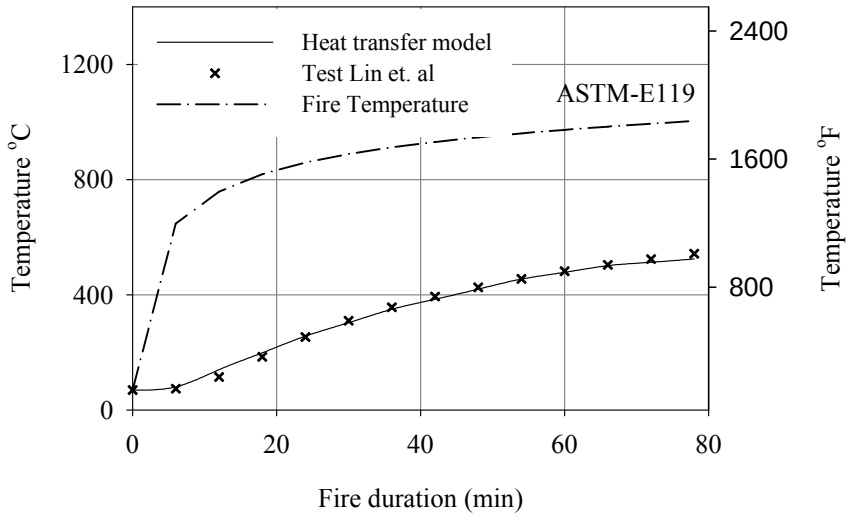

Fig. 2-3-Validation of the heat transfer model (average temperature of bottom reinforcing bars)

2.3.2.1 Average layer temperature

The methodology proposed by El-Fitiany and Youssef[3] is adopted. The square mesh elements are grouped into horizontal fibers to simplify the use of sectional analysis. Therefore, an equivalent temperature T_i has to be assigned for each fiber to allow estimating the concrete compressive strength, its modulus of elasticity, transient creep and thermal strains. To accurately predict the behavior using sectional analysis, El-Fitiany and Youssef[3] suggested the use of two different T_i's, one for estimating stresses and the other for strain values. It is clear from Eq. (1) that the tangential modulus of elasticity is the most important factor, thus it is proposed to estimate the first average layer temperature such that it produces the average modulus of elasticity for the square elements within the layer. At elevated temperatures, initial modulus of elasticity of loaded concrete is proportional to its reduced compressive strength[6]. Therefore, the first average temperature distribution for each fiber is based on the average strength of the square mesh elements, Fig. 2-2d, composing this layer. The second average temperature distribution is used to estimate the thermal and transient creep strains. Eqs. (4) and (5) show that they are proportional to the fire temperature and, this second temperature is equal to the algebraic average of the square mesh elements composing this layer. Fig. 2-4 shows the two distributions for the analyzed beam B1 after one hour of ASTM-E119 standard fire exposure. The temperature of steel bars can be assumed to be the same as the temperature of the square mesh element within which they are located[1].

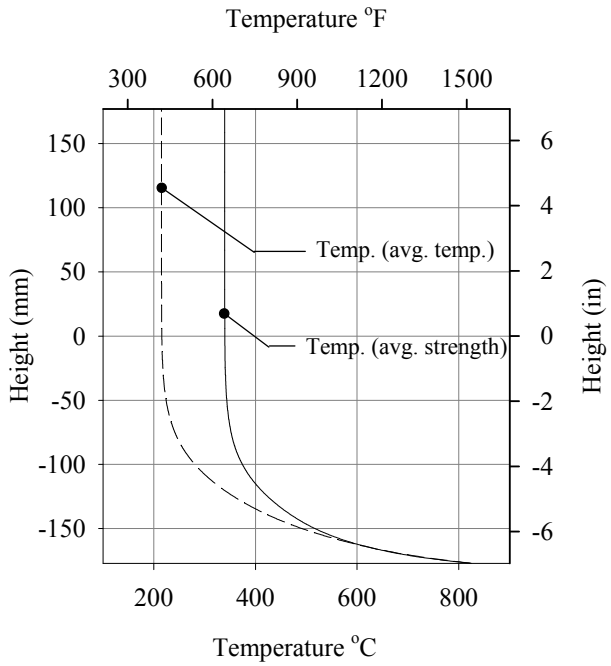

Fig. 2-4-Average temperature distributions for B1 after 1hr ASTM-E119 fire exposure

2.3.2.2 Thermal and effective strain calculation

Fig. 2-5 shows the expected linear distribution of total strains (ε) under a pure bending moment (M). This linear shape is based on the fact that plane sections remain plane after loading, which is still valid at elevated temperatures[11,12]. El-Fitiany and Youssef[3] used the same principle but the total strain was a constant value representing the case for a section exposed to fire from four sides. The distribution of ε_{th} for a rectangular cross-section subjected to fire temperature from three sides is shown in Fig. 2-5.

For unrestrained concrete sections, the effective strain (ε_{cT}) can be calculated by subtracting the concrete and steel's thermal strains from the total strain. The nonlinear distribution of thermal strains results in a nonlinear effective (mechanical) strain distribution, Fig. 2-5. As Eq. (1) is only applicable for linear strain distributions, the following sub-sections propose a methodology to conduct sectional analysis for the non-linear varying effective strain distribution.

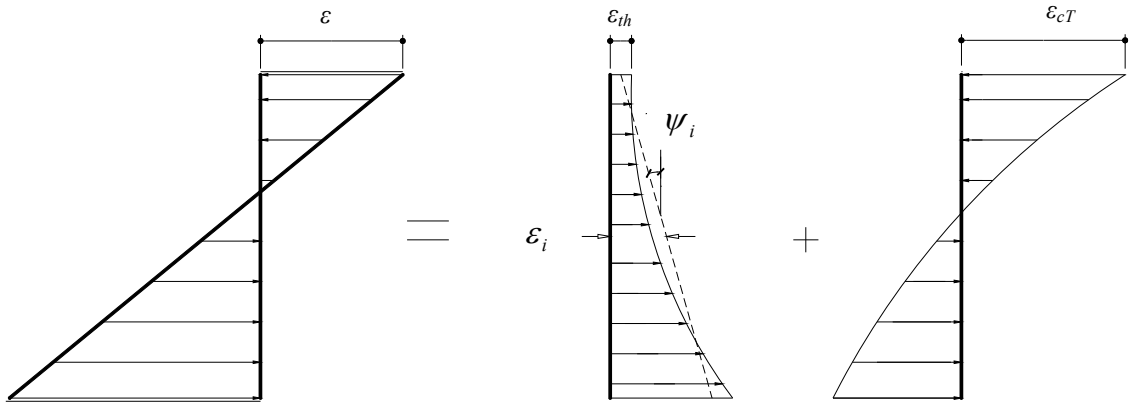

Fig. 2-5-Components of total strain at elevated temperatures

2.3.2.3 Isolation of thermal strain component for beam sections

For square column sections exposed to fire temperature from four sides, details for thermal strain equilibrium are given by El-Fitiany and Youssef[3]. For the case of a rectangular cross-section exposed to fire from three sides, the thermal strain is expected to be asymmetric as shown in Fig. 2-5. The equivalent shape is defined by the mid-height axial strain (ε_i) and the curvature (ψ_i), Figs. 2-5 and 2-6. The values of ε_i and ψ_i are evaluated such that the axial forces and bending moments in concrete and steel layers resulting from the difference between the actual thermal strain distribution and ε_i are in self equilibrium. An iterative procedure is used to calculate the values of ε_i and ψ_i such that the forces, shown in Fig. 2-6b, produce zero axial force and zero moment. Concrete tensile strength is neglected in the analysis.

Fig. 2-6a shows the nonlinear thermal strain distribution for the studied beam B1 after 1 hr standard ASTM-E119 fire exposure. The presented thermal strain distribution is converted to a linear distribution by considering section equilibrium. The equivalent uniform strain reflects the actual deformation of the concrete section under zero external loads and moments. Differences between the non-linear and equivalent uniform strains represent concrete and steel internal stresses that are in equilibrium.

2.3.2.4 Thermally induced stresses

The conversion from the actual nonlinear strain distribution to the equivalent linear distribution induces self-equilibrating internal strains (ε_{st}), Fig. 2-6b. These internal strains are part of mechanical strains required to retain the geometric linearity of B1's cross-section. To account for these strains, they are included as initial strains for each concrete and/or steel fiber.

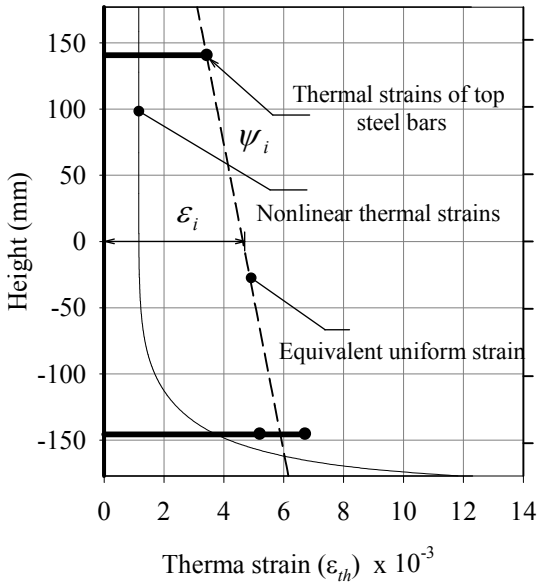

a) Thermal strains

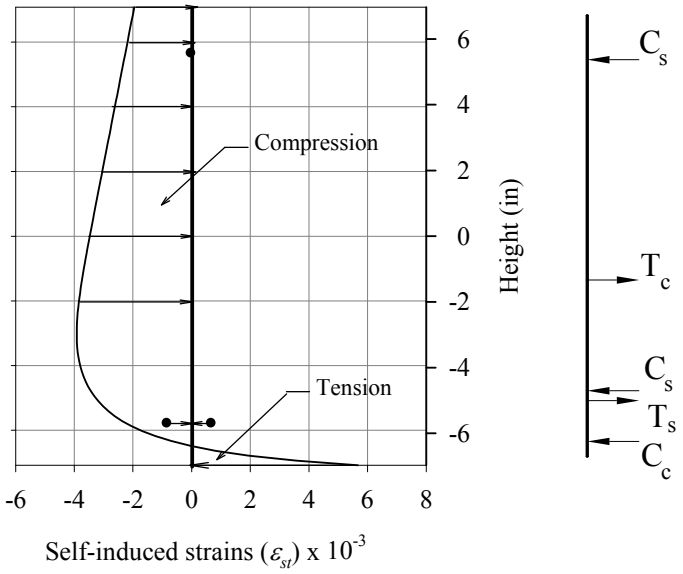

$(\varepsilon_{st} = \varepsilon_{th} - \overline{\varepsilon_{th}})$

b) Self-equilibrating strains

Fig. 2-6-Strain distribution and self-equilibrating forces along B1 height

2.4 Analysis Steps of RC Beams under Fire Loading

It can be concluded from the previous sections that the sectional analysis can be divided into three main steps;

1. The heat transfer model is applied and the heat gradient through the cross section is predicted. The average temperatures for each layer are then obtained.

2. The equivalent uniform thermal strain ε_i and the curvature ψ_i are then calculated by equilibrating the forces in the concrete and steel layers resulting from the actual thermal strain distribution. The difference between the actual and uniform strain distributions represents the induced strains ε_{st} in concrete and steel layers to satisfy the section geometry. These strains are considered as initial strains in the following step.

3. Sectional analysis is conducted to construct the moment-curvature diagrams.

2.4.1 Validation of the sectional analysis methodology

Moment-curvature curves represent the flexural behavior of a RC section under specified axial load level (λ). Fig. 2-7 shows the effect of 1 hr standard ASTM-E119 fire exposure on the studied unrestrained section of beam B1 (λ equals to zero). As shown in Fig. 2-7, elevated temperatures increase the ductility and reduce the capacity of RC sections during fire exposure. The initial point of the moment-curvature diagram after 1 hr fire exposure defines the equilibrium curvature ψ_i. This curvature value represents the initial rotation of B1 due to the non-linear thermal distribution combined with the material weakening. This initial curvature will occur regardless of the external effect of the applied moments.

The moment-curvature diagrams were constructed for beam B1 at different fire durations. The vertical deflection *w** at each time step was estimated by applying the moment-area method to the estimated curvature distribution along the beam length. The effect of

elevated temperatures on the shear capacity, bond loss between steel bars and concrete, and concrete spalling were not considered in the sectional analysis. The obtained results are plotted in Fig. 2-8. An excellent match is found between the sectional analysis, the FEM conducted by Kodur and Dwaikat[2] , and the experimental results (up to 80 minutes). Failure criteria proposed by BS 476 and adopted by Kodur and Dwaikat[2] are used. These criteria are setting limits for the maximum allowable deflection, Eq. (11), and maximum rate of deflection, Eq. (12).

$$\Delta_{max} = \frac{L}{20} = 305 \text{ mm} \quad [12 \text{ in}] \tag{11}$$

$$\left(\frac{\partial \Delta}{\partial t}\right)_{max} = \frac{L^2}{9000d} = 13 \quad \text{mm/minute} \ [0.51 \text{ in/minute}] \tag{12}$$

Where L is the span between the supports (mm) and d is the effective depth of the beam (mm) [1 in = 25.4 mm]

As shown in Fig. 2-8, the proposed sectional analysis results in about 17 minutes difference in predicting failure compared with the reported fire test resistance.

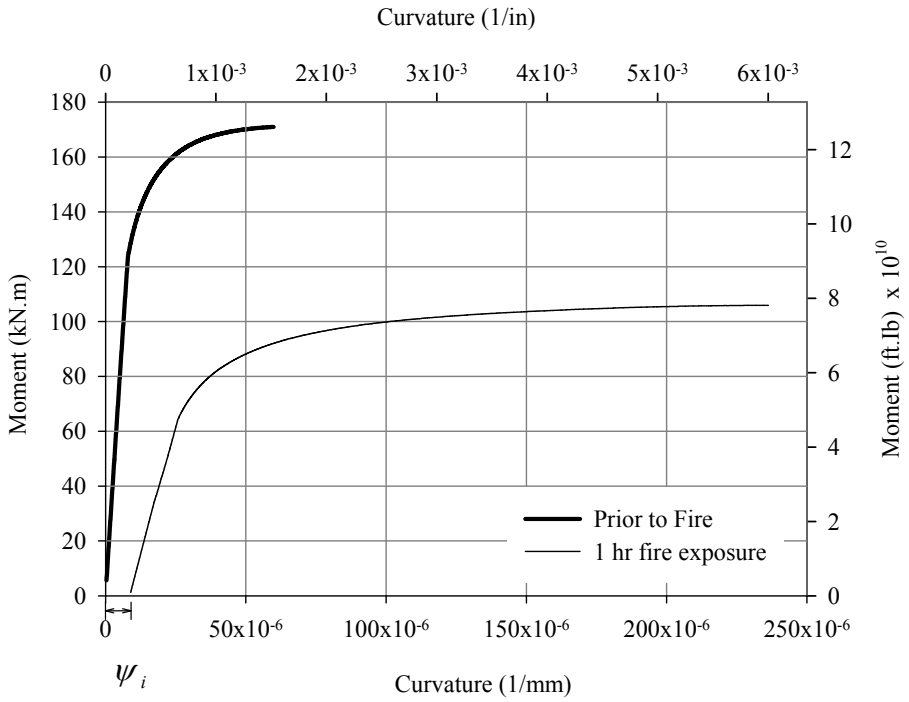

Fig. 2-7-Effect of fire temperature on the moment – curvature relationship for B1

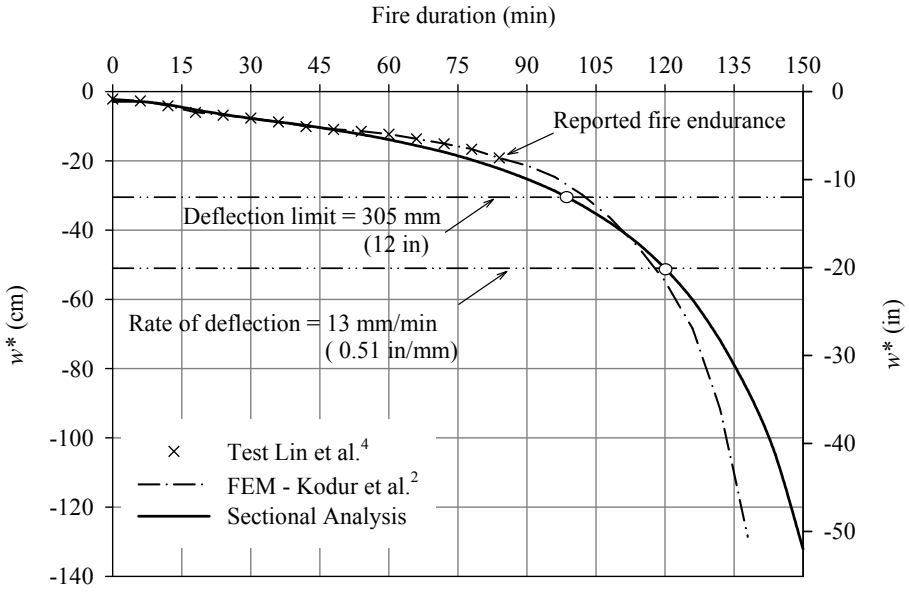

Fig. 2-8-Validation of sectional analysis methodology by prediction the deflections of B1 during fire exposure

2.5 Stress-Block Parameters at Ambient Temperature

Reinforced concrete beams are currently designed for flexure at ambient conditions by assuming a linear strain distribution and converting the nonlinear stress distribution to an equivalent stress-block. This conversion is done using the stress-block parameters α_1 and β_1. The recommended values for the stress-block parameters at ambient temperature in the Canadian code CSA A23.3-04[10] depend on f'_c to account for high strength concrete and are given by:

$$\alpha_1 = 0.85 - 0.0015 \times f'_c \tag{13a}$$

$$\beta_1 = 0.97 - 0.0025 \times f'_c \tag{13b}$$

The nominal moment at failure M_n can therefore be calculated from section equilibrium as follows

$$C = \alpha_1 \times f'_c \times \beta_1 \times c \times b \tag{14a}$$

$$T_s = f_y \times A_s \tag{14b}$$

$$C = T_s \quad \text{(calculate } c\text{)} \tag{14c}$$

$$M_n = (C \text{ or } T_s) \times (d - \frac{\beta_1 \times c}{2}) \tag{14d}$$

Where C is the compression force in the concrete, c is the depth of neutral axis, b is the width of the compression zone, T_s is the tension force in steel assuming yielding or reinforcement, f_y is the yield stress of steel bars, A_s is the area of tensile steel bars, and d is the effective depth of the section.

2.6 Stress-Block Parameters at Elevated Temperatures

The effect of fire temperature on the ambient stress-block parameters α_1 and β_1 is evaluated in this section through an extensive parametric study. A total of 28 rectangular cross-sections are analyzed to study the stress distribution at different fire durations. Table 2-1 shows details of the beams that are subjected to sagging bending moments (positive moments). On the other hand, Table 2-2 shows details of beams that are subjected to hogging bending moments (negative moments). The studied parameters are; fire duration (t), geometry of the sections (b and h), reinforcement ratio (ρ) and configuration, concrete compressive strength (f'_c), and aggregate type. The effect of compression reinforcement is neglected for simplicity.

Fig. 2-9 shows details for the studied cross-sections. All the beams are subjected to the standard ASTM-E119 fire from three faces, i.e. the two sides and the bottom surface of each beam. A sectional analysis was conducted for each beam at different fire durations starting from 0.0 hr and up to 2.5 hr with time intervals of 15 min. For each time step, the stress-block parameters at elevated temperature α_{1T} and β_{1T} are evaluated by predicting the total strain distribution (ε) at failure using the proposed sectional analysis methodology. The mechanical strain (ε) is then isolated and the stress distribution is obtained based on it. The following sub-sections explain these steps for beams B4, sagging moment, and B18, hogging moment.

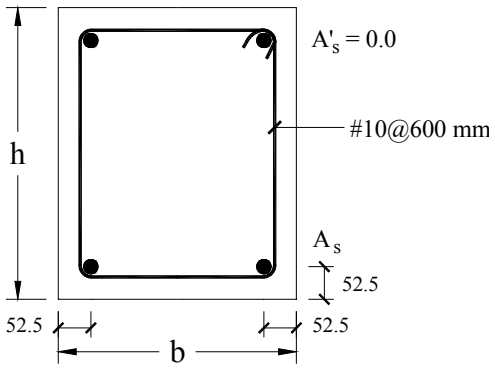

Fig. 2-9-Details of the studied RC beam "B4" in the parametric study

Dimensions in mm [1 in = 25.4 mm]

Table 2-1–Parametric study cases (sagging moment)

Beam #	f_y (MPa) [psi]	f'_c (MPa) [psi]	b (mm) [in]	h (mm) [in]	ρ ($\%A_g$)	Studied variables	Notes
B2	400 [58015]	30 [4351]	300 [11.8]	502.5 [19.8]	1.0	h, ρ	
B3					2.0	h, ρ	
B4				705.0 [27.8]	1.0	h, ρ, b , agg. type	
B5					2.0	h, ρ, b , agg. type	
B6				907.5 [35.7]	1.0	h, ρ	
B7					2.0	h, ρ	
B8			400 [15.7]	700.0 [27.6]	1.0	f'_c, b	
B9					2.0	f'_c, b	
B10			300 [11.8]	705.0 [27.8]	1.0	aggregate type	carbonate aggregate
B11					2.0	aggregate type	carbonate aggregate
B12				907.5 [35.7]	1.0		
B13					2.0		
B14		40 [5802]		705.0 [27.8]	1.0	RFT configuration	
B15					1.0	RFT configuration	2 layers RFT
B16			400 [15.7]	700.0 [27.6]	1.0	f'_c	
B17					2.0	f'_c	

Table 2-2–Parametric study cases (hogging moment)

Beam #	f_y (MPa)	f'_c (MPa)	b (mm)	h (mm)	ρ ($\%A_g$)	Studied variables	notes
B18	400 [58015]	30 [4351]	300 [11.8]	705.0 [27.8]	1.0	h, b, ρ, agg. type	
B19					2.0	h, b, ρ, agg. type	
B20				907.5 [35.7]	1.0	h, b, ρ	
B21					2.0	h, b, ρ	
B22				705.0 [27.8]	1.0	aggregate type	carbonate aggregate
B23					2.0	aggregate type	carbonate aggregate
B24				700.0 [27.6]	1.0	b, f'_c	
B25					2.0	b, f'_c	
B26			400 [15.7]	900.0 [35.4]	1.0	b	
B27					2.0	b	
B28		40 [5802]		700.0 [27.6]	1.0	f'_c	
B29		40 [5802]			2.0	f'_c	

2.6.1 Behavior of beams subjected to sagging moments during fire

A heat transfer analysis was conducted for beam B4. The height of the beam was slightly increased to 705 mm [27.8 in] to retain the aspect ratio of the 45 degree heat transfer mesh. Fig. 2-10 shows the average temperature distributions along B4 cross-section height.

The studied beam B4 was analyzed using the proposed sectional analysis methodology. A constant spacing for stirrups of 600 mm [23.6 in] was assumed. Fig. 2-10 shows the predicted total linear strain distribution at failure. The mechanical strain ε_{cT} can be isolated from the total strain ε by subtracting the thermal strain ε_{th}. Knowing the constitutive model for the stress-strain relationship of concrete at elevated temperatures, i.e. Eq. (7), the stress distribution can be plotted as explained earlier in this chapter.

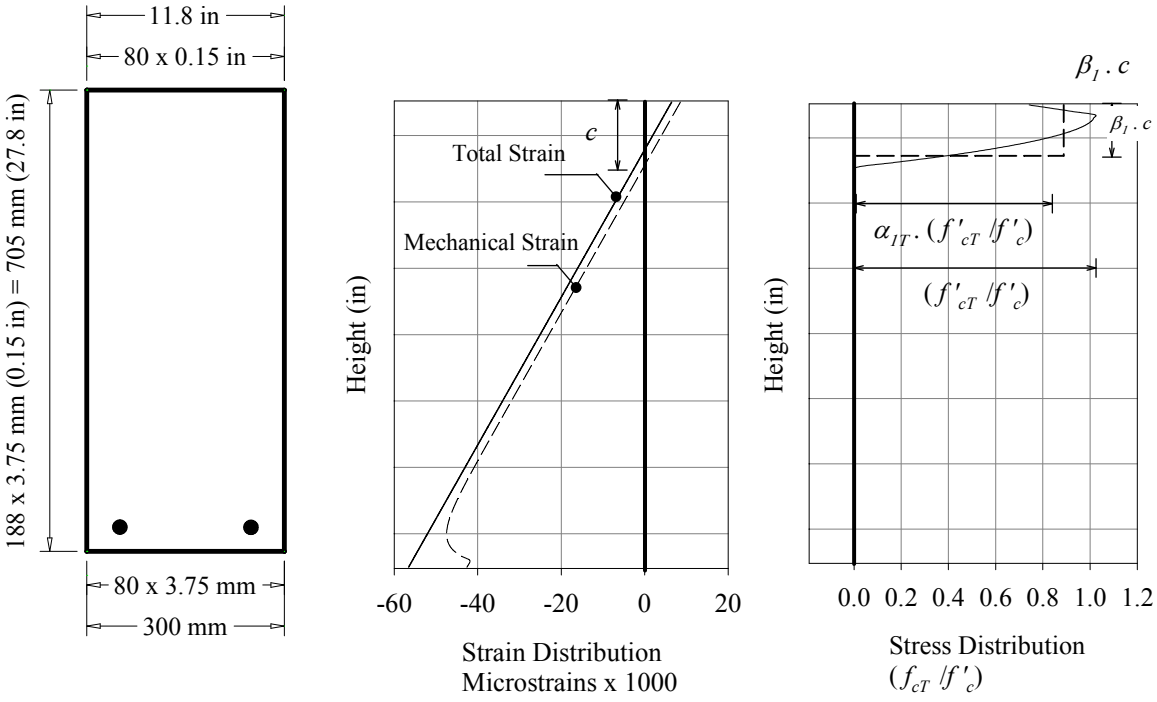

Fig. 2-10-Strain and stress distributions of B4 at 1.0 hr fire exposure

The equivalent rectangular stress-block can be obtained by considering the equilibrium in forces and moments between the equivalent block and the actual stress distribution. The stress-block parameters α_{1T} and β_{1T} of beam B4 after 1 hr fire exposure were found to be 0.87 and 0.80, respectively.

Fig. 2-10 indicates that the nonlinear effect of the bottom surface heating is limited to the bottom zone of the beam cross-section where the tensile reinforcement is allocated while temperature distribution is uniform in the concrete compression zone. This uniform temperature has consequently resulted in a linear mechanical strain distribution, because of the constant thermal strain ε_{th}, at the top of the concrete section. The uniform temperature has also resulted in a constant concrete stress-strain relationship for concrete at different locations in the compression zone. This explains why the stress distributions at elevated temperatures for beams subjected to sagging moments have similar shape to the ambient temperature. The uniform average temperatures in the compression zone were found to be functions of the section width and aggregate type. Fig. 2-11 allow predicting the average temperature (based on the average strength) in the concrete compression zone for both siliceous and carbonate aggregate. Fig. 2-12 shows the algebraic average temperature in the concrete compression zone for different aggregate types.

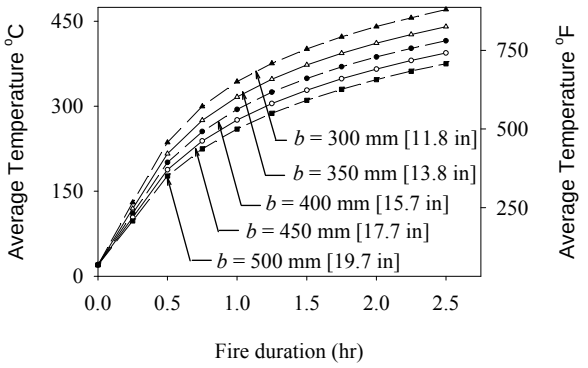

Fig. 2-11-Effect of ASTM-E119 fire duration and section width on the average strength temperatures

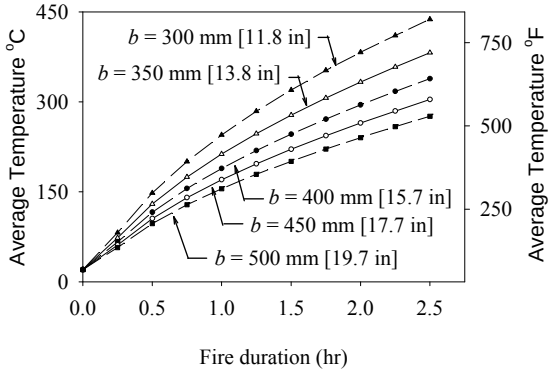

a) Siliceous aggregate

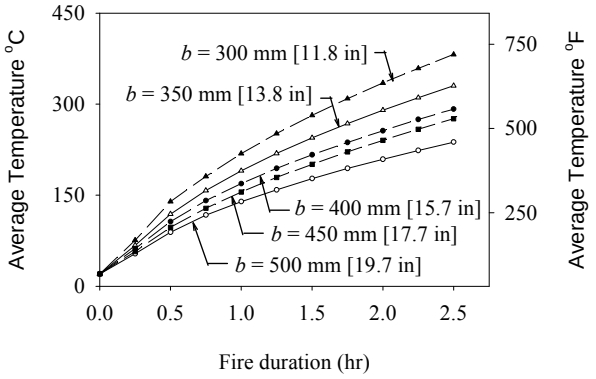

b) Carbonate aggregate

Fig. 2-12-Effect of ASTM-E119 fire duration and section width on the average temperature

2.6.2 Stress-block parameters for beams subjected to sagging moments

Tables 2-3 and 2-4 show the results of the parametric study for the beams described in Table 2-1. The effect of reinforcement ratio and section height on α_{1T} and β_{1T} is negligible as shown Fig. 2-13. The effect of the concrete compressive strength f'_c, distribution of reinforcing bars, and aggregate type on the shape of the equivalent stress-block is negligible. On the other hand, the effect of the section width b is found to have the greatest influence on the studied stress-block parameters α_{1T} and β_{1T}. This conclusion is reasonable since the effect of the fire temperature is usually limited to the outer concrete layers exposed to the flames while the beam core remains mostly undamaged.

A statistical study was conducted based on the results presented in Tables 2-3 and 2-4 to propose a simplified expression for α_{1T} and β_{1T}. The effects of fire duration t, concrete compressive strength f'_c, and section width b were accounted for in a multiple regression analysis using the Ordinary Least Square method (OLS). Based on the results of the parametric study, Equations (15a) and (15b) were proposed and plotted in Fig. 2-13. A good match can be found for all the results up to 2.50 hr fire duration.

$$\alpha_{1T} = \alpha_1 - 1.533\times10^{-2} + 24.397\times10^{-3}t + 15.758\times10^{-4} f'c - 10.089\times10^{-5} b \tag{15a}$$

$$\beta_{1T} = \beta_1 - 2.907\times10^{-2} + 20.734\times10^{-3}t^2 - 94.794\times10^{-3}t - 75.057\times10^{-5} f'_c + 15.413\times10^{-5} b \tag{15b}$$

Table 2-3–Parametric study results (sagging moment)

t (hr)	B2		B3		B4		B5		B6		B7		B8		B9	
	α_{IT}	β_{IT}	α_{IT}	β_{IT}	α_{IT}	β_{IT}	α_{IT}	β_{IT}	α_{IT}	β_{IT}	α_{IT}	β_{IT}	α_{IT}	β_{IT}	α_{IT}	β_{IT}
0.00	0.846	0.881	0.847	0.880	0.842	0.881	0.845	0.879	0.836	0.886	0.829	0.891	0.834	0.888	0.837	0.885
0.25	0.856	0.852	0.855	0.852	0.847	0.856	0.850	0.860	0.846	0.857	0.844	0.858	0.839	0.869	0.842	0.865
0.50	0.860	0.828	0.863	0.825	0.860	0.830	0.850	0.830	0.854	0.831	0.851	0.833	0.843	0.846	0.847	0.844
0.75	0.861	0.817	0.866	0.813	0.860	0.816	0.861	0.815	0.857	0.818	0.858	0.817	0.850	0.832	0.851	0.831
1.00	0.870	0.803	0.874	0.800	0.870	0.802	0.872	0.800	0.870	0.802	0.873	0.799	0.850	0.826	0.858	0.820
1.25	0.879	0.796	0.882	0.790	0.879	0.793	0.880	0.790	0.877	0.792	0.878	0.791	0.857	0.817	0.862	0.811
1.50	0.880	0.789	0.886	0.782	0.882	0.786	0.885	0.782	0.883	0.784	0.884	0.782	0.862	0.809	0.868	0.803
1.75	0.885	0.782	0.887	0.778	0.885	0.779	0.887	0.777	0.886	0.778	0.888	0.776	0.867	0.803	0.873	0.796
2.00	0.891	0.778	0.891	0.772	0.887	0.775	0.890	0.772	0.888	0.774	0.890	0.771	0.870	0.799	0.878	0.792
2.25	0.887	0.775	0.891	0.769	0.890	0.772	0.892	0.768	0.889	0.771	0.892	0.768	0.876	0.793	0.880	0.787
2.50	0.887	0.772	0.892	0.766	0.890	0.768	0.892	0.765	0.892	0.767	-----	-----	0.882	0.791	-----	-----

Table 2-4–Parametric study results (sagging moment) - Cont'd

t (hr)	B2		B3		B4		B5		B6		B7		B8		B9	
	α_{IT}	β_{IT}	α_{IT}	β_{IT}	α_{IT}	β_{IT}	α_{IT}	β_{IT}	α_{IT}	β_{IT}	A_{IT}	β_{IT}	α_{IT}	β_{IT}	α_{IT}	β_{IT}
0.00	0.844	0.881	0.845	0.879	0.802	0.902	0.806	0.899	0.810	0.898	0.811	0.897	0.801	0.906	0.802	0.902
0.25	0.846	0.860	0.845	0.861	0.819	0.869	0.817	0.871	0.824	0.868	0.823	0.868	0.811	0.882	0.809	0.882
0.50	0.854	0.834	0.858	0.831	0.831	0.841	0.837	0.837	0.833	0.842	0.834	0.840	0.822	0.859	0.826	0.853
0.75	0.858	0.822	0.859	0.820	0.839	0.826	0.840	0.825	0.838	0.828	0.839	0.826	0.824	0.845	0.830	0.840
1.00	0.869	0.806	0.871	0.804	0.854	0.810	0.854	0.810	0.854	0.813	0.854	0.810	0.826	0.837	0.833	0.832
1.25	0.877	0.796	0.879	0.793	0.863	0.800	0.869	0.794	0.862	0.801	0.866	0.797	0.836	0.830	0.841	0.823
1.50	0.883	0.787	0.885	0.785	0.870	0.791	0.875	0.786	0.869	0.792	0.873	0.790	0.839	0.822	0.852	0.811
1.75	0.888	0.781	0.889	0.779	0.876	0.783	0.881	0.779	0.874	0.786	0.878	0.782	0.845	0.817	0.856	0.806
2.00	0.889	0.777	0.892	0.773	0.879	0.779	0.883	0.775	0.881	0.782	0.881	0.778	0.855	0.811	0.862	0.799
2.25	0.892	0.772	0.893	0.769	0.883	0.775	0.886	0.771	0.881	0.777	0.886	0.773	0.859	0.803	0.866	0.795
2.50	0.895	0.769	0.895	0.765	0.885	0.771	0.888	0.767	0.881	0.775	0.887	0.768	0.856	0.804	0.868	0.792

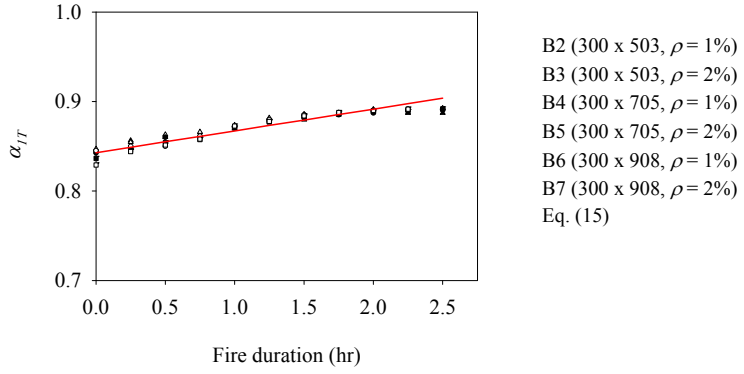

a) Variation of α_{1T}

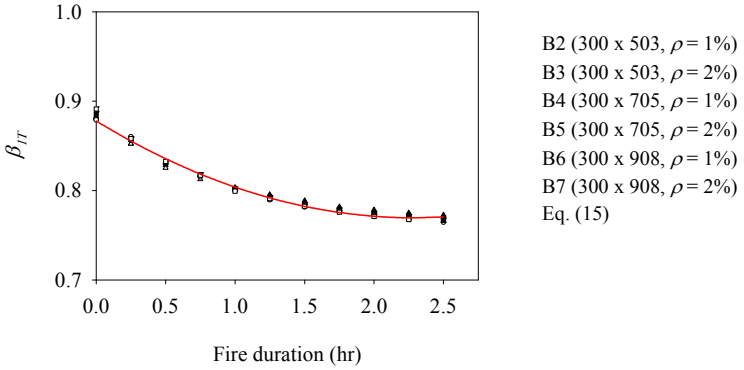

b) Variation of β_{1T}

Fig. 2-13-Effect of fire duration, RFT ratio, and section height on α_{1T} and β_{1T}

Dimensions in mm [1 in = 25.4 mm]

2.6.3 Flexural capacity for beams subjected to sagging moments

This section presents a methodology that can be used by designers to predict the reduced nominal flexural resistance M_{nT} for beams subjected to positive moments under ASTM-E119 standard fire exposure. This procedure is illustrated considering a 350×750 mm [13.8×29.5 in] rectangular beam (B30), Fig. 2-14, cast with a 35 MPa [5076 psi] siliceous aggregate concrete. The beam has reinforcement ratio ρ (grade 400) of 1.5%. The sectional analysis methodology predicted a reduced resistance moment after 1.5 hr ASTM-E119 fire exposure of 541 kN.m [3.99×10^{11} ft.Ib]. The designer can reasonably predict the reduced resistance using the proposed equation, Eq. (15), as explained in Appendix I. Eq. (15) estimates a nominal failure moment of 536 kN.m [3.95×10^{11} ft.Ib] with a difference of 1% from the sectional analysis. The ASCE simplified method[1] estimates 496 kN.m [3.66×10^{11} ft.Ib] (the difference is 8% from the sectional analysis methodology). Applying the 500 ^{o}C [932 ^{o}F] isotherm method as described in the ENV 1992-1-2[13] requires constructing the elevated temperatures contour map within the beam cross section, Fig. 2-15. The next step is to neglect the concrete where the temperature is above 500 ^{o}C [932 ^{o}F] in calculating the reduced flexural strength. As shown in Fig. 2-15, the reduced cross section is 289×750 mm [11.4×29.5 in]. Considering this reduced cross section results in 487 kN.m [3.59×10^{11} ft.Ib] nominal failure moment, Appendix I. The difference between the 500 ^{o}C [932 ^{o}F] isotherm method and the sectional analysis methodology is 10%.

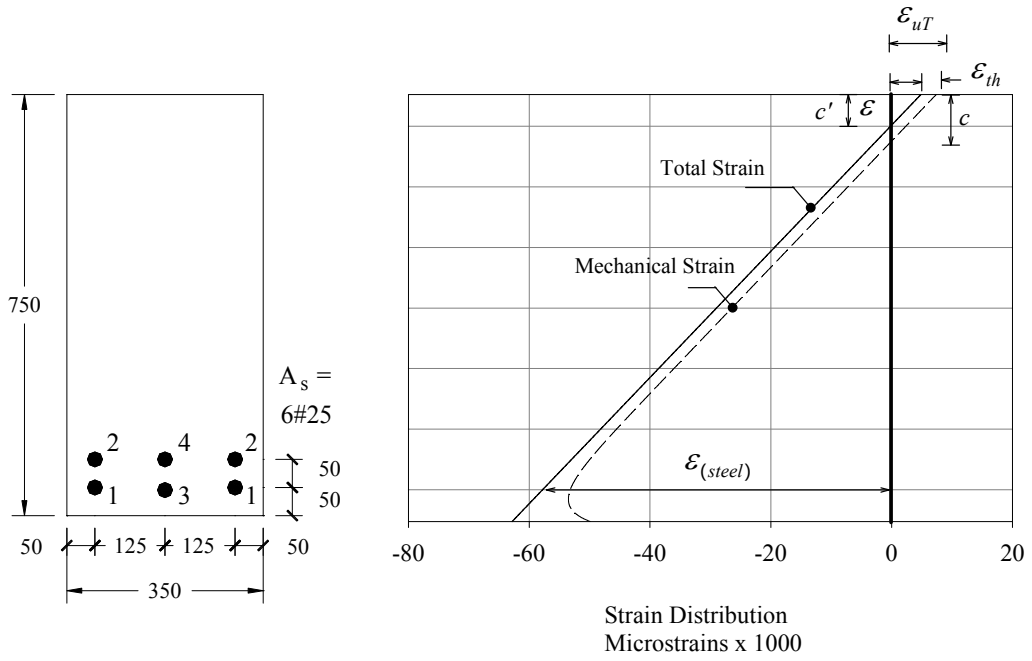

Fig. 2-14- Example beam (B30) for calculating the nominal failure moment M_{nT} using the proposed α_{1T} and β_{1T} - Dimensions in mm [1 in = 25.4 mm]

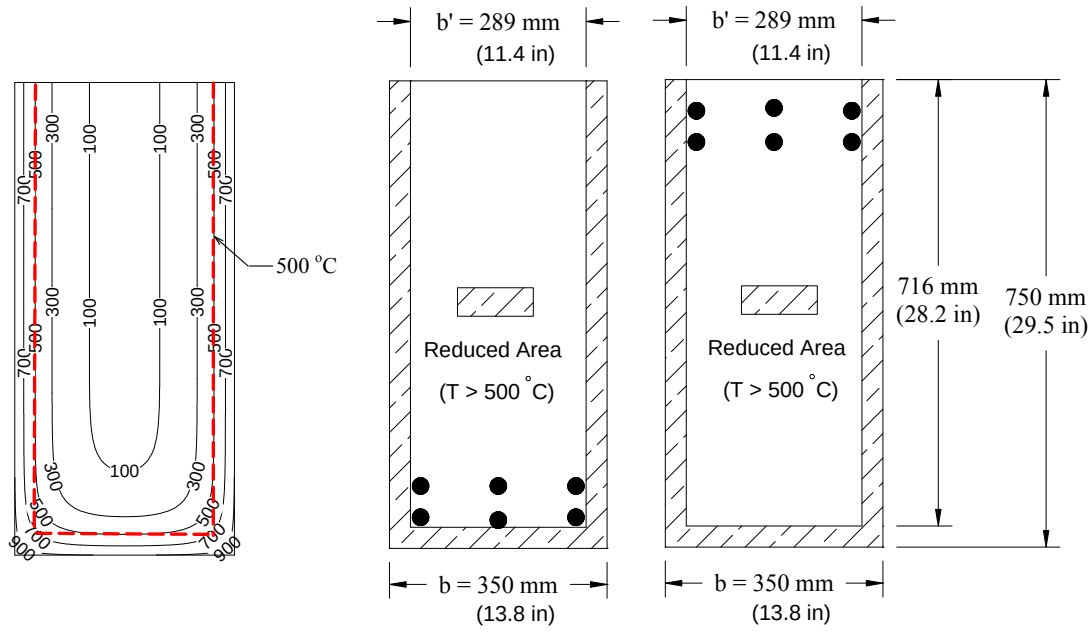

a) sagging moment b) hogging moment

Fig. 2-15- Temperature contour map in ^{o}C of B30 [1 ^{o}F = 1.8 ^{o}C + 32]

2.6.4 Calculation of stress-block parameters for beams subjected to Hogging moments

The same procedure illustrated for beams subjected to sagging moments is repeated here. A heat transfer analysis followed by a sectional analysis is conducted for beam B18 as an illustrative example. The mechanical strain ε_{cT} is isolated from the total strain ε by subtracting the thermal strain ε_{th}, Fig. 2-16. By knowing the constitutive model for the stress-strain relationship of concrete at elevated temperatures, the stress distribution can be predicted at different fire durations as shown in Fig. 2-16. The effect of fire on the concrete compression zone becomes more pronounced in the case of negative moments. This effect is characterized by the significant reduction in the concrete compressive strength and the shape of the compression stress distribution. Fig. 2-10 shows a steep variation in the average temperature in the concrete compression zone allocated close to the heat source. This variation results in different stress-strain relationships for concrete at different heights in the compression zone, similar stress distribution was recommended by Tan and Yao[14]. Therefore, the stress-distribution after 1.0 hr fire exposure has two different peak points. Tan and Yao have suggested values for α_{1T} and β_{1T} by replacing f'_c with f'_{cT} in Eq. (13) without having a rational basis for this modification. f'_c in Eq. (13) accounts for the compressive strength enhancement for high strength concrete rather than material weakening at the top concrete allocated close to fire flames.

It should also be noted that concrete failure, i.e. Eq. (8), has to occur at the top compression fibers where the maximum mechanical strain occurs. The top concrete fibers should sustain higher transient strains ε_{tr} because of the higher temperatures they experience which subsequently increase the failure strain ε_{uT} predicted by Eq. (10). The equivalent stress-block can be obtained by considering the equilibrium in forces and moments between the equivalent block and the actual stress distribution at different fire durations.

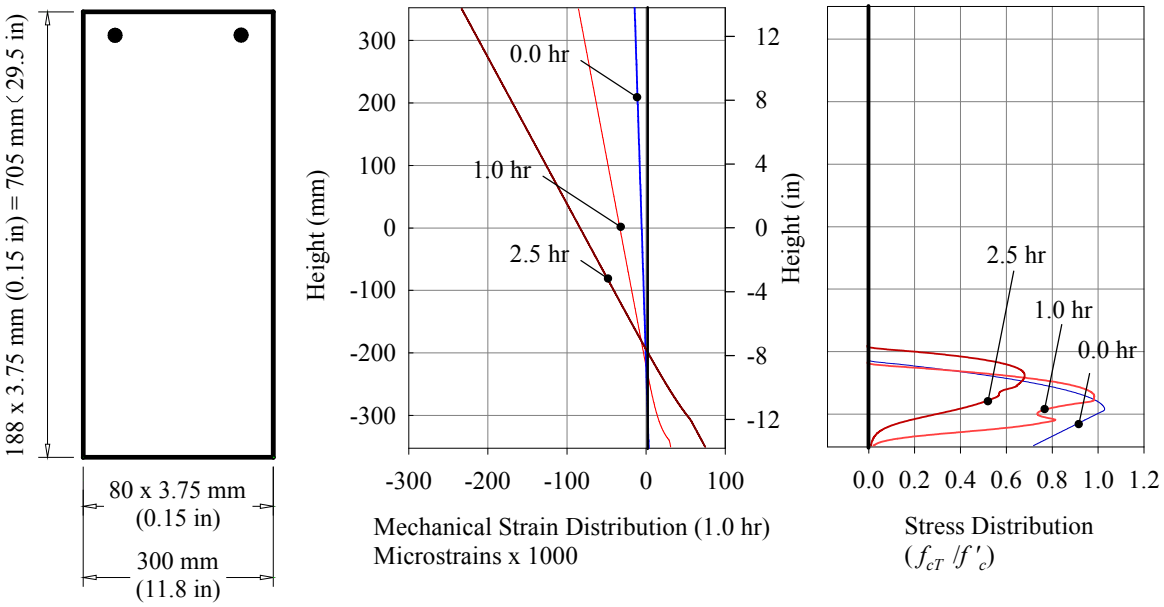

Fig. 2-16-Mechanical strain and stress distributions of B18 at different fire durations

2.6.5 Stress-block parameters for beams subjected to hogging moments

Tables 2-5 and 2-6 show the results of the parametric study for the beams presented in Table 2-2. The force equilibrium factor α_{1T} is found to be better described in terms of the fire duration t only, Fig. 2-17. The moment equilibrium factor β_{1T} is described in terms of the fire duration t, reinforcement ratio ρ, aggregate type, concrete compressive strength f'_c, and section width b. Fig. 2-18 is presented as a sample figure for the results. For simplicity and practicality, the reduction in the concrete compressive strength R was accounted for in the parameters α_{1T} and β_{1T} for beams subjected to negative moments.

A statistical study was conducted on the results presented in Tables 2-5 and 2-6 to propose a simplified expression for α_{1T} and β_{1T} for beams subjected to hogging moments. Eq. (16.a) and (16.b) were proposed based a multiple regression analysis using the Ordinary Least Square (OLS) method plotted in Figs 3-17 and 3-18. A good match is found for all the results up to 2.50 hr fire duration.

$$\alpha_{1T} = \alpha_1 - 2.735\times10^{-2} - 1.497\times10^{-1} t + 7.579\times10^{-2} F_{agg.} \tag{16a}$$

$$\beta_{1T} = \beta_1 - 1.965\times10^{-1} - 4.054\times10^{-2}\left(\frac{t}{\rho}\right)^2 + 2.448\times10^{-1}\left(\frac{t}{\rho}\right) - 3.456\times10^{-2} F_{agg.} + 3.687\times10^{-3} f'_c + 2.342\times10^{-4} b \tag{16b}$$

where $F_{agg.}$ is a factor to account for the aggregate type; 0.0 for siliceous concrete and 1.0 for carbonate concrete.

Table 2-5–Parametric study results (hogging moment)

t (hr)	B2		B3		B4		B5		B6		B7	
	α_{IT}	β_{IT}	α_{IT}	β_{IT}	α_{IT}	β_{IT}	α_{IT}	β_{IT}	α_{IT}	β_{IT}	α_{IT}	β_{IT}
0.00	0.843	0.845	0.835	0.829	0.842	0.845	0.834	0.837	0.833	0.832	0.797	0.801
0.25	0.805	0.820	0.813	0.817	0.838	0.839	0.798	0.818	0.800	0.815	-----	0.773
0.50	0.696	0.755	0.722	0.765	-----	0.788	-----	0.752	0.685	0.736	-----	-----
0.75	0.631	0.705	0.659	0.719	0.743	0.758	0.638	0.691	0.663	0.694	-----	-----
1.00	0.557	0.660	0.598	0.691	0.707	0.761	0.572	0.662	0.613	0.653	0.518	0.605
1.25	0.491	0.604	0.536	0.640	0.668	0.739	0.515	0.627	0.559	0.615		0.575
1.50	0.439	0.553	0.483	0.593	0.631	0.717	0.464	0.585	0.510	0.573	0.410	0.530
1.75	0.396	0.508	0.437	0.548	0.596	0.693	0.422	0.543	0.468	0.532	0.371	0.492
2.00	0.359	0.468	0.399	0.507	0.564	0.667	0.387	0.505	0.431	0.495	-----	0.452
2.25	0.327	0.432	0.366	0.471	0.534	0.641	0.357	0.473	0.399	0.462	0.310	0.423
2.50	0.298	0.400	0.336	0.438	0.507	0.616	0.330	0.442	0.371	0.433	0.285	-----

Table 2-6–Parametric study results (hogging moment) - Cont’d

t (hr)	B2		B3		B4		B5		B6		B7	
	α_{IT}	β_{IT}	α_{IT}	β_{IT}	α_{IT}	β_{IT}	α_{IT}	β_{IT}	α_{IT}	β_{IT}	α_{IT}	β_{IT}
0.00	0.881	0.879	0.886	0.891	0.881	0.879	0.888	0.885	0.887	0.887	0.906	0.902
0.25	0.927	0.902	0.915	0.898	0.912	0.892	0.933	0.908	0.925	0.909	-----	0.930
0.50	0.995	0.933	0.968	0.919	-----	0.918	-----	0.944	0.994	0.953	-----	-----
0.75	1.047	0.964	1.012	0.944	0.989	0.937	1.055	0.982	1.021	0.982	-----	-----
1.00	1.101	0.993	1.057	0.961	1.022	0.945	1.110	1.005	1.063	1.013	1.167	1.050
1.25	1.140	1.021	1.091	0.984	1.057	0.964	1.157	1.033	1.106	1.043	-----	1.081
1.50	1.173	1.045	1.123	1.002	1.089	0.985	1.191	1.063	1.142	1.074	1.250	1.115
1.75	1.200	1.068	1.150	1.022	1.114	1.007	1.223	1.087	1.170	1.098	1.276	1.140
2.00	1.221	1.089	1.173	1.042	1.130	1.028	1.246	1.110	1.196	1.121	-----	1.166
2.25	1.240	1.108	1.193	1.059	1.140	1.047	1.268	1.131	1.218	1.143	1.318	1.187
2.50	1.255	1.126	1.209	1.075	1.150	1.060	1.287	1.152	1.239	1.163	1.333	-----

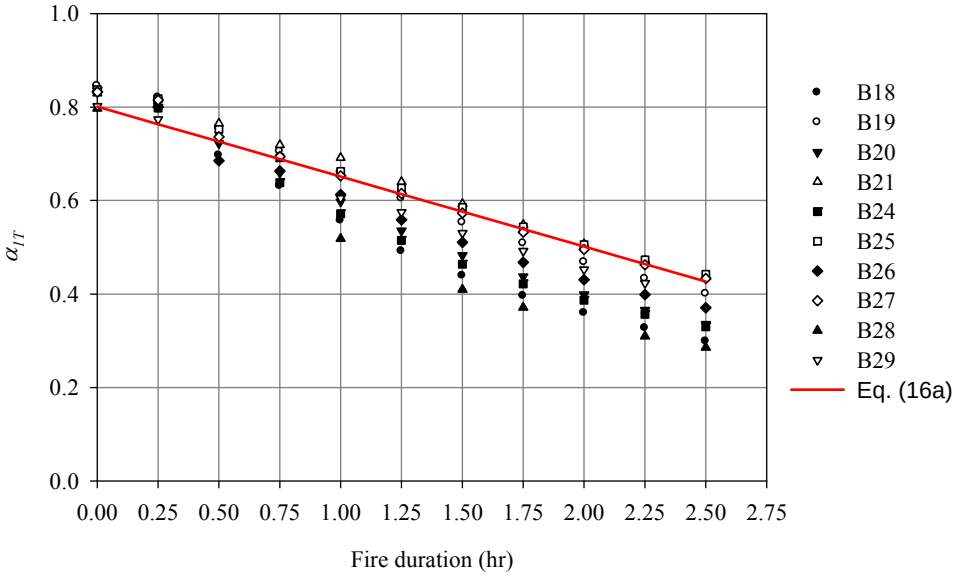

Fig. 2-17- Effect of fire duration and other studied factors on α_{1T}

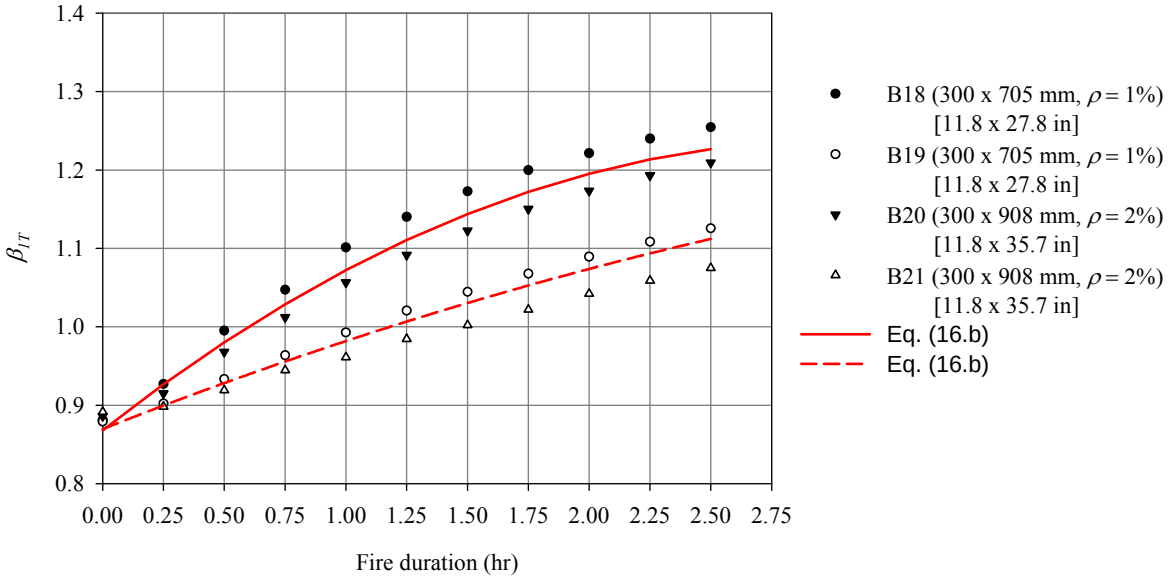

Fig. 2-18- Effect of fire duration, RFT ratio, and section height on β_{1T}

2.6.6 Flexural capacity for beams subjected to hogging moments

This section presents a methodology that can be used by designers to predict the flexural resistance M_{nT} for beam B30 in the case of negative bending. The sectional analysis methodology predicted a reduced resistance moment, after 1.5 hr ASTM-E119 fire exposure, of 627 kN.m [4.62×10^{11} ft.Ib]. On the other hand, structural engineers can predict a reduced flexural resistance of 593 kN.m [4.37×10^{11} ft.Ib] using Eq. (16), Appendix II. The ASCE manual[1] recommends using a reasonable average value for the compressive strength. The 500 ^{o}C [932 ^{o}F] isotherm method recommended by the ENV EC2, 1992[13] results in 571 kN.m [4.21×10^{11} ft.Ib] failure moment with 9% difference than the sectional analysis.

2.7 Summary and Conclusions

The sectional analysis methodology, introduced by the authors in a previous publication, is extended in the first part of this chapter to cover RC beams subjected to fire from three sides. The proposed methodology is found to be a simple, yet accurate method to track the behavior of rectangular RC beams at elevated temperatures. In a similar fashion to ambient temperature analysis of RC beams, temperature-dependent stress-block parameters are developed in the second part of this chapter to convert the non-linear compression stresses distribution to a linear and constant stress distribution.

A parametric study aiming at investigating the effect of ASTM-E119 fire temperature on the stress distribution is conducted by applying the proposed methodology on a number of unrestrained rectangular beams. The studied parameters are; fire duration (t), geometry of the sections (b and h), reinforcement ratio (ρ) and configuration, concrete compressive strength (f'_c), and aggregate type. The studied cross-sections were subjected to a standard ASTM-E119 fire durations up to 2.5 hour. For each time step, the total strain and stress distributions were predicted at failure. The actual distributions of compression stresses at different fire durations were approximated to their equivalent

stress-blocks. The equivalent stress-block parameters were evaluated for the studied sagging and hogging moment cases by applying multiple regression analysis on the parametric study results. Failure of the beams subjected to sagging moments was found to occur at the top compression fibers similar to ambient temperature. On the other hand, failure of the beams subjected to hogging moments occurs at a location within the compression block where the mechanical strain in concrete reaches the failure strain at this location. Simplified expressions for the proposed stress-block parameters were derived and verified in this chapter for nominal failure moment prediction. The use of the proposed parameters is relatively easy and practical to be implemented in design codes. Prediction of nominal flexural strength of fire-damaged concrete beams can also be useful to check the capacity design of beam-column assemblage in seismic design.

2.8 Acknowledgments

This research was funded by the Natural Sciences and Engineering Research Council of Canada (NSERC).

2.9 References

1. Lie, T.T., ed., "Structural Fire Protection," ASCE Manuals and Reports on Engineering Practice, no. 78, New York, NY, 1992, 241 pp.
2. Kodur, V.K.R., and Dwaikat, M., "Performance-based fire safety design of reinforced concrete beams," Journal of Fire Protection Engineering, vol. 17, no. 4, 2007, pp. 293-320.
3. El-Fitiany, S., Youssef, M.A. 2009, "Assessing the flexural and axial behaviour of reinforced concrete members at elevated temperatures using sectional analysis", Fire Safety Journal, vol. 44, no. 5, pp. 691-703.

4. Lin, T.D., Gustaferro, A.H., and Abrams, M.S., "Fire Endurance of Continuous Reinforced Concrete Beam", Portland Cement Association, Bulletin RD072.01B, Skokie, 1981.
5. Youssef, M.A., and Rahman, M., "Simplified seismic modelling of reinforced concrete flexural members," Magazine of Concrete Research, vol. 59, no. 9, 2007, pp. 639-649.
6. Youssef, M.A. and Moftah, M., "General stress-strain relationship for concrete at elevated temperatures," Engineering Structures, vol. 29, no. 10, 2007, pp. 2618-2634.
7. Hertz, K.D., "Concrete Strength for Fire Safety Design," Magazine of Concrete Research, vol. 57, no. 8, 2005, pp. 445-453.
8. Terro, M.J., "Numerical modeling of the behavior of concrete structures in fire," ACI Structural Journal, vol. 95, no. 2, 1998, pp. 183-193.
9. Bratina, S., Saje, and M., Planinc, I., "The effects of different strain contributions on the response of RC beams in fire," Engineering Structures, vol. 29, no. 3, 2007, pp. 418-430.
10. Cement Association of Canada, "Concrete design handbook, CAN/CSA A23.3-04," 3rd Ed., Ottawa, 2006.
11. Collins, M.P., Mitchell, D. 1987, "Prestressed Concrete Basics," Canadian Prestress Concrete Institute, Ottawa, ON, Canada.
12. Tassios, T.P., Chronopoulos, M.P., "Structural response of RC elements under fire," The Structural Engineer, vol. 69, no. 15, 1991, pp. 277-281.
13. Eurocode 2, "Design of Concrete Structures," ENV EC2, 1992.
14. Tan, K.H., and Yao, Y., "Fire resistance of four-face heated reinforced concrete columns," Journal of Structural Engineering, vol. 129, no. 9, 2003, pp. 1220-1229.
15. Anderberg, Y, and Thelandersson, S., "Stress and deformation characteristics of concrete at high temperatures: 2 experimental investigation and material behaviour model", Bulletin 54, Lund institute of Technology, Sweden, 1976.
16. Youssef, M.A., El-Fitiany, S.F., and Elfeki, M.A., "Flexural Behavior of Protected Concrete Slabs After Fire Exposure," Designing Concrete Structures for Fire Safety, ACI SP-255-4, 2008, pp. 47-74.

2.10 Appendix I

Simplified calculation of the M_{nT} for beams subjected to sagging moments

1. The reduced concrete compressive strength can be calculated using Fig. 2-15 and Eq. (2.b)

for b = 350 mm [13.8 in] and t = 1.50 hr $\rightarrow$ $T_{av.\ str}$ = 373 ^{o}C [703 ^{o}F] [Fig. 2-15]

R = 1.0 [Eq. (2b)]

$f'_{cT} = 1.25 \times (1.0 \times f'_c) \leq f'_c$ [25% increase because beam is loaded before fire]

$\therefore f'_{cT} = f'_c = 35\,\text{MPa}$ [5076 psi]

$f'_{cT} = K_{hT} \times f'_{cT} = 1.0 \times 35\,\text{MPa}$ [neglect confinement]

2. The compression force in the concrete is calculated as follows

$C = \alpha_{1T} \times f'_{cT} \times \beta_{1T} \times c \times b$ [Eq. (15a) and (15b)]

$\alpha_1 = 0.85 - 0.0015 \times 35 = 0.80$

$\therefore \alpha_{1T} = 0.80 - 1.533 \times 10^{-2} + 24.397 \times 10^{-3} \times 1.50 + 15.758 \times 10^{-4} \times 35 - 10.089 \times 10^{-5} \times 350$
$= 0.84$

$\beta_1 = 0.97 - 0.0025 \times 35 = 0.88$

$\therefore \beta_{1T} = 0.88 - 2.907 \times 10^{-2} + 20.734 \times 10^{-3} \times 1.5^2 - 94.794 \times 10^{-3} \times 1.5 - 75.057 \times 10^{-5} \times 35$
$+ 15.413 \times 10^{-5} \times 350 = 0.78$

$C = 0.83 \times 35 \times 0.79 \times c \times 350 = 8{,}026.2 \times c$

assume c = 105.9 mm [4.2 in] $\rightarrow$ $\therefore C = 849991\,\text{N}$ [191.1 kps]

3. The tension force in the steel is calculated as follows

$\varepsilon_{cuT} = \varepsilon_{cu} + \varepsilon_{tr}$

for b = 350 mm [13.8 in] and t = 1.50 hr $\rightarrow$ $T_{av.\ temp}$ = 278 °C [532 °F] [Fig. 2-16a]

$\varepsilon_{tr} = 0.00593$ [Eq. (5)]

$\varepsilon_{cuT} = 0.0035 + 0.00593 = 0.00943$ [Eq. (8)]

$\varepsilon_{tot} = \varepsilon_{cuT} - \varepsilon_{th} = 0.00943 - 0.00167 = 0.00776$ [Fig. 2-22]

$$c' = \frac{c}{\varepsilon_{cuT}} \times \varepsilon_{tot} = 0.823 \times c$$

$$\varepsilon_{tot(steel)} = \frac{\varepsilon_{tot}}{c'} \times d$$ [Fig. 2-22]

$T_1 = 558\ ^\circ\text{C}$ [1036 °F], $T_2 = 420\ ^\circ\text{C}$ [788 °F], $T_3 = 376\ ^\circ\text{C}$ [709 °F], and $T_4 = 163\ ^\circ\text{C}$ [325 °F]

$\varepsilon_{sT} = \varepsilon_{tot} - \varepsilon_{th}$ [Fig. 2-22]

The coefficient of thermal expansion of steel α_s is given by Lie et al. as follows

$\alpha_s = (0.004T + 12) \times 10^{-6}$ C^{-1} $T < 1000\ ^oC$ [1832 °F]

$\alpha_s = 16 \times 10^{-6}$ C^{-1} $T \geq 1000\ ^oC$ [1832 °F]

Thus,

$\varepsilon_{sT1} = 0.04661,\ \varepsilon_{sT2} = 0.04436,\ \varepsilon_{sT3} = 0.04949$, and $\varepsilon_{sT4} = 0.04805$

$f_{sT1} = 219\,\text{MPa}$ [31764 psi], $f_{sT2} = 282\,\text{MPa}$ [40901 psi], $f_{sT3} = 303\,\text{MPa}$ [43947 psi], and $f_{sT4} = 397\,\text{MPa}$ [57581 psi]

$$T_s = \sum_{i=1}^{4} f_{sTi} \times A_{si} = 849991\,\text{N} \quad [191.1\ \text{kps}]$$

$C = T_s$ O.K.

$$M_{nT} = \sum_{i=1}^{4} f_{sTi} \times A_{si} \times (d_i - \frac{\beta_{1T} \times c}{2}) = 536\ \text{kN.m} \qquad [39.54 \times 10^4\ \text{ft.Ib}]$$

2.11 Appendix II

Simplified calculation of the M_{nT} for beams subjected to hogging moments

1. The compression force in the concrete is calculated as follows

$$C = \alpha_{1T} \times f'_c \times \beta_{1T} \times c \times b$$

$$\alpha_1 = 0.85 - 0.0015 \times 35 = 0.80$$

$$\alpha_{1T} = \alpha_1 - 2.735 \times 10^{-2} - 1.497 \times 10^{-1} \times 1.50 + 7.579 \times 10^{-2} \times 0.0 = 0.55$$

$$\beta_1 = 0.97 - 0.0025 \times 35 = 0.88$$

$$\beta_{1T} = \beta_1 - 1.965 \times 10^{-1} - 4.054 \times 10^{-2}\left(\frac{1.5}{1.5}\right)^2 + 2.448 \times 10^{-1}\left(\frac{1.5}{1.5}\right) - 3.456 \times 10^{-2} \times 0.0$$
$$+ 3.687 \times 10^{-3} \times 35 + 2.342 \times 10^{-4} \times 350 = 1.10$$

assume c = 132.9 mm [5.2 in]

$\therefore C = 984734$ N [221.4 kps]

2. The tension force in the steel is calculated as follows

$T_1 = 366\,^{\circ}\text{C}$ [691 ^{o}F], $T_2 = 366\,^{\circ}\text{C}$ [691 ^{o}F], $T_3 = 58\,^{\circ}\text{C}$ [136 ^{o}F], and $T_4 = 58\,^{\circ}\text{C}$ [136 ^{o}F]

$f_{yT1} = 296\,\text{MPa}$ [42932 psi], $f_{yT2} = 296\,\text{MPa}$ [42932 psi], $f_{yT3} = 393\,\text{MPa}$ [57001 psi], and $f_{yT4} = 393\,\text{MPa}$ [57001 psi]

$$T_s = \sum_{i=1}^{4} f_{sTi} \times A_{si} = 984734 \text{ N [221.4 kps]}$$

$C = T_s$ O.K.

$$M_{nT} = \sum_{i=1}^{4} f_{sTi} \times A_{si} \times (d_i - \frac{\beta_{1T} \times c}{2}) = 593 \quad \text{kN.m} \qquad [43.75 \times 10^4 \text{ ft.lb}] \qquad (\text{Diff.} \approx 5\%)$$

Chapter 3

3 Simplified Method to Analyze Continuous RC beams during Fire Exposure

Fire safety is an important design aspect that engineers must consider while designing Reinforced Concrete (RC) structures. Fire is initiated by the ignition of combustible materials and spreads horizontally and vertically based on the compartment boundaries[1]. The exposed RC elements are heated and a temperature gradient is generated through them. The developed elevated temperatures cause the element's stiffness to degrade and produce thermal deformations[2, 3]. The only available approach to predict the behavior of a RC element during a fire event is to conduct a nonlinear coupled thermal-stress Finite Element (FE) analysis[4]. The FE method has proven to be a powerful method to predict the behavior of concrete structures during exposure to fire events[4]. Drawbacks of using the FE method including: the need for a comprehensive computer program, the difficulty to comprehend its results and to identify potential modeling errors, and the long running time make it impractical for design engineers. Its complexity becomes obvious in indeterminate structures where different regions of the structure have different heating regimes, cross-section dimensions, reinforcing bars configuration, and axial restrain conditions[5]. A simplified method to estimate the capacities and deformations of statically determinate RC elements during fire exposure was developed and validated by the authors[2, 6, 7]. Although this method is relatively easy to apply as compared to the FE method, it still requires knowledge of heat transfer principles and ability to conduct analysis at elevated temperatures.

In this chapter, the fire behavior of statically determinate and indeterminate RC beams is discussed. A practical method for tracking the deflection of indeterminate RC beams during fire exposure is presented and illustrated. The rectangular RC beams tested by Lin et al.[5] are used to validate the proposed method. A number of RC rectangular sections with different cross-section dimensions, reinforcement configuration, material properties, and loading levels are then analyzed during the standard ASTM-E119 fire exposure. Results of the parametric study are used to provide designers with simplified expressions

for the effective flexural stiffness and thermal deformations of fire exposed RC beams. These expressions will allow them to easily apply the proposed approach and have a quick idea about the serviceability of RC beams during fire events.

3.1 Research Significance

Analysis of RC continuous beams for structural fire safety can only be conducted at the research level and requires long computation time. This limitation is due to the complexity of the fire problem and the need for comprehensive FE tools. Fire ratings are currently satisfied using prescriptive methods that include specifying the minimum required cover[8]. Engineers need simplified tools to predict the behavior of RC structures during fire events. These tools are mostly needed by emergency response teams as a quick assessment of the integrity of a fire-damaged structure ensures the safety of their field members. This chapter presents such a tool for RC beams.

3.2 Sectional Analysis at Elevated Temperatures

Fire temperature drastically decreases concrete and steel mechanical properties and induces thermal and transient strains. Total concrete strain at elevated temperatures (ε) is composed of three terms: unrestrained thermal strain (ε_{th}), instantaneous stress related strain (ε_c), and transient creep strain (ε_{tr}). Fire performance of RC beams can be predicted by summing these strain components as shown in Eq. (1).

$$\varepsilon = \varepsilon_{th} + \varepsilon_c + \varepsilon_{tr} \quad (1)$$

A sectional analysis approach suitable for the analysis of rectangular RC beams at elevated temperatures was proposed by El-Fitiany and Youssef [2, 6, 7]. Fig. 3-1a shows the fiber model of a typical RC cross-section. The section is assumed to be exposed to fire from three sides. The approach can be briefly explained by the following main steps:

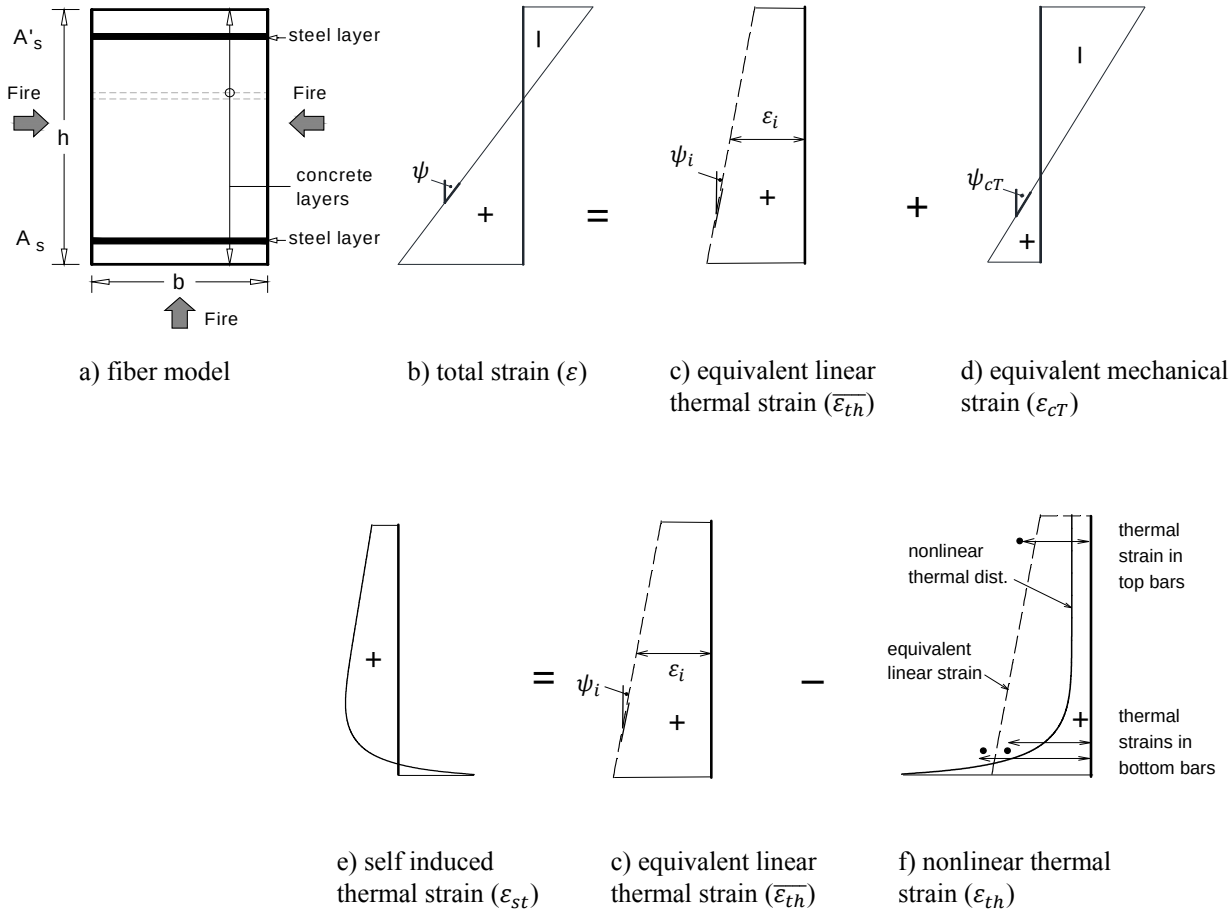

a) fiber model | b) total strain (ε) | c) equivalent linear thermal strain ($\overline{\varepsilon_{th}}$) | d) equivalent mechanical strain (ε_{cT})

e) self induced thermal strain (ε_{st}) | c) equivalent linear thermal strain ($\overline{\varepsilon_{th}}$) | f) nonlinear thermal strain (ε_{th})

Fig. 3-1-Modified sectional analysis approach for RC sections exposed to fire

1. At specific fire duration, a heat transfer analysis is conducted to predict the temperature distribution using the Finite Difference Method (FDM)[1]. The cross-section is then divided into horizontal layers and two average temperatures, T_σ and T_{th} are calculated for each layer. T_σ produces the same average concrete compressive strength for the layer, and thus is suitable for strength calculations. T_{th} represents the algebraic average temperature of the elements within each layer and is suitable for calculating the thermal and transient creep strains as they are temperature dependent[2].

2. The nonlinear thermal strain (ε_{th}) distribution, shown in Fig. 3-1f, is calculated using T_{th}. The thermal strain of steel bars is calculated based on the concrete temperature at

their location. ε_{th} is then converted to an equivalent linear thermal strain ($\overline{\varepsilon_{th}}$), Fig. 3-1c, by considering self equilibrium of internal thermal forces in concrete and steel layers. The linear distribution is characterized by the unrestrained thermal axial strain, ε_i, and curvature, ψ_i. Fig. 3-1e shows the differences between the equivalent linear and nonlinear thermal strains, which represent the self induced thermal strains (ε_{st}). These strains are assigned as initial strains for the concrete and steel layers to model the corresponding self-induced thermal stresses at a given point of the fire temperature-time curve. The total strain (ε) can be described as follows:

$$\varepsilon = \overline{\varepsilon_{th}} + \varepsilon_{st} + \varepsilon_c + \varepsilon_{tr} \quad (2)$$

3. The terms ε_{st} , ε_c , and ε_{tr} are lumped into an equivalent mechanical strain ε_{cT} that is used to calculate the corresponding stresses. The constitutive stress-strain relationships for concrete and steel, which are proposed by Youssef and Moftah[3] and are based on T_σ, are adapted. The concrete model implicitly accounts for transient creep as the strain corresponding to the maximum concrete stress is shifted using the transient creep strain given by Terro[9].

4. By considering the equilibrium of the stresses developed in all of the layers, the corresponding moment can be calculated. The behavior of the analyzed cross-section is presented by moment (M)–curvature (ψ) diagram.

The following section presents application of the method to two fire-exposed determinate beams.

3.3 Statically Determinate RC Beams during Fire

Beams B-123 and B-123a have a cross-section of $305 \times 355\ mm$ [$12 \times 14\ in$] and are fabricated with carbonate aggregate. The compressive strength for concrete, f'_c, is $30\ MPa$ [$4{,}350\ psi$]. The yield strength, f_y, for longitudinal reinforcing bars is $435.8\ MPa$ [$63{,}200\ psi$]. The tensile strength for concrete is neglected[3,10]. The effect of elevated temperatures on the shear capacity, bond loss between steel bars and concrete, and concrete spalling were not considered in the sectional analysis. The thermal properties proposed by Lie et al.[1] are used for the heat transfer analysis. The constitutive stress-strain relationships for concrete and steel proposed by Youssef and Moftah[3] are used in the analysis of B-123 and B123-a.

3.3.1 Simply supported beam (sagging moments)

The $6.10\ m$ [$1.86\ ft$] simply supported beam (B-123) was tested by Lin et al.[5] and subjected to four-$20\ kN$ [$4.5\ kips$] concentrated loads. Fig. 3-2a shows the test setup, loading, and beam cross-section. The applied loads were kept constant during exposure to ASTM-E119 standard fire. At ambient temperature, the applied loads induce an external moment that equals 42% of the beam nominal flexural capacity. A sectional analysis is conducted at different fire durations and the moment (M)–curvature (ψ) diagrams are constructed for each duration. Fig. 3-2b shows the $M-\psi$ diagrams at ambient temperature and after $30\ min$ of fire exposure. The mid-span deflection is then calculated by integrating the curvature distribution along the beam length. An ABAQUS FE model is also developed[11]. The thermal and stress FE analyses are assumed to be uncoupled. The concrete and steel are modeled using 8-node brick linear elements. Fig. 3-2c shows a good match between the sectional analysis predictions, ABAQUS FE results, and the experimental data. The sectional analysis has the advantages of ease of application and speed over the FE method.

a) beam loading (B-123)

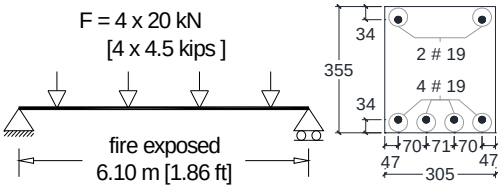

b) M – ψ diagram (B-123)

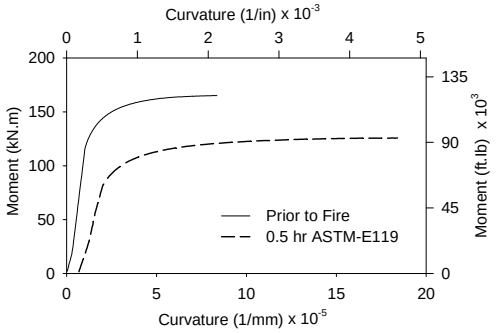

c) mid-span deflection (B-123)

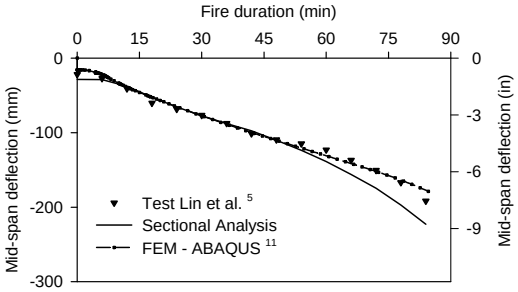

d) beam loading (B-123a)

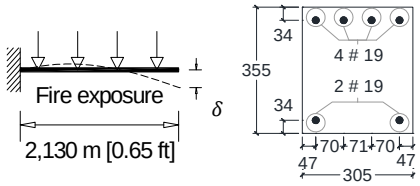

e) cantilever deflection (B-123a)

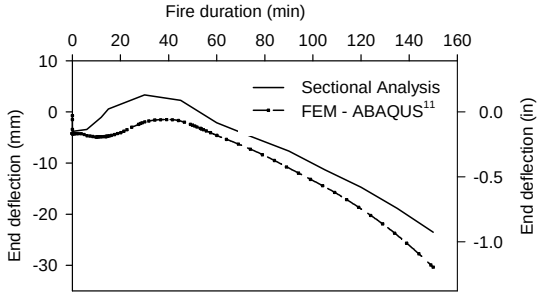

Fig. 3-2-Validation beams (B-123) and (B-123a)

3.3.2 Cantilever beam (hogging moments)

Experimental and analytical results addressing the fire performance of rectangular beams subjected to hogging (negative) moments is limited in the literature. The behavior of a cantilever beam, B-123a, is analytically studied during exposure to ASTM-E119 fire. As shown in Fig. 3-2d, the beam supports a uniformly distributed gravity load ($w = 34\ kN/m$) [$25.1\ kips/ft$] and is exposed to fire at three of its surfaces. An ABAQUS uncoupled thermal-stress FE analysis is conducted to predict its behavior. The concrete and steel are modeled using 8-node brick linear elements. The change of the deflection at the end of the cantilever as function of the fire duration is plotted in Fig. 3-2e. Using the sectional analysis method, the M–ψ diagrams are constructed at different fire durations and the end displacement is then predicted. Fig. 3-2e shows an acceptable agreement between the sectional analysis and the ABAQUS results. At the beginning, the bottom fibers of the beam, which are located close to the fire temperature, tend to expand relative to the top fibers causing an upward deflection. As fire continues, the stiffness of the beam degrades and the effect of gravity loads becomes more predominant causing a downward deflection. The difference between the FE method and the sectional analysis results can be due to the use of an average layer temperature and/or the method used to model the tensile reinforcing bars (lumped at one point in the sectional analysis method and represented using the actual circular cross-section area of the bar in the ABAQUS FE model).

3.4 Moment–Curvature Relationships of Fire-Heated RC Sections

Fig. 3-3 shows schematics for the M–ψ curves for RC sections subjected to sagging and hogging moments at a specific fire duration[4, 7]. The end point on the curve defines the nominal moment capacity (M_n) that corresponds to the curvature capacity of the analyzed cross-section[3]. The secant slope of the M–ψ diagram represents the cross-section's stiffness at a specific moment (M_{app}) or at a specific load level (λ), $\lambda = M_{app}/M'_n$ and M'_n is the nominal flexural capacity at ambient temperature.

For a specific fire duration, the effect of thermal strain on the M–ψ relationship is not governed by the load level. It represents the free thermal expansion of the unloaded concrete element and results in shifting the M–ψ diagram by a value ψ_i. This shift can be predicted by calculating the nonlinear thermal strain distribution and converting it to an equivalent linear distribution as discussed earlier in this chapter. The $M-\psi$ diagram includes the effects of material degradation, transient creep strain (ε_{tr}), and self induced thermal strain (ε_{st}). The total curvature (ψ) is the sum of the unrestrained thermal curvature (ψ_i) and the mechanical curvature (ψ_{cT}) and can be expressed in terms of the effective stiffness (EI_{eff}) as follows.

$$\psi = \psi_i + M_{app}/EI_{eff} \tag{3}$$

As shown in Fig. 3-3, heating RC beams from the bottom face and the two sides cause the bottom concrete fibers to thermally expand more than the top concrete fibers and results in ψ_i. The acting moment induces a mechanical curvature (ψ_{cT}), which is either added to or deducted from ψ_i. As shown in Fig. 3-3a, a positive (sagging) moment induces a curvature that adds to the initial curvature. For negative (hogging) moments, compression stresses are applied on the bottom fibers. Curvature caused by these stresses opposes the initial curvature, Fig. 3-3b. Such a moment-curvature diagram is similar to that of a prestressed concrete beam section. While the initial curvature in such a beam is caused by prestressing, it results from the thermal expansion in a fire-exposed beam. The

moment required to shift the behavior from sagging to hogging is a function of the fire duration that is proportional to the value of the initial curvature and the section properties that affects flexural deformations. The effect of fire duration and different section properties are discussed in details in the parametric study conducted at the end of this chapter.

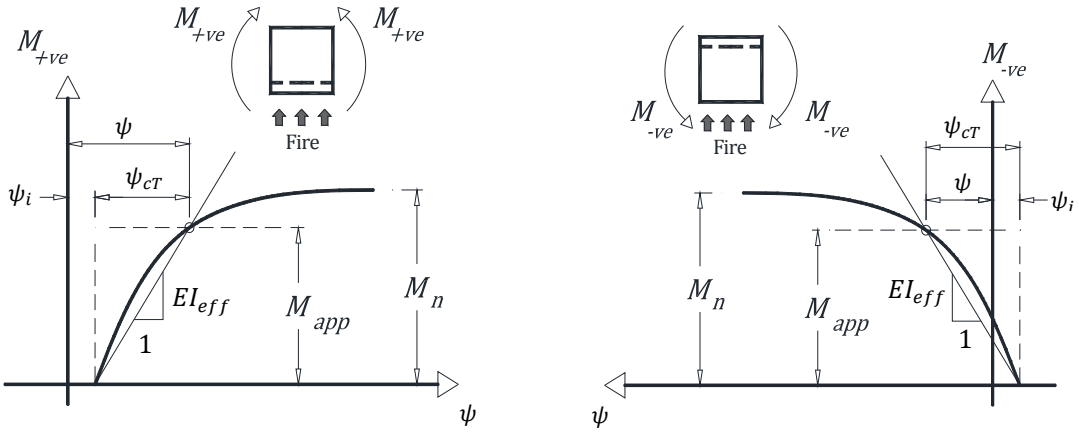

a) sagging moments (M_{+ve})

b) hogging moments (M_{-ve})

Fig. 3-3-(M)–(ψ) diagrams for RC beams during fire

3.5 Statically Indeterminate RC Beams during Fire

Indeterminacy restrains thermal deformations and induces secondary moments. The following sections propose and validate a method to track the behavior of statically indeterminate beams during fire exposure. The effect of elevated temperatures on the shear capacity, bond loss between steel bars and concrete, and concrete spalling were not considered in the sectional analysis.

3.5.1 Proposed method for continuous RC beams

The main assumptions of the proposed method are:

1) The effect of heat transfer along the beam longitudinal axis is neglected, i.e. two-dimensional heat transfer for the beam cross-section is conducted using the FDM.

2) The effect of concrete cracking on the heat transfer calculations is neglected.

3) The tensile resistance of concrete is assumed equal to zero.

4) Plane sections remain plane during fire exposure. This assumption has been validated using available experimental results up to a fire temperature of 1100 ℃ [2012 °F][2].

5) The thermal expansion is not affected by the load level.

6) The beam can be divided into elements, each with a constant stiffness EI_{eff}.

7) Transient $creep\ strains$ are calculated using Terro's model[9] and are implicitly accounted for by using the stress-strain relationship proposed by Youssef and Moftah[3].

Fig. 3-4a shows a schematic for a two span RC continuous beam subjected to fire from its bottom face and two sides. The beam is divided into five segments (S1, S2, S3, S2, and S1) based on the reinforcement configuration. The ambient temperature (primary) BMD is shown in Fig. 3-4b. The behavior of this beam at specific fire duration (t) is affected by

the values of the degraded stiffness (EI) and the thermal deformations. To capture this behavior, the following steps are proposed.

I) Evaluating the degraded flexural stiffness

A sectional analysis is conducted for the beam sections and the $M-\psi$ diagram is constructed for each segment at the given fire duration (t), Fig. 3-4c. The effective flexural stiffness (EI_{eff}) for each segment is then evaluated as the secant slope of the $M-\psi$ diagram at the applied ambient moment level. As a conservative simplification, a constant value of EI_{eff} is assigned to each segment based on its maximum flexural moment[12], Fig. 3-4d. Revised values for M_1, M_2, and M_3 are to be calculated based on the degraded EI_{eff} values.

II) Evaluating the restrain effect on thermal deformations

The unrestrained thermal curvature ψ_i is the curvature value at zero moment. Fig. 3-4d shows the distribution of ψ_i along the beam length during fire exposure. The continuity of the beam prevents this distribution from forming. Assuming that the middle support is removed, the curvature distribution, shown in Fig. 3-4d, can be obtained by applying two imaginary concentrated thermal moments (M_{th}) at the ends of each segment, Fig. 3-4e. Because of the continuity of the beam (the middle support in this example), the applied thermal curvatures cannot form. Secondary moments are developed in the beam redistributing these curvatures. These secondary moments can be evaluated by analyzing the indeterminate beam under the effect of the thermal moments (M_{th}), shown in Fig. 3-4e. Such analysis leads to defining the reaction at the middle support that can be used to calculate the moment diagram, Fig. 3-4f. The final moment acting on the beam equals the summation of the primary and secondary moments. This method is similar to the one used to account for the effect of restraint in continuous prestressed concrete beams.

The mentioned steps are repeated by recalculating the values for EI_{eff} that corresponds to the final moment distribution. These values are used to recalculate the primary and secondary moments. Iterations are performed until convergence is reached.

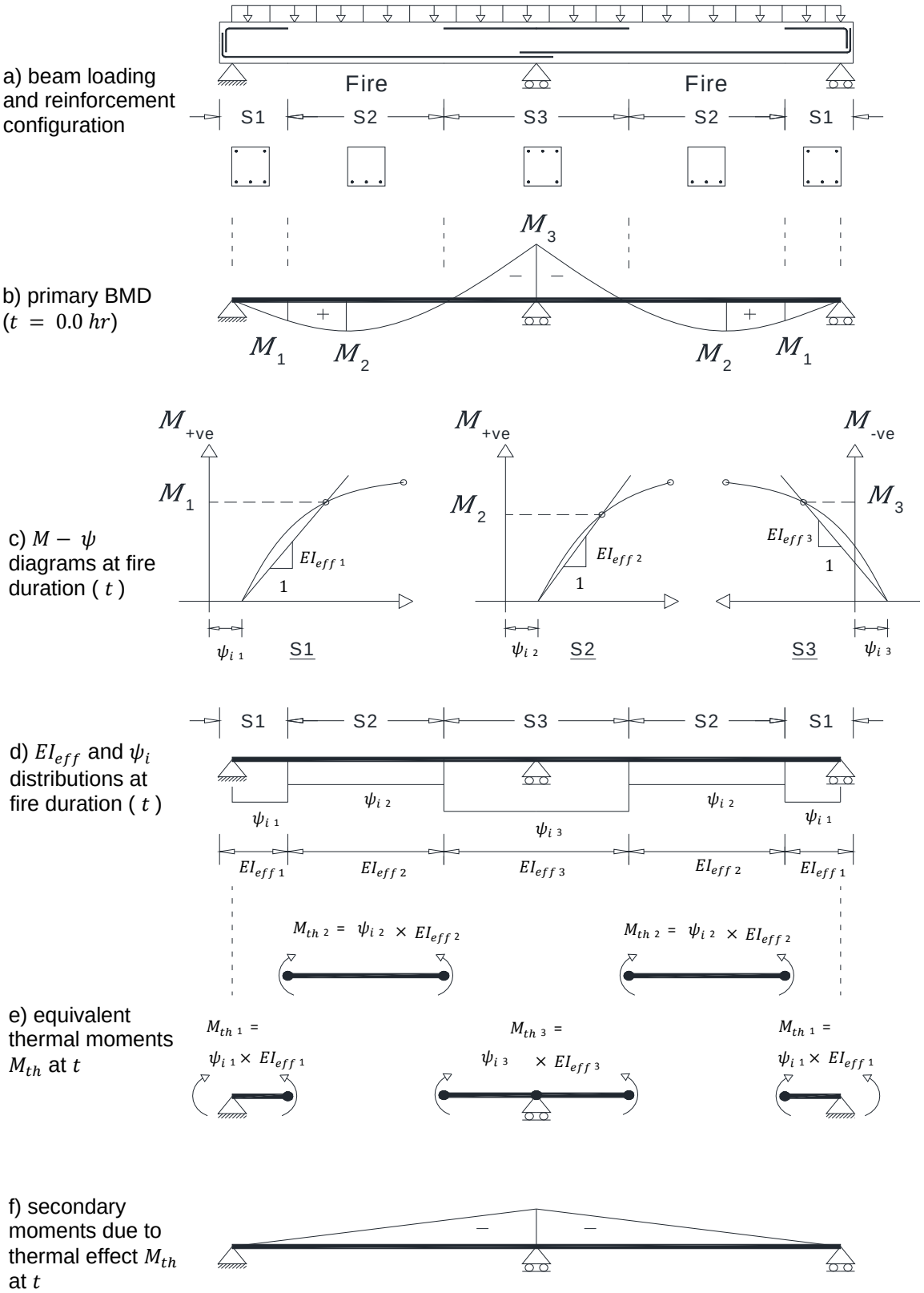

Fig. 3-4-Analysis steps for a two-span continuous RC beam during fire

3.5.2 Validation of the proposed methodology

Lin et al.[5] have experimentally investigated the effect of continuity on the behavior of RC beams during fire exposure. Fig. 3-5a shows a schematic of beam B-124 and Fig. 3-5b shows its reinforcement. The beam dimensions are the same as B-123. The beam was exposed to a 3.5 hrs of ASTM-E119 standard fire over a length of 5.486 m [18 ft], Fig. 3-5a, while supporting four equally spaced concentrated loads ($P3$) and two end loads ($P1$) and ($P2$). $P3$ was kept constant at 50.2 kN [11.27 kips] during the fire test. Prior to the fire test, $P1$ and $P2$ were equal to about 59.0 kN [13.26 kips]. They were adjusted during the fire test such that the deflections at points A and B are kept constant. The beam own weight is 2.57 kN/m [0.175 kips/ft]. The beam supports an additional load at the center span of 0.53 kN/m [0.036 kips/ft], which represents the weight of the furnace cover. At ambient temperature, the applied loads induce flexural negative and positive moments of about 43% of the beam nominal flexural capacity. Fig. 3-5c shows the moment diagram as compared to the nominal moment capacity. The beam was fabricated using carbonate concrete having a compressive strength of 29.7 MPa [4310 psi]. The yield strength of the reinforcing bars was 435.8 MPa [63,200 psi]. The mid-span deflection of the intermediate span and the variable loads $P2$ and $P3$ were monitored during the fire test. These values are predicted using the proposed method in the following section.

3.5.3 Modeling and analysis of B-124

The RC continuous beam is modeled using SAP2000[13] software as a series of frame elements. For simplicity, the beam is considered symmetric in terms of loading and material properties. To account for concrete cracking at ambient temperature, the M–ψ diagrams are constructed for both positive and negative moment sections and used to define (EI_{eff}) for the three cross-sections shown in Fig. 3-5b. The vertical loads are applied on the beam and the corresponding deflections are shown in Fig. 3-5d. The calculated mid-span deflection at ambient temperature is 0.015 m [0.57 in]. The upward deflection at the beam ends is 0.003 m [0.11 in]. During fire exposure, the behavior of beam B-124 is studied by super-positioning the thermal and load effects.

a) beam loading

(Dimensions in m [$1\ m\ =\ 3.28\ ft$])

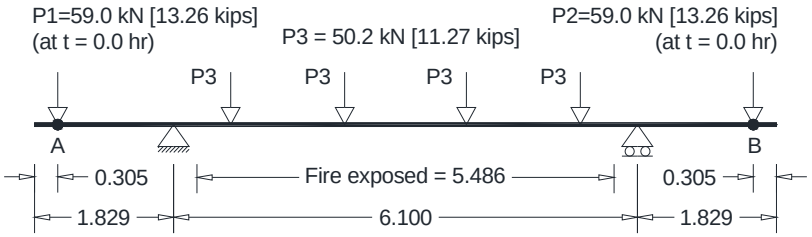

b) reinforcement configuration

(Dimensions in m [$1\ m\ =\ 3.28\ ft$])

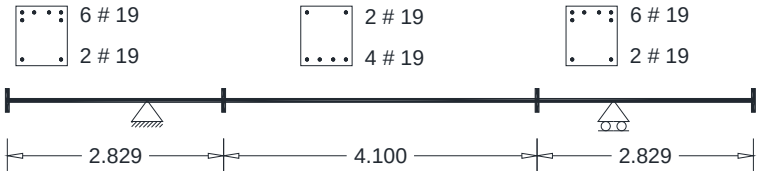

c) Primary BMD ($t\ =\ 0.0\ hr$)

(Moments in $kN.m$
[$1\ kN.m\ =\ 737.56\ Ib.ft$])

(Stiffnesses in $N.mm^2$)
[$1\ N.mm^2\ =\ 1/2870\ Ib.in^2$]

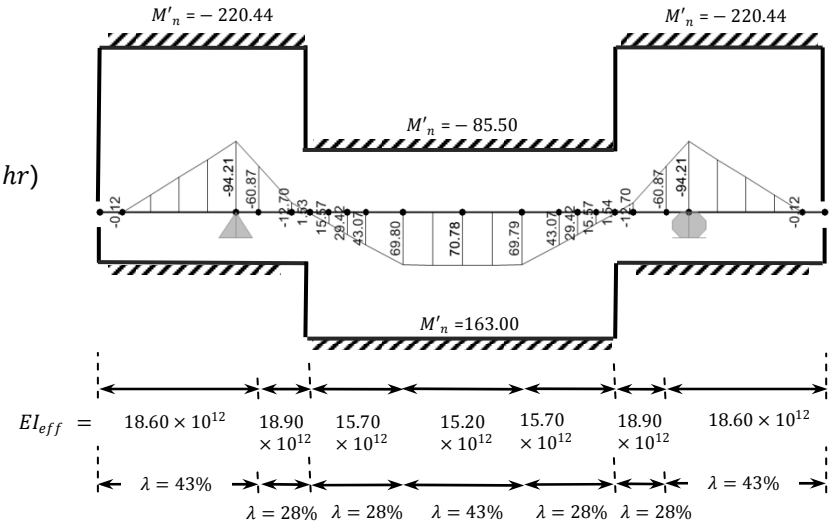

d) beam deflection ($t\ =\ 0.0\ hr$)

(Dimensions in m [$1\ m\ =\ 3.28\ ft$])

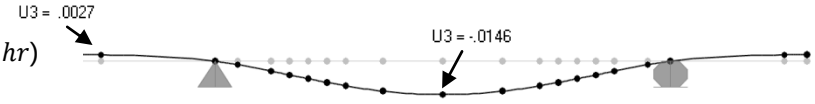

e) fire loading ($t\ =\ 1.0\ hr$)

(Dimensions in m
[$1\ m\ =\ 3.28\ ft$])

(Stiffnesses in $N.mm^2$)
[$1\ N.mm^2\ =\ 1/2870\ Ib.in^2$]

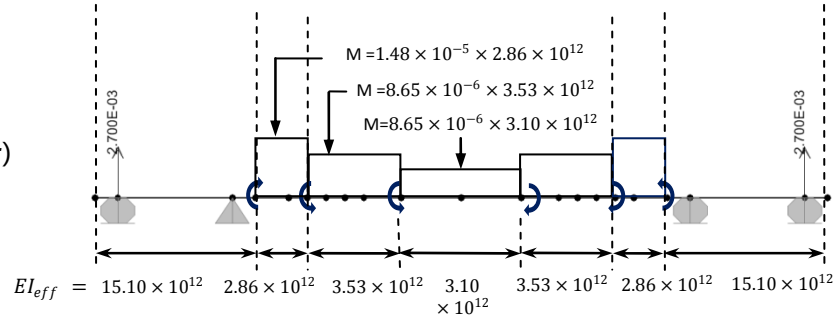

f) beam deflection and reactions ($t\ =\ 1.0\ hr$)

(Dimensions in m [$1\ m\ =\ 3.28\ ft$])

(Reactions in kN [$1\ kN\ =\ 224.81\ Ib$])

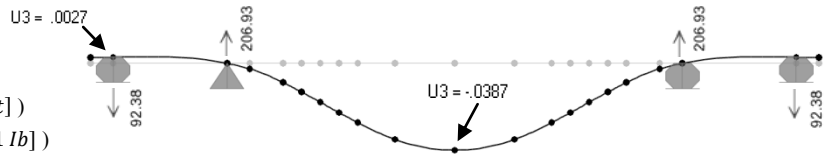

Fig. 3-5-Validation beam B-124

3.5.3.1 Unrestrained thermal curvature

A heat transfer analysis is conducted for B-124 using the FDM and the thermal properties given by Lie et al.[1]. The obtained temperature distributions, at different fire durations, are used to evaluate the equivalent linear thermal strain distributions for both the maximum negative and maximum positive moment sections. Fig. 3-6 shows the variation of the unrestrained thermal curvature (ψ_i) at different fire durations up to 3.5 hrs.

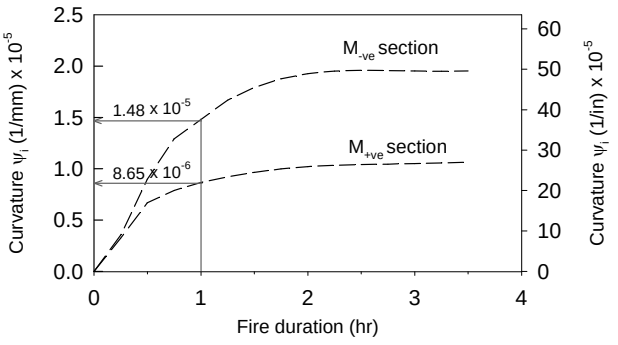

Fig. 3-6-Unrestrained thermal curvature ψ_i for B-124

3.5.3.2 Flexural stiffness during fire exposure

The beam is divided based on the applied load level and fire exposure conditions to seven segments as shown in Fig. 3-5e. Sectional analysis is conducted for each segment at different fire durations. Using the obtained moment-curvature diagrams, the secant modulus of elasticity, (EI_{eff}), is estimated. Fig. 3-7a shows the degradation of EI_{eff} for the heated positive moment section at load level (λ) equals to 43% and 28% up to 3.5 hr of ASTM-E119 fire exposure. The reduction in EI_{eff} for the fire exposed negative moment section is shown in Fig. 3-7b. The temperature of steel bars is considered uniform along the beam length because of the high thermal conductivity of steel material2.9.

3.5.3.3 Applying the proposed approach on B-124

The performance of B-124 after 1 hr of ASTM-E119 standard fire exposure is predicted by applying the following steps:

1- To simulate the support conditions during the fire test, the vertical displacement calculated at ambient condition, i.e. U3 = 0.0027 m [0.106 in], is applied as an induced displacement at the cantilever ends.

2- From Fig. 3-7, the reduced (effective) flexural stiffnesses, (EI_{eff}), are 3.10 × 10^{12} $N.mm^2$ and 3.53 × 10^{12} $N.mm^2$ for the positive moment segments and 2.86 × 10^{12} $N.mm^2$ and 15.10 ×

10^{12} $N.mm^2$ for the negative moment segments. [1 $N.mm^2$ = 1/2870 $Ib.in^2$]

a) M_{+ve} section

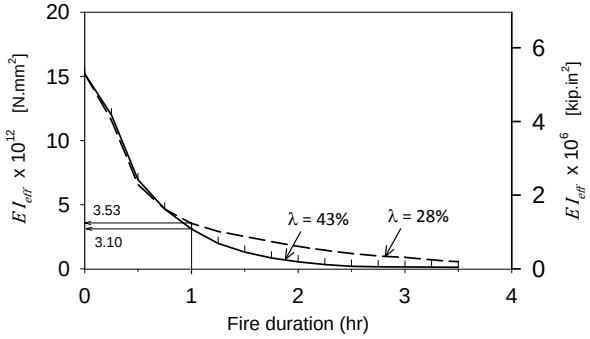

b) M_{-ve} section

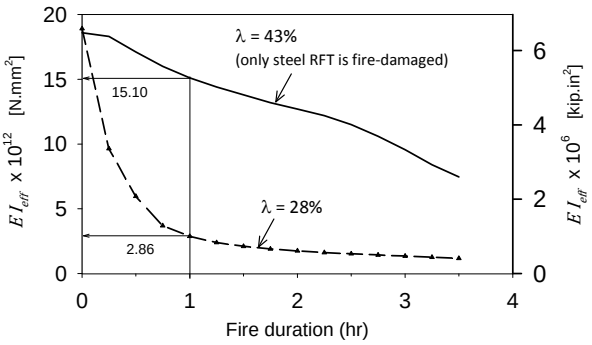

Fig. 3-7-Effective stiffness of B-124 during fire test

3- An arrangement of concentrated moments is applied on the beam to represent the unrestrained thermal curvatures. Fig. 3-5e. The corresponding curvature values, Fig. 3-6, are $8.65 \times 10^{-6}\ \frac{1}{mm}$ and $1.48 \times 10^{-5}\ \frac{1}{mm}$ for the positive and negative moment sections, respectively. ($\frac{1}{mm} = 25.4\ \frac{1}{in}$).

The mid-span deflection and the vertical reactions at the outer supports are recorded, Fig. 3-5f. These reactions are used to calculate the secondary moment that is induced during fire exposure, Fig. 3-8a. The total BMD is the summation of the primary moment, i.e. at ambient temperature, and the secondary moment as shown in Fig. 3-8b.

4- The final moment distribution changes the applied load levels (λ) along the beam length, Fig. 3-8b. The new λ values are used to recalculate EI_{eff} in the second iteration.

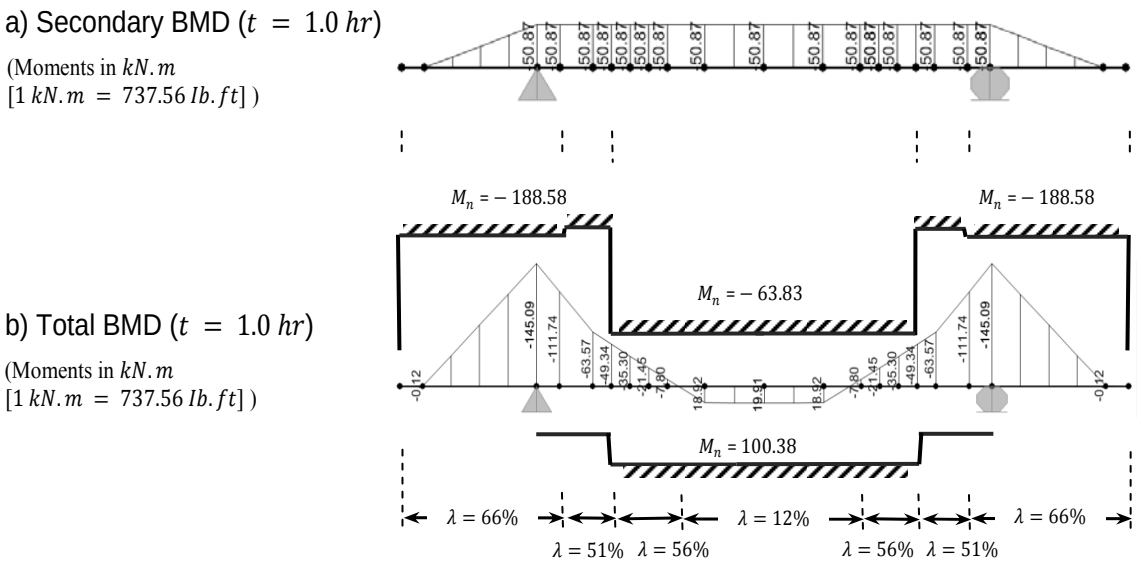

Fig. 3-8-Moment redistribution of B-124 after $1.0\ hr$ ASTM-E119 fire exposure

This procedure is repeated till convergence for EI_{eff} is achieved. Fig. 3-8b indicates that the reduced negative flexural capacity for the main span, i.e. $M_n = -63.83\ kN.m$ $[-47.08\ kips.ft]$, governs the overall capacity of the beam. Since the location of the zero moment is shifted from its original position at ambient temperature, the behavior of a section within the main span subjected to negative moment is studied in the subsequent analysis cycle. The convergence of B-124 is achieved after three analysis iterations.

The previous steps are repeated each $15\ min$ up to $3.5\ hrs$. Fig. 3-9 shows the variation of mid-span deflection during the fire test. B-124 should theoretically fail after 160 min of ASTM-E119 fire exposure if the moment redistribution is neglected. By accounting for the secondary moments generated during fire exposure, the prediction of the mid-span deflection is significantly improved and matches the measured deflection data experimentally with a maximum error of 22% at 105 min. The difference between the analytical and test results can be due to the inaccurate predictions of λ during the analysis and the complexity of test conditions. The effect of beam continuity and moment redistribution on the cantilever loads $P1$ and $P2$ is shown in Fig. 3-10. The proposed approach has acceptable predicted the variation of $P1$ and $P2$ during fire exposure with an acceptable error in the order of 15%.

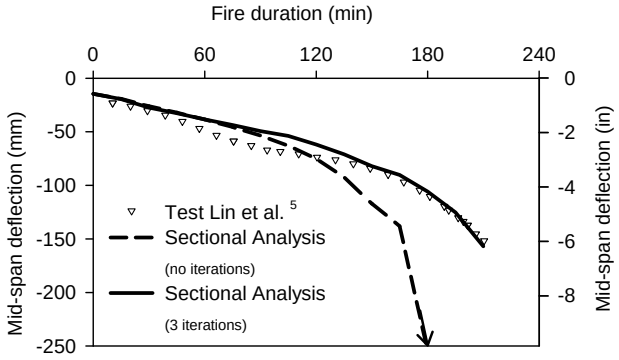

Fig. 3-9-Mid-span deflection of B-124

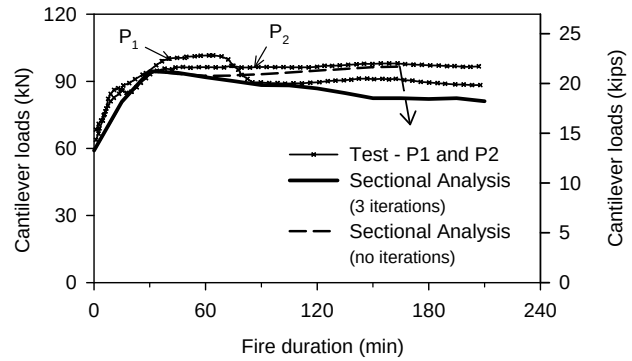

Fig. 3-10-Outer span loads of B-124

3.6 Evaluation of Thermal and Effective Stiffness Parameters

In this section, the effects of different geometric and material factors on the unrestrained thermal curvature (ψ_i) and on the effective flexural stiffness (EI_{eff}) are discussed using a comprehensive parametric study. The study aims at providing structural engineers with simple expressions to evaluate these parameters without the need for heat transfer and sectional analysis calculations.

Table 3-1 summarizes the properties of the analyzed beams. All the beams have rectangular cross-section and are subjected to ASTM-E119 standard fire exposure from three sides as shown in Fig. 3-11. The considered parameters are width (b), height (h), concrete compressive strength (f'_c), flexural moment at ambient temperature ($\lambda = 15\% - 60\%$), number of tensile steel layers ($n = 1, 2$), aggregate type (Agg) (siliceous, carbonate), compression reinforcement ratio ($\rho' = 0.06\% - 0.65\%$), and tensile reinforcement ratio ($\rho = 0.5\% - 2.5\%$). Each of the shown sections is analyzed twice, considering its performance in positive and negative bending. The standard reinforcement layout, shown Fig. 3-11, is assumed in this study. The parametric study is limited to siliceous and carbonate concretes with compressive strength (f'_c) ranging between 20 and 50 MPa [1 MPa = 145.04 psi]. The fire duration (t) ranges from 0.0 to 2.5 hr.

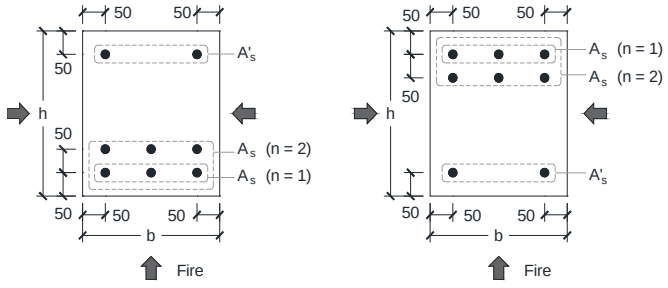

a) sagging moments (M_{+ve})

b) hogging moments (M_{-ve})

Fig. 3-11-Typical cross-sections for the parametric study beams
(Dimensions in mm [1 mm = 1/25.4 in])

Table 3-1–Parametric study cases

Beam #	b (mm) [in]	h (mm) [in]	f'_c (MPa) [psi]	n	ρ' % (A_g)	ρ % (A_g)
B1	300 [11.8]	500 [19.7]	30 [4351]	1	0.13	0.5
B2						1.0
B3				2		1.5
B4						2.5
B5	300 [11.8]	700 [27.6]		1	0.10	0.5
B6						1.0
B7				2		1.5
B8						2.5
B9	400 [15.7]	700 [27.6]		2	0.07	1.0
B10						2.5
B11	500 [19.7]	700 [27.6]		2	0.06	1.0
B12						2.5
B13	300 [11.8]	300 [11.8]		1	0.22	1.5
D1	300 [11.8]	500 [19.7]	20 [2901]	1	0.13	0.5
D2						1.0
D3				2		1.5
D4						2.5
D5	300 [11.8]	700 [27.6]	40 [5802]	1	0.10	0.5
D6						1.0
D7				2		1.5
D8						2.5
D9	400 [15.7]	700 [27.6]	50 [7252]	2	0.07	1.0
D10						2.5
D11	500 [19.7]	700 [27.6]	50 [7252]	2	0.06	1.0
D12						2.5
I1 *	300 [11.8]	500 [19.7]	30 [4351]	1	0.13	1.0
I2 *				2	0.13	2.5
I4	300 [11.8]	700 [27.6]	40 [5802]	2	0.25	1.0
I5					0.45	
I6					0.65	
I7 *	300 [11.8]	700 [27.6]	30 [5802]	2	0.10	1.5
I8 *	300 [11.8]	700 [27.6]	40 [5802]	2	0.10	0.5
I9 *					0.10	1.5
I10	400 [15.7]	700 [27.6]	50 [7252]	2	0.15	2.5
F1	300 [11.8]	500 [19.7]	30 [4351]	2	0.13	1.5
F2	300 [11.8]	500 [19.7]	30 [4351]	2	0.13	1.5
F3	300 [11.8]	700 [27.6]	30 [4351]	2	0.10	2.5

* carbonate aggregate

3.6.1 Unrestrained thermal curvature

A heat transfer analysis is conducted for each of the assumed sections and the nonlinear thermal distribution is converted to a uniform thermal distribution. The unrestrained thermal curvature ψ_i is estimated at each time step up to $2.5\,hr$. Fig. 3-12 shows the variation of ψ_i for the studied sections considering both positive and negative bending. As fire temperature/duration increases, larger thermal strains develop and the initial curvature ψ_i is increased. Assuming the same ρ and ρ', ψ_i for sections subjected to negative moments is found to be higher than ψ_i for sections subjected to positive moments. This can be explained by the fact that both sections have almost the same thermal expansion at their bottom layers. However, the top thermal strain will be lower for sections subjected to negative moments as the increased area of top steel bars that have relatively low temperatures limit the expansion of the top layers. The effect of tensile reinforcement ratios (ρ) and compressive concrete strengths (f'_c) on ψ_i is found to be negligible.

The effect of the cross-section dimensions, b and h, is shown in Figs. 3-12a and 3-12b. Increasing the section height (h), or decreasing the section width (b), decreases ψ_i. Deep sections spread the thermal expansion over longer length. This results in decreasing ψ_i. ψ_i is significantly increased for wide sections. This is due to the low thermal conductivity of concrete, which results in a substantial thermal expansion difference between the lower and top concrete masses.

Distributing the tensile steel bars on two layers ($n = 2$) instead of one layer ($n = 1$) has a minor effect on ψ_i for sections subjected to negative moment. For sections subjected to positive moments, the effect of n is clear because of the lower temperature in the second row. Increasing the compression reinforcement ratio ρ'reduces ψ_i for sections subjected to positive moments. The effect of compression reinforcement in the case of negative moment is minimal as it is exposed to high temperatures, which reduce its effectiveness in controlling ψ_i.

Concrete with carbonate aggregate is found to have less thermal expansion than concrete with siliceous aggregate[1, 3]. The effect of the aggregate type on the curvature is minor for the case of positive moment as the thermal expansion of the lower concrete is highly dependent on the expansion of the bottom steel reinforcement. The thermal expansion of the lower concrete mass is more predominant in case of negative moments as its expansion is not controlled by substantial amount of steel bars.

a) effect of section height h

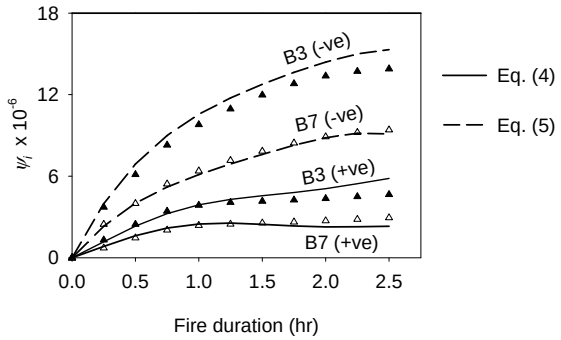

b) effect of section width b

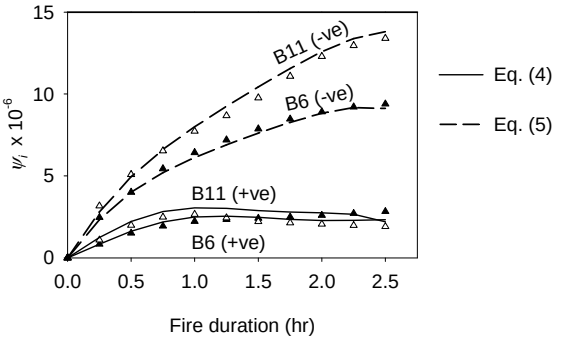

Fig. 3-12- Effect of section dimensions (b, h) on ψ_i
(Curvature in $1/mm$ [$1/mm = 25.4 \times 1/in$])

3.6.2 Proposed expressions for the unrestrained thermal curvature ψ_i

The values obtained from the parametric study for ψ_i are analyzed using a multiple regression analysis technique[14]. This has resulted in equations (4) and (5) that can be used to predict the unrestrained thermal curvature ψ_i for rectangular RC sections subjected to ASTM-E119 fire exposure up to $2.5\,hr$. Eq. (4) is for sections subjected to positive (sagging) moments and Eq. (5) is for sections subjected to negative moments. The predictions of the proposed equations are shown in Fig. 3-12.

$$\psi_i = 10^{-7} \times \left[-0.1994 - 1.023 \times 10^{-2}\, b\,.\, t^5 \right.$$

$$+(4.072 \times 10^{-2}\, b + 8.683)\ t^4$$

$$-(38.884 + 2.025 \times 10^{-2}\, b)\, t^3$$

$$+(46.997 - 8.670 \times 10^{-2}\, b)\, t^2$$

$$+(68.490 - 0.07108\, h + 0.103\, b - 5.968\, \rho')\, t$$

$$\left. +(11.131\, n\,.\ Agg - 23.381\, Agg - 8.897\, n)\, t \right] \qquad (4)$$

$$\psi_i = 10^{-7} \times \left[-0.9604 - 6.698\, t^4 \right.$$

$$+(62.166 - 3.430 \times 10^{-2}\, h)\, t^3$$

$$+(-214.634 + 0.185\, h)\, t^2 + (348.066$$

$$\left. -0.372\, h + 0.09388\, b - 13.252\, Agg\,)\, t \right] \qquad (5)$$

Where,

ψ_i is the unrestrained thermal curvature at fire duration $t \geq 0.25\, hrs$

t is the ASTM-E119 fire duration in hrs

b is the cross-section width in mm [$1\ mm = \ 1/25.4\ in$]

h is the cross-section height in mm [$1\ mm = \ 1/25.4\ in$]

ρ' percentage of compression reinforcement relative to $(b \times d)$

d is the effective depth of tensile reinforcement in mm [$1\ mm = \ 1/25.4\ in$]

n is the number of tensile reinforcement layers

Agg is a factor to account for the aggregate type (0.0 for siliceous concrete and 1.0 for carbonate concrete)

Fig. 3-13 shows the relationship between the analytical predictions, using the sectional analysis, and the values obtained by applying the proposed expressions.

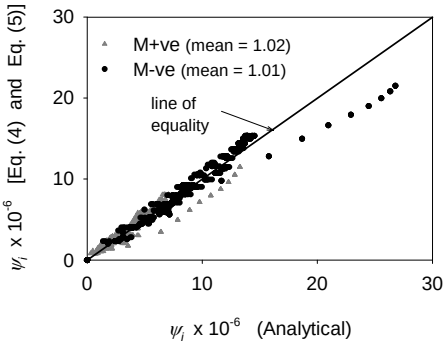

Fig. 3-13- Regression analysis of ψ_i results
(Curvature in $1/mm$ [$1/mm\ = \ 25.4\ \times \ 1/in$])

3.6.3 Effective flexural stiffness

Using the obtained moment-curvature relationships, the secant slope (EI_{eff}) is evaluated at four load levels, $\lambda = 15\%, 30\%, 45\%, and\ 60\%$, for different fire durations. As a sample of the results, Fig. 3-14 shows the effect of tensile reinforcement ratio, ρ, and duration of fire exposure on EI_{eff} for a number of the studied rectangular RC beams. Similar to ambient temperature, EI_{eff} of RC beams depends on the tensile reinforcement ratio (ρ)[12]. While for positive bending, fire severely affects the yielding strength of the tensile reinforcing bars, it degrades the compressive concrete strength in case of negative bending. Both the loading level (λ) and the aggregate type (Agg) have a minor effect on the stiffness degradation.

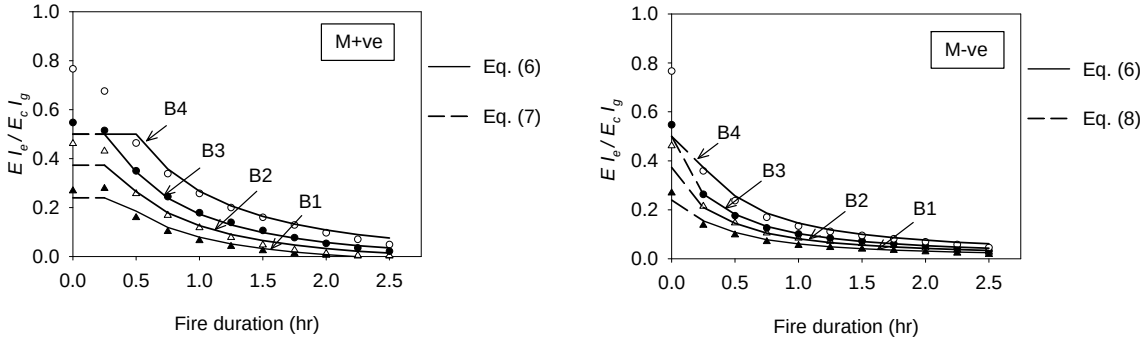

Fig. 3-14- Effect of tensile reinforcement ratio (ρ) on EI_{eff}

3.6.4 Proposed expressions for the effective flexural stiffness EI_{eff}

The effective flexural stiffness at ambient temperature can be estimated using Eq. (6) that was developed based on an analytical study[12] and was included in ACI 318-08[15].

$$\frac{EI_{eff}}{E_c I_g} = (0.10 + 0.25\,\rho)\left(1.2 - 0.2\,\frac{b}{d}\right) \leq 0.5 \qquad (6)$$

Where,

EI_{eff} is the effective flexural stiffness at ambient temperature (i.e. $t = 0.0\ hrs$)

E_c is the ambient secant modulus for concrete and can be evaluated in MPa as $4500\sqrt{f'_c}$ [$1\ MPa = 145.04\ psi$] 10

f'_c concrete compressive strength in MPa [$1\ MPa = 145.04\ psi$]

I_g gross sectional second moment of inertia

b is the cross-section width in mm [$1\ mm = 1/25.4\ in$]

d is the effective depth of tensile reinforcement in mm [$1\ mm = 1/25.4\ in$]

ρ percentage of tensile reinforcement relative to $(b \times d)$

During ASTM-E119 fire exposure, Eqs. (7) and (8) are proposed to predict the degradation of the effective flexural stiffness EI_{eff} for sections subjected to positive and negative moments, respectively. These equations are developed based on a multiple regression analysis of the parametric study results, Fig. 3-15. The proposed equations are shown in Fig. 3-14. An upper limit for these equations is considered to be given by Eq. (7).

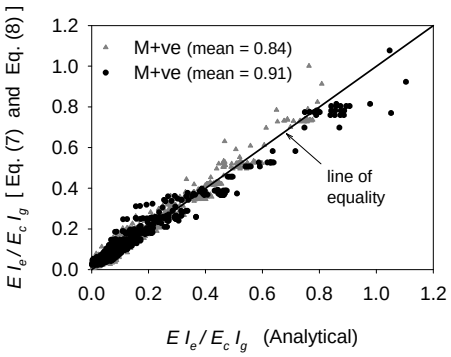

Fig. 3-15- Regression analysis of EI_{eff}

For sections subjected to positive moments

$$\frac{EI_{eff}}{E_c I_g} = 2.032 \times 10^{-2}$$

$$-(0.180 + 1.408\,\rho)\,{}^{1}\!/_{t^2} \times 10^{-2}$$

$$+(\,5.897 + \,10.806\,\rho) \times \frac{1}{t} \times 10^{-2}$$

$$+(2.590\,\lambda + 0.651\,Agg)t^2 \times 10^{-2}$$

$$-(12.676\,\lambda + 0.375\,Agg)\,t \times 10^{-2} \;\; \leq \text{Eq. (6)} \qquad (7)$$

For sections subjected to negative moments

$$\frac{EI_{eff}}{EI_g} = -0.210 \times 10^{-2} - (1.329 + 0.506\,\rho$$

$$-1.762\,\lambda - 0.14\,\rho')\frac{1}{t^2} \times 10^{-2} + (\,5.414 + 4.2\,\rho'$$

$$-2.948\,\lambda + 4.747\,\rho)\,\frac{1}{t} \times 10^{-2} \qquad \leq \text{Eq. (6)} \qquad (8)$$

Where,

t is the ASTM-E119 fire duration in hrs ($t \geq 0.25\ hr$)

Agg is a factor to account for the aggregate type (0.0 for siliceous concrete and 1.0 for carbonate concrete)

λ is the flexural level at ambient temperature

3.6.5 Practical application of the proposed method

The proposed method described in this chapter can be used by designers to check the fire ratings of simple and continuous RC beams subjected to standard ASTM-E119 fire exposure. The steps of the proposed method can be summarized as follows:

- analyze the beam at ambient temperature and calculate the primary BMD. The beam is then divided into a number of segments based on the calculated BMD and fire exposure conditions.

- evaluate the degraded flexural stiffness (EI_{eff}) at specific fire duration using Eqs. (7) and (8). A constant value of EI_{eff} is assigned to each segment of the beam based on its maximum flexural moment.

- estimate the unrestrained thermal curvature ψ_i for each beam segment using Eqs. (4) and (5).

A set of concentrated moments are applied to the fire exposed region of the beam to induce the unrestrained thermal curvature distribution during fire exposure.

- analyze the beam and estimate the secondary moment distribution as well as the deflected shape. The secondary moments are added to the primary moments to predict the total moment distribution. Revised values for EI_{eff} are assigned to each beam segment based on the predicted total moment distribution. An iterative procedure should be done

till convergence is achieved.

The previous steps are repeated at different fire durations to predict the fire performance of the considered beam.

3.7 Summary and Conclusions

A sectional analysis methodology was proposed by the authors in previous publications[2,7]. The application of this methodology for statically determinate beams is presented in this chapter and extended to predict the fire performance of statically indeterminate RC beams. A practical approach based on superimposing the effects of thermal expansion and material degradation is introduced. The nonlinear thermal expansion is converted to an equivalent uniform thermal distribution, which can be represented by the unrestrained thermal axial strain ε_i and curvature ψ_i. The degradation effect in material strength is considered by accounting for the reduction in the effective flexural strength (EI_{eff}). The RC continuous beam tested by Lin et al.[5] is used to validate the proposed terminology. The mid-span deflections as well as the outer supports` reactions are predicted up to 3.5 hrs of standard ASTM-E119 fire exposure. A good agreement is found between the experimental data and the results of the proposed methodology.

A comprehensive parametric study is conducted in the second part of the chapter to investigate the effect of different material, geometric, and loading factors on the unrestrained thermal curvature (ψ_i) and the effective flexural strength (EI_{eff}). For simplicity, the parametric study is limited to rectangular RC beams subjected to 2.5 hr ASTM-E119 standard fire exposure and typical reinforcement configurations. Based on the results of the parametric study, a number of expressions are proposed to predict ψ_i and EI_{eff} for sections subjected to both sagging (positive) and hogging (negative) moments. Designers can apply the proposed methodology using these expressions to conduct a quick assessment for the structural fire safety of RC continuous beams.

3.8 Acknowledgments

This research was funded by the Natural Sciences and Engineering Research Council of Canada.

3.9 References

1. Lie, T.T., ed., "Structural Fire Protection," ASCE Manuals and Reports on Engineering Practice, no. 78, New York, NY, 1992, 241 pp.

2. El-Fitiany, S., Youssef, M.A., "Assessing the flexural and axial behaviour of reinforced concrete members at elevated temperatures using sectional analysis", Fire Safety Journal, vol. 44, no. 5, 2009, pp. 691-703.

3. Youssef, M.A. and Moftah, M., "General stress-strain relationship for concrete at elevated temperatures," Engineering Structures, vol. 29, no. 10, 2007, pp. 2618-2634.

4. Kodur, V.K.R., and Dwaikat, M., "Performance-based fire safety design of reinforced concrete beams," Journal of Fire Protection Engineering, vol. 17, no. 4, 2007, pp. 293-320.

5. Lin, T.D., Gustaferro, A.H., and Abrams, M.S., "Fire Endurance of Continuous Reinforced Concrete Beam", Portland Cement Association, Bulletin RD072.01B, Skokie, 1981.

6. El-Fitiany S.F. and Youssef M.A., “A Simplified Sectional Analysis Approach for RC Elements during Fire Events”, 6th International Conference on Structures in Fire, Michigan State University in East Lansing, MI, 2010, pp. 239-246.

7. El-Fitiany, S.F., and Youssef, M.A., “Stress Block Parameters for Reinforced Concrete Beams During Fire Events,” Innovations in Fire Design of Concrete Structures, ACI SP-279, 2011, pp. 1-39.

8. Cement Association of Canada, “Concrete design handbook, CAN/CSA A23.3-04," 3rd Ed., Ottawa, 2006.

9. Terro, M.J., "Numerical modeling of the behavior of concrete structures in fire", ACI Structural Journal, vol. 95, no. 2, 1998, pp. 183-193.

10. Youssef, M.A., EL Fitiany, S.F., and Elfeki, M.A., "Flexural Behavior of Protected Concrete Slabs after Fire Exposure", Designing Concrete Structures for Fire Safety, ACI SP-255, 2008, pp. 47-74.

11. ABAQUS theory and user manuals version 6.9. USA: ABAQUS Inc..

12. Khuntia, M., and Ghosh, S. K., “Flexural Stiffness of Reinforced Concrete Columns and Beams: Analytical Approach,” ACI Structural Journal, vol. 101, no. 3, May-June, 2004, pp. 351-363.

13. Wilson EL. SAP2000 analysis reference manual. Berkeley, California: Computers and Structures Inc.; 2002.

14. Ronald J. Wonnacott. & Wonnacott, Thomas H., (fourth edition), “Introductory statistics”, New York: John Wiley & Sons, 1985.

15. ACI Committee 318,“Building Code Requirements for Structural Concrete (ACI 318-08) and Commentary,” American Concrete Institute, Farmington Hills, MI, 2005, 465 pp.

Chapter 4

4 Practical Method to Predict the Axial Capacity of RC Columns Exposed to Fire

During fire events, elevated temperatures dramatically reduce the mechanical properties of concrete and steel. They also induce thermal and transient creep strains[1] 1. To ensure that a fire exposed structure retains its integrity during the fire fighting process; capacities of RC columns need to be monitored at different durations of fire exposure.

Current North America's building codes achieve the required fire ratings using prescriptive methods. These methods specify minimum cross-section dimensions and minimum clear cover to the reinforcing bars[2]. Capacity of RC columns during fire events can be evaluated using nonlinear coupled thermal-stress Finite Element (FE) analysis. Raut and Kodur [3] concluded that the FE method is a powerful tool to predict the behavior of RC columns during fire exposure. Drawbacks of using the FE method, including: the need for a comprehensive computer program, the difficulty to comprehend its results and to identify potential modeling errors, and the long running time, make it impractical for design engineers. A simplified sectional analysis method to estimate the axial behavior of RC columns during fire exposure was proposed and validated by El-Fitiany and Youssef[4, 6, 6]. The method involves dividing the cross-section into horizontal layers and converting the two-dimensional (2D) temperature distribution within the section to a rational average one-dimensional (1D) distribution. The average temperature is used to predict the section tangent stiffness and the axial load-axial deformation relationship. Although sectional analysis is relatively easy to apply as compared to FE, it requires evaluating the temperature distribution within the concrete section based on knowledge of heat transfer principles. It also requires solving the equilibrium and kinematic equations utilizing different constitutive relationships for the section layers [7, 8].

Dotreppe et al. [9] proposed a simple equation to predict the fire resistance of RC columns. This equation was based on a number of FE numerical simulations, and thus is limited to the studied cases: standard fire exposure (ISO 834, ASTM-E119, and ULC-S101),

columns with cross-sectional areas less than $0.2\ m^2$ and aspect ratios (h/b) greater than 0.5 (where h and b are the section's height and width, respectively).

In this chapter, a simplified method to predict the axial capacity of RC columns exposed to fire is developed. The method involves simple substitution to evaluate the average concrete temperature, the average concrete stress, the stress in the steel bars, and the column's reduced axial capacity. The chapter discusses the axial behavior of RC columns, evaluates errors associated with some simplifying assumptions, and provides the derivation and validation of the proposed method.

4.1 Axial Behavior of RC Columns Exposed to Fire

4.1.1 Section Analysis Method

Fig. 4-1a shows a $305\ mm$ square column, column $C1$ in Table 4-1, exposed to fire from its four sides and tested by Lie et. al[10]. The sectional analysis method developed and validated by El-Fitiany and Youssef [4] is used to calculate the axial capacity of this column using the following steps:

1. At specific fire duration, the section is divided into a number of elements, Fig. 4-1a, and the temperature distribution is predicted using the Finite Difference Method (FDM) [1]. The effect of steel bars is neglected in the heat transfer analysis. Fig. 4-1b shows the predicted elevated temperatures after 1 hr of ASTM-E119 fire exposure.

2. The cross-section is divided into horizontal layers and two average temperatures, T_σ and T_{avg}, are calculated for each layer, Fig. 4-2. T_σ results in the same average concrete compressive strength for the considered layer, and thus is suitable for strength calculations. T_{avg} represents the algebraic average temperature of the elements within each layer and is suitable for thermal and transient creep strains calculations[11].

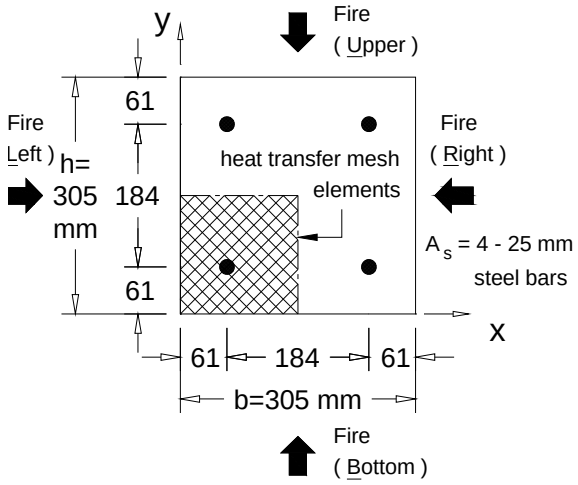

a) column section and mesh

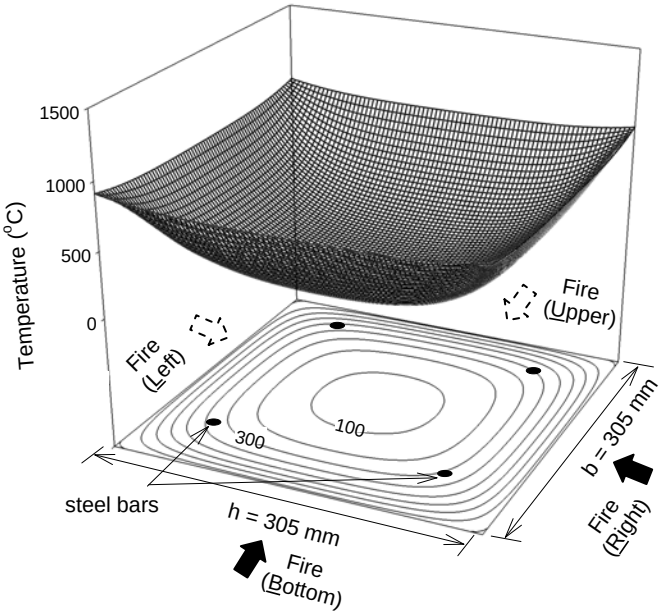

b) 1 hr ASTM-E119 temperature contour

Fig. 4-1. Heat transfer analysis using FDM

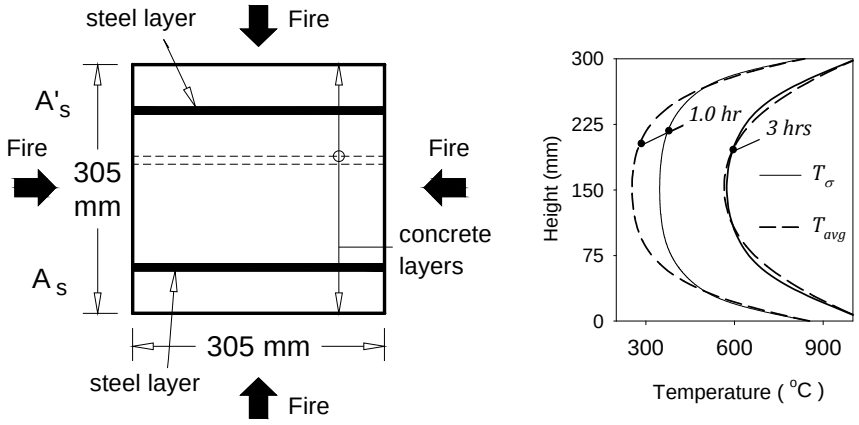

Fig. 4-2. Average temperature distribution

3. The total concrete strain at elevated temperatures (ε) is composed of three terms: unrestrained thermal strain (ε_{th}), instantaneous stress related strain (ε_c), and transient creep strain (ε_{tr}). The total strain is given by Eq. (1).

$$\varepsilon = \varepsilon_{th} + \varepsilon_c + \varepsilon_{tr} \quad (1)$$

The nonlinear thermal strain (ε_{th}) distribution, Fig. 4-3f, is calculated using T_{avg}. The thermal strain of steel bars is calculated based on the concrete temperature at their locations. ε_{th} is then converted to an equivalent linear thermal strain (ε_i), Fig. 4-3c, by considering self-equilibrium of internal thermal forces in concrete and steel layers. Fig. 4-3e shows the differences between the equivalent linear and nonlinear thermal strains, which represent the self-induced thermal strains (ε_{st}). These strains are assigned as initial strains for the concrete and steel layers to model the corresponding self-induced self-equilibrating thermal stresses. The terms ε_{st}, ε_c, and ε_{tr} are lumped into an equivalent mechanical strain ε_{cT}, Eq. (2), which can be used in the constitutive stress-strain relationship for concrete developed by Youssef and Moftah[11].

$$\varepsilon = \varepsilon_i + (\varepsilon_{st} + \varepsilon_c + \varepsilon_{tr}) = \varepsilon_i + \varepsilon_{cT} \quad (2)$$

4. For different values of ε_{cT} , the constitutive relationship by Youssef and Moftah[11] is used to evaluate the internal stress for each layer. Considering equilibrium of the stresses for different layers, the corresponding axial force is calculated.

5. The previous steps are repeated at different fire temperatures. The axial load (P)–axial strain (ε) curves at $t = 0.0$, 1.0 , and 3.0 hrs are shown in Fig. 4-4. The peak points of these diagrams define the axial capacities of the analyzed section at different fire durations.

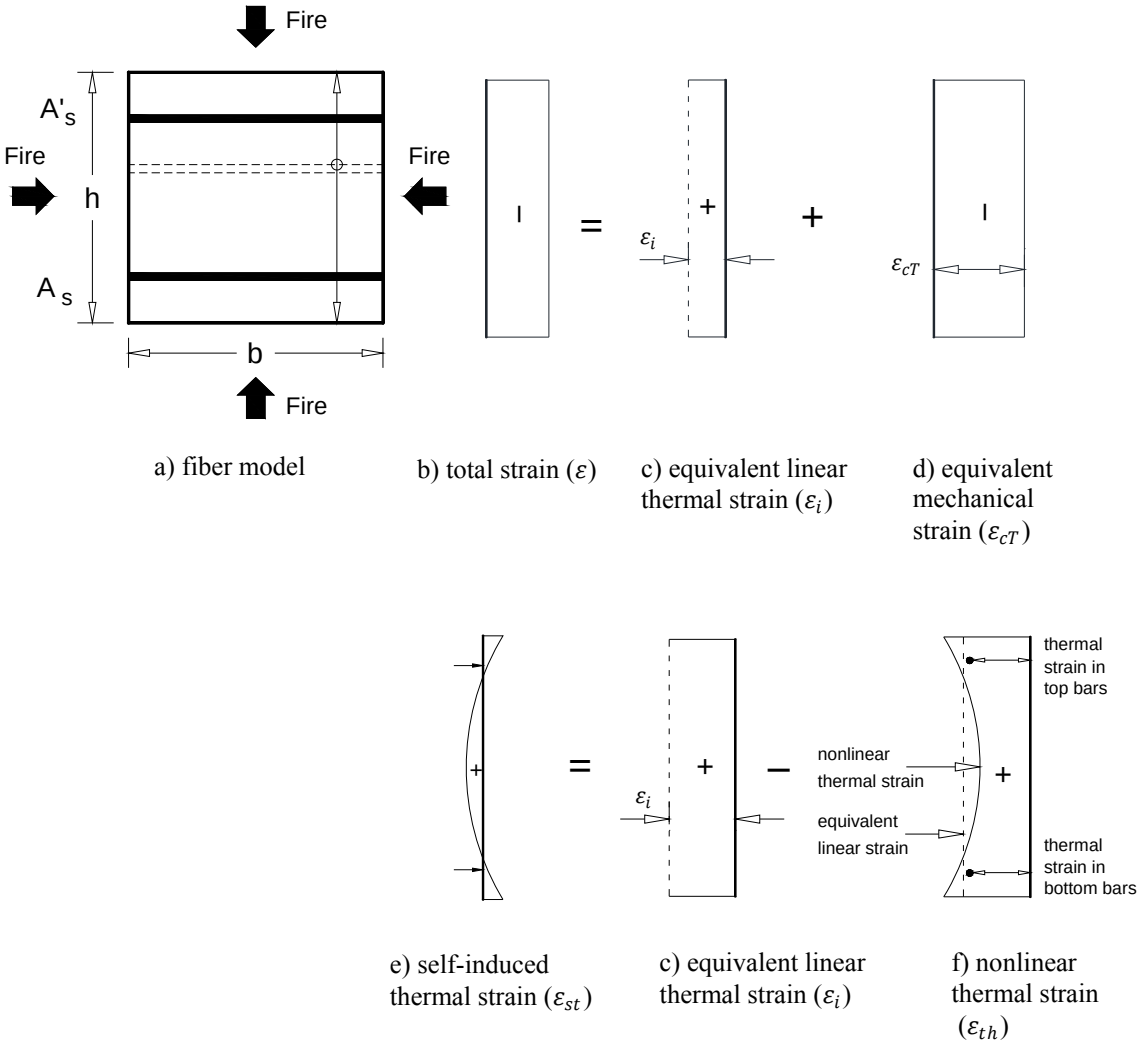

Fig. 4-3. Sectional analysis approach for axially loaded RC sections exposed to fire

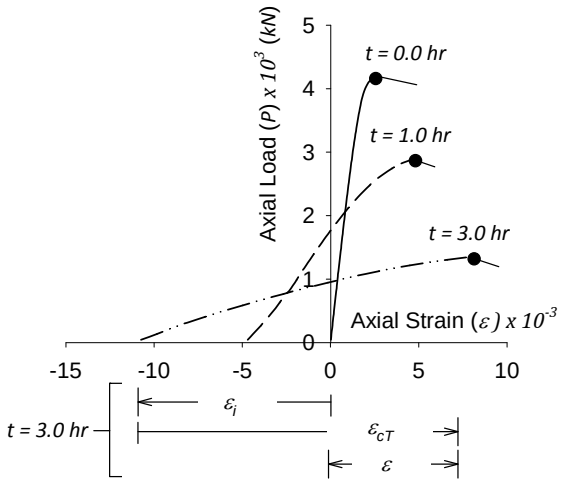

Fig. 4-4. P–ε relationships for a $305\ mm$ square column at different fire durations

4.1.2 Error Analysis

The errors corresponding to ignoring ε_{st} or using T_{avg} for strength calculations are assessed by analyzing the columns shown in Table 4-1. Comparisons between the analytical axial capacities obtained by considering all parameters, ignoring ε_{st}, and using T_{avg} are shown in Figs. 4-5a and 4-5b. While ignoring ε_{st} results in slightly underestimating the axial capacity, using T_{σ} for stress calculations has a minor effect on the axial capacity of the examined concrete columns.

Table 4-1–Parametric study cases

Col #	b (mm)	h (mm)	f'_c (MPa)	f_y (MPa)	ρ $\%\ (A_g)$
$C1$	305	305	36.1	443.7	2.1
$C2$	400	400	30	400	1.5
$C3$	600	600	40	400	1.5
$C4$	400	700	50	400	1.0
$C5$	500	700	25	400	1.0

***** all columns are analyzed up to 4 hrs of standard ASTM-E119 fire exposure

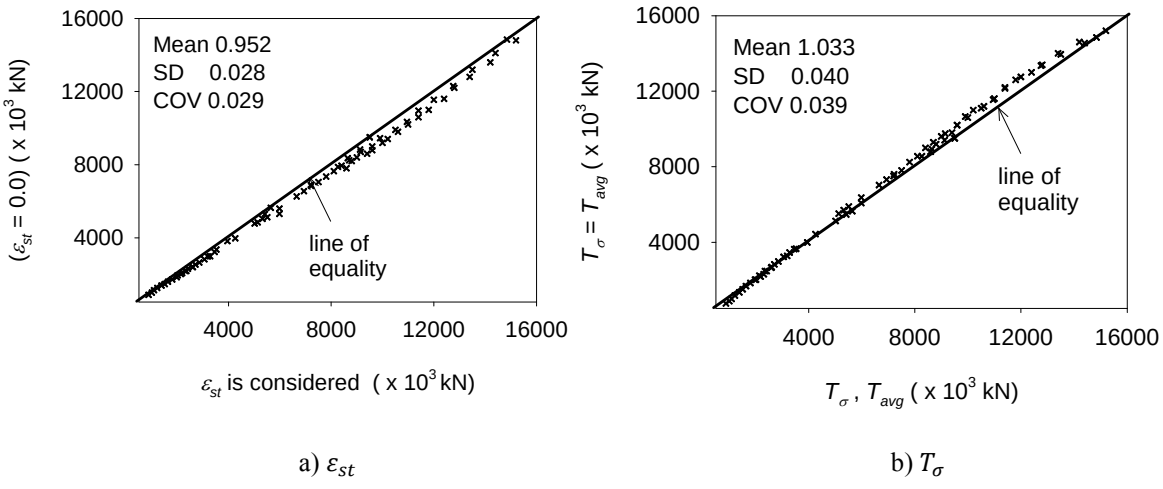

Fig. 4-5. Effect of different parameters on sectional analysis results

4.2 Proposed Method

The proposed method is based on the fact that the temperature distribution is steep close to the heated faces and almost constant at the core of the column section, Fig. 4-1b. Consequently, the concrete strength is variable near the heated faces and constant at the inner concrete core. Application of the proposed method involves the following steps:

1) Evaluating a one-dimensional average temperature distribution.

2) Estimating the concrete strains.

3) Evaluating concrete and steel stresses at failure.

4) Determining the axial capacity of the section.

Derivations of simplified equations to conduct each of the mentioned steps are given in the following sections.

4.3 Average Temperature Distribution

In this section, a simplified method to calculate the temperature distribution within a fire exposed concrete section is first presented. The section is then divided into regions of constant and variable temperatures. Equations to evaluate the average temperature profile for the cross-section are also derived.

4.3.1 Wickstrom Simplified Formulas

Wickstrom[12] proposed and validated a set of handy formulas to calculate the temperature distribution within a fire exposed concrete section. Wickstrom's formulas can be applied for any type of concrete and fire scenario. However, they are practically easy for ISO 834 standard fire and normal weight concrete. Wickstorm's formulas do not account for variability in the thermal conductivity of concrete, moisture content, and nonlinear boundary conditions which include prescribed temperature and heat flux[12].

Fig. 4-6 shows a RC concrete column subjected to fire from four sides; Left (L), Right (R), Bottom (B), and Top (T) faces. Application of Wickstrom's formulas to calculate the temperature distribution within this section can be summarized as follows:

1) The fire temperature T_f in Celsius is first calculated at a specific fire duration t (hr) using a given fire temperature-time relationship.
2) A modified time (t^*) that evaluates the corresponding time of exposure to the standard ISO 834 standard fire is then calculated. The ratio between the modified time (t^*) and the actual fire duration (t) defines a dimensionless compartment time factor (Γ). The ISO 834 standard fire can be described by Eq. (3).

$$T_{f\,(\mathrm{ISO})} = 345\ \log(480\ t^* + 1) \tag{3}$$

where $T_{f\,(\mathrm{ISO})}$ is the ISO 834 standard fire temperature in Celsius at a modified fire duration t^* in hrs.

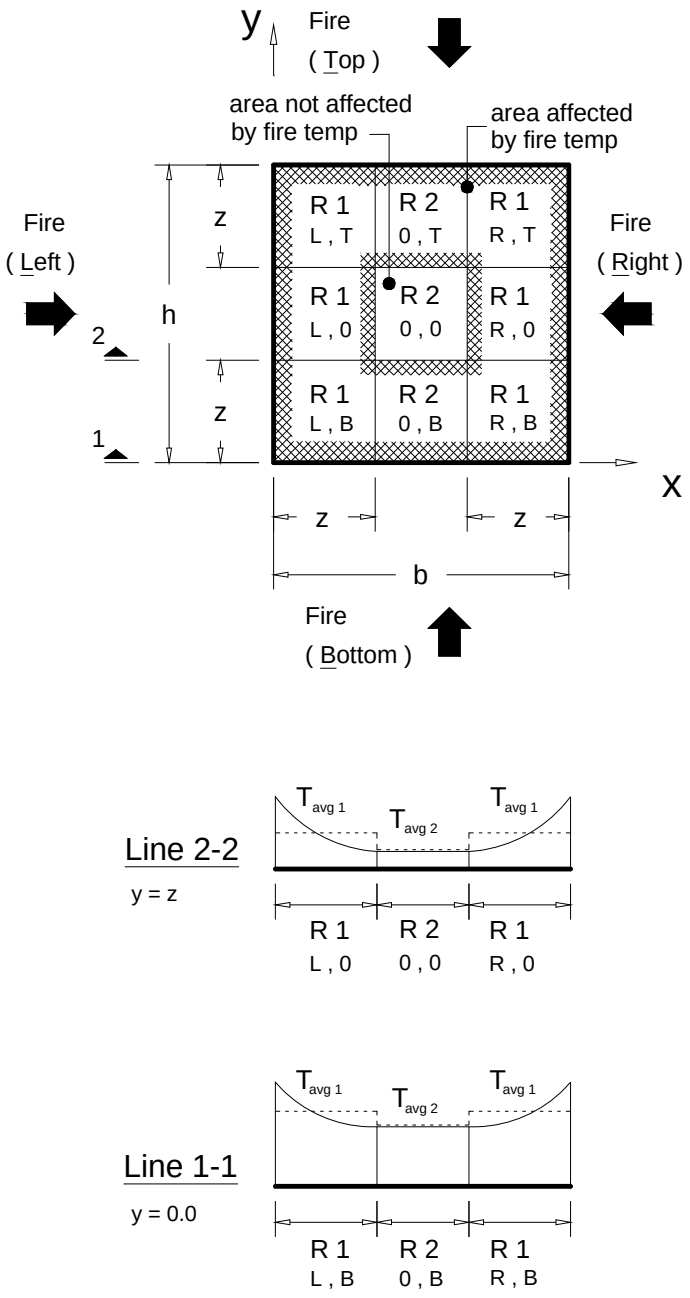

Fig. 4-6. Temperature calculation of example RC column ($z \leq b/2$)

3) The temperature rise at any point (x, y) within the section due to heating from four sides can be estimated using Eq. (4).

$$T_{xy} = \left[n_w \left(n_x + n_y - 2n_x.n_y\right) + n_x.n_y\right] T_f \quad (4a)$$

$$n_w = 1 - 0.0616 \left(\sqrt{\Gamma}.\ t\right)^{-0.88} \quad \geq 0.0 \quad (4b)$$

$$n_x = \left[0.18 \ln\left(\frac{t}{x^2}\right) - 0.81\right]_{\text{Fire (L)}} + \left[0.18\ \ln\left(\frac{t}{(b-x)^2}\right) - 0.81\right]_{\text{Fire (R)}} \quad \geq 0.0 \quad (4c)$$

$$n_y = \left[0.18 \ln\left(\frac{t}{y^2}\right) - 0.81\right]_{\text{Fire (B)}} + \left[0.18\ \ln\left(\frac{t}{(h-y)^2}\right) - 0.81\right]_{\text{Fire (T)}} \quad \geq 0.0 \quad (4d)$$

where b is the section width, h is the section height, T_{xy} is the temperature rise at any point (x, y) in Celsius, n_w is the ratio between the surface temperature and the fire temperature, and n_x and n_y are the ratios between the internal and surface temperatures due to heating in the x and y directions, respectively.

4.3.2 Temperature Regions

Figs. 4-6 and 4-7 show different temperature regions within a concrete section. The values shown in each region indicate the heating surface causing temperature variation in x and y directions. Values of zero indicate that the temperature is constant in the given direction. While region R2(0,0), Fig. 4-6, is not affected by the fire temperature, region R3(L+R, T+B), Fig. 4-7, is affected by fire temperature from the four sides. The value of z that defines the boundaries of these regions can be evaluated by equating n_x and n_y in Eqs. (4c) and (4d) to zero, which will result in Eq. (5). Value of z is less than $b/2$ and $h/2$ in Fig. 4-6 and are greater than them in Fig. 4-7.

$$z = \sqrt{e^{-4.5\ t}} \quad (5)$$

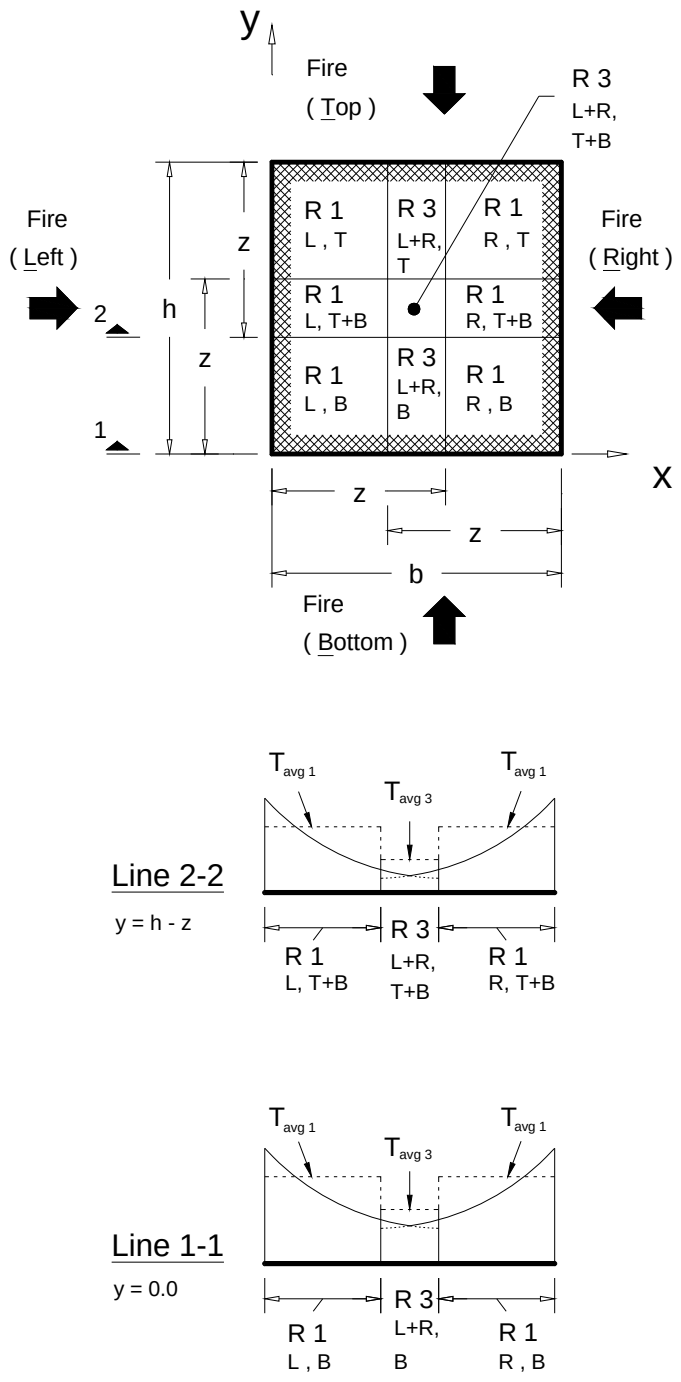

Fig. 4-7. Temperature calculation of example RC column ($z > b/2$)

The schematic temperature profiles for lines 1-1 and 2-2 in Fig. 4-6 present the variation of temperature in x direction at $y \leq z$ and $y = y_o \rightarrow (h - z)$, respectively. Both profiles show varying temperature for R1 and constant temperature for R2. The schematic temperature profiles for lines 1-1 and 2-2 in Fig. 4-7 present the variation of temperature in the x direction at $y \leq (h - z)$ and $y = (h - z) \rightarrow z$, respectively. All regions have variable temperature profile.

4.3.3 Average Temperatures

Eq. (4) predicts the temperature rise at different locations within the studied concrete section. For each of lines 1-1 and 2-2, n_y is constant and n_x value defines the temperature along the line. To conduct uniaxial stress analysis for the fire exposed section, the average temperature for each line needs to be calculated. Three equations are derived to evaluate the average temperature within each region at a given y value. $T_{avg\,1}$, Eq. (6a), represents the average temperature for regions affected by heating from either L or R. $T_{avg\,2}$, Eq. (6b), represents the average temperature for regions not affected by heating from L or R. $T_{avg\,3}$, Eq. (6c), represents the average temperature due to heating from the left and right sides simultaneously, i.e. (L + R).

$$T_{avg\,1} = \left[0.18\, n_w - 0.36\, n_w.n_y + 0.18\, n_y\right]\left[x_2\ ln\left(\frac{t}{{x_2}^2}\right) - x_1\, ln\left(\frac{t}{{x_1}^2}\right)\right]\frac{T_f}{(x_2 - x_1)}$$

$$-0.45\, T_f.n_w + 1.9\, T_f.n_w.n_y - 0.45\, T_f.n_y \qquad x = x_1 \rightarrow x_2 \qquad (6a)$$

$$T_{avg\,2} = T_f.n_w.n_y \qquad (6b)$$

$$T_{avg\,3} = \left(0.18\, n_w + 0.18\, n_y - 0.36\, n_w.n_y\right)\left[ln\left(\frac{t}{(b-x_2)^2}\right)\ x_2 - ln\left(\frac{t}{(b-x_1)^2}\right)\ x_1\right]\frac{T_f}{(x_2 - x_1)}$$

$$+ b\left(0.36\, n_w.n_y - 0.18\, n_w - 0.18\, n_y\right)\left[ln\left(\frac{t}{(b-x_2)^2}\right) - ln\left(\frac{t}{(b-x_1)^2}\right)\right]\ \frac{T_f}{(x_2 - x_1)}$$

$$-0.45\, T_f.n_w + 0.9\, T_f.n_w.n_y - 0.45\, T_f.n_y + T_{avg\,1} \qquad x = x_1 \rightarrow x_2 \qquad (6c)$$

The average temperatures $T_{avg\,1}$, $T_{avg\,2}$, and $T_{avg\,3}$ are represented in Figs. 4-6 and 4-7 by the dashed lines. The ambient temperature (20 ℃) is added to the calculated average temperatures. A weighted average temperature can then be calculated for each line to facilitate sketching the final average temperature distribution along the section height. The final temperature profile can be idealized using Eq. (7) where z_1 and z_2 are constants that can be estimated using average temperature values at $y = 0.0$ and $y = z$. This equation was chosen as it can be easily integrated.

$$T_{avg} = z_1 \,.\, e^{(z_2 \,.\, y)} \tag{7}$$

where $z_1 = T_{avg\,(y=0.0)}$; and $z_2 = \frac{\ln\left[\frac{T_{avg\,(y=z)}}{z_1}\right]}{z}$

4.4 Concrete Fire-induced Strains

The total concrete strain at elevated temperatures (ε) is given by Eq. (2) [6, 9]. The thermal deformations shift the axial load (P)–axial strain (ε) diagrams but do not affect the axial capacity of the studied section, Fig. 4-4. This fact allows ignoring ε_i in the proposed method as it will not affect the member capacity. The effect of self-induced strains (ε_{st}) on the axial capacity is found to have minor effect on the predicted member capacity, Fig. 4-5a.

The value of ε_c at the peak stress (f'_{cT}), i.e. ε_{oT}, defines the stress-strain relationship during fire exposure. For loaded RC columns, the effect of elevated temperatures on ε_{oT} is negligible[11]. Fig. 4-8 shows the variation of $\varepsilon_{oT} + \varepsilon_{tr}$ with fire temperature [Eurocode 2]. A linear relationship, i.e. Eq. (8), is chosen to represent the Eurocode 2 recommendation. Such a relationship allows reaching a closed form solution while accounting for concrete nonlinearity as will be discussed in the next section. To evaluate the error associated with using the approximate Eq. (8), the axial capacities of the columns shown in Table 4-1 are calculated up to 4 hrs of ASTM-E119 standard fire exposure. Fig. 4-9a shows that this approximation has a negligible effect on the axial capacity predictions calculated using sectional analysis method.

$$\varepsilon_{oT} + \varepsilon_{tr} = 2.52 \times 10^{-5}\, T_{avg} \qquad 80\,℃ < T_{avg} \leq 1200\,℃ \qquad (8)$$

Concrete subjected to lower T_{avg} develops their compressive capacity at lower ε_{cT}. Thus, failure strain is defined using the lowest T_{avg} in the section.

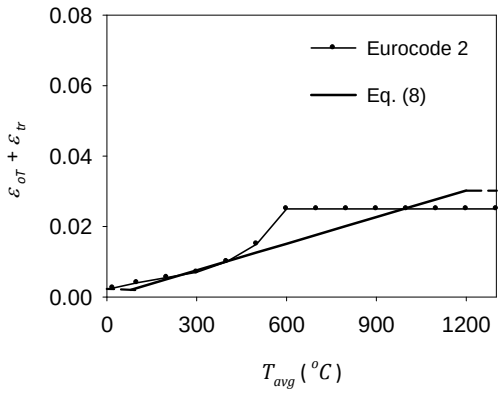

Fig. 4-8. Variation of $\varepsilon_{oT} + \varepsilon_{tr}$ at elevated temperatures

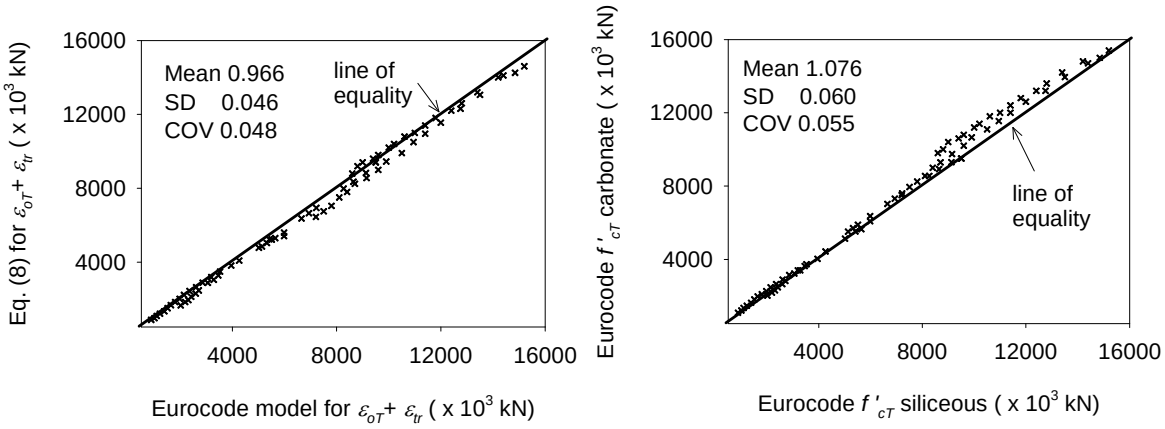

a) proposed Eq. (11)

b) aggregate type

Fig. 4-9- Effect of different parameters on sectional analysis results

4.5 Stress-Strain Relationships

4.5.1 Concrete

Concrete compressive strength experiences significant degradation at elevated temperatures. Eurocode 2 predicts the reduced compressive strength (f'_{cT}) for siliceous and carbonate concretes as a ratio from its ambient value (f'_c) [14]. The reduction in f'_{cT} for siliceous concrete is fitted by a polynomial equation, Eq. (9). For $T_{avg} \leq 900$ ℃, the proposed equation results in coefficient of variations of 0.067 and 0.195 for siliceous and carbonate concrete, respectively. Fig. 4-9b shows the axial load capacities of the columns in Table 4-1 considering either siliceous or carbonate concrete. Carbonate aggregate slightly increases the axial capacity of RC columns during fire exposure, and thus the use of Eq. (9) yields conservative predictions.

$$\frac{f'_{cT}}{f'_c} = 1.76 \times 10^{-9}\, {T_{avg}}^3 - 3.00 \times 10^{-6}\, {T_{avg}}^2 + 2.50 \times 10^{-4}\, T_{avg} + 1.00 \qquad (9)$$

where T_{avg} is the weighted average temperature, in ℃, calculated in previous section

The relationship between the compression stress, f_{cT}, and the corresponding mechanical strain, ε_{cT}, at elevated temperatures was studied by a number of researchers. Among the available models, Youssef and Moftah [11] proposed a stress-strain model, Eq. (10), which includes a simplified representation of transient creep strains and better matches the available experimental data. It is also consistent with the Eurocode 2 stress-strain relationship [14]. Fig. 4-10 shows the concrete stress-strain relationship at three average temperatures ($T_{avg} = 230$, 400, and 600 ℃). f'_{cT} and $\varepsilon_{oT} + \varepsilon_{tr}$ are calculated using Eqs. (8) and (9), respectively.

$$f_{cT} = f'_{cT} \left[2 \left(\frac{\varepsilon_{cT}}{\varepsilon_{oT} + \varepsilon_{tr}} \right) - \left(\frac{\varepsilon_{cT}}{\varepsilon_{oT} + \varepsilon_{tr}} \right)^2 \right] \qquad \varepsilon_{cT} \leq (\varepsilon_{oT} + \varepsilon_{tr}) \qquad (10)$$

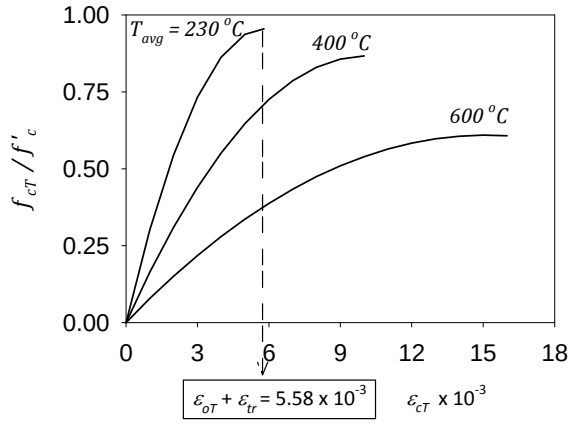

Fig. 4-10. Concrete stress-strain relationship at different T_{avg} values

The axial behavior of RC columns during fire exposure can be predicted by assuming different mechanical strains (ε_{cT}). At each ε_{cT}, the corresponding concrete stresses at different y values are calculated using Eqs. (9) and (10). The axial load is then predicted by summing the normal concrete stresses.

Using the average temperature distribution defined by Eq (7), the distribution of $\varepsilon_{oT} + \varepsilon_{tr}$ and f'_{cT}/f'_c over the section height can be evaluated using Eqs. (8) and (9). The minimum value of $\varepsilon_{oT} + \varepsilon_{tr}$ defines the failure strain ε_{cT}. The distribution of stresses over the section height can then be evaluated using Eq. (10). Integrating these stresses over a distance y of the section height results in an average concrete stress, Eq. (11).

$$\left(\frac{f_{cT\,avg}}{f'_c}\right) = 2\left(\frac{f_{cT\,avg}}{f'_c}\right)_L - \left(\frac{f_{cT\,avg}}{f'_c}\right)_N \tag{11}$$

where

$$\left(\frac{f_{cT\,avg}}{f'_c}\right)_L = \left(\frac{6.566\times10^{-6}\,\varepsilon_{cT}}{z\,z_1\,z_2}\right)\,[5.3\,{z_1}^3\,e^{2\,z\,z_2} - 1.815\times10^4\,{z_1}^2\,e^{\,z\,z_2}$$

$$-6.055\times10^9\,e^{-z\,z_2} + 1.516\times10^6\,y_o\,z_2\,z_1 - 5.3\,{z_1}^3 + 1.815\times10^4\,{z_1}^2$$

$$+6.055\times10^9] \quad \text{, and}$$

$$\left(\frac{f_{cT\,avg}}{f'_c}\right)_N = \left(\frac{52\times10^{-2}\ \varepsilon_{cT}{}^2}{z\ z_1{}^2\ z_2}\right) * [5.3\ z_1{}^3\ e^{z\,z_2} - 1.514\times10^9\ e^{-2\,z\,z_2}$$

$$-7.58\times\ 10^5\ z_1\ e^{-z\,z_2} - 9.077\times10^3\ z\ z_2\ z_1{}^2 - 5.3\ z_1{}^3$$

$$+ 7.58\times10^5\ z_1 + 1.514\times10^9]$$

4.6 Steel

Lie et al.'s model[1] is used to predict the reduced yield strength of reinforcing bars (f_{yT}), Eq. (12), and the stress-strain ($f_{sT} - \varepsilon_{sT}$) relationship, Eq. (13).

$$f_{yT} = \left[1 + \frac{T}{900\ \ln(T/1750)}\right] f_y \qquad 0 < T \leq 600\ ℃ \tag{12a}$$

$$= \left[\frac{340-0.34\,T}{T-240}\right] f_y \qquad 600 < T \leq 1000\ ℃ \tag{12b}$$

$$f_{sT} = \frac{f[T\,,0.001]}{0.001}\ \varepsilon_{sT} \qquad \varepsilon_{sT} \leq \varepsilon_p \tag{13a}$$

$$f_{sT} = \frac{f[T\,,0.001]}{0.001}\ \varepsilon_p + f\left[T\,,\left(\varepsilon_{sT} - \varepsilon_p + 0.001\right)\right] - f[T\,,0.001] \qquad \varepsilon_{sT} > \varepsilon_p \tag{13b}$$

$$\varepsilon_p = 4\times10^{-6}\ f_y \tag{13c}$$

$$f[T, 0.001] = (50 - 0.04\,T)\left[1 - e^{(-30+0.03\,T)\sqrt{0.001}}\right] \times 6.9 \tag{13d}$$

$$f\left[T\,,\left(\varepsilon_{sT} - \varepsilon_p + 0.001\right)\right] = (50 - 0.04\,T)\left[1 - e^{(-30+0.03\,T)\sqrt{\left(\varepsilon_{sT}-\varepsilon_p+0.001\right)}}\right] \times 6.9 \tag{13e}$$

4.7 Predicting the Axial Capacity

The axial compression capacity is finally calculated by summing the forces in concrete and steel. The effect of elevated temperatures on bond loss between steel bars and concrete and concrete spalling were not considered in the analysis. The following section provides example calculations for the proposed method.

4.8 Illustrative Example

The column tested by Lie et al[10], Fig. 4-1, is used as an example to explain the proposed method. It has a section of $305\ mm$ by $305\ mm$. It is reinforced with four $25\ mm$ steel bars and has $10\ mm$ ties spaced at $305\ mm$. The compressive and yield strengths of the siliceous concrete and reinforcing steel bars are 36.1 and $443.7\ MPa$, respectively. The column is exposed to a standard ASTM-E119 fire while being axially loaded. The calculated ambient axial compressive capacity of the column is $4120\ kN$. The following steps are conducted to calculate the axial capacity of the tested column after 1 hr and 3 hrs of ASTM-E119 fire exposure.

1) The ASTM-E119 fire temperature (T_f) is first calculated at fire durations of $t = 1.0\ hr$ and $3.0\ hrs$ using Eq. (14) (Lie et al., 2001).

$$T_f = 750\left(1 - e^{-3.79553\sqrt{t}}\right) + 170.41\sqrt{t} \quad (14)$$

where T_f is the fire temperature in Celsius and t (hrs) is the fire duration.

For t of $1\ hr$ and $3\ hrs$, values of T_f are 904 ℃ and 1044 ℃, respectively.

2) Γ values of 0.86 and 0.74 for t of $1.0\ hr$ and $3.0\ hrs$, respectively, are evaluated using Eq. (3).

3) n_w values of 0.93 and 0.97 for t of $1.0\ hr$ and $3.0\ hrs$, respectively, are estimated using Eq. (4b).

4) z values of 0.105 m and 0.183 m for t of 1.0 hr and 3.0 hrs are calculated using Eq. (5).

5) The average temperatures for each region are calculated and are shown in Figs. 4-6 and 4-7 by the dashed lines.

   For 1 hr fire exposure (Fig. 4-6): z of 0.105 is used to define the region boundaries. Substituting in Eq. (6a) using $x_1 = 0.0\,m$, and $x_2 = 0.105\,m$ results in $T_{avg\,1} = 304 + 562\,n_y$. Substituting in Eq. (6b) using $x_1 = 0.0\,m$, and $x_2 = 0.105\,m$ results in $T_{avg\,2} = 844\,n_y$.

   For 3 hrs fire exposure (Fig. 4-7): z of 0.183 m is greater than $b/2$, thus the region boundary is defined by the value of ($b - 0.183\,m = 0.122\,m$). Using Eq. (6a), $x_1 = 0.0\,m$, and $x_2 = 0.122\,m$ results in $T_{avg\,1} = 512 + 518\,n_y$. Substituting in Eq. (6c) using x_1 of $0.122\,m$, and x_2 of $0.183\,m$ results in $T_{avg\,R3} = 136 + 884\,n_y$.

6) The ambient temperature (20 ℃) is added to the calculated average temperatures. Weighted average temperatures for t of 1.0 hr and 3.0 hrs are then calculated at different y values. For 1 hr fire exposure, $T_{avg}(y = 0.0\,m) = 879$ ℃ and $T_{avg}(y = 0.105\,m) = 230$ ℃. For 3 hrs of fire exposure, $T_{avg}(y = 0.0\,m) = 1048$ ℃ and $T_{avg}(y = 0.153\,m) = 534$ ℃. The average temperature distribution is shown in Fig. 4-11. The figure shows that the values calculated using the developed simplified method matches the values predicted using the FDM method.

7) The constants (z_1 and z_2) of Eq. (7) are evaluated using values of T_{avg} at y_1 of 0.0 m and y_2 of 0.105 m for t of 1 hr and at y_1 of 0.0 m and y_2 of 0.153 m for t of 3 hrs. The equations representing the average temperature distribution over the section height are:

   For 1 hr of exposure, $T_{avg} = 879\ e^{(-12.12\ y)}$

   For 3 hrs of exposure, $T_{avg} = 1048\ e^{(-4.41\ y)}$

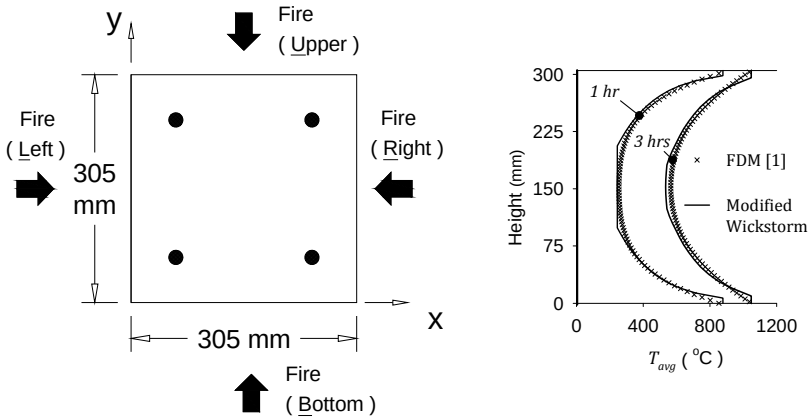

a) four-face heated RC section b) T_{avg} dist

Fig. 4-11. T_{avg} distribution of the example RC column

8) The lowest average temperatures in the section for $t = 1\ hr$ and $t = 3\ hrs$ are 230 ℃ and 534 ℃, respectively. The failure strain ε_{cT} can be assumed to be equal to $\varepsilon_{oT} + \varepsilon_{tr}$ at these temperatures. For t of $1\ hr$ and $3\ hrs$, ε_{cT} equals to 5.80×10^{-3} and 13.47×10^{-3}, respectively.

9) Fig. 4-12 shows the constant strain distribution. The corresponding f_{cT} distributions for t of $1\ hr$ and $3\ hrs$ are also shown. Values of f_{cT} are evaluated using Eq. (10). $f_{cT\ avg}$ is calculated as follows:

   a. For t of $1\ hr$: substituting in Eq. (11) using $y = 0.105\ m$, $z_1 = 879$, $z_2 = -12.12$, and $\varepsilon_{cT} = 5.80 \times 10^{-3}$ yields $\left(f_{cT\ avg}/f'_c\right)_L = 0.358$, $\left(f_{cT\ avg}/f'_c\right)_N = 0.236$, and $\left(f_{cT\ avg}/f'_c\right) = 0.481$. $\left(f_{cT\ avg}/f'_c\right)$ for the constant temperature zone is calculated directly using Eq. (12) as 0.920.

   b. For t of $3\ hrs$: substituting in Eq. (11) using $y = 0.153\ m$, $z_1 = 1048$, $z_2 = -4.41$, and $\varepsilon_{cT} = 13.47 \times 10^{-3}$ yields $\left(f_{cT\ avg}/f'_c\right)_L = 0.204$, $\left(f_{cT\ avg}/f'_c\right)_N = 0.171$, and $\left(f_{cT\ avg}/f'_c\right) = 0.237$.

10) The temperature of steel bars in the example column can be calculated using the Wickstrom method[10], Eq. (4). In this example, all bars have the same temperature that can be calculated as follows:

a. For 1 hr of fire exposure: using Eqs. (4c) and (4d), n_x and n_y are equal to 0.2. Eq. (4a) yields $T_{avg} = 322$ ℃.

b. For 3 hrs of fire exposure, n_x and n_y are equal to 0.39. Eq. (4a) yields $T_{avg} = 668$ ℃.

11) The steel stress is calculated using Eqs. (9) to (13). For 1 hr of fire exposure, $f_{yT} = 0.79\ f_y$. $\varepsilon_{sT} = 5.80 \times 10^{-3}$, $\varepsilon_p = 0.0018$, $f[T, 0.001] = 122\ MPa$, $f\left[T, (\varepsilon_{sT} - \varepsilon_p + 0.001)\right] = 196\ MPa$, and $f_{sT} = 290\ MPa$. For 3 hrs of fire exposure, $f_{yT} = 0.26\ f_y$. $\varepsilon_{sT} = 12.47 \times 10^{-3}$, $\varepsilon_p = 0.0018$, $f[T, 0.001] = 108\ MPa$, $f\left[T, (\varepsilon_{sT} - \varepsilon_p + 0.001)\right] = 108\ MPa$, and $f_{sT} = 142\ MPa$.

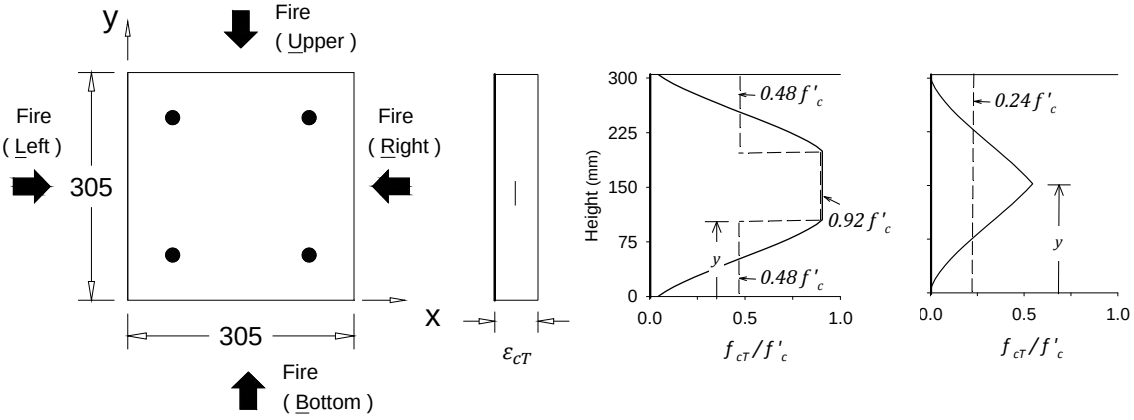

a) four-face heated b) ε_{cT} dist. c) f_{cT} dist.. ($t = 1.0\ hr$) d) f_{cT} dist.. ($t = 3.0\ hrs$)

Fig. 4-12. Average compression stresses distribution

12) Using the steel and concrete stresses, the axial capacity of the example column is predicted as $2{,}618\,kN$ and $1{,}077\,kN$ after $1\,hr$ and $3\,hrs$ fire exposure, respectively.

The steps mentioned above are repeated for the studied RC column at different fire durations. The reduced axial capacity is estimated at each fire duration up to $3.75\,hrs$, Fig. 4-13. Although the proposed method results in conservative predictions, i.e. around 15% less than test results, it was able to match the profile of degradation of the axial capacity and provided values of good accuracy for a design engineer. The proposed method can be applied to have a quick idea about the structural fire safety of RC columns.

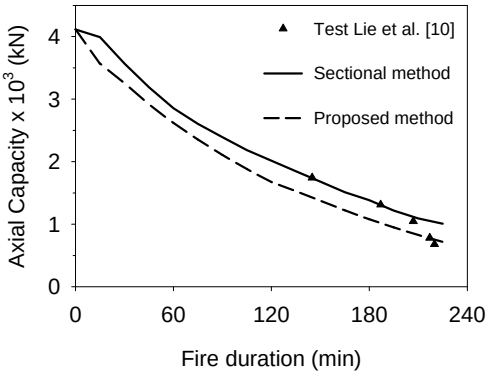

Fig. 4-13. Axial capacity predictions of example column

4.9 Validation

The proposed method is used to predict the axial compression capacity of three concentrically loaded RC columns tested by Lie and Wollerton[15]; Dotreppe et al[16]; and Hass[17].

4.9.1 Lie and Wollerton [15]

Table 4-2 shows the geometric and reinforcement properties of eighteen RC columns tested by Lie and Wollerton[15]. All columns were axially loaded with a load P_{app} and subjected to a standard ASTM-E119 fire. Values for P_{app}were kept constant during testing of all columns. The fire endurance time (t) was recorded at the end of each column test. The reinforcing steel cover was $48\ mm$ for all columns except column NO. 16, where it was $64\ mm$. Fig. 4-14a shows a comparison between P_{app} and the predicted axial capacity using the proposed method and the method proposed by Dotreppe et al. [9]and applied by Tan and Tang[18]. The proposed method results have good accuracy given the complexity of the problem. . The proposed method resulted in better accuracy compared to Doterppe et al.'s simple method.

Table 4-2–Details of Lie and Wollerton[15]

No	b (mm)	h (mm)	steel bars (mm)	f'_c (MPa)	f_y (MPa)	P_{app} (kN)	t (min)
1	305	305	4Ø25.5	36.9	444	1333	170
2	305	305	4Ø25.5	34.2	444	800	218
3	305	305	4Ø25.5	35.1	444	711	220
4	203	203	4Ø20.0	42.3	442	169	180
5	305	305	4Ø25.5	36.1	444	1067	208
6	305	305	4Ø25.5	34.8	444	1778	146
7	305	305	4Ø25.5	38.3	444	1333	187
8	305	305	4Ø25.5	43.6	444	1044	201
9	305	305	4Ø25.5	35.4	444	916	210
10	305	305	4Ø25.5	52.9	444	1178	227
11	305	305	4Ø25.5	49.5	444	1067	234
12	305	305	8Ø25.5	42.6	444	978	252
13	305	305	8Ø25.5	37.1	444	1333	225
14	406	406	8Ø25.5	38.8	444	2418	262
15	406	406	8Ø32.3	38.4	414	2795	285
16	406	406	8Ø32.3	46.2	414	2978	213
17	305	305	4Ø25.5	39.6	444	800	242
18	305	305	4Ø25.5	39.2	444	1000	220

* all columns have length (L) of 3.81 m long

4.9.2 Dotreppe et al. [16]

Table 4-3 shows the properties of eight RC columns tested by Dotreppe et al. [16]. The columns were loaded by the shown loads, P_{app}. The heights of columns 1 to 3 and columns 4 to 8 were $3.90\ m$ and $2.10\ m$, respectively. All the columns were subjected to a standard ISO 834 fire exposure and the fire endurance (t) for each column was recorded. The reinforcing steel cover was $25\ mm$ for all columns and the end conditions were pinned-pinned (p-p). Although all the loads were concentrically applied at the beginning of the fire test, the columns were affected by buckling. Dotreppe et al. [9] proposed reducing the axial capacity by a buckling factor $\chi(\lambda)$, Eq. (15).

$$\chi(\lambda) = 1 - \frac{\lambda}{100} \qquad \lambda \leq 20 \qquad (15a)$$

$$\chi(\lambda) = 0.80\left[\frac{20}{\lambda}\right]^{0.7\left(\frac{225-c}{200}\right)^5} \qquad 20 < \lambda \leq 70 \qquad (15b)$$

$$\chi(\lambda) = 0.80\left[\frac{20}{\lambda}\right]^{0.7\left(\frac{\lambda}{70}\right)\left(\frac{225-c}{200}\right)^5} \qquad 70 < \lambda \qquad (15c)$$

where λ is the column slenderness ratio and c is the concrete cover in mm.

The predicted axial capacities by the proposed method are reduced by the factor $\chi(\lambda)$. Fig. 4-14b shows a comparison between applied concentric loads (P_{app}) and the reduced axial capacity predictions. The estimated axial capacities are in good agreement with the applied loads. Dotreppe et al.'s method results in slightly better accuracy than the proposed method as shown in Fig. 4-14b. This can be due to the fact that this method was calibrated using these experimental results.

Table 4-3- Details of Dotreppe et al. [16]

No	b (mm)	h (mm)	steel bars (mm)	f'_c (MPa)	f_y (MPa)	P_{app} (kN)	t (min)
1*	300	300	4Ø16	33.9	576	950	61
2*	300	300	4Ø16	35.4	576	622	120
3*	300	300	4Ø16	29.3	576	422	116
4‡	300	300	4Ø16	29.3	576	1270	63
5‡	300	300	4Ø16	28.6	576	803	123
6‡	300	300	4Ø25	26.2	591	878	69
7‡	200	300	4Ø12	30.6	493	611	107
8‡	200	300	4Ø12	27.3	493	620	97

* $L = 3.9\ m$
‡ $L = 2.1\ m$

4.9.3 Hass [17]

Table 4-4 shows properties of seven RC columns tested by Hass[17]. All the columns were subjected to a standard ISO 834 fire exposure. The reinforcing steel cover was $38\,mm$ and the end conditions were pinned-pinned (p-p). The predicted axial capacities by the proposed method are reduced by Dotreppe et al.'s buckling factor $\chi(\lambda)$ to account for buckling[9]. Fig. 4-14c shows a comparison between applied concentric loads (P_{app}) and the reduced axial capacity predictions. As shown in the figure, the proposed method underestimates the axial capacity of the tested RC columns. A similar scatter in the results was found by Tan and Tang [18] using Dotreppe et al.'s method[9]. It should be noted that columns No. 1 and 2 have the same geometric, material, and loading conditions but their fire endurance differs by 64%. This can be due to errors in conducting the fire test.

Table 4-4-Details of Hass [17]

No	b (mm)	h (mm)	steel bars (mm)	f'_c (MPa)	f_y (MPa)	P_{app} (kN)	t (min)
1*	300	300	6Ø20	24.1	487	930	84
2*	300	300	6Ø20	24.1	487	930	138
3‡	300	300	6Ø20	34.1	487	880	108
4**	300	300	6Ø20	24.1	487	800	58
5*	200	200	4Ø20	24.1	487	420	58
6*	200	200	4Ø20	24.1	487	420	66
7‡	200	200	4Ø20	24.1	487	340	48

* $L = 3.76\,m$
‡ $L = 4.76\,m$
** $L = 5.76\,m$

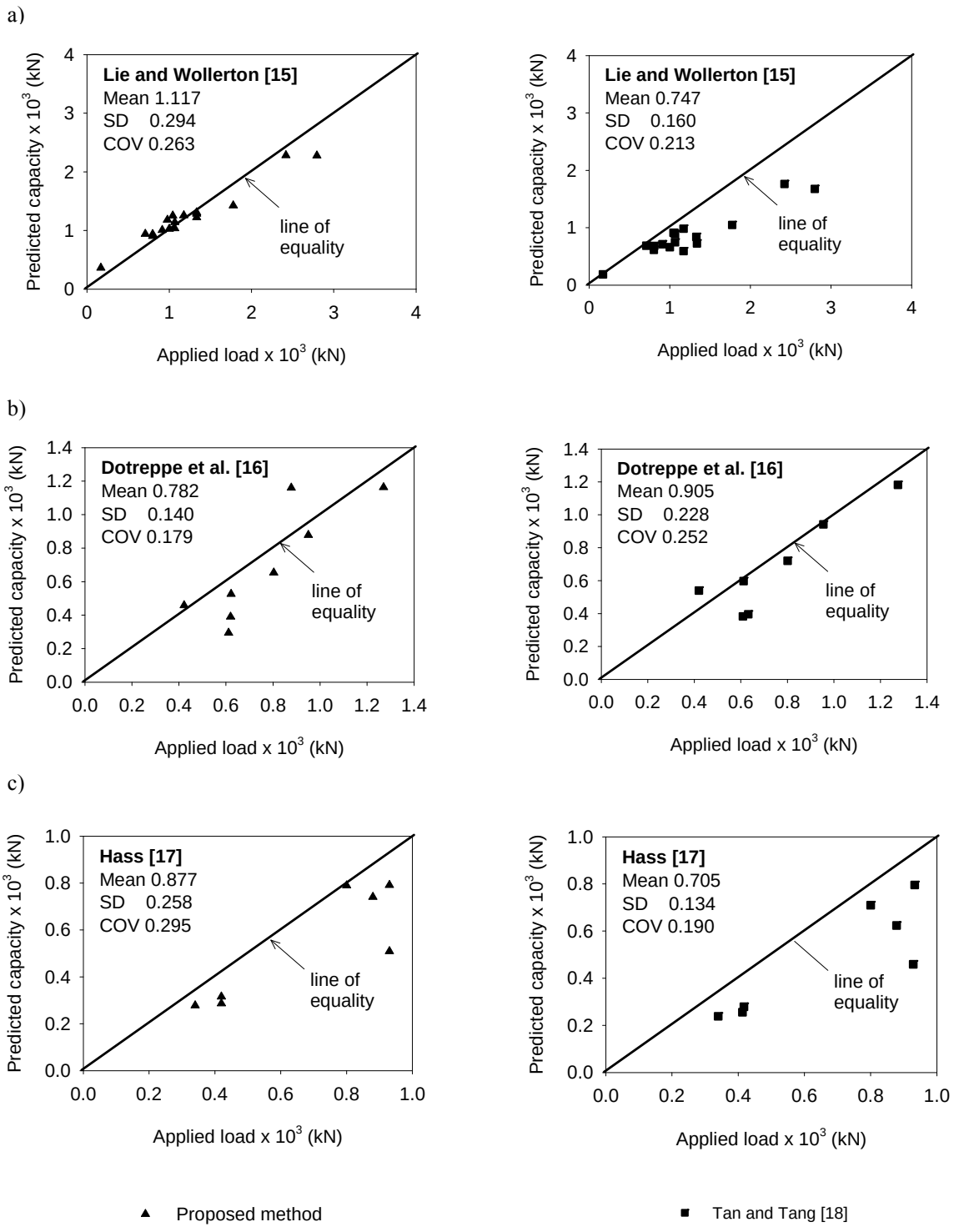

Fig. 4-14. Proposed method predictions for different experimental works

4.10 Summary and Conclusion

This chapter provides structural engineers with a rational tool to predict the axial compression capacity of four-faces heated RC columns during fire events. The proposed tool can be applied using a simple spreadsheet. The proposed method starts by dividing the analyzed section into different temperature zones. Equations to evaluate the average temperature with each zone are developed. The average temperature distribution is then used to estimate the failure strain. Equations to evaluate the corresponding average concrete stress were developed by integrating the concrete stresses along the height of the cross section. The failure strain is used to evaluate the reinforcing bar stresses. The axial compressive capacity is then calculated by using the concrete average stress and the reinforcing bar stresses.

The proposed method is validated by comparing its predictions with the test results of thirty three RC columns. A good agreement is found between the proposed method and the experimental results.

4.11 Acknowledgments

This research was funded by the Natural Sciences and Engineering Research Council of Canada (NSERC).

4.12 References

1. Lie, T.T., ed. 1992, "Structural fire protection." ASCE Manuals and Reports on Engineering Practice, no. 78, New York, 241 pp.

2. Cement Association of Canada 2006, “Concrete design handbook, CAN/CSA A23.3-04," 3rd Ed., Ottawa.

3. Raut, N., and Kodur, V.K.R. 2011. "Modeling the fire response of reinforced concrete columns under biaxial bending." ACI Struct. J., 108(6), pp. 1-24.

4. El-Fitiany, S., and Youssef, M.A. 2009. "Assessing the flexural and axial behaviour of reinforced concrete members at elevated temperatures using sectional analysis.", FSJ, 44(5), pp. 691-703.

5. El-Fitiany S.F. and Youssef M.A. 2010, "A Simplified Sectional Analysis Approach for RC Elements during Fire Events", 6th International Conference on Structures in Fire, Michigan State University in East Lansing, MI, pp. 239-246.

6. El-Fitiany, S.F., and Youssef, M.A. 2011, "Stress Block Parameters for Reinforced Concrete Beams During Fire Events," Innovations in Fire Design of Concrete Structures, ACI SP-279, pp. 1-39.

7. Law, A., and Gillie, M. 2010. "Interaction diagrams for ambient and heated concrete sections." Eng. Struct., 32(6), pp. 1641-1649.

8. Caldas, Rodrigo Barreto, Sousa Jr., João Batista M., and Fakurya, Ricardo Hallal 2010. "Interaction diagrams for reinforced concrete sections subjected to fire." Eng. Struct., 32(9), pp. 2832–2838.

9. Dotreppe, J.C., Franssen, J.M., and Vanderzeypen, Y. 1999, "Calculation method for design of reinforced concrete columns under fire conditions." ACI Struct. J., 96(1), pp. 9-18.

10. Lie, T.T., Lin, T.D., Allen, D.E., Abrams, M.S. 1984, "Fire resistance of reinforced concrete columns." Technical Paper No. 378, Division of Building Research, National Research Council of Canada, Ottawa, Ontario, Canada.

11. Youssef, M.A., and Moftah, M. 2007, "General stress-strain relationship for concrete at elevated temperatures." Eng. Struct., 29(10), pp. 2618-2634.

12. Wickstrom, U. 1986, "A very simple method for estimating temperature in fire exposed concrete structures." Fire Technology Technical report SP-RAPP 1986, 46, Swedish National Testing Institute, pp. 186-194.

13. Terro, M.J. 1998, "Numerical modeling of the behavior of concrete structures in fire." ACI Struct. J., 95(2), pp. 183-193.

14. Eurocode 2 1992, “Design of concrete structures.” ENV EC2.

15. Lie, T. T., and Woollerton, J. L. 1998, "Fire resistance of reinforced-concrete columns: Test results." Internal Rep. No. 569, National Research Council of Canada, Quebec, Canada.

16. Dotreppe, J.-C., Franssen, J.-M., Bruls, A., Baus, R., Vandevelde, P., Minne, R., Nieuwenburg, D. van, and Lambotte, H. 1997, “ Experimental research on the determination of the main parameters affecting the behaviour of reinforced concrete columns under fire conditions.” Mag. Concrete Res., 49(179), pp. 117-127

17. Hass, R. 1986, “Practical rules for the design of reinforced concrete and composite columns submitted to fire.” Technical Rep. No. 69, Institute fur Baustoffe, Massivbau and Brandschutz der Technischen Universita Branschweig. (in German)

18. Tan, K.H., Tang, C.Y. 2004, “Interaction Formula for Reinforced Concrete Columns in Fire Conditions.” ACI Struct. J., 101(1), pp. 19-28.

Chapter 5

5 Simplified Interaction Diagrams for Fire-Exposed RC Columns

Ongoing development in material and construction technology drives structural engineers to consider new design challenges including significantly taller high-rise buildings. For such buildings, fire evacuation of occupants and safety of fire fighters must be carefully considered at the design stage. During fire events, Reinforced Concrete (RC) columns are subjected to elevated temperatures, which significantly reduce the mechanical properties of concrete and steel[1]. Fire temperatures also induce nonlinear thermal and transient creep strains[2]. As a result, the capacity of the fire exposed columns varies during fire exposure.

Fire testing is the most reliable approach to assess the fire endurance of RC columns[3,4]. However, its cost and limitations make it unsuitable for regular design. The capacity of heated RC columns can be analytically assessed using axial force-moment interaction diagrams[5]. These diagrams can be constructed using the Finite Element (FE) method[5, 6] by assuming a load eccentricity and varying the applied axial force until failure occurs. This procedure is repeated for different load eccentricities to construct the interaction diagram for a given fire duration. Such method is computationally expensive, which makes the FE method unpractical for design engineers.

El-Fitiany and Youssef [7,8,9] proposed a sectional analysis method that converts the two-dimensional (2D) temperature distribution to an average one-dimensional (1D) temperature distribution which then predicts the uniaxial behavior of the heated section at different axial load levels (λ). Law and Gillie simplified the sectional analysis method by defining the failure point for the concrete section as the one causing the section tangent modulus matrix to be singular[5].

Eurocode 2[10] recommends the use of the 500 ℃ isotherm method. The method assumes that concrete heated to a temperature lower than 500 ℃ retains its full strength while concrete heated to a temperature higher than 500 ℃ is fully damaged. Ignoring the

damage to concrete heated to temperatures up to 500 ℃ can result in unsafe predictions as explained by Law and Gillie[5, 7].

This chapter proposes a practical approach to construct the interaction diagrams for RC columns during fire exposure. The proposed method extends the work done by El-Fitiany and Youssef [8]. The chapter provides the development of an efficient heat transfer method to calculate an average 1D temperature distribution, the derivation of closed form solutions for concrete internal stresses, and the application to construct the interaction diagram. The proposed method is validated by comparing its predictions with the experimental and analytical results by others.

5.1 Research Significance

Numerical methods can be used to construct the interaction diagrams for fire exposed RC columns. However, they are computationally expensive, which limit their use for design engineers. This chapter presents a simple method that can be used to construct the axial force-moment interaction diagram for RC sections. The method includes the derivation of a simple technique to calculate an average 1D temperature distribution for RC sections and a number of mathematical expressions to calculate the internal forces.

5.2 Interaction Diagrams using Sectional Analysis

Fire temperature decreases concrete and steel mechanical properties considerably and induces thermal and transient strains. A sectional analysis approach suitable for the analysis of rectangular RC sections at elevated temperatures was proposed by El-Fitiany and Youssef[7]. Fig. 5-1a shows a RC section subjected to fire from four faces. The use of sectional analysis to evaluate the interaction diagram for this column involves the following steps:

1. At specific fire duration, the section is divided into a number of elements, Fig. 5-1a, and the temperature distribution is predicted using the Finite Difference Method (FDM)[1]. The effect of steel bars is neglected in the heat transfer analysis.

2. The cross-section is divided into horizontal layers and two average temperatures, T_σ and T_{avg}, are calculated for each layer, Fig. 5-1a. T_σ results in the same average concrete compressive strength for the considered layer, and thus is suitable for strength calculations. T_{avg} represents the algebraic average temperature of the elements within each layer and is suitable for thermal and transient creep strains calculations[8].

3. The total concrete strain at elevated temperatures (ε) is composed of three terms: unrestrained thermal strain (ε_{th}), instantaneous stress related strain (ε_c), and transient creep strain (ε_{tr}). The total strain is given by Eq. (1).

$$\varepsilon = \overline{\varepsilon_{th}} + \varepsilon_c + \varepsilon_{tr} \quad (1)$$

The nonlinear thermal strain (ε_{th}) distribution, Fig. 5-1f, is calculated using T_{avg}. The thermal strain of steel bars is calculated based on the concrete temperature at their locations. ε_{th} is then converted to an equivalent linear thermal strain ($\overline{\varepsilon_{th}}$), Fig. 5-1c, by considering self-equilibrium of internal thermal forces in concrete and steel layers. $\overline{\varepsilon_{th}}$ is represented by the value of the center axial strain (ε_i). The curvature ψ_i is equal to zero for sections heated from four faces. Fig. 5-1e shows the differences between the equivalent linear and nonlinear thermal strains, which represent the self-induced thermal strains (ε_{st}). These strains are assigned as initial strains for the concrete and steel layers to model the corresponding self-induced self-equilibrating thermal stresses. The terms ε_{st}, ε_c, and ε_{tr} are lumped into an equivalent mechanical strain ε_{cT} as shown in Eq. (2).

$$\varepsilon = \overline{\varepsilon_{th}} + \left(\varepsilon_{st} + \varepsilon_c + \varepsilon_{tr}\right) = \overline{\varepsilon_{th}} + \varepsilon_{cT} \quad (2)$$

4. For assumed values of axial load, ε_{cT} at the top of the section and ψ_{cT}, the constitutive stress-strain relationship for concrete developed by Youssef and Moftah[2] are used to evaluate the corresponding stresses in the concrete and steel layers. The corresponding internal axial forces are then calculated. To satisfy equilibrium between

the calculated internal forces and the applied axial load, iterations are executed by changing the value of ε_{cT} . Using the final strain distribution, the moment acting on the section is evaluated. This process is repeated for different values of ψ_{cT} and the relationship between ψ_{cT} and the applied moment is sketched, Fig. 5-2. The maximum applied moment defines the moment of resistance at the assumed axial load.

5. Repeating step 4 for different axial loads (λ) allows evaluating the interaction diagram for the given section at given fire duration.

6. Steps 1 to 5 are to be repeated at different fire durations.

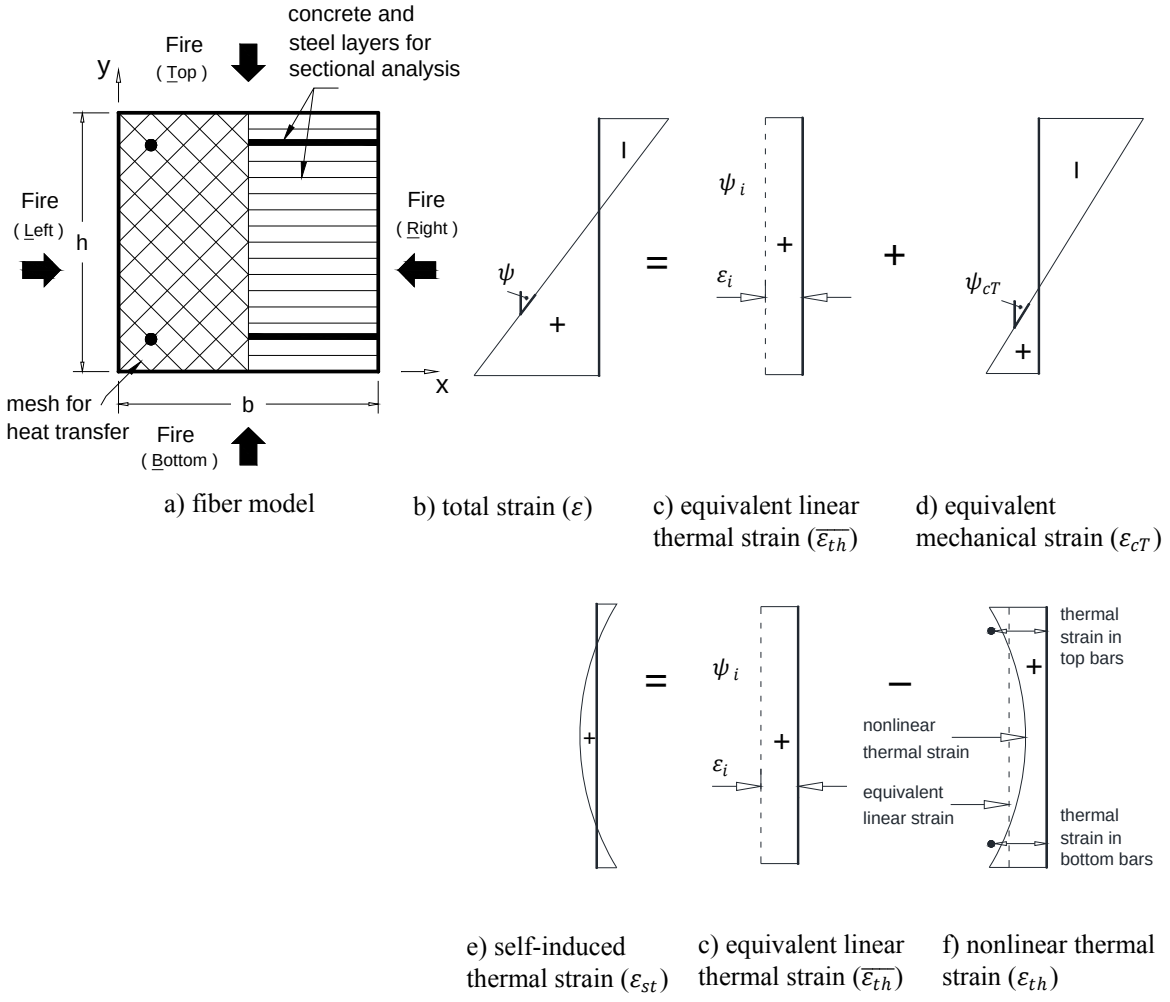

a) fiber model | b) total strain (ε) | c) equivalent linear thermal strain ($\overline{\varepsilon_{th}}$) | d) equivalent mechanical strain (ε_{cT})

e) self-induced thermal strain (ε_{st}) | c) equivalent linear thermal strain ($\overline{\varepsilon_{th}}$) | f) nonlinear thermal strain (ε_{th})

Fig. 5-1-Sectional analysis approach for four-face fire exposed RC columns

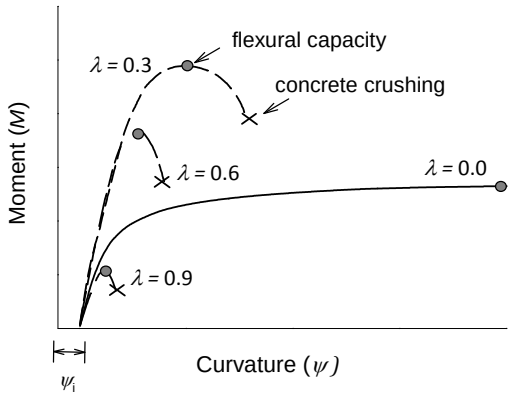

Fig. 5-2-Schematic for M–ψ relationships at different axial load levels

The errors corresponding to ignoring ε_{st} or using T_{avg} for strength calculations are assessed by analyzing the columns shown in Table 5-1 at different axial load levels (λ = 0.0 - 0.9). Comparisons between the analytical flexural capacities obtained by considering all parameters, ignoring ε_{st}, and using T_{avg} are shown in Figs. 5-3 and 5-4. While ignoring ε_{st} results in slightly underestimating the flexural capacity, using T_{σ} for stress calculations has a negligible effect on the flexural capacity of the examined concrete columns.

Although the sectional analysis method is relatively easy to apply as compared to the FE method, it requires knowledge of heat transfer principles and the ability to conduct iterative analysis at elevated temperatures. The following sections present a simplified approach to predict the interaction diagram of RC column during fire exposure.

Table 5-1–Parametric study cases

Col #	b (mm)	h (mm)	f'_c (MPa)	f_y (MPa)	ρ $\%\ (A_g)$
$C1$	305	305	36.1	443.7	2.1
$C2$	400	400	30	400	1.5
$C3$	600	600	40	400	1.5
$C4$	400	700	50	400	1.0
$C5$	500	700	25	400	1.0

***** all columns are analyzed up to 4 hrs of standard ASTM-E119 fire exposure

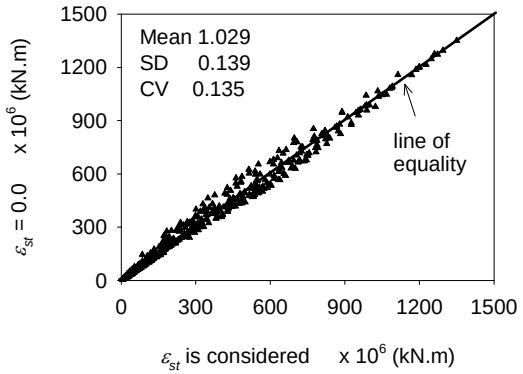

Fig. 5-3. Effect of ignoring ε_{st} on the flexural capacity of fire-exposed columns

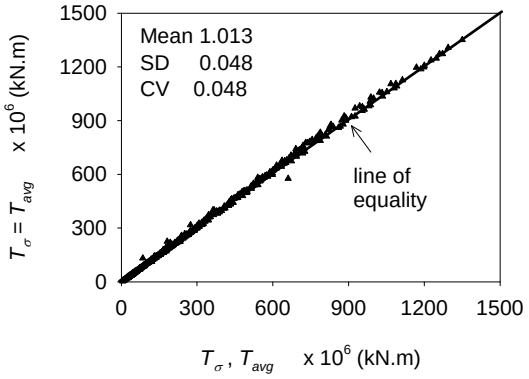

Fig. 5-4. Effect of neglecting T_σ on the flexural capacity of fire-exposed columns

5.3 Proposed Method

Concrete has low thermal conductivity, which results in a steep temperature distribution near the heated faces and almost constant at the core of the heated section. Thus, the concrete strength becomes variable near the heated faces and constant at the inner concrete core. The effect of elevated temperatures on the shear capacity, bond loss between steel bars and concrete, and concrete spalling were not considered in the sectional analysis. For a given fire duration and axial load, the proposed method provides simplified equations to evaluate:

1) a one-dimensional average temperature distribution.

2) the concrete strains at failure.

3) the concrete and steel stresses at failure.

4) the flexural capacity of the section.

The following sections provide the derivations of the simplified equations.

5.4 Average Temperature Distribution

A simplified method to calculate the temperature distribution within a fire exposed concrete section was presented in chapter 4. In this method, the heated section is divided into regions of constant and variable temperatures and the average temperature (T_{avg}) profile is predicted based on the average temperature of each region. The predicted T_{avg} profile, Eq. (3), is used in the proposed method.

$$T_{avg} = z_1 \,.\, e^{(z_2 \,.\, y)} \tag{3}$$

where $z_1 = T_{avg\,(y=0.0)}$; and $z_2 = \frac{\ln\left[\frac{T_{avg\,(y=z)}}{z_1}\right]}{z}$

5.5 Concrete and Steel Constitutive Relationships

Concrete and steel models used in the proposed method are discussed in this section. Concrete tensile strength is neglected in the analysis.

5.5.1 Concrete compressive strength

Concrete compressive strength experiences significant degradation at elevated temperatures. Eurocode 2 predicts the reduced compressive strength (f'_{cT}) for siliceous and carbonate concretes as a ratio from its ambient value (f'_c) [10]. The reduction in f'_{cT} for siliceous concrete is fitted by a polynomial equation, Eq. (4), such that it can be integrated in the following sections to calculate concrete internal forces and moments. For $T_{avg} \leq 900$ ℃, the proposed equation results in coefficient of variation of 0.067 and 0.195 for siliceous and carbonate concrete, respectively. Fig. 5-5 shows the flexural capacities of the columns in Table 5-1 considering either siliceous or carbonate concrete. Carbonate aggregate slightly increases the flexural capacity of RC columns during fire exposure, and thus the use of Eq. (4) yields conservative predictions. The equation can be conservatively applied for carbonate aggregate concrete.

$$f'_{cT} / f'_c = 1.76 \times 10^{-9}\, T_{avg}{}^3 - 3 \times 10^{-6}\, T_{avg}{}^2 + 2.5 \times 10^{-4}\, T_{avg} + 1.00 \qquad (4)$$

where T_{avg} is the weighted average temperature, in ℃, calculated in the previous section

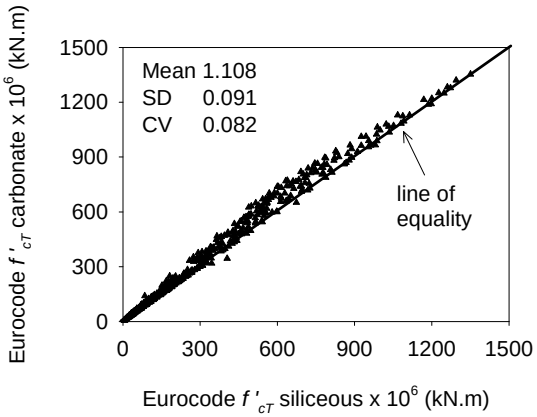

Fig. 5-5. Effect of aggregate type on the flexural capacity of fire-exposed columns

5.5.2 Thermal strains

The total concrete strain at elevated temperatures (ε) is given by Eq. (2). The thermal deformation, $\overline{\varepsilon_{th}}$, shifts the moment ($M$)–curvature ($\psi$) diagrams but does not affect the flexural capacity of the studied section, Fig. 5-2. This fact allows ignoring $\overline{\varepsilon_{th}}$ in the proposed method as it does not affect the member capacity.

5.5.3 Concrete strain at peak stress

The value of ε_c at the peak stress (f'_{cT}), i.e. ε_{oT}, defines the stress-strain relationship during fire exposure, Fig. 5-6. For loaded RC columns, the effect of elevated temperatures on ε_{oT} is negligible[2]. Fig. 5-7 shows the variation of $\varepsilon_{oT} + \varepsilon_{tr}$ with fire temperature as proposed by Eurocode 2. The shown values of $\varepsilon_{oT} + \varepsilon_{tr}$ are consistent with Terro's model[9] within its validated temperature range, i.e. up to 600 ℃. A linear relationship, Eq. (5), is chosen to represent the Eurocode 2 recommendation. Such a relationship allows reaching a closed form solution while accounting for concrete nonlinearity as will be discussed in the next section. To evaluate the error associated with using the approximate Eq. (5), the flexural capacities, at different axial load levels ($\lambda = 0.0 - 0.9$), of the columns shown in Table 5-1 are calculated up to 4 hrs of ASTM-

E119 standard fire exposure. Fig. 5-8 shows that this approximation has a minor effect on the flexural capacity predictions calculated using sectional analysis method.

$$\varepsilon_{oT} + \varepsilon_{tr} = 2.52 \times 10^{-5}\, T_{avg} \qquad 80\ ℃ < T_{avg} \leq 1200\ ℃ \qquad (5)$$

5.5.4 Concrete ultimate strain

Concrete ultimate strain is the strain at which concrete crushing occurs. Elevated temperatures increase this strain. Models evaluating the effect of elevated temperatures on the ultimate concrete compressive strain (ε_{uT}) are limited in the literature. Meda et al.[13] assumed that ε_{uT} corresponds to a maximum post peak stress of 0.85 f'_{cT}. Eurocode 2 proposes a linear relationship between ε_{uT} and T_{avg}, Fig. 5-7. This relationship can be represented by Eq. (6). ε_{uT} is defined in Eurocode 2 as the strain corresponding to zero compression stress. The difference between ε_{uT} and $\varepsilon_{oT} + \varepsilon_{tr}$ when evaluated using Eqs. (5) and (6) is constant and equal to 0.02.

$$\varepsilon_{uT} = 2.52 \times 10^{-5}\, T_{avg} + \Delta\varepsilon = \varepsilon_{oT} + \varepsilon_{tr} + 0.02 \qquad (6)$$

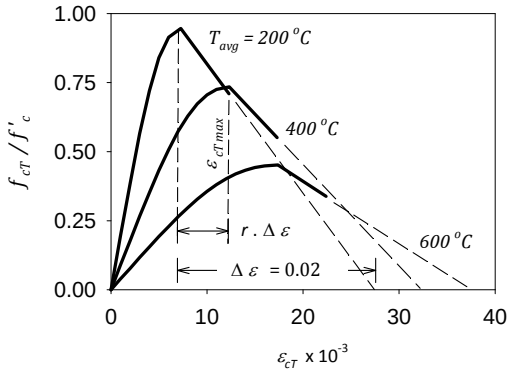

Fig. 5-6- Concrete stress-strain relationships at different elevated temperatures

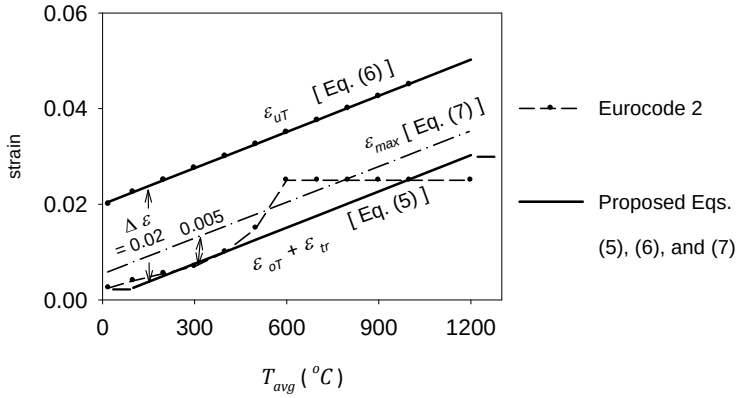

Fig. 5-7-Variation of ($\varepsilon_{oT} + \varepsilon_{tr}$), ε_{uT}, and $\varepsilon_{cT\,max}$ at elevated temperatures

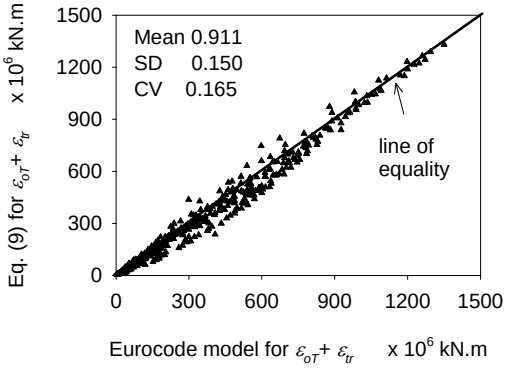

Fig. 5-8. Effect of using Eq. (5) on the flexural capacity of fire-exposed columns

5.5.5 Maximum concrete strain

The maximum concrete strain is defined as the strain corresponding to the maximum moment resistance. As shown in Fig. 5-2, this strain is usually lower than ε_{uT}. Elbahy et al.[14] studied the variation of this strain with the axial load level at ambient temperature.

At elevated temperatures, a parametric study is conducted to evaluate the compression strain ($\varepsilon_{cT\,max}$) corresponding to the flexural capacity, i.e. peak points in Fig. 5-2. To identify the point of maximum moment in a typical M–ψ diagram (Fig. 5-2), the flexural capacity must be evaluated assuming different values of failure strain ($\varepsilon_{cT\,max}$) ranging from ($\varepsilon_{oT} + \varepsilon_{tr}$) to ε_{uT}. The flexural capacities of the columns shown in Table 5-1 are determined at different axial load levels ($\lambda = 0.0 - 0.9$) using sectional analysis method. For each column section, the M–ψ diagrams are constructed assuming different lengths ($r\,.\,\Delta\varepsilon$) for the descending branch as shown in Fig. 5-8, where r values of 0.0, 0.25, 0.50, 0.75, and 1.0 are assumed.

Fig. 5-9 shows the $P - M$ diagrams of column $C2$ at 1.0 hr ASTM-E119 fire exposure. The dashed line represents the correct flexural capacities as determined by the peak points of the constructed M–ψ diagrams at different axial loads. Terminating the descending branch at $r < 0.0$ results in conservative flexural capacity. On the other hand, considering the full descending branch, i.e. $r = 1.0$, significantly underestimates the flexural capacity. Fig. 5-10 shows a comparison between the correct flexural capacities and the predicted flexural capacities, for all columns in Table 5-1, at fire durations up to 4.0 hrs of standard ASTM-E119 fire exposure. Reasonable predictions are obtained at r equals to 0.25. Thus, $\varepsilon_{cT\,max}$ is defined by adding $0.25\,\Delta\varepsilon$ to ($\varepsilon_{oT} + \varepsilon_{tr}$), where $\Delta\varepsilon$ equals to 0.02. ε_{max} is given by Eq. (7).

$$\varepsilon_{cT\,max} = (\varepsilon_{oT} + \varepsilon_{tr}) + 0.005 \tag{7}$$

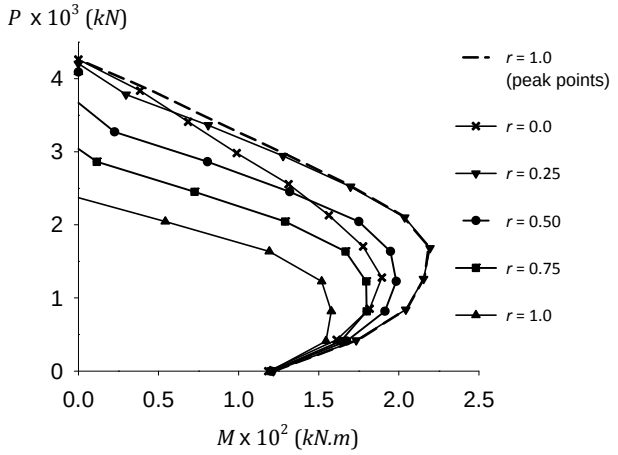

Fig. 5-9-P-M diagrams for column $C2$ with using different r values

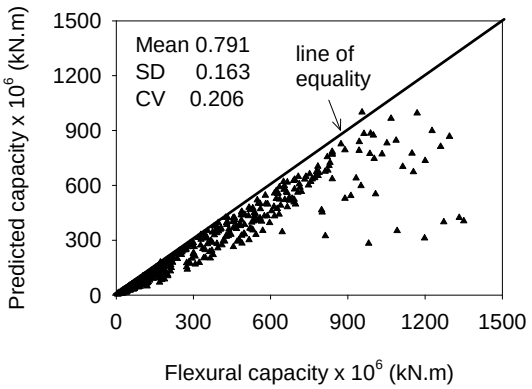

a) $r = 0.00\ \Delta\varepsilon$

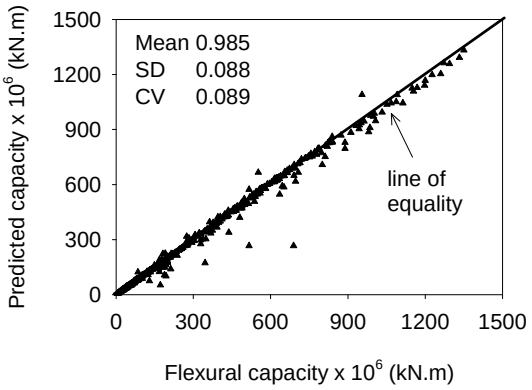

b)) $r = 0.25\ \Delta\varepsilon$

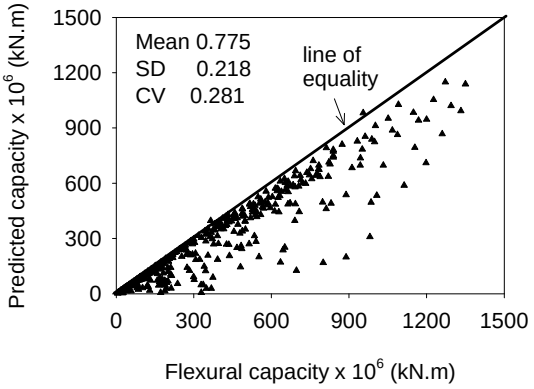

c)) $r = 0.50\ \Delta\varepsilon$

Fig. 5-10. Effect of descending branch length on flexural capacity

5.5.6 Concrete stress-strain relationships

The relationship between the compression stress, f_{cT}, and the corresponding mechanical strain, ε_{cT}, at elevated temperatures was studied by a number of researchers. Among the available models, Youssef and Moftah[2] proposed a stress-strain model that includes a simplified representation of transient creep strains (ε_{tr}) and better matches the available experimental data. It is also consistent with the stress-strain relationship recommended by Eurocode 2[10]. Youssef and Moftah's concrete stress-strain relationship, up to the peak stress (f'_{cT}), is given by Eq. (8a).

The descending branch of $f_{cT} - \varepsilon_{cT}$ relationship depends on the level of confinement provided by transverse reinforcement. Youssef and Moftah proposed a comprehensive post-peak behavior, which includes a linear descending branch followed by a constant stress zone at $0.2\, f'_{cT}$. Meda et al.[13] assumed a constant post-peak behavior up to ε_{uT}. A general and simple approach to estimate the $f_{cT} - \varepsilon_{cT}$ descending branch is proposed by Eurocode 2 and represented by Eq. (8b). The full curve of Eurocode 2 is adopted in this study due to its simplicity and ease of implementation in the proposed method. Fig. 5-8 shows the application of Eq. (8) at three average temperatures ($T_{avg} = 200$, 400, and 600 ℃). Eqs. (4) and (5) are used to calculate f'_{cT}/f'_{c} and $(\varepsilon_{oT} + \varepsilon_{tr})$, respectively.

$$f_{cT} = f'_{cT}\left[2\left(\frac{\varepsilon_{cT}}{\varepsilon_{oT}+\varepsilon_{tr}}\right) - \left(\frac{\varepsilon_{cT}}{\varepsilon_{oT}+\varepsilon_{tr}}\right)^2\right] \qquad \varepsilon_{cT} \le (\varepsilon_{oT} + \varepsilon_{tr}) \quad (8a)$$

$$= f'_{cT}\left[\frac{\varepsilon_{uT}-\varepsilon_{cT}}{0.02}\right] \qquad (\varepsilon_{oT} + \varepsilon_{tr}) < \varepsilon_{cT} \le \varepsilon_{uT} \quad (8b)$$

5.5.7 Steel stress-strain relationships

Lie et al.'s model[1] is used to predict the reduced yield strength of reinforcing bars (f_{yT}), Eq. (9), and the stress-strain ($f_{sT} - \varepsilon_{sT}$) relationship, Eq. (10).

$$f_{yT} = \left[1 + \frac{T}{900\ \ln(T/1750)}\right] f_y \qquad 0 < T \leq 600\ ℃ \tag{9a}$$

$$= \left[\frac{340 - 0.34\,T}{T - 240}\right] f_y \qquad 600 < T \leq 1000\ ℃ \tag{9b}$$

$$f_{sT} = \frac{f[T\,,0.001]}{0.001}\ \varepsilon_{sT} \qquad \varepsilon_{sT} \leq \varepsilon_p \tag{10a}$$

$$f_{sT} = \frac{f[T\,,0.001]}{0.001}\ \varepsilon_p + f\left[T\,,\left(\varepsilon_{sT} - \varepsilon_p + 0.001\right)\right] - f[T\,,0.001] \qquad \varepsilon_{sT} > \varepsilon_p \tag{10b}$$

$$\varepsilon_p = 4 \times 10^{-6}\, f_y \tag{10c}$$

$$f[T, 0.001] = (50 - 0.04\,T)\left[1 - e^{(-30 + 0.03\,T)\sqrt{0.001}}\right] \times 6.9 \tag{10d}$$

$$f\left[T\,,\left(\varepsilon_{sT} - \varepsilon_p + 0.001\right)\right] = (50 - 0.04\,T)\left[1 - e^{(-30 + 0.03\,T)\sqrt{\left(\varepsilon_{sT} - \varepsilon_p + 0.001\right)}}\right] \times 6.9 \tag{10e}$$

5.6 Evaluation of Concrete Internal Forces

The following sections propose a simplified approach to calculate concrete internal forces using the predicted T_{avg} distribution and material models presented earlier in this chapter.

5.6.1 Concrete strain profile

The average temperature profile (T_{avg}) is a function of the distance y. Utilizing the predicted T_{avg} distribution, ($\varepsilon_{oT} + \varepsilon_{tr}$) and $\varepsilon_{cT\,max}$ distributions can be evaluated using Eqs. (5) and (7), respectively. Fig. 5-11 shows these distributions for the column section shown in Fig. 5-1. A linear ε_{cT} distribution is assumed as follows

$$\varepsilon_{cT} = z_3\, y + z_4 \tag{11}$$

where z_3 and $z_4$are constants to define ε_{cT} variation in y direction. By varying z_3 and z_4, different ε_{cT} distributions are obtained. The flexural capacity occurs when the value of ε_{cT} at any point approaches maximum strain $\varepsilon_{cT\,max}$ at this location. Therefore, three possible failure scenarios should be considered in the sectional analysis [15]:

1) concrete fails at extreme top fibers of the section, i.e. $y = h$. The slope of ε_{cT} distribution (z_3) can take any value between zero (horizontal line) and the tangent of $\varepsilon_{cT\,max}$ profile at $y = h$, Figs. 5-11a and 5-11c.

2) concrete fails at the boundaries of the constant T_{avg} zone, i.e. $y = h - z$. The slope of ε_{cT} distribution (z_3) can take any value between infinity (vertical line) and the tangent of $\varepsilon_{cT\,max}$ profile at $y = h - z$.

3) concrete fails at any point between $y = h - z$ and $y = h$. In this case, ε_{cT} distribution is the tangent line of $\varepsilon_{cT\,max}$ profile, Figs. 5-11b and 5-11d.

5.6.2 Calculation of concrete internal forces and their locations

Average concrete compressive stresses $(f_{cT})_{avg}$ can be estimated using Eq. (8) and concrete mechanical strain ε_{cT}. These stresses are integrated over the section area to calculate the internal compression force in concrete (C_c) and its location (y), Eqs. (12) and (13).

$$C_c = \int_{y=(h-c)}^{h} (f_{cT})_{avg} \; b \; dy \tag{12}$$

$$C_c \, . \, y = \int_{y=(h-c)}^{h} (f_{cT})_{avg} \; b \; y \; dy \tag{13}$$

where b and h are the section width and depth (m), respectively and c is the neutral axis depth (m). $(f_{cT})_{avg}$ is the average concrete compressive stress (kPa) at different y values.

The following substitutions are made in Eqs. (12) and (13) to allow reaching a closed form solution: (1) $(f_{cT})_{avg}$ = Eq. (8), (2) $(\varepsilon_{oT} + \varepsilon_{tr})$ = Eq. (5), (3) f'_{cT} = Eq. (4), (5) ε_{uT} = Eq. (6), (5) T_{avg} = either a constant value or Eq. (3), and (6) ε_{cT} =Eq. (11). This solution is given by Eqs. (14) to (21), which are shown in the Appendix. For values of $\varepsilon_{cT} \leq (\varepsilon_{oT} + \varepsilon_{tr})$, two equations are given for the compressive force in concrete, Eqs. (14) and (18). They allow evaluating $C_{c\,o(v)}$ and $C_{c\,o(c)}$ for variable and constant T_{avg} distributions, respectively. The centroids of these compressive forces are given by Eqs. (15) and (19). For values of $\varepsilon_{cT} > (\varepsilon_{oT} + \varepsilon_{tr})$, the compressive force in concrete, $C_{c\,u(v)}$ or $C_{c\,u(c)}$, can be evaluated using Eqs. (16) and (20) for variable or constant T_{avg} distributions. The centroids of these forces are given by Eqs. (17) and (21).

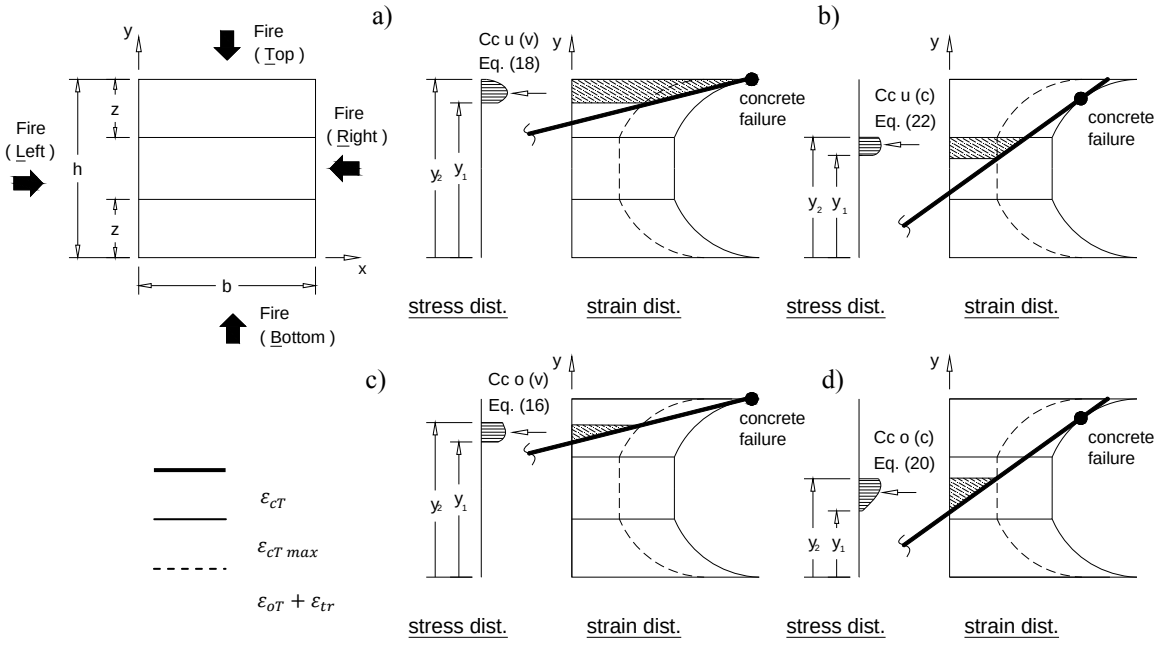

Fig. 5-11-Different cases for concrete internal compression force

Application of these equations is explained with reference to Fig. 5-11, which shows a four-face heated RC column section with four potential mechanical strain (ε_{cT}) distributions. z_1 and z_2 are constants of average temperature fitting equation, Eq. (3). z_3 and z_4 are constants defining the linear variation of ε_{cT} in y direction, Eq. (11). y_1 and y_2 define the location of internal concrete stresses used to calculate the corresponding force. Their values are determined for each case based on the assumed ε_{cT} distribution and using $(\varepsilon_{oT} + \varepsilon_{tr})$ and $\varepsilon_{cT\,max}$ profiles. A_1 and A_2 are constants equal to $e^{y_1\ z_2}$ and $e^{y_2\ z_2}$, respectively. The magnitude and location of $C_{c\,u(c)}$, Fig. 5-11b, are evaluated using Eqs. (20) and (21), respectively. The magnitude and location of $C_{c\,o(v)}$, Fig. 5-11c, are evaluated using Eqs. (14) and (15), respectively. The magnitude and location of $C_{c\,o(c)}$, Fig. 5-11d, are evaluated using Eqs. (18) and (19), respectively. The total internal compression force C_c is calculated by summing two or more components in Fig. 5-11.

5.6.3 Interaction Diagram

The interaction diagram for a fire-exposed RC column can be constructed using the following main steps. At specific fire duration,

1) an external axial load (P_{app}) is assumed.

2) an average temperature (T_{avg}) distribution is predicted using Eq. (3). Based T_{avg} distribution, ($\varepsilon_{oT} + \varepsilon_{tr}$) and $\varepsilon_{cT\,max}$ distributions are evaluated using Eqs. (5) and (7)

3) different linear mechanical strain (ε_{cT}) distributions are assumed, i.e. z_3 and z_4 in Eq. (11). For each ε_{cT} distribution, Eqs. (14) to (21) are used to calculate the corresponding concrete force and its location. Equilibrium is then conducted between internal forces in concrete and steel and the assumed external axial load, P_{app}. An iterative procedure requires changing z_3 and z_4 till force equilibriums is achieved.

4) the corresponding flexural capacity is calculated. For simplicity, P_{app} can be assumed acting at the heated section's centroid.

5) The above steps are repeated considering different axial loads and the corresponding flexural capacities are evaluated. These capacities define the interaction diagram of the analyzed column section at specific fire duration.

5.7 Illustrative Example

The 600 mm square column analyzed by Meda et al.[13], Fig. 5-12a, is used as an example to explain the proposed method. The column is reinforced by $24-20\,mm$ steel bars uniformly distributed with $40\,mm$ concrete cover to main reinforcement. The compressive and yield strength of the siliceous concrete and reinforcing bars are 40 MPa and 430 MPa, respectively. The column is subjected to a standard ISO 834 fire from four directions. Sectional analysis was used to predict the interaction diagram after $t=$ 0.0 hr, 1.5 hrs, and 3.0 hrs of fire exposure. The FDM mesh used for the heat transfer calculations is shown in Fig. 5-12a. The corresponding average temperature distribution is shown in Fig. 5-12b as discrete points**.** The interaction diagrams were constructed using the iterative method mentioned at the beginning of this chapter and are shown in Fig. 5-13. The proposed simplified method is used to predict the interaction diagram for the column section after $t=1.5\,hr$s of fire exposure. A simple excel spreadsheet was created to apply the following steps of the proposed method.

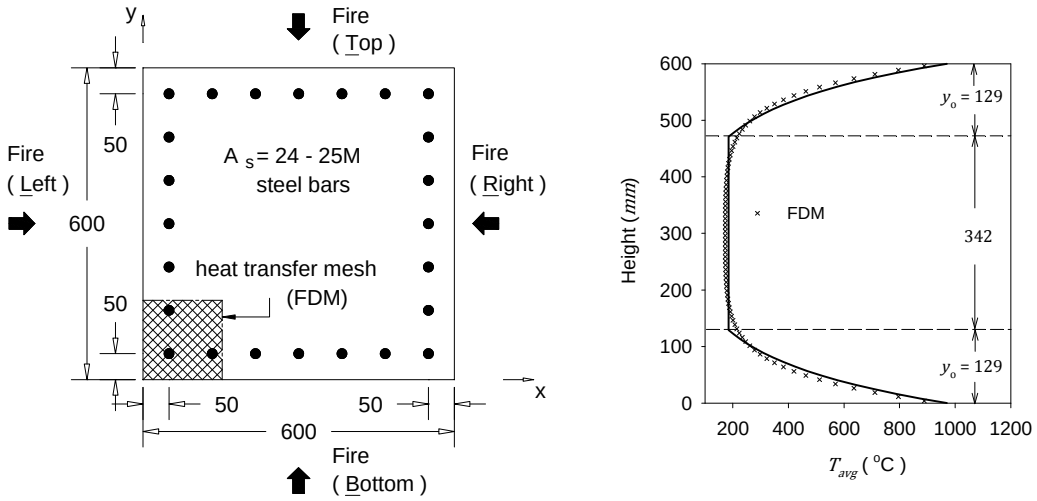

a) four-face heated RC section

b) T_{avg} dist.

Fig. 5-12. T_{avg} distribution of example RC column
[Dimensions in mm]

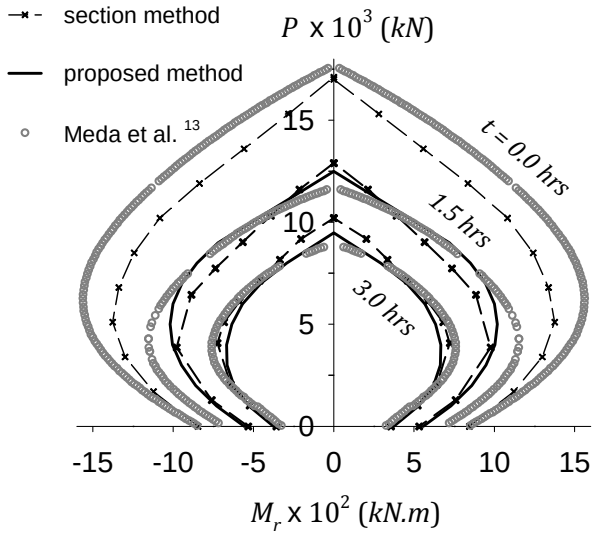

Fig. 5-13-*P*-*M* diagrams for example column

1) ISO 834 fire temperatures T_f of 986 ℃ is calculated. Γ is equal to 1 as no conversion is necessary.

2) n_w value of 0.96 is estimated.

3) z value of 0.129 for t of 1.5 hrs is calculated. Fig. 5-14 shows the different regions of the example column.

4) The average temperatures for each region are calculated as follows,
   z value of 0.129 is used to define the region boundaries. Substituting in the average temperature equation for R1 using $x_1 = 0.0\,m$, and $x_2 = 0.129\,m$ results in $T_{avg\,1} = 320 + 619\,n_y$. Substituting in the average temperature equation for R2 results in $T_{avg\,2} = 923\,n_y$.

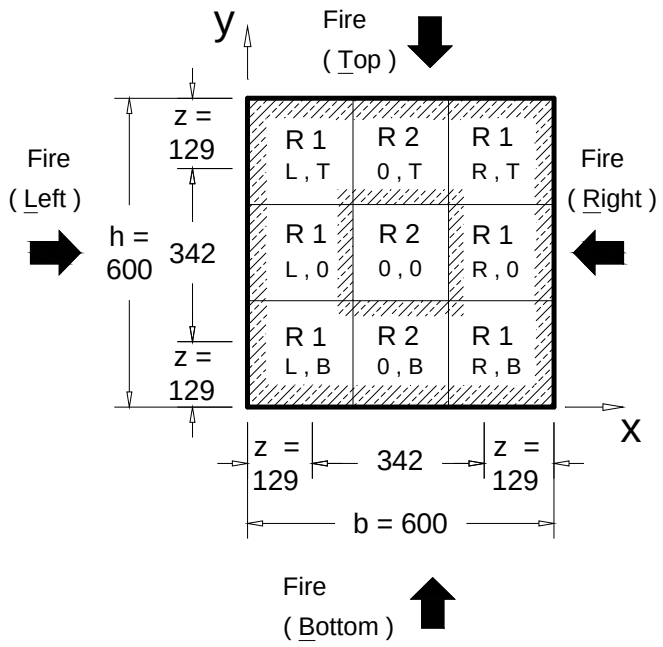

Fig. 5-14. Temperature calculation of a example column
[Dimensions in mm]

5) The ambient temperature (20 ℃) is added to the calculated average temperatures. Weighted average temperatures are then calculated at different values of y. The average temperature distribution is shown in Fig. 5-12b as a solid line. The figure shows that the values calculated using the developed simplified method matches the values predicted using the FDM method.

6) The constants (z_1 and z_2) of Eq. (3) are evaluated using values of T_{avg} at y_1 of $0.0\ m$ and y_2 of $0.129\ m$.

   The predicted T_{avg} distribution is used to plot ($\varepsilon_{oT} + \varepsilon_{tr}$) and $\varepsilon_{cT\,max}$ distributions along y direction using Eqs. (5) and (7), respectively, Fig. 5-15b.

7) A strain distribution is assumed as shown by the heavy line in Fig. 5-15b (z_3 and $z_4$of Eq. (11) are equal to 0.089 and -0.033, respectively). The line is tangent to the concrete crushing curve, which assumes that concrete crushing occurs at the point highlighted in Fig. 5-15b.

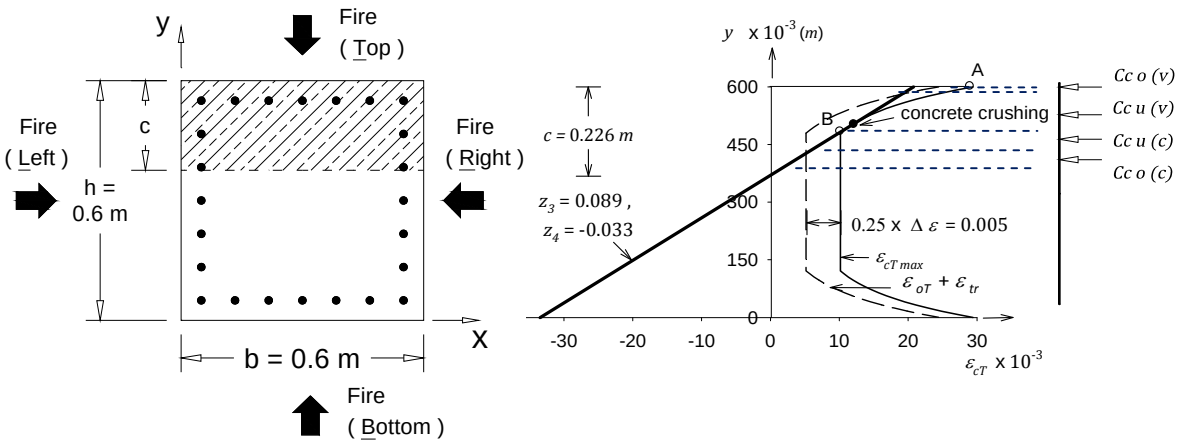

a) four-face heated RC section

b) ε_{cT} dist.

c) concrete forces

Fig. 5-15-Concrete internal compression force for example column

8) concrete compressive forces and corresponding centroids are calculated using expressions provided in Appendix I as follows:

a. For $y = 0.374 \rightarrow 0.421\ m$ [constant temperature and $\varepsilon_{cT} \leq (\varepsilon_{oT} + \varepsilon_{tr})$]

Eqs. (18) and (19) → $C_{c\,o\,(c)} = -745{,}905\ N$, $C_{c\,o\,(c)}.y = -301\ kN.m$ (i.e. $y = 0.404\ m$)

b. For $y = 0.421 \rightarrow 0.471\ m$ [constant temperature and $\varepsilon_{cT} > (\varepsilon_{oT} + \varepsilon_{tr})$]

Eqs. (20) and (21) → $C_{c\,u\,(c)} = -1{,}014{,}715\ N$, $C_{c\,u\,(c)}.y = -452\ kN.m$ (i.e. $y = 0.445\ m$)

c. For $y = 0.471 \rightarrow 0.581\ m$ [variable temperature and $\varepsilon_{cT} > (\varepsilon_{oT} + \varepsilon_{tr})$]

Eqs. (16) and (17) → $C_{c\,u\,(v)} = -1{,}520{,}285\ N$, $C_{c\,u\,(v)}.y = -789\ kN.m$ (i.e. $y = 0.519\ m$)

d. For $y = 0.581 \rightarrow 0.600\ m$ [variable temperature and $\varepsilon_{cT} \leq (\varepsilon_{oT} + \varepsilon_{tr})$]

Eqs. (14) and (15) → $C_{c\,o\,(v)} = -60{,}833\,N$, $C_{c\,o\,(v)}.y = -36\,kN.m$ (i.e. $y = 0.592\,m$)

9) The temperature of steel bars in the example column can be calculated using the Wickstrom method, explained in chapter 4. The calculated temperatures for steel bars are given in Table 5-2.

10) The steel stresses are calculated using Eq. (10) and given in Table 5-2.

11) The calculated concrete and steel forces are in equilibrium with external forces. The flexural capacity of the example column is predicted after $1.5\,hr$ ISO 834 fire exposure as $957\,kN.m$. The corresponding applied axial load (P_{app}) is calculated by summing the internal forces in concrete and steel (P_{app} is $3{,}000\,kN$).

The proposed method is repeated for the example RC column using different ε_{cT} distributions. The flexural capacity and corresponding axial load are calculated for each distribution. Fig. 5-13 shows the interaction diagrams for the example column at $1.5\,hr$ and $3\,hrs$ fire exposures. The proposed method's predictions and the sectional analysis method results are in a good match. Meda et al.[13] overestimates the flexural capacity. This can be due to the approximate concrete stress-strain relationship used by Meda et al.[13].

Table 5-2-Calculation of steel internal forces

A_s (mm^2)	x (mm)	y (mm)	T_{xy} (℃)	ε_{sT}	$\frac{f_{yT}}{f_y}$	$f[T, 0.001]$ (MPa)	$f[T, (\varepsilon_{sT} - \varepsilon_p + 0.001)]$ (MPa)	f_{sT} (MPa)	P_s (kN)	$P_s . y$ $(kN.m)$
			Eq. (4)	Eq. (18)	Eq. (16)	Eq. (17d)	Eq. (17e)	Eq. (17a,b)	$f_{sT} \times A_s$	
600	50	50	559	0.029	0.46	65	170	217	130,028	6,501,391
600	133	50	342	0.029	0.77	116	241	325	195,071	9,753,525
600	217	50	342	0.029	0.77	116	241	325	195,071	9,753,525
300	300	50	342	0.029	0.77	116	241	325	97,535	4,876,763
600	50	133	342	0.021	0.77	116	236	320	191,761	25,561,774
600	50	217	342	0.014	0.77	116	225	308	185,048	40,099,867
600	50	300	342	0.007	0.77	116	195	279	167,236	50,170,885
600	50	383	342	-0.001	0.77	116	52	100	-59,970	-22,986,365
600	50	467	342	-0.008	0.77	116	205	289	-173,526	-80,984,368
600	50	550	559	-0.016	0.46	65	153	200	-119,815	-65,898,443
600	133	550	342	-0.016	0.77	116	228	312	-187,129	-102,920,724
600	217	550	342	-0.016	0.77	116	228	312	-187,129	-102,920,724
300	300	550	342	-0.016	0.77	116	228	312	-93,564	-51,460,362
									$\sum P_s =$	$\sum P_s . y =$
									340,617	-280,453,254

5.8 Validation

The proposed method is validated in this section by comparing its results with analytical and experimental results by others.

5.8.1 Law and Gillie (2010)

Fig. 5-16 shows a rectangular RC section subjected to a standard ISO 834 fire from three sides. Law and Gillie[5] constructed, using sectional analysis, the interaction diagrams for this section at $t = 1\ hr$ and $2\ hrs$. The distortion in the interaction diagrams is due to the change of plastic centroid location as a result of the uneven heating of the section during fire exposure. As shown in Fig. 5-17, the proposed method results are in close agreement with the results of Law and Gillie.

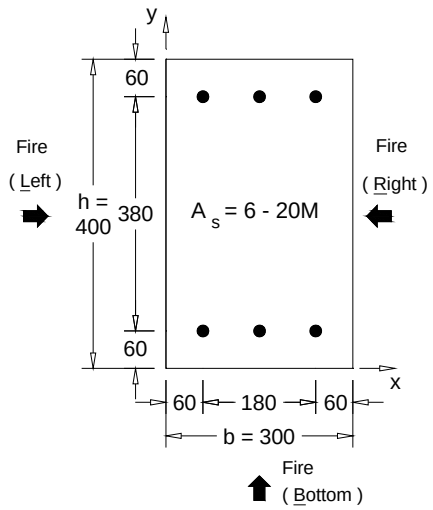

Fig. 5-16- Column section analyzed by Law and Gillie[5]

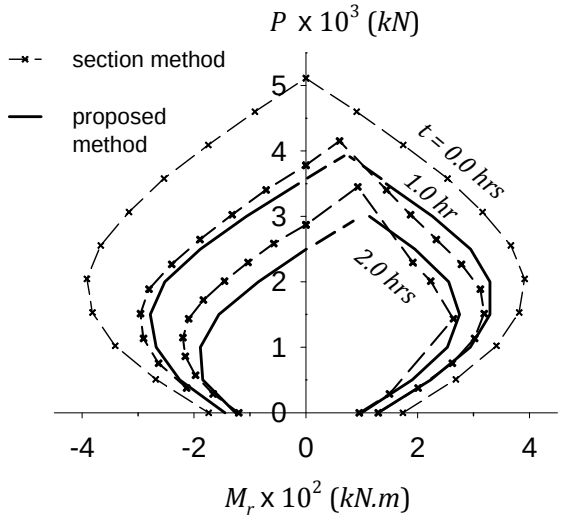

Fig. 5-17- *P-M* diagrams for Law and Gillie[5] column

5.8.2 Lie and Wollerton (1986)

Fig. 5-18a shows the cross-section and reinforcement for a RC column tested by Lie and Wollerton3. The tested column was subjected to a standard ASTM-E119 fire exposure under 25 mm eccentric load ($P = 1{,}000\ kN$), which was kept constant during the whole test. The fire endurance recorded at the end of the fire test was 181 min ($t = 3.0\ hrs$). The reinforcing steel cover was 48 mm and the end conditions of the tested column were pinned-pinned. Fig. 5-18b shows the predicted T_{avg} distribution through the section height. T_{avg} distribution does not include a constant distribution due to heating overlap from the Top and Bottom faces. Based on T_{avg} distribution, $(\varepsilon_{oT} + \varepsilon_{tr})$ and $\varepsilon_{cT\,max}$ profiles are calculated and are shown in Fig. 5-18b. A linear ε_{cT} distribution is then assumed, Fig. 5-18c, i.e. concrete crushing occurs at top fibers of the section. The internal forces and moments for concrete and steel are calculated using the equations provided in the appendix. Fig. 5-18d shows the values for internal concrete compressive forces and their locations. By conducting equilibrium between external and internal forces, the proposed method estimates a 25 mm eccentric load capacity of 890 kN, i.e. a small error of -11%.

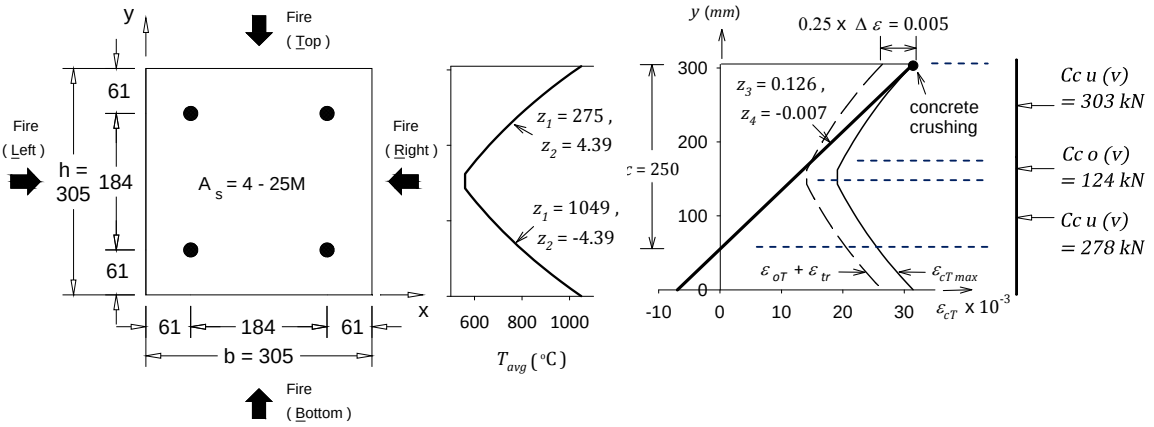

a) four-face heated RC section — b) T_{avg} dist. — c) ε_{cT} dist. — d) concrete forces

Fig. 5-18- Concrete internal compression force for Lie and Woollerton3 column

5.9 Summary and Conclusions

Interaction diagrams represent an efficient tool to predict the flexural capacity of RC columns at ambient and fire conditions. Sectional analysis method can be used to construct interaction diagrams for fire exposed RC columns. However, it is computationally expensive for design engineers as it requires dividing the column section into layers to conduct heat transfer and stress analysis during fire exposure. A simple technique to calculate an average 1D temperature distribution is presented and validated in this chapter. Based on this temperature distribution, the heated RC section is divided into different zones to conduct stress analysis. A number of approximations are assumed to allow integrating concrete stress-strain relationships with respect to mechanical strain and temperature distributions. The main assumptions include:

1) using a 1D average temperature distribution, i.e. T_{avg}, instead of 2D elevated temperature contours with the RC sections,

2) choosing an appropriate algebraic function to represent T_{avg} variation along the section height, i.e. Eq. (3),

3) using an integrable stress-strain constitutive relationships for concrete at elevated temperatures, i.e. Eq. (8), and

4) identifying the envelope for concrete failure strain by plotting the variation of maximum strain ($\varepsilon_{cT\ max}$) along section height, i.e. Eq. (7)

Mathematical expressions are then derived to calculate the internal compressive forces and their locations. Structural engineers can use these expressions to easily construct the interaction diagrams for fire exposed RC columns using first principles. The predictions of the proposed method are in good agreement with other analytical and experimental results.

5.10 Acknowledgments

This research was funded by the Natural Sciences and Engineering Research Council of Canada.

5.11 References

1. Lie, T.T., ed., "Structural Fire Protection", ASCE Manuals and Reports on Engineering Practice, no. 78, New York, NY, 1992, 241 pp.

2. Youssef, M.A. Moftah, M., "General stress-strain relationship for concrete at elevated temperatures", Engineering Structures, vol. 29, no. 10, 2007, pp. 2618-2634.

3. Lie, T. T., Woollerton, J. L., "Fire resistance of reinforced-concrete columns: Test results", Internal Rep. No. 569, 1998, National Research Council of Canada, Quebec, Canada.

4. Lie, T.T., Lin, T.D., Allen, D.E., Abrams, M.S., "Fire resistance of reinforced concrete columns", Technical Paper No. 378, 1984, Division of Building Research, National Research Council of Canada, Ottawa, Ontario, Canada.

5. Law, A., Gillie, M., “Interaction diagrams for ambient and heated concrete sections", Eng. Struct., vol. 32, no. 6, 2010, pp. 1641-1649.

6. Raut, N., Kodur, V.K.R., "Modeling the fire response of reinforced concrete columns under biaxial bending", ACI Struct. J., vol. 108, no. 6, 2011, pp. 1-24.

7. El-Fitiany, S.F., and Youssef, M.A., “Stress Block Parameters for Reinforced Concrete Beams During Fire Events,” Innovations in Fire Design of Concrete Structures, ACI SP-279, 2011, pp. 1-39.

8. El-Fitiany, S., Youssef, M.A., "Assessing the flexural and axial behaviour of reinforced concrete members at elevated temperatures using sectional analysis", Fire Safety Journal, vol. 44, no. 5, 2009, pp. 691-703.

9. El-Fitiany S.F. and Youssef M.A., “A Simplified Sectional Analysis Approach for RC Elements during Fire Events”, 6th International Conference on Structures in Fire, Michigan State University in East Lansing, MI, 2010, pp. 239-246.

10. Eurocode 2, “Design of concrete structures", ENV EC2, 1992.

11. Wickstrom, U., "A very simple method for estimating temperature in fire exposed concrete structures", Fire Technology Technical report SP-RAPP 1986, 46, Swedish National Testing Institute, pp. 186-194.

12. Terro, M.J., "Numerical modeling of the behavior of concrete structures in fire", ACI Struct. J., vol. 95, no. 2, 1998, pp. 183-193.

13. Meda, Alberto, G. Gambarova, Pietro, Bonomi, Marco, "High-Performance Concrete in Fire-Exposed Reinforced Concrete Sections ", ACI Struct. J., vol. 99, no. 3, 2002, pp. 277-287.

14. Elbahy Y.I., Youssef M.A., Nehdi M., “Stress Block Parameters for Concrete Flexural Members Reinforced with Superelastic Shape Memory Alloys”, Materials and Structures, vol. 42, no. 10, 2009, pp 1335-1351.

15. Caldas, Rodrigo Barreto, Sousa Jr., João Batista M., Fakurya, Ricardo Hallal, “Interaction diagrams for reinforced concrete sections subjected to fire", Eng. Struct., vol. 32, no.9, 2010, pp. 2832–2838.

5.12 Appendix I

The following symbols are used in this appendix:

ε_{uT} = ultimate compressive strain of concrete, Eq. (10)

$\Delta\varepsilon_1$ = difference between ε_{uT} and $(\varepsilon_{oT} + \varepsilon_{tr})$ equals to 0.02

b = column width in x direction

$C_{c\,o\,(v)}$ = concrete compression force at $\varepsilon_{cT} \leq (\varepsilon_{oT} + \varepsilon_{tr})$ for variable T_{avg} distribution

$C_{c\,o\,(v)}\,.\,y$ = concrete moment about x axis at $\varepsilon_{cT} \leq (\varepsilon_{oT} + \varepsilon_{tr})$ for variable T_{avg} distribution

$C_{c\,u\,(v)}$ = concrete compression forces at $\varepsilon_{cT} > (\varepsilon_{oT} + \varepsilon_{tr})$ for variable T_{avg} distribution

$C_{c\,u\,(v)}\,.\,y$ = concrete moment about x axis at $\varepsilon_{cT} > (\varepsilon_{oT} + \varepsilon_{tr})$ for variable T_{avg} distribution

$C_{c\,o\,(c)}$ = concrete compression force corresponding to $\varepsilon_{cT} \leq (\varepsilon_{oT} + \varepsilon_{tr})$ for constant T_{avg}

$C_{c\,o\,(c)}\,.\,y$ = concrete moment about x axis at $\varepsilon_{cT} \leq (\varepsilon_{oT} + \varepsilon_{tr})$ for constant T_{avg}

$C_{c\,u\,(c)}$ = concrete compression force corresponding to $\varepsilon_{cT} > (\varepsilon_{oT} + \varepsilon_{tr})$ for constant T_{avg}

$C_{c\,u\,(c)}\,.\,y$ = concrete moment about x axis at $\varepsilon_{cT} > (\varepsilon_{oT} + \varepsilon_{tr})$ for constant T_{avg}

f'_c = concrete compressive strength at ambient condition

x, y = horizontal and vertical coordinates for any point within the column section, origin located at bottom left of the section

y_1, y_2 = boundaries of internal concrete compression force measured in y direction

z_1, z_2 = constants of average temperature fitting equation, Eq. (7)

z_3, z_4 = constants define the linear variation of mechanical strain (ε_{cT}) in y direction, Eq. (15)

A_1 $e^{y_1 \ z_2}$

A_2 $e^{y_2 \ z_2}$

$$C_{c\,o(v)} = 2\,C_{c\,o(v)\,L} - C_{c\,o(v)\,N} \tag{14a}$$

$$C_{c\,o(v)\,L} = \left(\frac{1}{30.465}\,\frac{b\;\;f'_c}{{z_2}^2\,z_1}\right)[\tag{14b}$$

$$-\left({A_2}^2\,y_2 - {A_1}^2\,y_1\right) \times 1065\,{z_1}^3\,z_3\,z_2$$
$$+(A_2\,y_2 - A_1\,y_1) \times 3630767\,{z_1}^2\,z_3\,z_2$$

$$+\left({A_2}^2 - {A_1}^2\right) \times 1065\,{z_1}^3\,(0.5\,z_3 - z_4\,z_2)$$
$$+(A_2 - A_1) \times 3630767\,{z_1}^2\,(z_4\,z_2 - z_3)$$

$$+\left(\frac{y_2}{A2} - \frac{y_1}{A_1}\right) \times 1210.981 \times 10^9\;\; z_3\,z_2$$

$$+\left(\frac{1}{A_2} - \frac{1}{A_1}\right) \times 1210.981 \times 10^9\,(\,z_3 + z_4\,z_2)$$

$$-({y_2}^2 - {y_1}^2) \times 1515.812 \times 10^5 z_1\,z_3\,{z_2}^2$$

$$-(y_2 - y_1) \times 3031.623 \times 10^5\,z_1\,z_4\,{z_2}^2]$$

$$C_{c\,o(v)\,N} = \left(\frac{5.21026\ \ b\ \ f'_c}{{z_2}^3\,{z_1}^2}\right)[\tag{14c}$$

$$+\left(\frac{{y_2}^2}{{A_2}^2}-\frac{{y_1}^2}{{A_1}^2}\right)\times 1.5137262\times 10^{14}\,{z_3}^2\,{z_2}^2$$

$$+\left(\frac{y_2}{{A_2}^2}-\frac{y_1}{{A_1}^2}\right)\times 3.0274525\times 10^{14}(\,z_3\,z_4\,{z_2}^2+0.5\,{z_3}^2\,z_2)$$

$$+\left(\frac{1}{{A_2}^2}-\frac{1}{{A_1}^2}\right)\times 1.5137262\times 10^{14}(z_3\,z_4\,z_2+0.5\,{z_3}^2+{z_4}^2\,{z_2}^2)$$

$$+\left(\frac{{y_2}^2}{A_2}-\frac{{y_1}^2}{A_1}\right)\times 7.579058\times 10^{10}\,z_1\,{z_3}^2\,{z_2}^2$$

$$+\left(\frac{y_2}{A_2}-\frac{y_1}{A1}\right)\times 1.5158116\times 10^{11}(z_1\,{z_3}^2\,z_2+z_1\,z_3\,z_4\,{z_2}^2)$$

$$+\left(\frac{1}{A_2}-\frac{1}{A_1}\right)\times 1.5158116\times 10^{11}(z_1\,z_3\,z_4\,z_2+0.5\,z_1\,{z_4}^2\,{z_2}^2+z_1\,{z_3}^2)$$

$$-(A_2\,{y_2}^2-A_1\,{y_1}^2)\times 532.5016\times 10^3\,{z_1}^3\,{z_3}^2\,{z_2}^2$$

$$+(A_2\,y_2-A_1\,y_1)\times 1065.0032\times 10^3(\,{z_1}^3\,{z_3}^2\,z_2-{z_1}^3\,z_3\,z_4\,{z_2}^2)$$

$$+(A_2-A_1)\times 1065.0032\times 10^3({z_1}^3\,z_3\,z_4\,z_2-0.5{z_1}^3\,{z_4}^2\,{z_2}^2-{z_1}^3\,{z_3}^2)$$

$$+({y_2}^3-{y_1}^3)\times 3.025639\times 10^8\,{z_1}^2\,{z_3}^2\,{z_2}^3$$

$$+({y_2}^2-{y_1}^2)\times 9.0769173\times 10^8\,{z_1}^2\,z_3\,{z_2}^3\,z_4$$

$$+(y_2-y_1)\times 9.0769173\times 10^8\,{z_1}^2\,{z_4}^2\,{z_2}^3]$$

$$C_{c\,o(v)}.y \;=\; 2\,C_{c\,o(v)\,L}.y - \;C_{c\,o(v)\,N}.y \tag{15a}$$

$$C_{c\,o(v)\,L}.y \;= \left(\frac{1}{9.1395}\frac{b\;\;f'_c}{{z_2}^3\,z_1}\right)[\tag{15b}$$

$$-\left({A_2}^2\,{y_2}^2 - {A_1}^2\,{y_1}^2\right) \times 3195 \times 10^{-4}\;\;{z_1}^3\,z_3\,{z_2}^2$$

$$+(A_2\,{y_2}^2 - A_1\,{y_1}^2) \times\; 1.08923 \times 10^3\;\;{z_1}^2\,z_3\,{z_2}^2$$

$$+\left({A_2}^2\,y_2 - {A_1}^2\,y_1\right) \times 3195 \times 10^{-4}\,{z_1}^3\,z_2\,(z_3 - z_4\,z_2)$$

$$+\left({A_2}^2 - {A_1}^2\right) \times 15975 \times 10^{-5}\,{z_1}^3(z_4\,z_2 - z_3)$$

$$+(A_2\,y_2 - A_1\,y_1) \times 1.08923 \times 10^3\,{z_1}^2\,z_2\,(-2\;\;z_3 +\;\;z_4\,z_2\;)$$

$$+\left(\frac{{y2}^2}{A_2} - \frac{{y1}^2}{A_1}\right) \times 3.632943 \times 10^8\,z_3\,{z_2}^2$$

$$+\left(\frac{y_2}{A_2} - \frac{y_1}{A_1}\right) \times 3.632943 \times 10^8(2\;\;z_3\,z_2 +\;\;z_4\,{z_2}^2\;)$$

$$+\left(\frac{1}{A_2} - \frac{1}{A_1}\right) \times 3.632943 \times 10^8(2\,z_3 +\;\;z_4\,z_2)$$

$$+(A_2 - A_1) \times 1.08923 \times 10^3(2\;\;{z_1}^2\,z_3 -\;\;{z_1}^2\,z_4\,z_2)$$

$$-({y_2}^2 - {y_1}^2) \times 4.547435 \times 10^4\,z_1\,z_4\,{z_2}^3 +$$

$$-({y_2}^3 - {y_1}^3) \times 3.031623 \times 10^4\;\;z_1\,z_3\,{z_2}^3]$$

$$C_{c\,o(v)\,N}\,.y\; = \left(\frac{5.21026\,b\;\;f'c}{{z_2}^4\,{z_1}^2}\right)[\tag{15c}$$

$$+({y_2}^4 - {y_1}^4) \times 2.2692293 \times 10^5\,{z_3}^2\,{z_2}^4\,{z_1}^2$$

$$+\left(\frac{{y_2}^3}{{A_2}^2} - \frac{{y_1}^3}{{A_1}^2}\right) \times 1.5137262 \times 10^{11}\;\;{z_3}^2\,{z_2}^3$$

$$+({y_2}^3 - {y_1}^3) \times 6.0512782 \times 10^5\,z_3\,{z_2}^4\,z_4\,{z_1}^2$$

$$-(A_2\,{y_2}^3 - A_1\,{y_1}^3) \times 532.5016\;\;{z_1}^3\,{z_3}^2\,{z_2}^3$$

$$+\left(\frac{{y_2}^3}{A_2} - \frac{{y_1}^3}{A_1}\right) \times 7.57906 \times 10^7\;\;z_1\,{z_3}^2\,{z_2}^3$$

$$+\left(\frac{{y_2}^2}{{A_2}^2} - \frac{{y_1}^2}{{A_1}^2}\right) \times 3.0274525 \times 10^{11}(\,z_3\,z_4\,{z_2}^3 + 0.75\,{z_3}^2\,{z_2}^2)$$

$$+\left(\frac{{y_2}^2}{A_2} - \frac{{y_1}^2}{A_1}\right) \times 1.5158116 \times 10^5(1.5\,z_1\,{z_3}^2\,{z_2}^2 + \;z_1\,z_3\,{z_2}^3\,z_4)$$

$$+(A_2\,{y_2}^2 - A_1\,{y_1}^2) \times 1065.0032\;(1.5\,{z_1}^3\,{z_3}^2\,{z_2}^2 - {z_1}^3\,z_3\,{z_2}^3\,z_4)$$

$$+({y_2}^2 - {y_1}^2) \times 4.5384586 \times 10^5\,{z_4}^2\,{z_2}^4\,{z_1}^2$$

$$+(A_2\,y_2 - A_1\,y_1) \times 532.5016\;(4\;\;{z_1}^3\,z_3\,z_4\,{z_2}^2 - 6\,{z_1}^3\,{z_3}^2\,z_2 - \;\;{z_1}^3\,{z_4}^2\,{z_2}^3)$$

$$+\left(\frac{y_2}{{A_2}^2} - \frac{y_1}{{A_1}^2}\right) \times 3.0274525 \times 10^{11}(\;\,z_3\,z_4\,{z_2}^2\;\; + 0.75\;\,{z_3}^2\,z_2 + 0.5\;\,{z_4}^2\,{z_2}^3)$$

$$+\left(\frac{y_2}{A_2} - \frac{y_1}{A_1}\right) \times 0.757906 \times 10^8(6\,z_1\,{z_3}^2\,z2 + 4\,z_1\,z_3\,z_4\,{z_2}^2 + \;z_1\,{z_4}^2\,{z_2}^3)$$

$$+\left(\frac{1}{{A_2}^2} - \frac{1}{{A_1}^2}\right) \times 0.756863 \times 10^{11}(1.5\,{z_3}^2 + \;{z_4}^2\,{z_2}^2 + 2\,z_3\,z_4\,z_2)$$

$$+\left(\frac{1}{A_2} - \frac{1}{A_1}\right) 0.757906 \times 10^8\;(4\,z_1\,z_3\,z_4\,z_2 + z_1\,{z_4}^2\,{z_2}^2 + 6\,z_1\,{z_3}^2)$$

$$+(A_2 - A_1) \times 532.5016\;(-4\;\;{z_1}^3\,z_3\,z_4\,z_2 + \;{z_1}^3\,{z_4}^2\,z_2^2 + 6\,{z_1}^3\,{z_3}^2)]$$

$$C_{c\,u\,(v)} = \left(\frac{1}{2.67609}\frac{b\ \ f'_c}{{z_2}^2\,\Delta\varepsilon}\right)[\tag{16}$$

$$+({y_2}^2 - {y_1}^2) \times 1.3403194 \times 10^6\ z_3\ {z_2}^2$$

$$+(A_2\ y_2 - A_1\ y_1) \times 6.71083 \times 10^2\ z_1\ z_3\ z_2$$

$$+\left({A_2}^3\ y_2 - {A_1}^3\ y_1\right) \times 1.571667 \times 10^{-3}\ {z_1}^3\ z_3\ z_2$$

$$-\left({A_2}^2\ y_2 - {A_1}^2\ y_1\right) \times 4.01855\ \ {z_1}^2\ z_3\ z_2$$

$$-\left({A_2}^4 - {A_1}^4\right) \times 2.97045 \times 10^{-8}\ {z_1}^4\ z_2$$

$$+\left({A_2}^3 - {A_1}^3\right) \times (-5.23889 \times 10^{-4}\ {z_1}^3\ z_3 + 3.607829 \times 10^{-5}\ {z_1}^3\ z_2$$

$$+ 1.571667 \times 10^{-3}\ {z_1}^3\ z_4\ z_2)$$

$$+\left({A_2}^2 - {A_1}^2\right) \times 4.01855\ (0.5\ {z_1}^2\ z_3 -\ {z_1}^2\ z_4\ z_2)$$

$$+\left({A_2}^2 - {A_1}^2\right) \times 7.191535 \times 10^{-2}\ {z_1}^2\ z_2$$

$$+(A_2 - A_1) \times 6.71083 \times 10^2(-\ z_1\ z_3 +\ z_1\ z_4\ z_2)$$

$$-(A_2 - A_1) \times 80.97376\ \ z_1\ z_2\ \ ]$$

$$C_{c\,u\,(v)}\,.y\; = \left(\frac{1}{3.2113}\frac{-b\;\; f'_c}{{z_2}^3\,\Delta\varepsilon}\right)[\tag{17}$$

$$-({y_2}^3 - {y_1}^3) \times 1.0722555 \times 10^3\; z_3\; {z_2}^3$$

$$+({y_2}^2 - {y_1}^2) \times 32.16767(-50\; z_4\; {z_2}^3 +\; {z_2}^3)$$

$$+\left({A_2}^2\; {y_2}^2 - {A_1}^2\; {y_1}^2\right) \times 4.82226 \times 10^{-3}\; {z_1}^2\; z_3\; {z_2}^2$$

$$-\left({A_2}^3\; {y_2}^2 - {A_1}^3\; {y_1}^2\right) \times 1.886 \times 10^{-6}\; {z_1}^3\; z_3\; {z_2}^2$$

$$-(A_2\; {y_2}^2 - A_1\; {y_1}^2) \times 0.8053\;\; z_1\; z_3\; {z_2}^2$$

$$+\left({A_2}^2\; y_2 - {A_1}^2\; y_1\right) \times 4.82226 \times 10^{-3}(-\,{z_1}^2\; z_3\; z_2 + {z_1}^2\; z_4\; {z_2}^2)$$

$$-\left({A_2}^2\; y_2 - {A_1}^2\; y_1\right) \times 8.62984 \times 10^{-5}\; {z_1}^2\; {z_2}^2$$

$$+\left({A_2}^3\; y_2 - {A_1}^3\; y_1\right) \times 1.257334 \times 10^{-6}(\,{z_1}^3\; z_3\; z_2 - 1.5\; {z_1}^3\; z_4\; {z_2}^2)$$

$$-\left({A_2}^3\; y_2 - {A_1}^3\; y_1\right) \times 4.3294 \times 10^{-8}\; {z_1}^3\; {z_2}^2$$

$$+(A_2\; y_2 - A_1\; y_1) \times 0.8053\; (-\,z_1\; z_4\; {z_2}^2 + 2\; z_1\; z_3\; z_2)$$

$$+(A_2\; y_2 - A_1\; y_1) \times 9.7169 \times 10^{-2}\; z_1\; {z_2}^2$$

$$+\left({A_2}^4\; y_2 - {A_1}^4\; y_1\right) \times 3.56454 \times 10^{-11}\; {z_1}^4\; {z_2}^2$$

$$+\left({A_2}^3 - {A_1}^3\right) \times 4.19113 \times 10^{-7}(1.5\; {z_1}^3\; z_4\; z_2 -\; {z_1}^3\; z_3)$$

$$+\left({A_2}^3 - {A_1}^3\right) \times 1.4431 \times 10^{-8}\; {z_1}^3\; z_2$$

$$+(A_2 - A_1) \times 0.8053\; (-0.5\; z_1\; z_3 +\; z_1\; z_4\; z_2)$$

$$-(A_2 - A_1) \times 9.7169 \times 10^{-2}\; z_1\; z_2$$

$$+\left({A_2}^2 - {A_1}^2\right) \times 2.4111 \times 10^{-3}(\;{z_1}^2\; z_3 -\; {z_1}^2\; z_4\; z_2)$$

$$+\left({A_2}^2 - {A_1}^2\right) \times 4.315 \times 10^{-5}\; {z_1}^2\; z_2\; - \left({A_2}^4 - {A_1}^4\right) \times 8.911 \times 10^{-12}\; {z_1}^4\; z_2]$$

$$C_{c\,o\,(c)} = (-1 \times 10^6\, b\, f'_{cT})\,[\,-\frac{1}{3}\,\frac{{z_3}^2}{{\varepsilon_{oT}}^2}\,({y_2}^3 - {y_1}^3) + \left(\frac{z_3}{\varepsilon_{oT}} - z_4\,\frac{z_3}{{\varepsilon_{oT}}^2}\right)({y_2}^2 - {y_1}^2) + \left(2\,\frac{z_4}{\varepsilon_{oT}} - \frac{{z_4}^2}{{\varepsilon_{oT}}^2}\right)(y_2 - y_1)\,] \quad (18)$$

$$C_{c\,o\,(c)}.y = (-1 \times 10^3\, b\, f'_{cT})[\,-\frac{1}{4}\,\frac{{z_3}^2}{{\varepsilon_{oT}}^2}\,({y_2}^4 - {y_1}^4) + \frac{1}{3}\left(2\,\frac{z_3}{\varepsilon_{oT}} - 2\,z_4\,\frac{z_3}{{\varepsilon_{oT}}^2}\right)({y_2}^3 - {y_1}^3) + \left(\frac{z_4}{\varepsilon_{oT}} - \frac{{z_4}^2}{2\,{\varepsilon_{oT}}^2}\right)({y_2}^2 - {y_1}^2)\,] \quad (19)$$

$$C_{c\,u\,(c)} = \left(\frac{-1\times10^6\, b\, f'_{cT}}{\Delta\varepsilon}\right)\left[\varepsilon_{uT}\,(y_2 - y_1) - \frac{1}{2}\,z_3\,({y_2}^2 - {y_1}^2) - z_4\,(y_2 - y_1)\right] \quad (20)$$

$$C_{c\,u\,(c)}.y = \left(\frac{-1\times10^3\, b\, f'_{cT}}{\Delta\varepsilon}\right)\left[-\frac{1}{3}\,z_3\,({y_2}^3 - {y_1}^3) + \frac{1}{2}\,(\varepsilon_{uT} - z_4)\,({y_2}^2 - {y_1}^2)\right] \quad (21)$$

Chapter 6

6 Fire Performance of RC Frames using Simplified Sectional Analysis

Fire initiates when combustible materials ignite. Then, it spreads horizontally and/or vertically depending on the compartment boundaries [1]. A temperature gradient is generated through exposed RC elements. These elevated temperatures cause the element's stiffness to degrade and produce thermal deformations [2]. Structural fire safety of RC structures is currently evaluated based on the fire ratings of single elements, i.e. columns, beams, walls, and slabs. However, the overall behavior of the structure during a fire should be assessed to ensure the safety of the occupants and the fire fighters during evacuation.

Fire testing is the most reliable approach to assess the fire endurance of a structure but its use for concrete frames is very limited [3]. This is mainly because of its cost, which makes it unsuitable for regular design. Finite Element (FE) tools are very powerful and capable of analyzing RC structures during fire events [4]. Drawbacks of using the FE method including: the need for a comprehensive computer program, the difficulty to comprehend its results and to identify potential modeling errors, and the long running time make it impractical for design engineers. To the best of the author's knowledge, simplified methods to analyze RC frames during fire exposure do not exist.

This chapter provides engineers with a practical approach to predict the fire response of statically determinate or indeterminate RC frames. The proposed method extends the work done by El-Fitiany and Youssef [5-8]. In this work, they proposed a sectional analysis method that converts the two-dimensional (2D) temperature distribution to an average one-dimensional (1D) temperature distribution and predicts the flexural behavior of the heated section at different axial load levels (λ). The chapter provides the derivation of closed form formulations for concrete flexural and axial stiffness, and the steps needed to apply these formulations to analyze RC frames during fire exposure. The proposed

method eliminates the need to divide a fire exposed section into finite elements or layers to conduct heat transfer and stress analyses. The proposed method is validated by comparing its predictions with experimental and analytical results by others.

6.1 Research Significance

Analysis of RC structures during fire events is usually conducted using numerical methods. However, they are computationally expensive, which limit their use for design engineers. This chapter presents a simple approach that can be used to predict the structural performance of fire-exposed RC frames. The method includes the derivation of a simple technique to calculate an average 1D temperature distribution for RC sections and a number of mathematical expressions to calculate the flexural and axial stiffnesses. The proposed method can be used by practitioners to conduct a quick assessment of the integrity of a fire exposed structure and to ensure the safety of emergency response teams during fire fighting. It can be easily applied using available commercial structural analysis software.

6.2 Proposed Method

Concrete has low thermal conductivity, which results in a steep temperature distribution near the heated faces and almost a constant temperature at the core of the heated section. Thus, the concrete strength becomes variable near the heated faces and constant at the inner concrete core. For a given fire duration, the proposed method can be applied using the following steps:

1. determining of an equivalent one-dimensional average temperature distribution for the cross-section of the heated elements.

2. identifying the needed constitutive models for the heated elements.

3. predicting the unrestrained thermal deformations for the heated elements.

4. evaluating the flexural and axial stiffnesses of the heated elements based on their axial forces and moments.

5. Analyzing the fire-exposed frame under the effect of the applied loads while accounting for the thermal deformations using linear elastic analysis. The flexural and axial stiffnesses obtained in step 4 are utilized in this step. The moments and axial forces are redistributed based on the assigned stiffness values.

6. Recalculating the flexural and axial stiffnesses in step 4 for the revised moments and axial forces obtained in step 5.

Steps 4, 5, and 6 are repeated until the change in the obtained axial forces and moments is less than an assumed tolerance. The following sections explain these steps.

6.3 Average Temperature Distribution

A simplified method to calculate the temperature distribution within a fire exposed concrete section was presented in chapter 4. In this method, the heated section is divided into regions of constant and variable temperatures and the average temperature (T_{avg}) profile is predicted based on the average temperature of each region. The predicted T_{avg} profile, Eq. (1), is used in the proposed method.

$$T_{avg} = z_1 \,.\, e^{(z_2 \,.\, y)} \tag{1}$$

where $z_1 = T_{avg\,(y=0.0)}$; and $z_2 = \frac{\ln\left[\frac{T_{avg\,(y=z)}}{z_1}\right]}{z}$

6.4 Concrete and Steel Constitutive Relationships

Fire temperature reduces the mechanical properties of concrete and steel. It also induces new strains, i.e. thermal and transient creep strains. The following sub-sections provide a brief summary of the concrete and steel models used in this chapter.

6.4.1 Concrete strains

The total concrete strain at elevated temperatures (ε) is composed of three terms: unrestrained thermal strain (ε_{th}), instantaneous stress related strain (ε_c), and transient creep strain (ε_{tr}). The total strain is given by Eq. (2).

$$\varepsilon = \varepsilon_{th} + \varepsilon_c + \varepsilon_{tr} \tag{2}$$

6.4.1.1 Thermal strains

The free thermal strain, ε_{th}, is a strain resulting from fire temperature and can be predicted using the Eurocode 2 model [10], Eq. (3).
For siliceous concrete:

$$\varepsilon_{th} = B_1 + B_2\left(T_{avg} - 20\right) + B_3\left(T_{avg} - 20\right)^3 \qquad 20\,℃ < T_{avg} \leq 720\,℃ \tag{3a}$$

$$= B_4 \qquad 720\,℃ < T_{avg}$$

where $B_1 = -1.8 \times 10^{-4}$, $B_2 = 9 \times 10^{-6}$, $B_3 = 2.3 \times 10^{-11}$, and $B_4 = 14 \times 10^{-3}$

For carbonate concrete:

$$\varepsilon_{th} = B_1 + B_2\left(T_{avg} - 20\right) + B_3\left(T_{avg} - 20\right)^3 \qquad 20\,℃ < T_{avg} \leq 824\,℃ \tag{3b}$$

$$= B_4 \qquad 824\,℃ < T_{avg}$$

where $B_1 = -1.2 \times 10^{-4}$, $B_2 = 6 \times 10^{-6}$, $B_3 = 1.4 \times 10^{-11}$, and $B_4 = 12 \times 10^{-3}$

6.4.1.2 Concrete strain at peak stress

The value of the instantaneous stress-related strain (ε_c) at the peak compressive stress (f'_{cT}), i.e. ε_{oT} , defines the stress-strain relationship during fire exposure. For loaded concrete, the effect of elevated temperatures on ε_{oT} is negligible[2]. Fig. 6-3 shows the variation of $\varepsilon_{oT} + \varepsilon_{tr}$ with fire temperature as proposed by Eurocode 2. The shown values of $\varepsilon_{oT} + \varepsilon_{tr}$ are consistent with Terro's model[11] within its validated temperature range, i.e. up to 600 ℃. A linear relationship, Eq. (8), is chosen to represent the Eurocode 2 recommendation. Such a relationship allows reaching a closed form solution while accounting for concrete nonlinearity.

$$\varepsilon_{oT} + \varepsilon_{tr} = 2.52 \times 10^{-5}\, T_{avg} \qquad 80\ ℃ < T_{avg} \leq 1200\ ℃ \qquad (4)$$

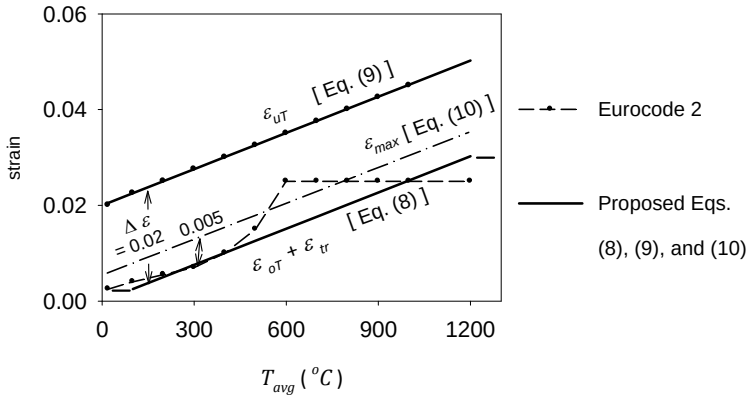

Fig. 6-1-Variation of ($\varepsilon_{oT} + \varepsilon_{tr}$) and ε_{uT} at elevated temperatures

6.4.1.3 Concrete ultimate strain

Concrete ultimate strain is the strain at which concrete crushing occurs. Elevated temperatures increase this strain. Eurocode 2 [10] proposes a linear relationship between ε_{uT} and T_{avg}, Fig. 6-3. This relationship can be represented by Eq. (9). ε_{uT} is defined in Eurocode 2 as the strain corresponding to zero compression stress. The difference between ε_{uT} and $\varepsilon_{oT} + \varepsilon_{tr}$ is constant and equal to 0.02.

$$\varepsilon_{uT} = 2.52 \times 10^{-5}\, T_{avg} + \Delta\varepsilon = \varepsilon_{oT} + \varepsilon_{tr} + 0.02 \quad (5)$$

6.4.1.4 Maximum concrete strain

The maximum concrete strain is defined as the strain corresponding to the maximum moment resistance. This strain is usually less than ε_{uT}. Elbahy et al.[13] studied the variation of this strain with the axial load level, λ, at ambient temperature. At elevated temperatures, a parametric study was conducted in the previous chapter to evaluate the compression strain ($\varepsilon_{cT\,max}$) corresponding to the flexural capacity at different λ values. Based on this parametric study, ε_{max} is given by Eq. (10).

$$\varepsilon_{cT\,max} = (\varepsilon_{oT} + \varepsilon_{tr}) + 0.005 \quad (6)$$

6.4.2 Concrete Compressive Strength

Concrete compressive strength experiences significant degradation at elevated temperatures. Eurocode 2 predicts the reduced compressive strength (f'_{cT}) for siliceous and carbonate concretes as a ratio from its ambient value (f'_{c}) [10]. The reduction in f'_{cT} for siliceous concrete is fitted by a polynomial equation, Eq. (11), as it allows reaching closed form solution for flexural stiffness.

$$f'_{cT}/f'_{c} = 1.76 \times 10^{-9}\, {T_{avg}}^{3} - 3 \times 10^{-6}\, {T_{avg}}^{2} + 2.5 \times 10^{-4}\, T_{avg} + 1.00 \quad (7)$$

where T_{avg} is the weighted average temperature, in ℃, calculated in previous section

6.4.3 Concrete Stress-Strain Relationships

The relationship between the compression stress, f_{cT}, and the corresponding mechanical strain, ε_{cT}, at elevated temperatures was studied by a number of researchers. Among the available models, Youssef and Moftah[2] proposed a stress-strain model that includes a simplified representation of transient creep strains (ε_{tr}) and better matches the available experimental data. It is also consistent with the stress-strain relationship recommended by Eurocode 2 [10]. Youssef and Moftah's concrete stress-strain relationship, up to the peak stress (f'_{cT}), is given by Eq. (12a).

A general and simple approach to estimate the $f_{cT} - \varepsilon_{cT}$ descending branch is proposed by Eurocode 2 [10] and represented by Eq. (12b). The Eurocode 2 descending curve is adopted in this study due to its simplicity and ease of implementation in the proposed method. Fig. 6-4 shows the application of Eq. (12) at three average temperatures ($T_{avg} =$ 200, 400, and 600 ℃). Eqs. (8) and (11) are used to calculate ($\varepsilon_{oT} + \varepsilon_{tr}$) and f'_{cT}/f'_{c}, respectively.

$$f_{cT} = f'_{cT}\left[2\left(\frac{\varepsilon_{cT}}{\varepsilon_{oT}+\varepsilon_{tr}}\right) - \left(\frac{\varepsilon_{cT}}{\varepsilon_{oT}+\varepsilon_{tr}}\right)^2\right] \qquad \varepsilon_{cT} \le (\varepsilon_{oT} + \varepsilon_{tr}) \qquad (8a)$$

$$= f'_{cT}\left[\frac{\varepsilon_{uT}-\varepsilon_{cT}}{0.02}\right] \qquad (\varepsilon_{oT} + \varepsilon_{tr}) < \varepsilon_{cT} \le \varepsilon_{uT} \qquad (8b)$$

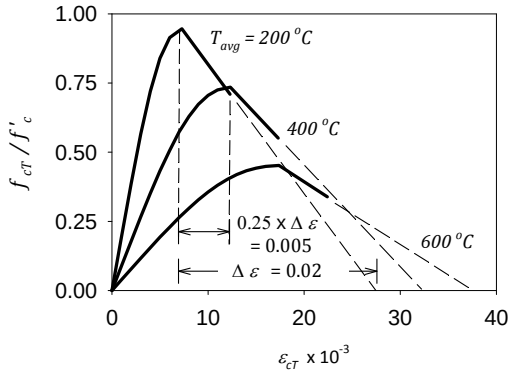

Fig. 6-2- Concrete stress-strain relationships at different elevated temperatures

6.4.4 Steel Stress-Strain Relationships

Lie et al.'s model[1] is used to predict the reduced yield strength of reinforcing bars (f_{yT}), Eq. (13), and the stress-strain ($f_{sT} - \varepsilon_{sT}$) relationship, Eq. (14).

$$f_{yT} = \left[1 + \frac{T}{900\ \ln(T/1750)}\right] f_y \qquad 0 < T \leq 600\ ℃ \tag{9a}$$

$$= \left[\frac{340 - 0.34\,T}{T - 240}\right] f_y \qquad 600 < T \leq 1000\ ℃ \tag{9b}$$

$$f_{sT} = \frac{f[T\,,0.001]}{0.001}\ \varepsilon_{sT} \qquad \varepsilon_{sT} \leq \varepsilon_p \tag{10a}$$

$$f_{sT} = \frac{f[T\,,0.001]}{0.001}\ \varepsilon_p + f\left[T\,,\left(\varepsilon_{sT} - \varepsilon_p + 0.001\right)\right] - f[T\,,0.001] \qquad \varepsilon_{sT} > \varepsilon_p \tag{10b}$$

$$\varepsilon_p = 4 \times 10^{-6}\, f_y \tag{10c}$$

$$f[T, 0.001] = (50 - 0.04\,T)\left[1 - e^{(-30 + 0.03\,T)\sqrt{0.001}}\right] \times 6.9 \tag{10d}$$

$$f\left[T\,,\left(\varepsilon_{sT} - \varepsilon_p + 0.001\right)\right] = (50 - 0.04\,T)\left[1 - e^{(-30 + 0.03\,T)\sqrt{\left(\varepsilon_{sT} - \varepsilon_p + 0.001\right)}}\right] \times 6.9 \tag{10e}$$

6.5 Prediction of the Unrestrained Deformation for a Heated Section

Fig. 6-5a shows a RC section subjected to fire from three faces. The average temperature (T_{avg}) distribution, Fig. 6-5b, can be calculated using the Finite Difference Method (FDM) or Eq. (5). T_{avg} induces thermal strains that can be evaluated using the following method:

1. The nonlinear thermal strain (ε_{th}) distribution, Fig. 6-5g, is calculated using T_{avg}. The thermal strain of steel bars is calculated based on the elevated temperature at their locations.

2. ε_{th} is then converted to an equivalent linear thermal strain ($\overline{\varepsilon_{th}}$), Fig. 6-5d, by considering self-equilibrium of internal thermal forces in concrete and steel layers. $\overline{\varepsilon_{th}}$ is represented by the value of the center axial strain (ε_i) and the curvature (ψ_i). ε_i and ψ_i define the unrestrained thermal deformation of a heated section.

3. Fig. 6-5f shows the differences between the equivalent linear and nonlinear thermal strains, which represent the self-induced thermal strains (ε_{st}). These strains are assigned as initial strains for the concrete and steel when calculating the flexural and axial stiffnesses. The following sections present a simplified approach to calculate ε_{st} using the predicted T_{avg} distribution and material models presented earlier in this chapter.

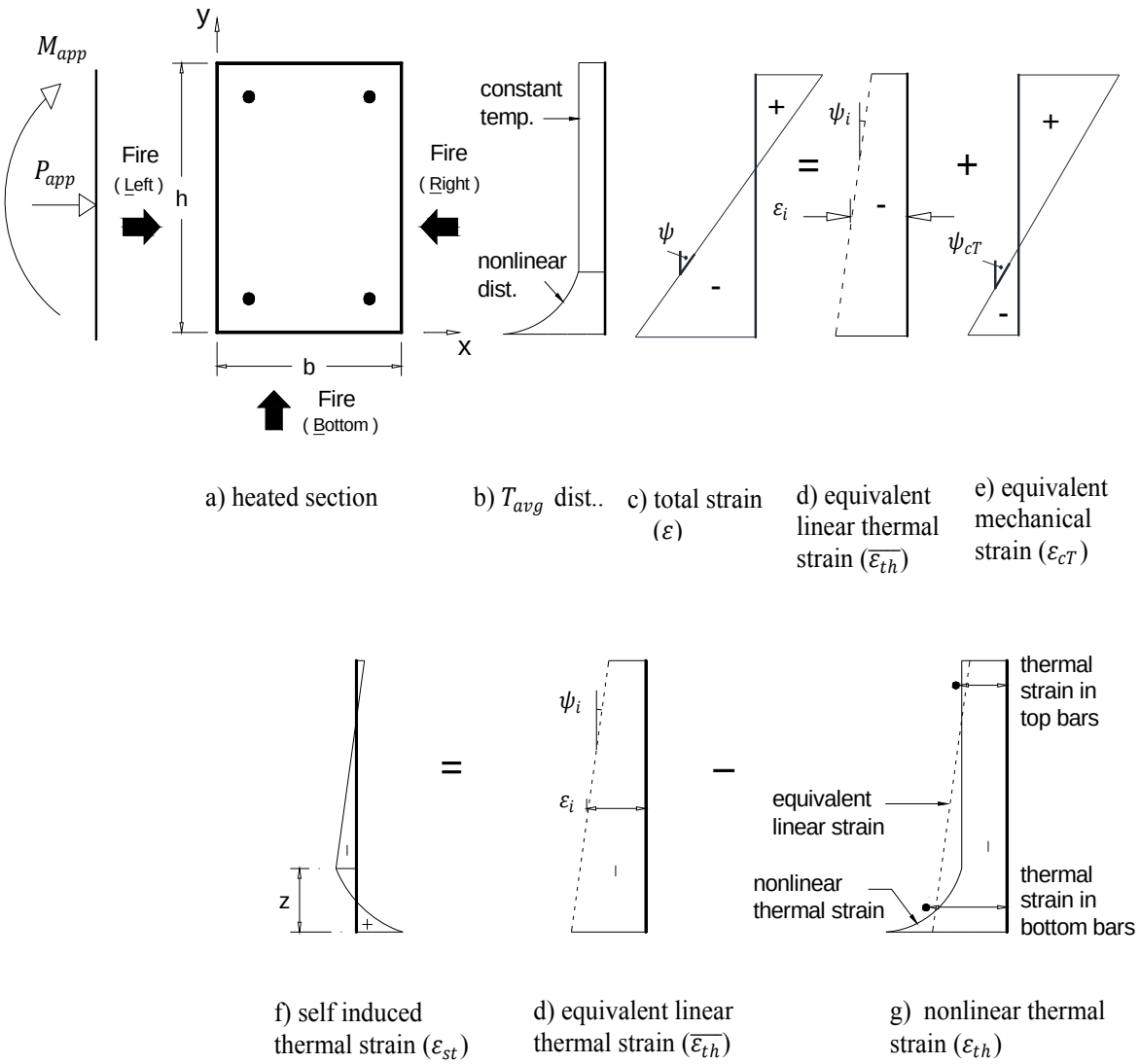

a) heated section

b) T_{avg} dist..

c) total strain (ε)

d) equivalent linear thermal strain ($\overline{\varepsilon_{th}}$)

e) equivalent mechanical strain (ε_{cT})

f) self induced thermal strain (ε_{st})

d) equivalent linear thermal strain ($\overline{\varepsilon_{th}}$)

g) nonlinear thermal strain (ε_{th})

Fig. 6-3-Sectional analysis approach for heated RC sections

6.5.1 Concrete strain profile

The average temperature profile (T_{avg}), Eq. (5), is a function of the distance y. Utilizing the predicted T_{avg} distribution, ($\varepsilon_{oT} + \varepsilon_{tr}$) distribution can be evaluated using Eq. (8). Fig. 6-6 shows these distributions for the concrete section subjected to fire from four faces. The difference between $\overline{\varepsilon_{th}}$ and ε_{th} represents the self-induced thermal strain (ε_{st}), Eq. (15).

$$\varepsilon_{st} = \overline{\varepsilon_{th}} - \varepsilon_{th} = (\bar{z}_3\, y + \bar{z}_4) - \varepsilon_{th} \tag{11}$$

where $\bar{z}_3$ and $\bar{z}_4$ are constants to define the linear variation of $\overline{\varepsilon_{th}}$ in y direction. ε_{th} is calculated using Eq. (7).

6.5.2 Calculation of concrete internal force and its location due to ε_{st}

Average concrete compressive stresses $(f_{cT})_{avg}$ can be estimated using Eq. (12) and self-induced strain ε_{st}. These stresses are integrated over the section area to calculate the internal compression force in concrete (C_{th}) and its location (y), Eqs. (16) and (17).

$$C_c \text{ (or } C_{th}) = \int_{y=(h-c)}^{h} (f_{cT})_{avg}\ b\ \ dy \tag{12}$$

$$C_c\,.\ y \text{ (or } C_{th}.y) = \int_{y=(h-c)}^{h} (f_{cT})_{avg}\ b\ y\ dy \tag{13}$$

where b and h are the section width and depth (m), respectively and c is the neutral axis depth (m). $(f_{cT})_{avg}$ is the average concrete compressive stress (kPa) at different y values.

To allow reaching a closed form solution, the following substitutions are made in Eqs. (16) and (17) to allow reaching a closed form solution: [1] $(f_{cT})_{avg}$ = Eq. (12), [2] $(\varepsilon_{oT} + \varepsilon_{tr})$ = Eq. (8), [3] f'_{cT} = Eq. (11), [4] ε_{uT} = Eq. (9), [5] T_{avg} = either a constant value or Eq. (5), and [6] ε_{cT} =Eq. (15).

As concrete stresses corresponding to ε_{st} are low compared to f'_{cT} and to simplify the closed form solution, the nonlinear term in concrete constitutive stress-strain relationship, Eq. (12), is neglected when integrating Eqs. (16) and (17) using Eq. (15). A parametric study is conducted later in this chapter to evaluate the error associated with this approximation. The closed form solutions of Eqs. (16) and (17) are given by Eqs. (21) to (26), which are shown in Appendix I.

Fig. 6-6 shows a four-face heated RC section with self-induced strain (ε_{st}) distribution. For variable T_{avg} distribution, two equations are given for the compressive force in concrete, Eqs. (21) and (23). They allow evaluating $C_{th\,c\,(v)}$ and $C_{th\,v\,(v)}$ for variable and uniform ε_{st} distributions, respectively. The centroids of these compressive forces are given by Eqs. (22) and (24). For constant T_{avg}, the compressive force in concrete, $C_{th\,c\,(c)}$, can be evaluated using Eq. (25) for uniform ε_{st} distribution. The centroid of this force is given by Eq. (26). Application of these equations is the same as explained in the previous section. The total internal compression force due to thermal incompatibility, C_{th}, is calculated by summing two or more components in Fig. 6-6.

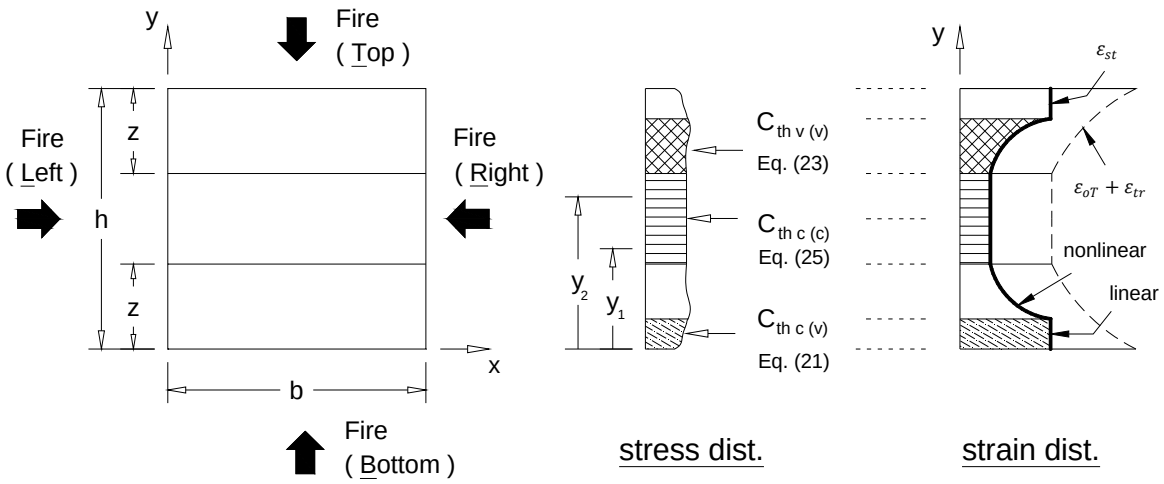

a) heated section

b) internal concrete forces

c) self induced thermal strain (ε_{st})

Fig. 6-4- Calculation of concrete internal forces corresponding to ε_{st}

6.6 Evaluation of the Flexural and Axial Stiffnesses for a Heated Section

A sectional analysis approach suitable for the analysis of rectangular RC sections at elevated temperatures was proposed by El-Fitiany and Youssef [6]. Fig. 6-5a shows the applied axial force (P_{app}) and moment (M_{app}) on a RC section exposed to fire from three faces. The use of sectional analysis to evaluate the flexural and axial stiffnesses for this section involves the following steps:

1. The self-induced thermal strains (ε_{st}), calculated in the previous section, are assigned as initial strains for the concrete and steel to model the corresponding self-induced self-equilibrating thermal stresses. The terms ε_{st} , ε_c , and ε_{tr} are lumped into an equivalent mechanical strain ε_{cT} , Eq. (18).

$$\varepsilon = \overline{\varepsilon_{th}} + \left(\varepsilon_{st} + \varepsilon_c + \varepsilon_{tr}\right) = \overline{\varepsilon_{th}} + \varepsilon_{cT} \tag{14}$$

2. For assumed values of ε_{cT} at the center of the section and ψ_{cT} , Eqs. (12) and (14) are used to evaluate the internal stresses in the concrete and steel, respectively. The corresponding internal axial forces are then calculated. Concrete tensile strength is neglected in the analysis. To satisfy equilibrium between the calculated internal forces and the external loads, i.e. P_{app} and M_{app}, iterations are executed by changing the values of center ε_{cT} and ψ_{cT} . This process can repeated for different values of M_{app}. A typical relationship between ψ_{cT} and M_{app}, for a constant P_{app}, is sketched in Fig. 6-7.

3. The secant slope of the $M-\psi_{cT}$ diagram represents the section's effective flexural stiffness (EI_{eff}) at M_{app} [8]. The corresponding effective axial stiffness (EA_{eff}) equals to P_{app} divided by the center axial strain (ε_{cT}).

As shown in Fig. 6-7, heating RC sections from the bottom face and the two sides cause the bottom concrete fibers to thermally expand more than the top concrete fibers and results in ψ_i . The acting moment induces a mechanical curvature (ψ_{cT}), which is either added to or deducted from ψ_i . As shown in Fig. 6-7a, a positive (sagging) moment

induces a curvature that adds to the initial curvature. For negative (hogging) moments, compression stresses are applied on the bottom fibers. Curvature caused by these stresses opposes the initial curvature, Fig. 6-7b. Such a moment-curvature diagram is similar to that of a prestressed concrete section. While the initial curvature in such a section is caused by prestressing, it results from the thermal expansion in a fire-exposed section [8].

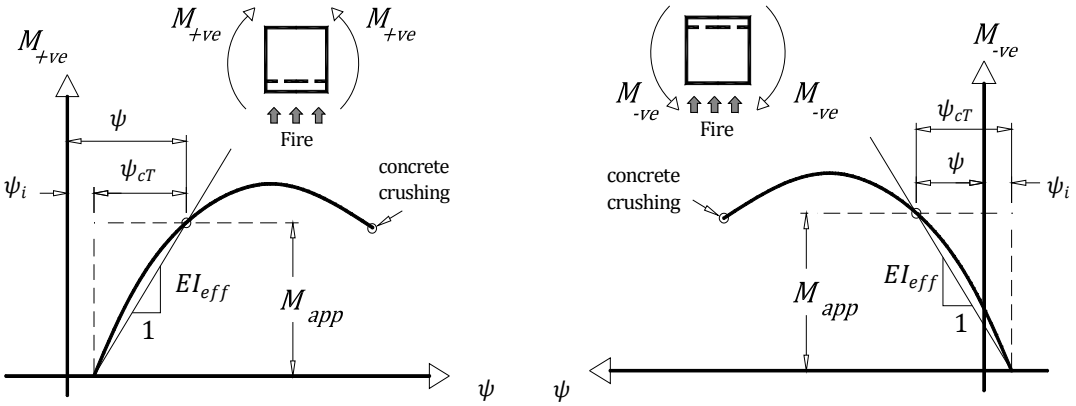

a) sagging moments (M_{+ve}) b) hogging moments (M_{-ve})

Fig. 6-5-(M)–(ψ) diagrams for RC sections during fire

For a specific fire duration, the effect of thermal strain on the M–ψ relationship is not governed by M_{app}. It represents the unrestrained/free thermal expansion of the unloaded concrete element and results in shifting the M–ψ and diagram by a value ψ_i, Fig. 6-7. Consequently, the total curvature (ψ) is the sum of the unrestrained thermal curvature (ψ_i) and the mechanical curvature (ψ_{cT}) and can be expressed in terms of the effective stiffness (EI_{eff}) as follows.

$$\psi = \psi_i + M_{app}/EI_{eff} \tag{15a}$$

Similarly, the total center axial strain (ε) is the sum of the unrestrained thermal strain (ε_i) and the center mechanical strain (ε_{cT}) and can be expressed in terms of the effective axial stiffness (EA_{eff}) as follows.

$$\varepsilon = \varepsilon_i + P_{app}/EA_{eff} \quad (15b)$$

The following sections present a simplified approach to calculate EI_{eff} and EA_{eff} using the predicted T_{avg} distribution and material models presented earlier in this chapter.

6.6.1 Concrete strain profile

The average temperature profile (T_{avg}), Eq. (5), is a function of the distance y. Utilizing the predicted T_{avg} distribution, $(\varepsilon_{oT} + \varepsilon_{tr})$ and $\varepsilon_{cT\,max}$ distributions can be evaluated using Eqs. (8) and (10), respectively. Fig. 6-8 shows these distributions for the concrete section subjected to fire from four faces. A linear ε_{cT} distribution is assumed as follows

$$\varepsilon_{cT} = z_3\, y + z_4 \quad (16)$$

where z_3 and z_4 are constants to define ε_{cT} variation in y direction. By varying z_3 and z_4, different ε_{cT} distributions are obtained. The flexural capacity occurs when the value of ε_{cT} at any point is equal to the maximum strain $\varepsilon_{cT\,max}$ at this point[12, 14].

6.6.2 Calculation of concrete internal force and its location due to ε_{cT}

Average concrete compressive stresses $(f_{cT})_{avg}$ can be estimated using Eq. (12) and concrete mechanical strain ε_{cT}. These stresses are integrated over the section area to calculate the internal compression force in concrete (C_c) and its location (y), Eqs. (16) and (17).

To allow reaching a closed form solution, the same substitutions used in the previous section are made in Eqs. (16) and (17) except for step [6] as using ε_{cT} = Eq. (20). This solution is given by Eqs. (27) to (34), which are shown in Appendix II. For values of $\varepsilon_{cT} \leq (\varepsilon_{oT} + \varepsilon_{tr})$, two equations are given for the compressive force in concrete, Eqs. (27) and (31). They allow evaluating $C_{c\,o(v)}$ and $C_{c\,o(c)}$ for variable and constant T_{avg} distributions, respectively. The centroids of these compressive forces are given by Eqs.

(28) and (32). For values of $\varepsilon_{cT} > (\varepsilon_{oT} + \varepsilon_{tr})$, the compressive force in concrete, $C_{c\,u(v)}$ or $C_{c\,u(c)}$, can be evaluated using Eqs. (29) and (33) for variable or constant T_{avg} distributions. The centroids of these forces are given by Eqs. (30) and (34).

Application of these equations is explained with reference to Fig. 6-8. z_1 and z_2 are constants of average temperature fitting equation, Eq. (5). z_3 and z_4 are constants defining the linear variation of ε_{cT} in y direction, Eq. (20). y_1 and y_2 define the location of internal concrete stresses used to calculate each force. Their values are determined for each case based on the assumed ε_{cT} distribution and using $(\varepsilon_{oT} + \varepsilon_{tr})$ and $\varepsilon_{cT\,max}$ profiles. A_1 and A_2 are constants equal to $e^{y_1\ z_2}$ and $e^{y_2\ z_2}$, respectively. The magnitude and location of $C_{c\,u(c)}$, Fig. 6-8b, are evaluated using Eqs. (33) and (34), respectively. The magnitude and location of $C_{c\,o(v)}$, Fig. 6-8a, are evaluated using Eqs. (27) and (28), respectively. The magnitude and location of $C_{c\,u(v)}$, Fig. 6-8a, are evaluated using Eqs. (29) and (30), respectively. The magnitude and location of $C_{c\,o(c)}$, Fig. 6-8b, are evaluated using Eqs. (31) and (32), respectively. The total internal compression force C_c is calculated by summing two or more components in Fig. 6-8.

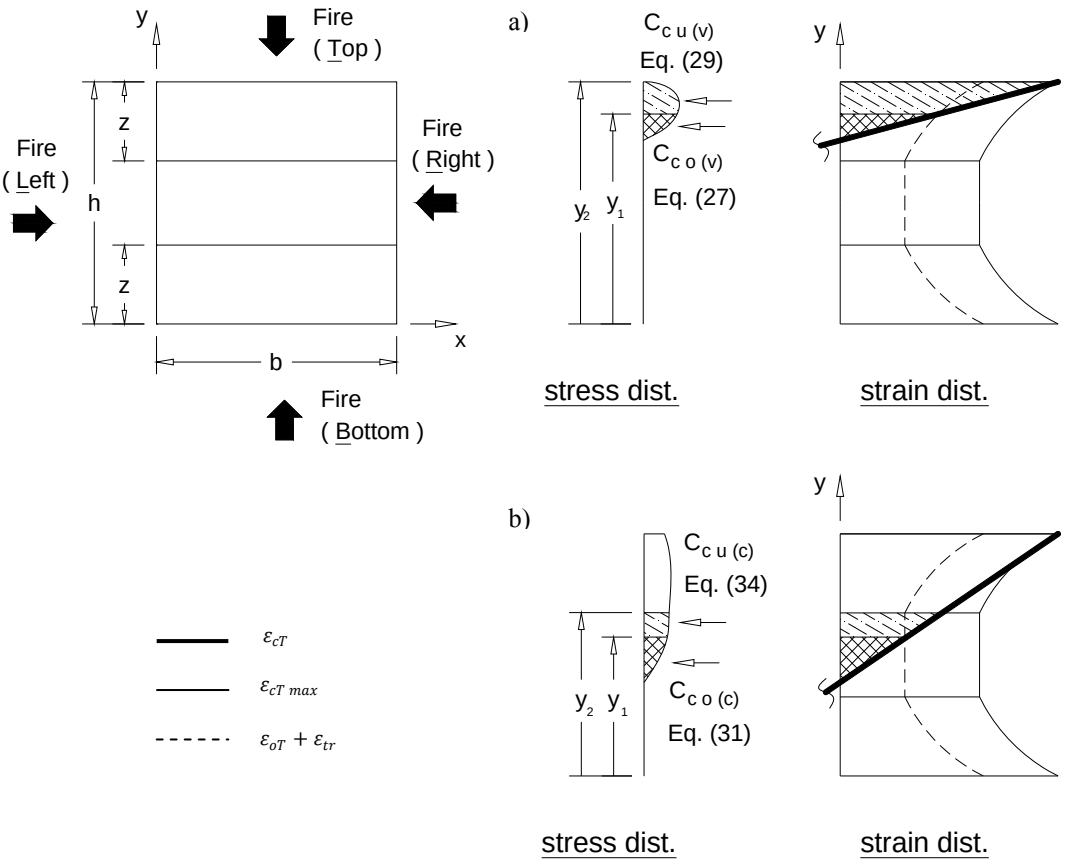

Fig. 6-6- Calculation of concrete internal forces corresponding to ε_{cT}

6.6.3 Calculation of concrete internal force and its location due to ε_{cT} and ε_{st}

ε_{st} can be considered as an initial/residual strain that is added to the mechanical strain ε_{cT} when calculating internal forces in concrete and steel. ε_{st} is to be divided into a series of straight lines, Fig. 6-6c. These lines can be then superimposed with ε_{cT} distribution, Eq. (20). This simplification allows using Eqs. (27) to (34) after modifying z_3 and z_4 only to account for ε_{st}. The modified ε_{cT} distribution consists of different zones based on ε_{st} idealization. Internal concrete and steel forces in each zone are calculated based on z_3 and z_4 for this zone.

6.7 Prediction of the Behaviour of RC Frames during Fire Exposure

The behavior of RC frames at specific fire duration can be predicted using the following main steps. These steps are applied for all fire-exposed RC members.

1) an average temperature (T_{avg}) distribution is predicted using Eq. (5). Based T_{avg} distribution, ($\varepsilon_{oT} + \varepsilon_{tr}$) and $\varepsilon_{cT\,max}$ distributions are evaluated using Eqs. (8) and (10)

2) an equivalent linear thermal strain ($\overline{\varepsilon_{th}}$) is assumed, i.e. $\overline{z_3}$ and $\overline{z_4}$, and the corresponding self-induced thermal strain (ε_{st}) distribution is estimated using Eq. (15). Eqs. (21) to (26) are used to calculate the self-equilibrating internal forces in concrete and steel based on the estimated ε_{st} distribution. $\overline{z_3}$ and $\overline{z_4}$ are changed in an iterative procedure till force/moment equilibrium are achieved. The final ε_{st} distribution is converted to a series of lines to allow adding it to the mechanical strain (ε_{cT}) in the next step.

3) different linear mechanical strain (ε_{cT}) distributions are assumed, i.e. z_3 and z_4 in Eq. (20), and modified based on ε_{st} calculated in step 2. For each modified ε_{cT} distribution, Eqs. (27) to (34) are used to calculate the corresponding concrete forces and their locations. Equilibrium is then conducted between internal forces in concrete and steel and external applied loads on the analyzed section. An iterative procedure requires changing z_3 and z_4 till force and moment equilibriums are achieved.

4) the degraded flexural and axial stiffnesses are then evaluated by dividing the applied flexural moment (M_{app}) and axial force (P_{app}) over the final ψ_{cT} (same as z_3) and center ε_{cT}, respectively.

5) The fire-exposed RC frame/subassemblage is then modeled, utilizing any linear elastic FE software, and analyzed using the degraded flexural and axial stiffnesses calculated in step 4. The effect of thermal expansion is considered by modeling ε_i and ψ_i as an induced deformation for all fire-exposed RC members.

The above steps are repeated till the external moments and axial forces are properly redistributed between the frame elements and results in the same flexural and axial stiffnesses. This approach for analyzing RC frames during fire exposure is illustrated and validated in the next sections.

6.8 Error Analysis

The error associated with proposed method approximations are evaluated in the following sections.

6.8.1 Average Temperatures

The error corresponding to using T_{avg} for strength calculations is assessed by analyzing the sections shown in Table 6- 1 at different load levels (λ = 0.2 - 0.5). All the sections are assumed exposed to ASTM-E119 standard fire from four faces. Comparisons between the analytical effective flexural and axial stiffnesses (EI_{eff} and EA_{eff}) obtained by considering the actual concrete strength and the strength calculated using T_{avg} are shown in Fig. 6-9. Using T_{avg} for stress calculations has a negligible effect on the flexural and axial stiffnesses of the examined concrete sections.

Table 6-1–Parametric study cases

Col #	b (mm)	h (mm)	f'_c (MPa)	f_y (MPa)	ρ $\%\ (A_g)$
$C1$	305	305	36.1	443.7	2.1
$C2$	400	400	30	400	1.5
$C3$	600	600	40	400	1.5
$C4$	400	700	50	400	1.0
$C5$	500	700	25	400	1.0

***** all sections are analyzed up to 4 hrs of standard ASTM-E119 fire exposure

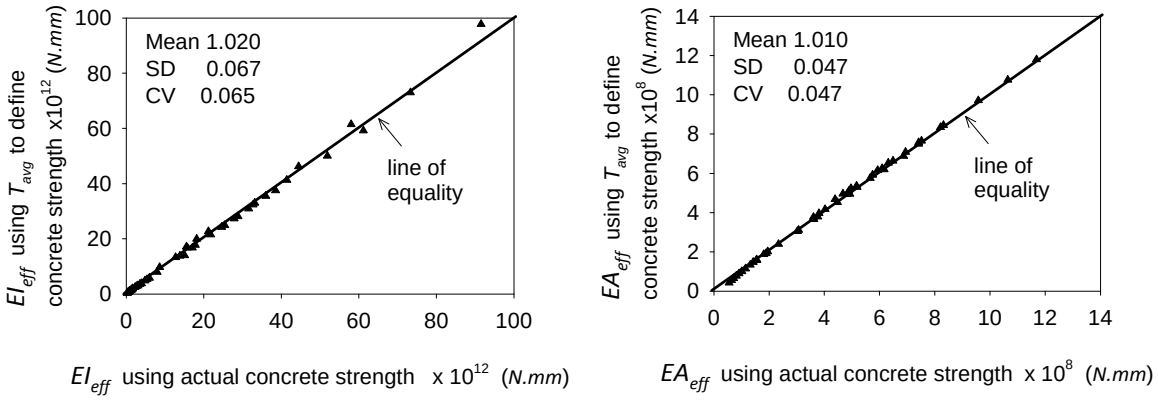

a) flexural stiffness EI_{eff}

b) axial stiffness EA_{eff}

Fig. 6-7. Effect of using T_{avg} on the stiffness of fire-exposed sections

6.8.2 Concrete strain at peak stress

To evaluate the error associated with using Eq. (8), the effective flexural and axial stiffnesses (EI_{eff} and EA_{eff}) of the four-face heated sections shown in Table 6- 1 are calculated, at different load levels ($\lambda = 0.2 - 0.5$), up to 4 hrs of ASTM-E119 standard fire exposure. Fig. 6-10 shows that this approximation has a minor effect on the flexural and axial stiffness predictions calculated using sectional analysis method.

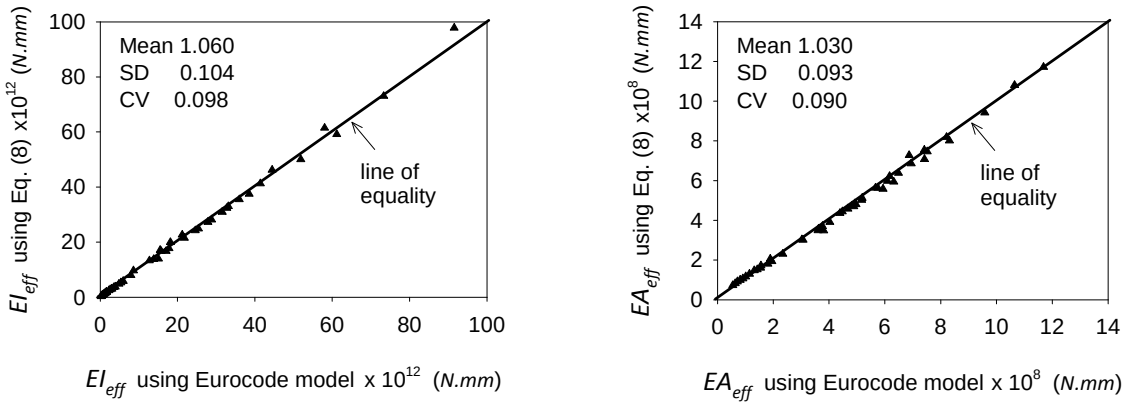

a) flexural stiffness EI_{eff}

b) axial stiffness EA_{eff}

Fig. 6-8. Effect of ($\varepsilon_{oT} + \varepsilon_{tr}$) model on the stiffness of fire-exposed sections

6.8.3 Concrete Compressive Strength

For $T_{avg} \leq 900$ ℃, Eq. (11) results in coefficient of variations of 0.067 and 0.195 for siliceous and carbonate concrete, respectively. The equation can be conservatively applied for carbonate aggregate concrete[8].

6.8.4 Effect of ignoring concrete nonlinearity on $\overline{\varepsilon_{th}}$

A parametric study is conducted in to evaluate the error in predicting $\overline{\varepsilon_{th}}$ due to ignoring concrete nonlinearity. The unrestrained thermal parameters ε_i and ψ_i are predicted using the sectional analysis method for the RC sections shown in Table 6- 1. All the sections are subjected to ASTM-E119 standard fire exposure up to 4 hrs. The studied sections are unevenly heated, i.e. from three faces, to generate ψ_i during fire exposure. ε_i and ψ_i are calculated considering the concrete nonlinearity, i.e. Eq. (12). Their values are recalculated ignoring the concrete nonlinearity, i.e. assuming a linear constitutive stress-strain relationship between f'_{cT} and $(\varepsilon_{oT} + \varepsilon_{tr})$. Fig. 6-11 shows a comparison between the correct ε_i and ψ_i and the approximate ε_i and ψ_i for all the RC sections. As shown in the figure, the effect of ignoring the concrete nonlinearity is negligible for ε_i and results in a minor difference for ψ_i.

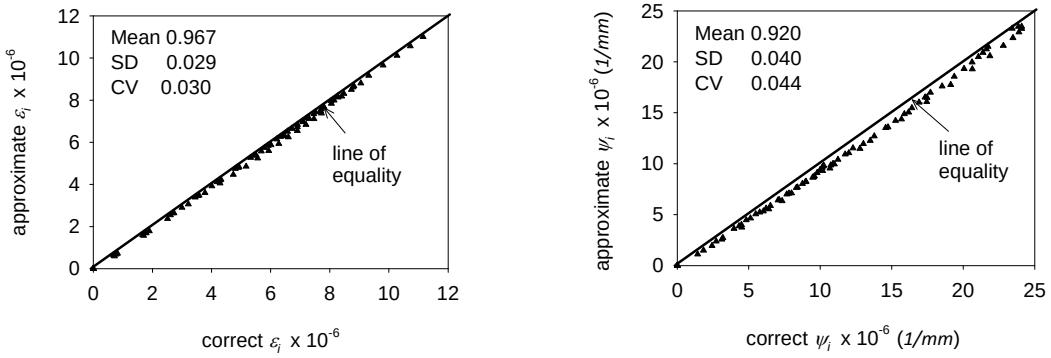

Fig. 6-9. Effect of concrete nonlinearity on thermal parameters ε_i and ψ_i

6.9 Validation Case 1 (Fang et al., 2012)

The proposed method is validated by comparing its predictions with experimental work by Fang et al.[3]. Fig. 6-12 shows a full-scale specimen that was exposed to a $3\,hrs$ standard ISO 834 fire. The top $150\,mm$ of the beam section was shielded by thick ceramic fiber to simulate the effect of floor slab. The outer $250\,mm$ of the column section was also shielded as the joint was insulated by thick ceramic fiber during fire exposure. The column has dimensions of $500\,mm$ by $500\,mm$ and a height of $2860\,mm$ and is reinforced with $12-22\,mm$ bars. The full length of the column was exposed to fire. The beam has dimensions of $400\,mm$ by $500\,mm$ and a fire exposed length of $5750\,mm$. It is reinforced with $4-22\,mm$ and $2-22\,mm$ bottom and top bars, respectively, and additional top $2-25\,mm$ bars at the beam end, i.e. SEC 2-2 in Fig. 6-12. The yield strength of the $22\,mm$ and $25\,mm$ reinforcing bars is $453\,MPa$ and $411\,MPa$, respectively. The 28 days compressive strength of the siliceous concrete was 34.47 MPa. Prior to test, the column was axially loaded by $1727\,kN$ and the beam was subjected to vertical loads P_1 of 78 and P_2 of 49 kN. All loads were maintained during the fire test and the variation of the deflection at P_1 and P_2 as well as the horizontal displacement and rotation at the roller support were continuously monitored during the whole test. These values are predicted using the proposed method in the following sections. Beam SEC 2-2 will be considered to provide sample calculations. The effect of elevated temperatures on the shear capacity, bond loss between steel bars and concrete, and concrete spalling were not considered in the analysis.

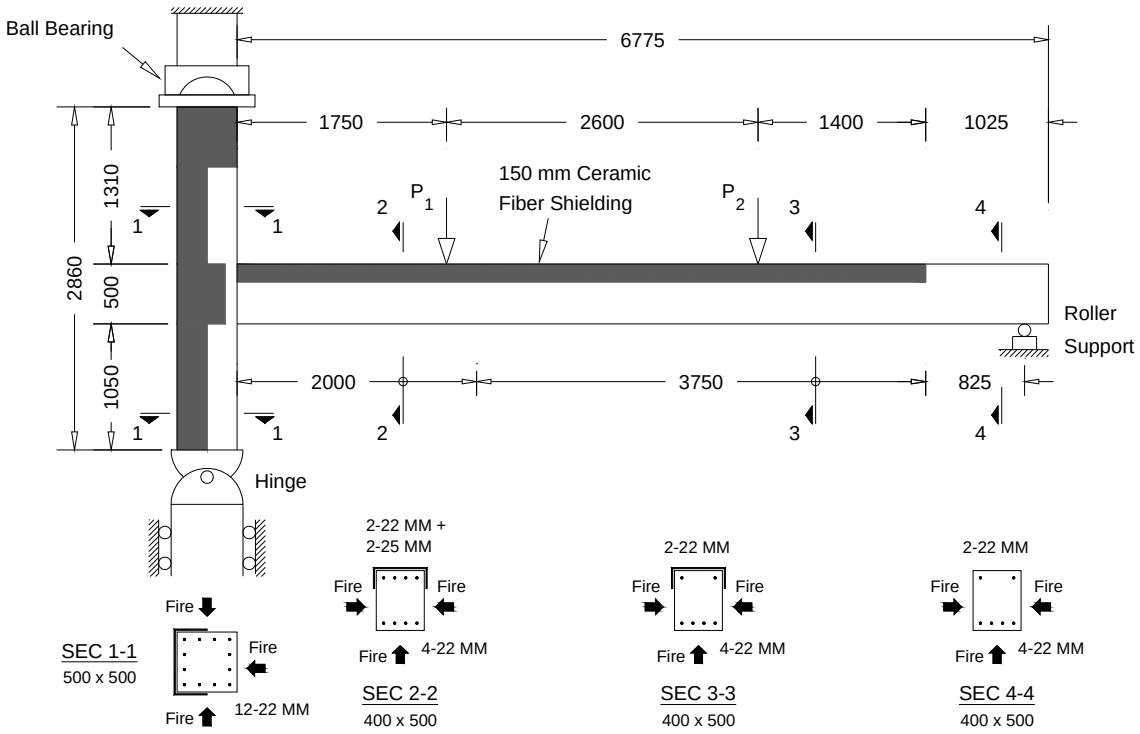

Fig. 6-10. Test setup for RC beam-column subassemblage [3]

[Dimensions in mm]

6.9.1 Predicting Average Temperature Distribution

The steps involved in applying Wickstrom's method to calculate the temperature distribution within the fire exposed beam section are given below. Due to the insulation, the concrete beam and column are assumed to be subjected to ISO 834 heating from three sides only; Left (L), Right (R), and Bottom (B) faces. The ISO 834 fire temperature (T_f) is calculated at fire duration of $t = 3.0\ hrs$ as 1090 ℃, Eq. (1). The ratio between the surface temperature and the fire temperature (n_w) can be estimated using Eq. (2b) as 0.98. The temperature rise in steel bars is calculated using n_y at top of the section equals to zero, Table 6- 2. To account for the effect of insulation, the temperature of top steel bars is limited to 100 ℃. This temperature was recorded during the fire test. The average temperature rise in concrete is calculated using the following steps:

1) z values of 0.183 for t of 3.0 hrs are calculated using Eq. (3).

2) The average temperatures for each region are calculated and are shown in Fig. 6-1 by the dashed lines.

For 3.0 hrs fire exposure: z of 0.183 is used to define the region boundaries. Substituting in Eq. (4a) using $x_1 = 0.0\ m$, and $x_2 = 0.183\ m$ results in $T_{avg\,1} = 383 + 690\ n_y$. Substituting in Eq. (4b) results in $T_{avg\,2} = 1064\ n_y$.

3) The ambient temperature (34 ℃) is added to the calculated average temperatures. Weighted average temperatures for t of 3.0 hrs are then calculated at different y values. For 3.0 hrs fire exposure, $T_{avg}(y = 0.0\ m) = 1107$ ℃ and $T_{avg}(y = 0.183\ m) = 384$ ℃.

4) The constants (z_1 and z_2) of Eq. (5) are evaluated using values of T_{avg} at y_1 of 0.0 m and y_2 of 0.183 m for t of 3.0 hrs. The equation representing the average temperature distribution over the section height is:

$T_{avg} = 1107\ e^{(-5.57\ y)}$.

The average temperature distribution, calculated using Eq. (5), is shown in Fig. 6-13b.

Table 6-2–Calculation of steel internal forces

(1)	(2)	(3)	(4)	(5)	(6)	(7)	(8)	(9)	(10)	(11)	(12)
A_s (mm^2)	x (mm)	y (mm)	T_{xy} (℃)	ε_{sT}	ε_{st}	$\varepsilon_{sT} + \varepsilon_{st}$	$\frac{f_{yT}}{f_y}$	$f[T, 0.001]$ (MPa)	$f[T, (\varepsilon_{sT} - \varepsilon_p + 0.001)]$ (MPa)	f_{sT} (MPa)	P_s (kN)
			Eq. (2a)	Eq. (20)	Eq. (15)		Eq. (13)	Eq. (14d)	Eq. (14e)	Eq. (14a,b)	$f_{sT} \times A_s$
774	----	439	**100**	-0.018	-0.002	-0.019	0.96	182	309	-458	-354,202
1000	----	439	**100**	-0.018	-0.002	-0.019	0.96	182	309	-458	-457,625
774	61	61	712	0.012	0.009	0.014	0.21	35	93	122	94,131
774	154	61	494	0.012	-0.009	0.010	0.57	80	160	225	173,979

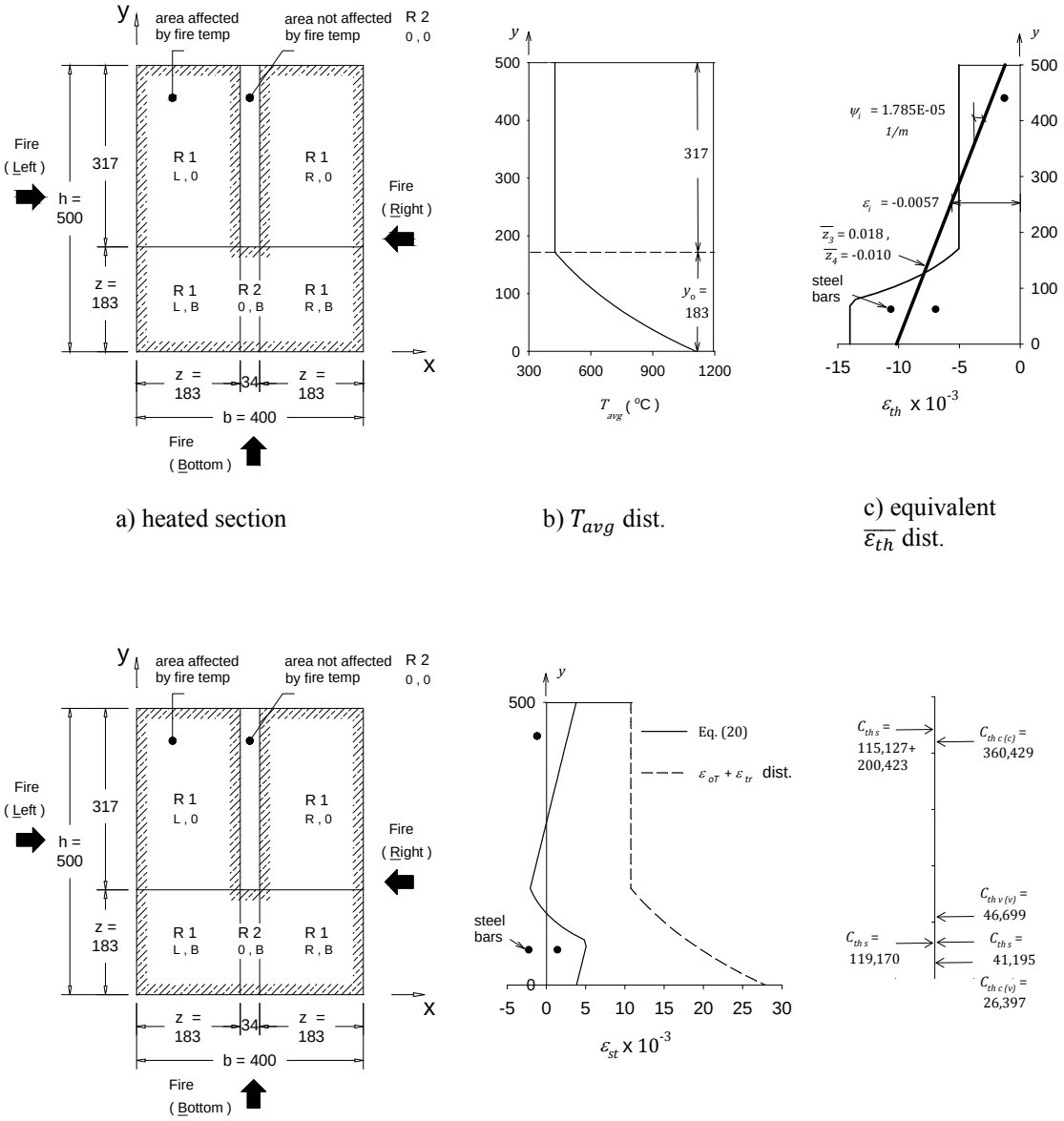

a) heated section

b) T_{avg} dist.

c) equivalent $\overline{\varepsilon_{th}}$ dist.

a) heated section

d) self induced thermal strain (ε_{st})

e) internal force equilibrium

Fig. 6-11-Thermal Deformation of beam SEC 2-2

[Dimensions in mm, forces in N]

6.9.2 Evaluation of Unrestrained Thermal Parameters

The unrestrained thermal parameters, ε_i and ψ_i, for the RC beam section at $t = 3\,hrs$ are calculated in this section.

5) The predicted T_{avg} distribution is used to plot ($\varepsilon_{oT} + \varepsilon_{tr}$) distribution along y direction using Eq. (8), Fig. 6-13d.

An equivalent linear thermal strain ($\overline{\varepsilon_{th}}$) distribution is assumed as shown in Fig. 6-13c, i.e. $\bar{z}_3 = 0.018$ and $\bar{z}_4 = -0.010$. Fig. 6-13d shows the difference between $\overline{\varepsilon_{th}}$ and ε_{th} which represents the self-induced thermal strain (ε_{st}) for concrete and steel. Concrete compression forces and corresponding moments are calculated using expressions provided in Appendix I as follows:

a. For $y = 0.000 \rightarrow 0.077\,m$ (constant ε_{th} and variable temperature)

   Eqs. (21) and (22) → $C_{th\,c\,(v)} = -26{,}397\,N$, $C_{th\,c\,(v)}.y = -1.58\,kN.m$ ($y = 0.060\,m$)

b. For $y = 0.077 \rightarrow 0.127\,m$ (variable ε_{th} and variable temperature)

   Eqs. (23) and (24) → $C_{th\,v\,(v)} = -46{,}699\,N$, $C_{th\,v\,(v)}.y = -4.56\,kN.m$ ($y = 0.098\,m$)

c. For $y = 0.288 \rightarrow 0.500\,m$ (constant ε_{th} and constant temperature)

   Eqs. (25) and (26) → $C_{th\,c\,(c)} = -360{,}429$ N , $C_{th\,c\,(c)}.y = -154.70$ kN.m ($y = 0.429\,m$)

The self-induced thermal strain (ε_{st}) in steel bars is shown in Table 6- 2. Fig. 6-13e shows that internal forces/moments in concrete and steel are in equilibrium, this means

that the assumed $\overline{\varepsilon_{th}}$ is correct. ε_i and ψ_i corresponding to the assumed $\overline{\varepsilon_{th}}$ are -0.0057 and $1.789 \times 10^{-5}\ 1/m$, respectively.

6.9.3 Evaluation of Degraded Flexural and Axial Stiffnesses

The analysis steps explained in the section titled "Proposed Method" are conducted following a number of iterations. The BMD acting on the beam-column subassemblage is shown Fig. 6-14c. The subassemblage is divided into a number of segments based on the applied loads, fire exposure conditions, and reinforcement configuration. A sectional analysis is conducted for a section in each segment using the maximum applied axial force and flexural moment in this segment. The temperature of steel bars is considered uniform along the beam length because of the high thermal conductivity of steel material[2.9]. Therefore, the reduction in EI_{eff} and EA_{eff} for the unexposed beam end (SEC 4-4) are calculated based on heated steel bars and full concrete strength, i.e. at ambient temperature. The required steps to calculate EI_{eff} and EA_{eff} for the RC beam (SEC 2-2) are explained below.

8) A mechanical strain (ε_{cT}) distribution is assumed as shown by the heavy line in Fig. 6-15c (z_3 and z_4 of Eq. (20) are equal to -0.080 and 0.017, respectively). The line does not intersect the concrete ($\varepsilon_{oT} + \varepsilon_{tr}$) curve, which indicates that concrete crushing does not occur at this mechanical strain.

9) ε_{st} is added to ε_{cT} as initial strains for concrete and steel. For the constant temperature zone ($0.183\ m < y < 0.5\ m$), ε_{st} is linear and can be added to ε_{cT} as shown in Figs. 13d and 15b. For the variable temperature zone ($y < 0.183\ m$), a linear ε_{st} distribution is assumed between $y = 0.0\ m$ and $y = 0.183\ m$. The modified ε_{cT} distribution is plotted as dashed lines in Fig. 6-15c.

10) concrete compressive forces and corresponding centroids are calculated using expressions provided in Appendix II as follows:

a. For $y = 0.000 \rightarrow 0.171\ m$ (average temperature and $\varepsilon_{cT} < (\varepsilon_{oT} + \varepsilon_{tr})$)

Eqs. (27) and (28) → $C_{c\,o(v)} = -517{,}203\ N$, $C_{c\,o(v)}\,.y\ = -57.60\ kN.m$

$(y = 0.111\ m)$

b. For $y\ =\ 0.171 \rightarrow 0.193\ m$ (constant temperature and $\varepsilon_{cT} < (\varepsilon_{oT} + \varepsilon_{tr})$)

Eqs. (31) and (32) → $C_{c\,o\,(c)} = -26{,}515\ N$, $C_{c\,o\,(c)}\ .y = -4.26\ kN.m$

$(y = 0.161\ m)$

11) the self-induced thermal strain (ε_{st}) in steel bars is added to the mechanical strain (ε_{sT}) as shown in Table 6- 2. The corresponding steel stresses are calculated using Eq. (14) and given in Table 6- 2.

12) the calculated concrete and steel forces are in equilibrium with external forces. The mechanical curvature and center strain, ψ_{cT} and ε_{cT}, are predicted after 3.0 hrs ISO 834 fire exposure as $-8.01 \times 10^{-5}\ 1/m$ and -0.0029, respectively.

13) the flexural stiffness is calculated by dividing the applied external moment over the calculated ψ_{cT}. The reduced (effective) flexural stiffness, (EI_{eff}), for the heated beam (SEC 2-2) is $3.47 \times 10^{12}\ N.mm^2$. Similarly, the axial stiffness (EA_{eff}) is calculated by dividing the applied external force over the calculated center ε_{cT}. The effect of fire temperature on the axial stiffness of the column is found to be negligible and not considered in the analysis. The RC beam is axially unrestrained at the roller support and no axial forces are generated in it during fire exposure.

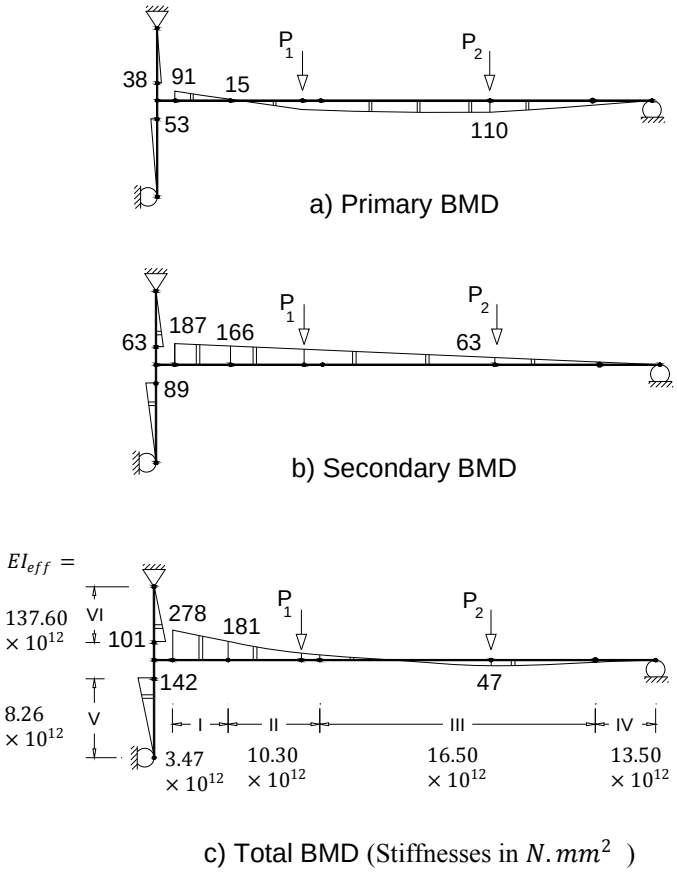

Fig. 6-12-Moment redistribution after 3 hrs ISO-834 fire exposure

[Moments are in $kN.m$]

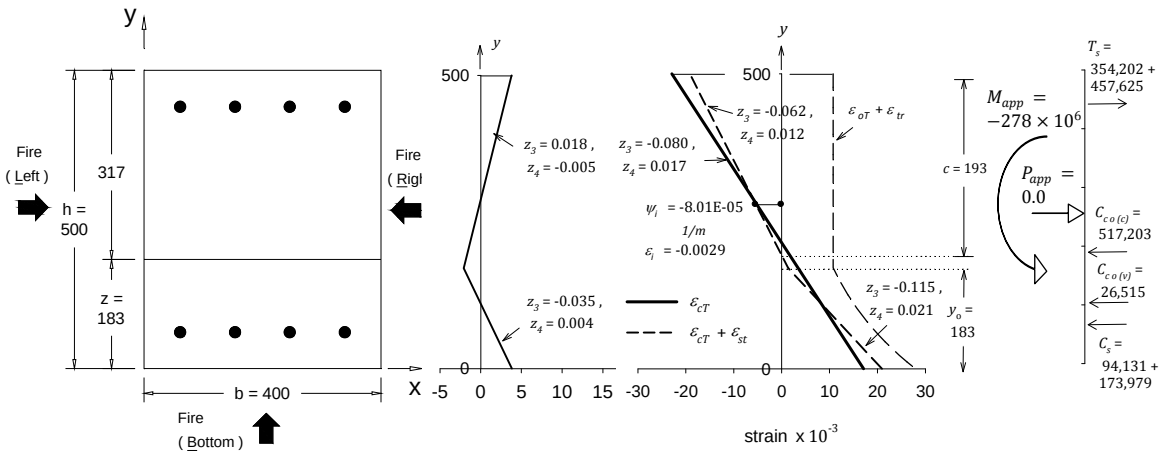

a) heated section

b) approximate ε_{st} dist.

c) ε_{cT} dist.

d) external-internal force equilibrium

Fig. 6-13-Mechanical stress analysis of beam SEC 2-2
[Dimensions in mm, forces in N, moments in $N.mm$]

6.9.4 Modeling and Analysis of RC Subassemblage

The RC beam-column subassembalge is modeled using SAP2000[15] software, Fig. 6-14. The insulated beam-column joint is modeled using rigid links.

14) a linear temperature loading is applied on the beam-column subassemblage to induce the calculated unrestrained thermal deformation. The temperature values are determined based on ε_i, ψ_i, coefficient of thermal expansion (defined by Sap2000), and section depth. The assigned temperature loading for the beam section based on 1.0×10^{-5} coefficient of thermal expansion is a $598\,℃$ uniform temperature in addition to a $1564\,℃/m$ gradient temperature in y direction.

15) the reduced EI_{eff} and EA_{eff} are assigned to each segment based on the applied moment and axial force.

6.9.5 Predicting the Fire Performance of the Beam-Column Subassemblage

The frame model is analyzed using SAP2000[13] and the BMD are obtained. Fig. 6-14a shows the primary moment due to vertical loads. A secondary moment is generated in the beam-column subassemblage due to the restrained rotation at the beam-column joint, Fig. 6-14b. The total BMD is the summation of the primary and the secondary moments as shown in Fig. 6-14c.

The total BMD is used to reevaluate EI_{eff} and EA_{eff} in the next iteration. This procedure is repeated till convergence for EI_{eff} and EA_{eff} is achieved and correct secondary moments are obtained. The convergence of the analyzed RC subassemblage is achieved after three iterations.

Fig. 6-16 shows the deflected shape of the subassemblage at $3\,hrs$ ISO 834 fire exposure. The predicted beam deflection reasonably matches the measured deflection data experimentally.

The recorded vertical deflection at P_2 during fire test was $62\,mm$ and the calculated deflection by SAP2000 is $68\,mm$ (10% error). The measured rotation (θ) at the roller support was 2.1° while SAP2000 estimate 2.2° (5% error). The measured displacement (Δ_1) at the roller support during fire test was $30\,mm$ and the calculated Δ_1 by SAP2000 is $37\,mm$ (23% error).

Although the proposed method reasonably predicts Δ_2 and θ, the difference in the roller support horizontal displacement (Δ_1) between the analytical and test results is due to overestimating the elevated temperature in the bottom steel bars in the beam which affects the thermal deformation of the beam.

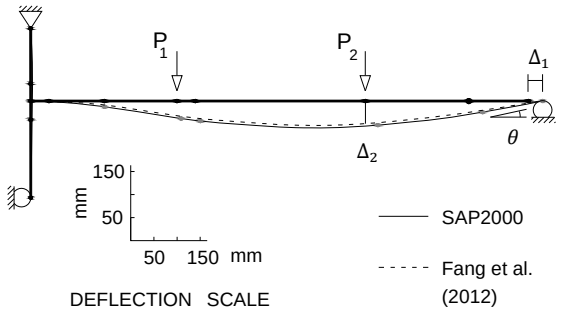

Fig. 6-14-Beam-column subassemblage deformation after 3 hrs ISO-834 fire exposure

6.10 Validation Case 2 (Iding et al., 1977)

Iding et al.[4] has analytically investigated the behavior of RC frames during fire exposure. Fig. 6-17 shows a schematic of a single bay RC frame analyzed using FIRES-RC II, a comprehensive FE software developed at University of California, Berkeley. The beam and column dimensions are $355\ mm \times 711\ mm$. The frame was exposed to a $1.0\ hr$ of ASTM-E119 standard fire over its entire length while supporting the vertical loads shown in Fig. 6-17. The frame was analyzed assuming siliceous concrete and a compressive strength of $27.6\ MPa$. The yield strength of the reinforcing bars was $275.8\ MPa$.

This frame is analyzed similar to validation case (1). The effect of elevated temperatures on the shear capacity, bond loss between steel bars and concrete, and concrete spalling were not considered in the analysis. Figs. 18 and 19 show sample calculations for the frame's column. The total moments and axial forces are estimated using the proposed method in this chapter and compared with the results of FIRES-RC II FE software, Fig. 6-20. The frame is analyzed using SAP2000[13] and the predicted deformed shape is shown in Fig. 6-21. A good match is found between the proposed method and the nonlinear FIRES-RC II FE software. The difference in deformations can be due to using different material models.

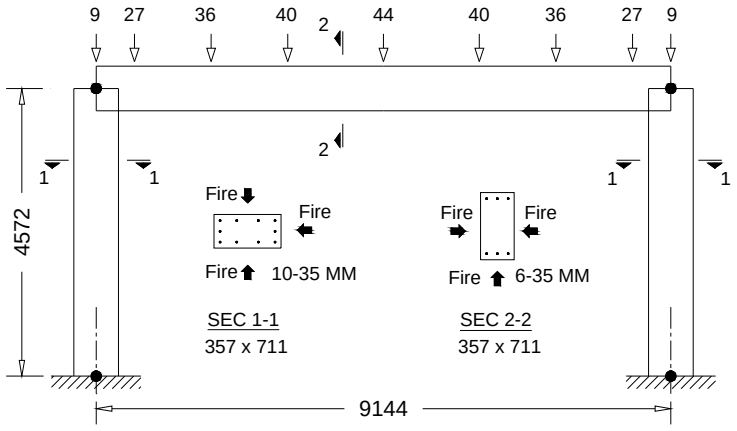

Fig. 6-15- Layout for a RC frame exposed to ASTM-E119 fire [4]
[Dimensions in mm, loads in kN]

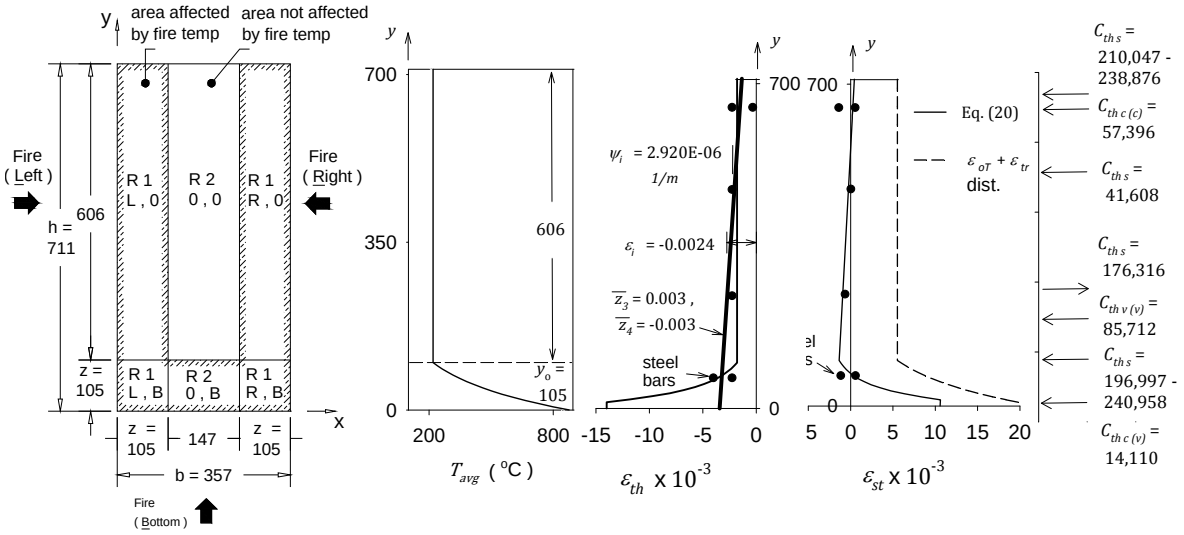

a) heated section | b) T_{avg} dist. | c) equivalent $\overline{\varepsilon_{th}}$ dist. | d) self induced thermal strain (ε_{st}) | e) internal force equilibrium

Fig. 6-16-Thermal Deformation of column SEC 1-1

[Dimensions in mm, forces in N]

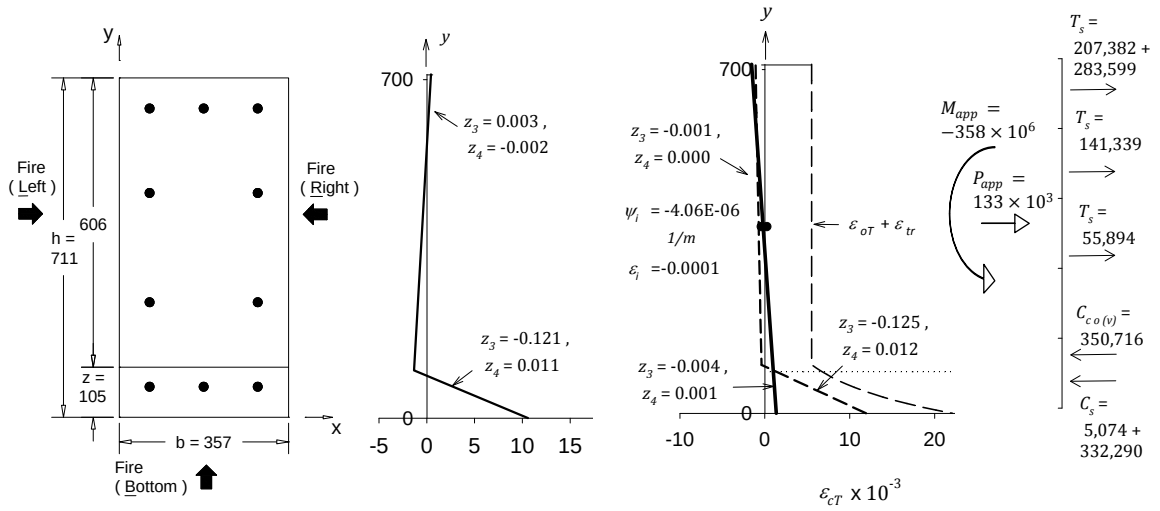

a) heated section | b) approximate ε_{st} dist. | c) ε_{cT} dist. | d) external-internal force equilibrium

Fig. 6-17- Mechanical stress analysis of column SEC 1-1

[Dimensions in mm, forces in N, moments in $N.mm$]

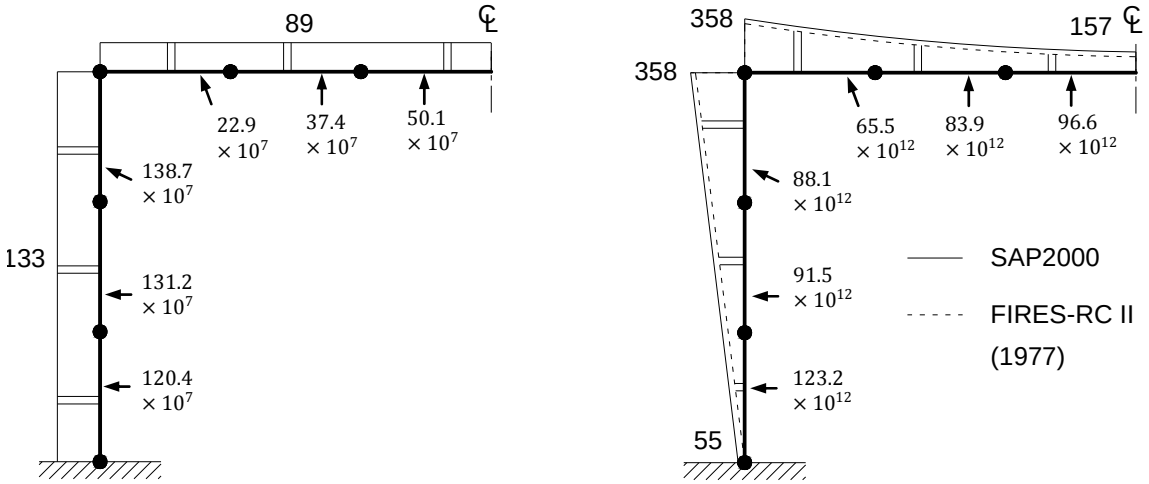

a) Axial (compression) force diagram (Stiffnesses in $N.mm^2$)

b) Total BMD (Stiffnesses in $N.mm^2$)

Fig. 6-18-External forces/moments after 1 *hr* ASTM-E119 fire exposure
[Axial forces in kN, moments in $kN.m$]

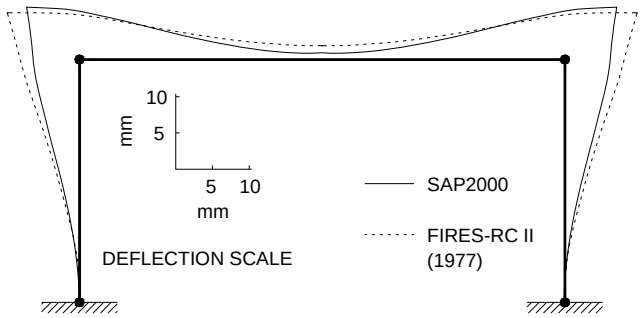

Fig. 6-19-RC frame deflection after 1 hr ASTM-E119 fire exposure

6.11 Summary and Conclusions

The overall behavior of RC framed structures is studied in this chapter. A practical approach based on superimposing the effects of thermal expansion and material degradation is introduced. The nonlinear thermal expansion is converted to an equivalent uniform thermal distribution, which can be represented by the unrestrained thermal axial strain ε_i and curvature ψ_i. The degradation effect in material strength is considered by accounting for the reduction in the effective flexural and axial stiffnesses, EI_{eff} and EA_{eff}, respectively.

A simple technique to calculate an average 1D temperature distribution is presented and validated in this chapter. Based on this temperature distribution, the heated RC column section is divided into different zones to conduct stress analysis. A number of approximations are assumed to allow integrating concrete stress-strain relationships with respect to mechanical strain and temperature distributions. The main assumptions include

1) using a 1D average temperature distribution, i.e. T_{avg}, instead of 2D elevated temperature contours with the RC sections,

2) choosing an appropriate algebraic function to represent T_{avg} variation along the section height, i.e. Eq. (5),

3) using an integrable stress-strain constitutive relationships for concrete at elevated temperatures, i.e. Eq. (12), and

4) ignoring the concrete nonlinearity in calculating the unrestrained thermal parameters ε_i and curvature ψ_i

Mathematical expressions are derived to calculate internal compression force and corresponding moment for the heated concrete. Structural engineers can use these expressions to predict the unrestrained thermal deformation and the effective flexural and axial stiffnesses, i.e. EI_{eff} and EA_{eff}.

The proposed method is validated by comparing its results with two case studies: a RC beam-column subassemblage tested by Fang et al. [3] , and a single storey RC frame analyzed by Iding et al. [4]. A good agreement is found between the experimental data and the results of the proposed method for both case studies.

6.12 Acknowledgments

This research was funded by the Natural Sciences and Engineering Research Council of Canada.

6.13 References

1. Lie, T.T., ed., "Structural Fire Protection", ASCE Manuals and Reports on Engineering Practice, no. 78, New York, NY, 1992, 241 pp.
2. Youssef, M.A. Moftah, M., "General stress-strain relationship for concrete at elevated temperatures", Engineering Structures, vol. 29, no. 10, 2007, pp. 2618-2634.
3. Fang, I.-Kuang, Sullivan, Patrick J. E., Lee, Chi-Chung, Fang, I.-Chung, Yeh Tzong-Yih, and Wu, Ming-Yuan, "Fire resistance of beam-column subassemblage", ACI Struct. J., vol. 109, no. 1, 2012, pp. 31-40.
4. Iding, R., Bresler, B., and Nizamuddin, Z., “FIRES-RC II, A computer program for the fire response of structures-reinforced concrete frames (revised version)”, Department of Civil Engineering (Division of structural engineering and structural mechanics),University of California Berkeley, 1977.
5. El-Fitiany, S.F., and Youssef, M.A., “Stress Block Parameters for Reinforced Concrete Beams During Fire Events,” Innovations in Fire Design of Concrete Structures, ACI SP-279, 2011, pp. 1-39.

6. El-Fitiany, S., Youssef, M.A., "Assessing the flexural and axial behaviour of reinforced concrete members at elevated temperatures using sectional analysis", Fire Safety Journal, vol. 44, no. 5, 2009, pp. 691-703.
7. El-Fitiany S.F. and Youssef M.A., “A Simplified Sectional Analysis Approach for RC Elements during Fire Events”, 6th International Conference on Structures in Fire, Michigan State University in East Lansing, MI, 2010, pp. 239-246.
8. El-Fitiany S.F. and Youssef M.A., “Simplified method to analyze continuous RC beams during fire exposure", ACI Struct. J., In press (accepted Oct 2012).
9. Wickstrom, U., "A very simple method for estimating temperature in fire exposed concrete structures", Fire Technology Technical report SP-RAPP 1986, 46, Swedish National Testing Institute, pp. 186-194.
10. Eurocode 2, “Design of concrete structures", ENV EC2, 1992.
11. Terro, M.J., "Numerical modeling of the behavior of concrete structures in fire", ACI Struct. J., vol. 95, no. 2, 1998, pp. 183-193.
12. Meda, Alberto, G. Gambarova, Pietro, Bonomi, Marco, "High-Performance Concrete in Fire-Exposed Reinforced Concrete Sections ", ACI Struct. J., vol. 99, no. 3, 2002, pp. 277-287.
13. Elbahy Y.I., Youssef M.A., Nehdi M., “Stress Block Parameters for Concrete Flexural Members Reinforced with Superelastic Shape Memory Alloys”, Materials and Structures, vol. 42, no. 10, 2009, pp 1335-1351.
14. Caldas, Rodrigo Barreto, Sousa Jr., João Batista M., Fakurya, Ricardo Hallal, “Interaction diagrams for reinforced concrete sections subjected to fire", Eng. Struct., vol. 32, no.9, 2010, pp. 2832–2838.

15. Wilson EL. SAP2000 analysis reference manual. Berkeley, California: Computers and Structures Inc.; 2002.

6.14 Appendices

The following symbols are used in Appendix I and II:

ε_{uT} = ultimate (crushing) compressive strain of concrete, Eq. (9)

$\Delta\varepsilon$ = difference between ε_{uT} and $(\varepsilon_{oT} + \varepsilon_{tr})$, equals to 0.02

b = column width in x direction

f'_c = concrete compressive strength at ambient condition

x, y = horizontal and vertical coordinates for any point within the column section, origin located at bottom left of the section

y_1, y_2 = boundaries of internal concrete compression force measured in y direction

z_1, z_2 = constants of average temperature fitting equation, Eq. (5)

z_3, z_4 = constants defining the linear variation of mechanical strain (ε_{cT}) in y direction, Eq. (20)

$\bar{z}_3, \bar{z}_4$ = constants defining the linear variation of equivalent thermal strain ($\overline{\varepsilon_{th}}$) in y direction, Eq. (15)

A_1 $e^{y_1 \ z_2}$

A_2 $e^{y_2 \ z_2}$

6.14.1 Appendix I

$C_{c\,o(v)\,L}$, $C_{c\,o(v)\,L}\,.\,y$, $C_{c\,o(v)\,L}$, and $C_{c\,o(v)\,L}\,.\,y$ are calculated from Appendix II using $\bar{z_3}$ and $\bar{z_4}$ instead of z_3 and z_4, respectively.

$$C_{th\,c\,(v)} = C_{c\,o(v)\,L} + \left(\frac{1}{30.465}\,\frac{b\;\;f'_c}{{z_2}^2\,z_1}\right)[+\left({A_2}^2 - {A_1}^2\right) \times 1065\,{z_1}^3\,(z_2\,\varepsilon_{th}) \tag{16}$$

$$+(A_2 - A_1) \times 3630767\,{z_1}^2\,(-z_2\,\varepsilon_{th})$$

$$+\left(\frac{1}{A_2} - \frac{1}{A_1}\right) \times 1210.981 \times 10^9\,(-z_2\,\varepsilon_{th})$$

$$-(y_2 - y_1) \times 3031.623 \times 10^5\,z_1\,(-\varepsilon_{th}\,){z_2}^2]$$

$$C_{th\,c\,(v)}\,.\,y\; = C_{c\,o(v)\,L}\,.\,y + \left(\frac{1}{9.1395}\frac{b\;\;f'_c}{{z_2}^3\,z_1}\right)[\tag{17}$$

$$+\left({A_2}^2\,y_2 - {A_1}^2\,y_1\right) \times 3195 \times 10^{-4}\,{z_1}^3\,z_2\,(\varepsilon_{th}\,z_2)$$

$$+\left({A_2}^2 - {A_1}^2\right) \times 15975 \times 10^{-5}\,{z_1}^3(-\varepsilon_{th}\,z_2)$$

$$+(A_2\,y_2 - A_1\,y_1) \times 1.08923 \times 10^3\,{z_1}^2\,z_2\,(-\varepsilon_{th}\,z_2)$$

$$+\left(\frac{y_2}{A_2} - \frac{y_1}{A_1}\right) \times 3.632943 \times 10^8(\,-\varepsilon_{th}\,{z_2}^2)$$

$$+\left(\frac{1}{A_2} - \frac{1}{A_1}\right) \times 3.632943 \times 10^8(-\varepsilon_{th}\,z_2)$$

$$+(A_2 - A_1) \times 1.08923 \times 10^3({z_1}^2\,\varepsilon_{th}\,z_2)$$

$$-({y_2}^2 - {y_1}^2) \times 4.547435 \times 10^4\,(-z_1\,\varepsilon_{th}\,{z_2}^3)\,]$$

$$C_{th\,v\,(v)} = C_{c\,o(v)\,L} + \left(\frac{1}{30.465}\ \frac{b\ \ f'_c}{{z_2}^2\ z_1}\right)[\tag{18}$$

$$+\left({A_2}^5 - {A_1}^5\right) \times 426\ {z_1}^6\ z_2\ B_3$$

$$-\left({A_2}^4 - {A_1}^4\right) \times 907700\ {z_1}^5\ z_2\ B_3$$

$$+\left({A_2}^3 - {A_1}^3\right) \times 710\ {z_1}^4\ z_2\ (B_2 + 142328.64\ B_3)$$

$$+\left({A_2}^2 - {A_1}^2\right) \times 1065\ {z_1}^3\ z_2\ (B_1 + 568535211.3\ {z_1}^3\ B_3 - 1704.58227\ {z_1}^3\ B_2)$$

$$+(A_2 - A_1) \times 3630767\ {z_1}^2\ (-z_2\ B_1 + 83.498\ z_2\ B_2)$$

$$+\left(\frac{1}{A_2} - \frac{1}{A_1}\right) \times 1210.981 \times 10^9\ (-z_2 B_1)$$

$$-(y_2 - y_1) \times 3031.623 \times 10^5\ z_1\ \ {z_2}^2\ (-B_1 - 3994.5\ B_2\ )]$$

$$C_{th\,c\,(v)}\,.\,y\; = C_{c\,o(v)\,L}\,.\,y + \left(\frac{1}{9.1395}\frac{b\;\;f'_c}{{z_2}^3\;z_1}\right)[\tag{19}$$

$$+\left({A_2}^5\,y_2 - {A_1}^5\,y_1\right) \times 1278 \times 10^{-4}\;\;{z_1}^6\,B_3\,{z_2}^2$$

$$-\left({A_2}^5 - {A_1}^5\right) \times 2556 \times 10^{-5}\;\;{z_1}^6\,B_3\,z_2$$

$$-\left({A_2}^4\,y_2 - {A_1}^4\,y_1\right) \times 272.308\;\;{z_1}^5\,B_3\,{z_2}^2$$

$$+\left({A_2}^4 - {A_1}^4\right) \times 68.077\;\;{z_1}^5\,B_3\,z_2$$

$$+\left({A_2}^3\,y_2 - {A_1}^3\,y_1\right) \times 30316.67\,{z_1}^4\,{z_2}^2\,(7.026 \times 10^{-6}\,B_2 + \;B_3)$$

$$-\left({A_2}^3 - {A_1}^3\right) \times 10105.33\,{z_1}^4\,z_2\,(7.026 \times 10^{-6}\,B_2 + \;B_3)$$

$$+\left({A_2}^2\,y_2 - {A_1}^2\,y_1\right) \times 181647333\,{z_1}^3\,{z_2}^2\,(\;B_3 - 3 \times 10^{-6}B_2 + 1.7589 \times 10^{-9}B_1)$$

$$+\left({A_2}^2 - {A_1}^2\right) \times 15975 \times 10^{-5}\,{z_1}^3(-B_1\,z_2 + 1704.59\,B_2\,z_2 - 568536 \times 10^3 B_3\,z_2)$$

$$+(A_2\,y_2 - A_1\,y_1) \times 1.08923 \times 10^3\,{z_1}^2\,z_2\,(-B_1\,z_2 + 83.5\,B_2\,z_2)$$

$$+\left(\frac{y_2}{A_2} - \frac{y_1}{A_1}\right) \times 3.63294 \times 10^8(\,-B_1\,{z_2}^2)$$

$$+\left(\frac{1}{A_2} - \frac{1}{A_1}\right) \times 3.63294 \times 10^8(-\,B_1\,z_2)$$

$$+(A_2 - A_1) \times 1.08923 \times 10^3({z_1}^2\,B_1\,z_2 - 83.5\,{z_1}^2\,B_2\,z_2)$$

$$-({y_2}^2 - {y_1}^2) \times 4.547435 \times 10^4\,(-z_1\,B_1\,{z_2}^3 - 3994.5\,z_1\,B_2\,{z_2}^3)\;]$$

$$C_{th\,c\,(c)} = (-1 \times 10^6\ b\ f'_{cT}) \left[\left(\frac{1}{2}\ \frac{z_3}{(\varepsilon_{oT}+\varepsilon_{tr})} \right)\ ({y_2}^2 - {y_1}^2) + \left(\frac{z_4-\varepsilon_{th}}{(\varepsilon_{oT}+\varepsilon_{tr})} \right) (y_2 - y_1) \right] \qquad (20)$$

$$C_{th\,c\,(c)}\,.y\ = (-1 \times 10^3\ b\ f'_{cT})[\ \frac{1}{3}\ \left(\frac{z_3}{(\varepsilon_{oT}+\varepsilon_{tr})} \right)\ ({y_2}^3 - {y_1}^3) + \frac{1}{2} \left(\frac{z_4-\varepsilon_{th}}{(\varepsilon_{oT}+\varepsilon_{tr})} \right)\ (\ {y_2}^2 -$$

$${y_1}^2\ )\ ] \qquad (21)$$

6.14.2 Appendix II

$$C_{c\,o(v)} = 2\,C_{c\,o(v)\,L} - C_{c\,o(v)\,N} \tag{22}$$

$$C_{c\,o(v)\,L} = \left(\frac{1}{30.465}\ \frac{b\ \ f'_c}{{z_2}^2\ z_1}\right)[\tag{22a}$$

$$-\left({A_2}^2\ y_2 - {A_1}^2\ y_1\right) \times 1065\ {z_1}^3\ z_3\ z_2$$
$$+(A_2\ y_2 - A_1\ y_1) \times 3630767\ {z_1}^2\ z_3\ z_2$$

$$+\left({A_2}^2 - {A_1}^2\right) \times 1065\ {z_1}^3\ (0.5\ z_3 - z_4\ z_2)$$
$$+(A_2 - A_1) \times 3630767\ {z_1}^2\ (z_4\ z_2 - z_3)$$

$$+\left(\frac{y_2}{A2} - \frac{y_1}{A_1}\right) \times 1210.981 \times 10^9\ \ z_3\ z_2$$

$$+\left(\frac{1}{A_2} - \frac{1}{A_1}\right) \times 1210.981 \times 10^9\ (\ z_3 + z_4\ z_2)$$

$$-({y_2}^2 - {y_1}^2) \times 1515.812 \times 10^5 z_1\ z_3\ {z_2}^2$$

$$-(y_2 - y_1) \times 3031.623 \times 10^5\ z_1\ z_4\ {z_2}^2]$$

$$C_{c\,o(v)\,N} = \left(\frac{5.21026\ b\ \ f'_c}{{z_2}^3\,{z_1}^2}\right)[\tag{22b}$$

$$+\left(\frac{{y_2}^2}{{A_2}^2}-\frac{{y_1}^2}{{A_1}^2}\right)\times 1.5137262\times 10^{14}\,{z_3}^2\,{z_2}^2$$

$$+\left(\frac{y_2}{{A_2}^2}-\frac{y_1}{{A_1}^2}\right)\times 3.0274525\times 10^{14}(\,z_3\,z_4\,{z_2}^2+0.5\,{z_3}^2\,z_2)$$

$$+\left(\frac{1}{{A_2}^2}-\frac{1}{{A_1}^2}\right)\times 1.5137262\times 10^{14}(z_3\,z_4\,z_2+0.5\,{z_3}^2+{z_4}^2\,{z_2}^2)$$

$$+\left(\frac{{y_2}^2}{A_2}-\frac{{y_1}^2}{A_1}\right)\times 7.579058\times 10^{10}\,z_1\,{z_3}^2\,{z_2}^2$$

$$+\left(\frac{y_2}{A_2}-\frac{y_1}{A1}\right)\times 1.5158116\times 10^{11}(z_1\,{z_3}^2\,z_2+z_1\,z_3\,z_4\,{z_2}^2)$$

$$+\left(\frac{1}{A_2}-\frac{1}{A_1}\right)\times 1.5158116\times 10^{11}(z_1\,z_3\,z_4\,z_2+0.5\,z_1\,{z_4}^2\,{z_2}^2+z_1\,{z_3}^2)$$

$$-(A_2\,{y_2}^2-A_1\,{y_1}^2)\times 532.5016\times 10^3\,{z_1}^3\,{z_3}^2\,{z_2}^2$$

$$+(A_2\,y_2-A_1\,y_1)\times 1065.0032\times 10^3(\,{z_1}^3\,{z_3}^2\,z_2-{z_1}^3\,z_3\,z_4\,{z_2}^2)$$

$$+(A_2-A_1)\times 1065.0032\times 10^3({z_1}^3\,z_3\,z_4\,z_2-0.5{z_1}^3\,{z_4}^2\,{z_2}^2-{z_1}^3\,{z_3}^2)$$

$$+({y_2}^3-{y_1}^3)\times 3.025639\times 10^8\,{z_1}^2\,{z_3}^2\,{z_2}^3$$

$$+({y_2}^2-{y_1}^2)\times 9.0769173\times 10^8\,{z_1}^2\,z_3\,{z_2}^3\,z_4$$

$$+(y_2-y_1)\times 9.0769173\times 10^8\,{z_1}^2\,{z_4}^2\,{z_2}^3]$$

$$C_{c\,o(v)}.y \;=\; 2\,C_{c\,o(v)\,L}.y - \;C_{c\,o(v)\,N}.y \tag{23}$$

$$C_{c\,o(v)\,L}.y \;=\left(\frac{1}{9.1395}\frac{b\;\;f'_c}{{z_2}^3\,z_1}\right)[\tag{23a}$$

$$-\left({A_2}^2\,{y_2}^2-{A_1}^2\,{y_1}^2\right)\times 3195\times 10^{-4}\;\;{z_1}^3\,z_3\,{z_2}^2$$

$$+\left(A_2\,{y_2}^2-A_1\,{y_1}^2\right)\times\;1.08923\times 10^3\;\;{z_1}^2\,z_3\,{z_2}^2$$

$$+\left({A_2}^2\,y_2-{A_1}^2\,y_1\right)\times 3195\times 10^{-4}\,{z_1}^3\,z_2\,(z_3-z_4\,z_2)$$

$$+\left({A_2}^2-{A_1}^2\right)\times 15975\times 10^{-5}\,{z_1}^3(z_4\,z_2-z_3)$$

$$+(A_2\,y_2-A_1\,y_1)\times 1.08923\times 10^3\,{z_1}^2\,z_2\,(-2\;\;z_3+\;\;z_4\,z_2\;)$$

$$+\left(\frac{{y2}^2}{A_2}-\frac{{y1}^2}{A_1}\right)\times 3.632943\times 10^8\,z_3\,{z_2}^2$$

$$+\left(\frac{y_2}{A_2}-\frac{y_1}{A_1}\right)\times 3.632943\times 10^8(2\;\;z_3\,z_2+\;\;z_4\,{z_2}^2\;)$$

$$+\left(\frac{1}{A_2}-\frac{1}{A_1}\right)\times 3.632943\times 10^8(2\,z_3+\;\;z_4\,z_2)$$

$$+(A_2-A_1)\times 1.08923\times 10^3(2\;\;{z_1}^2\,z_3-\;\;{z_1}^2\,z_4\,z_2)$$

$$-({y_2}^2-{y_1}^2)\times 4.547435\times 10^4\,z_1\,z_4\,{z_2}^3+$$

$$-({y_2}^3-{y_1}^3)\times 3.031623\times 10^4\;\;z_1\,z_3\,{z_2}^3]$$

$$C_{c\,o(v)\,N}\cdot y = \left(\frac{5.21026\,b\;\;f'_c}{{z_2}^4\,{z_1}^2}\right)[\tag{23b}$$

$$+({y_2}^4-{y_1}^4)\times 2.2692293\times 10^5\,{z_3}^2\,{z_2}^4\,{z_1}^2$$

$$+\left(\frac{{y_2}^3}{{A_2}^2}-\frac{{y_1}^3}{{A_1}^2}\right)\times 1.5137262\times 10^{11}\;\;{z_3}^2\,{z_2}^3$$

$$+({y_2}^3-{y_1}^3)\times 6.0512782\times 10^5\,z_3\,{z_2}^4\,z_4\,{z_1}^2$$

$$-(A_2\,{y_2}^3-A_1\,{y_1}^3)\times 532.5016\;\;{z_1}^3\,{z_3}^2\,{z_2}^3$$

$$+\left(\frac{{y_2}^3}{A_2}-\frac{{y_1}^3}{A_1}\right)\times 7.57906\times 10^7\;\;z_1\,{z_3}^2\,{z_2}^3$$

$$+\left(\frac{{y_2}^2}{{A_2}^2}-\frac{{y_1}^2}{{A_1}^2}\right)\times 3.0274525\times 10^{11}(\,z_3\,z_4\,{z_2}^3+0.75\,{z_3}^2\,{z_2}^2)$$

$$+\left(\frac{{y_2}^2}{A_2}-\frac{{y_1}^2}{A_1}\right)\times 1.5158116\times 10^5(1.5\,z_1\,{z_3}^2\,{z_2}^2+\;z_1\,z_3\,{z_2}^3\,z_4)$$

$$+(A_2\,{y_2}^2-A_1\,{y_1}^2)\times 1065.0032\,(1.5\,{z_1}^3\,{z_3}^2\,{z_2}^2-{z_1}^3\,z_3\,{z_2}^3\,z_4)$$

$$+({y_2}^2-{y_1}^2)\times 4.5384586\times 10^5\,{z_4}^2\,{z_2}^4\,{z_1}^2$$

$$+(A_2\,y_2-A_1\,y_1)\times 532.5016\,(4\;\;{z_1}^3\,z_3\,z_4\,{z_2}^2-6\,{z_1}^3\,{z_3}^2\,z_2-\;\;{z_1}^3\,{z_4}^2\,{z_2}^3)$$

$$+\left(\frac{y_2}{{A_2}^2}-\frac{y_1}{{A_1}^2}\right)\times 3.0274525\times 10^{11}(\;\;z_3\,z_4\,{z_2}^2\;\;+0.75\;\;{z_3}^2\,z_2+0.5\;\;{z_4}^2\,{z_2}^3)$$

$$+\left(\frac{y_2}{A_2}-\frac{y_1}{A_1}\right)\times 0.757906\times 10^8(6\,z_1\,{z_3}^2\,z2+4\,z_1\,z_3\,z_4\,{z_2}^2+\;\;z_1\,{z_4}^2\,{z_2}^3)$$

$$+\left(\frac{1}{{A_2}^2}-\frac{1}{{A_1}^2}\right)\times 0.756863\times 10^{11}(1.5\,{z_3}^2+\;\;{z_4}^2\,{z_2}^2+2\,z_3\,z_4\,z_2)$$

$$+\left(\frac{1}{A_2}-\frac{1}{A_1}\right)0.757906\times 10^8\;(4\,z_1\,z_3\,z_4\,z_2+z_1\,{z_4}^2\,{z_2}^2+6\,z_1\,{z_3}^2)$$

$$+(A_2-A_1)\times 532.5016\;(-4\;\;{z_1}^3\,z_3\,z_4\,z_2+\;\;{z_1}^3\,{z_4}^2\,z_2^2+6\,{z_1}^3\,{z_3}^2)]$$

$$C_{c\,u\,(v)} = \left(\frac{1}{2.67609}\frac{b\ \ f'_c}{{z_2}^2\,\Delta\varepsilon}\right)[\tag{24}$$

$$+({y_2}^2 - {y_1}^2) \times 1.3403194 \times 10^6\ z_3\ {z_2}^2$$

$$+(A_2\ y_2 - A_1\ y_1) \times 6.71083 \times 10^2\ z_1\ z_3\ z_2$$

$$+\left({A_2}^3\ y_2 - {A_1}^3\ y_1\right) \times 1.571667 \times 10^{-3}\ {z_1}^3\ z_3\ z_2$$

$$-\left({A_2}^2\ y_2 - {A_1}^2\ y_1\right) \times 4.01855\ \ {z_1}^2\ z_3\ z_2$$

$$-\left({A_2}^4 - {A_1}^4\right) \times 2.97045 \times 10^{-8}\ {z_1}^4\ z_2$$

$$+\left({A_2}^3 - {A_1}^3\right) \times (-5.23889 \times 10^{-4}\ {z_1}^3\ z_3 + 3.607829 \times 10^{-5}\ {z_1}^3\ z_2$$
$$+1.571667 \times 10^{-3}\ {z_1}^3\ z_4\ z_2\ )$$

$$+\left({A_2}^2 - {A_1}^2\right) \times 4.01855\ (0.5\ {z_1}^2\ z_3 -\ {z_1}^2\ z_4\ z_2)$$

$$+\left({A_2}^2 - {A_1}^2\right) \times 7.191535 \times 10^{-2}\ {z_1}^2\ z_2$$

$$+(A_2 - A_1) \times 6.71083 \times 10^2(-\ z_1\ z_3 +\ z_1\ z_4\ z_2)$$

$$-(A_2 - A_1) \times 80.97376\ \ z_1\ z_2\ \ ]$$

$$C_{c\,u\,(v)}\,.\,y\;=\left(\frac{1}{3.2113}\,\frac{-b\;\;f'_c}{{z_2}^3\,\Delta\varepsilon}\right)[\tag{25}$$

$$-({y_2}^3-{y_1}^3)\times 1.0722555\times 10^3\;z_3\;{z_2}^3$$

$$+({y_2}^2-{y_1}^2)\times 32.16767(-50\;z_4\;{z_2}^3+\;{z_2}^3)$$

$$+\left({A_2}^2\;{y_2}^2-{A_1}^2\;{y_1}^2\right)\times 4.82226\times 10^{-3}\;{z_1}^2\;z_3\;{z_2}^2$$

$$-\left({A_2}^3\;{y_2}^2-{A_1}^3\;{y_1}^2\right)\times 1.886\times 10^{-6}\;{z_1}^3\;z_3\;{z_2}^2$$

$$-({A_2}\;{y_2}^2-A_1\;{y_1}^2)\times 0.8053\;\;z_1\;z_3\;{z_2}^2$$

$$+\left({A_2}^2\;y_2-{A_1}^2\;y_1\right)\times 4.82226\times 10^{-3}(-\;{z_1}^2\;z_3\;z_2+{z_1}^2\;z_4\;{z_2}^2)$$

$$-\left({A_2}^2\;y_2-{A_1}^2\;y_1\right)\times 8.62984\times 10^{-5}\;{z_1}^2\;{z_2}^2$$

$$+\left({A_2}^3\;y_2-{A_1}^3\;y_1\right)\times 1.257334\times 10^{-6}(\;{z_1}^3\;z_3\;z_2-1.5\;{z_1}^3\;z_4\;{z_2}^2)$$

$$-\left({A_2}^3\;y_2-{A_1}^3\;y_1\right)\times 4.3294\times 10^{-8}\;{z_1}^3\;{z_2}^2$$

$$+({A_2}\;y_2-A_1\;y_1)\times 0.8053\;(-\;z_1\;z_4\;{z_2}^2+2\;z_1\;z_3\;z_2)$$

$$+({A_2}\;y_2-A_1\;y_1)\times 9.7169\times 10^{-2}\;z_1\;{z_2}^2$$

$$+\left({A_2}^4\;y_2-{A_1}^4\;y_1\right)\times 3.56454\times 10^{-11}\;{z_1}^4\;{z_2}^2$$

$$+\left({A_2}^3-{A_1}^3\right)\times 4.19113\times 10^{-7}(1.5\;{z_1}^3\;z_4\;z_2-\;{z_1}^3\;z_3)$$

$$+\left({A_2}^3-{A_1}^3\right)\times 1.4431\times 10^{-8}\;{z_1}^3\;z_2$$

$$+({A_2}-A_1)\times 0.8053\;(-0.5\;z_1\;z_3+\;z_1\;z_4\;z_2)$$

$$-({A_2}-A_1)\times 9.7169\times 10^{-2}\;z_1\;z_2$$

$$+\left({A_2}^2-{A_1}^2\right)\times 2.4111\times 10^{-3}(\;{z_1}^2\;z_3-\;{z_1}^2\;z_4\;z_2)$$

$$+\left({A_2}^2-{A_1}^2\right)\times 4.315\times 10^{-5}\;{z_1}^2\;z_2\;-\left({A_2}^4-{A_1}^4\right)\times 8.911\times 10^{-12}\;{z_1}^4\;z_2\;]$$

$$C_{c\,o\,(c)} = (-1 \times 10^6\ b\ f'_{cT})\ [\ -\frac{1}{3}\ \frac{{z_3}^2}{{\varepsilon_{oT}}^2}\ ({y_2}^3 - {y_1}^3) + \left(\frac{z_3}{\varepsilon_{oT}} -\ z_4\ \frac{z_3}{{\varepsilon_{oT}}^2}\right)\ ({y_2}^2 - {y_1}^2) + \left(2\ \frac{z_4}{\varepsilon_{oT}} - \frac{{z_4}^2}{{\varepsilon_{oT}}^2}\right)(y_2 - y_1)\ ] \quad (26)$$

$$C_{c\,o\,(c)}\ .y\ = (-1 \times 10^3\ b\ f'_{cT})\ [\ -\frac{1}{4}\ \frac{{z_3}^2}{{\varepsilon_{oT}}^2}\ \ ({y_2}^4 - {y_1}^4) + \frac{1}{3}\left(2\ \frac{z_3}{\varepsilon_{oT}} - 2\ z_4\ \frac{z_3}{{\varepsilon_{oT}}^2}\right)\ (\ {y_2}^3 - {y_1}^3\ ) + \left(\frac{z_4}{\varepsilon_{oT}} - \frac{{z_4}^2}{2\ {\varepsilon_{oT}}^2}\right)\ ({y_2}^2 - {y_1}^2)\ ] \quad (27)$$

$$C_{c\,u\,(c)} = \left(\frac{-1\times10^6\ b\ f'_{cT}}{\Delta\varepsilon}\right)\ \left[\varepsilon_{uT}\ (\ y_2 - y_1) - \frac{1}{2}\ z_3\ ({y_2}^2 - {y_1}^2) -\ z_4\ (y_2 - y_1)\right] \quad (28)$$

$$C_{c\,u\,(c)}\ .y\ = \left(\frac{-1\times10^3\ b\ f'_{cT}}{\Delta\varepsilon}\right)\left[-\frac{1}{3}\ z_3\ ({y_2}^3 - {y_1}^3) + \frac{1}{2}\ (\varepsilon_{uT} - z_4)\ ({y_2}^2 - {y_1}^2)\right] \quad (29)$$

Chapter 7

7 Summary and Conclusions

Performance-based fire design approach, recently adopted in building codes and standards, provides engineers with the main framework of the design methodology. Analytical tools that give engineers the ability to use this innovative design approach are needed.

This thesis has presented simple, practical, and rational tools to use this innovative approach to design RC flexural frames. These tools provide engineers with the ability to account for strength degradation in concrete and steel as well as thermal and transient creep strains due to fire temperature, while

1) evaluating the capacity of RC beams and columns.

2) analyzing RC continuous beams.

3) analyzing RC flexural frames.

All the proposed tools were validated using available experimental and analytical studies. This chapter summarizes the work done in each chapter and restates a number of general conclusions that can be withdrawn based on work conducted in each chapter. This is followed by the author's recommendation for further work.

7.1 Flexural capacity of RC Beams

The sectional analysis method was extended to cover RC beams subjected to fire from three sides. The proposed method was found to be a simple yet accurate method to track the behavior of rectangular RC beams at elevated temperatures. In a similar fashion to ambient temperature analysis of RC beams, temperature-dependent stress-block

parameters were developed to convert the non-linear compression stresses distribution to a rectangular block stress distribution.

A parametric study aiming at investigating the effect of ASTM-E119 fire temperature on the stress distribution was conducted by applying the proposed methodology on a number of unrestrained rectangular beams. The studied parameters were; fire duration, section geometry, reinforcement ratio and configuration, concrete compressive strength, and aggregate type. The studied cross-sections were subjected to a standard ASTM-E119 fire durations up to $2.5\ hr$. For each time step, the total strain and stress distributions were predicted at failure. The actual distributions of compression stresses at different fire durations were approximated to equivalent stress-blocks. The equivalent stress-block parameters were evaluated for the studied sagging and hogging moment cases by applying a multiple regression analysis. Failure of beams subjected to sagging moments was found to occur at top compression fibers similar to ambient temperature. On the other hand, failure of beams subjected to hogging moments occurs at a location within the compression block where the mechanical strain in concrete reaches the failure strain at this location. Simplified expressions for the proposed stress-block parameters were derived and validated for nominal failure moment prediction. The use of the proposed parameters is relatively easy and practical to be implemented in design codes.

7.2 Fire Performance of Continuous RC Beams

A practical approach based on superimposing the effects of thermal expansion and material degradation was introduced. The nonlinear thermal expansion was converted to an equivalent uniform thermal distribution, which can be represented by the unrestrained thermal axial strain and curvature. The degradation effect in material strength was considered by accounting for the reduction in the effective flexural stiffness. The RC continuous beam tested by Lin et al. (1981) was used to validate the proposed terminology. The mid-span deflections as well as the outer support reactions were

predicted up to 3.5 hrs of standard ASTM-E119 fire exposure. A good agreement was found between the experimental data and the results of the proposed methodology.

A comprehensive parametric study was conducted to investigate the effect of different material, geometric, and loading factors on the unrestrained thermal curvature and the effective flexural strength. For simplicity, the parametric study was limited to rectangular RC beams subjected to 2.5 hr ASTM-E119 standard fire exposure and typical reinforcement configurations. Based on the results of the parametric study, a number of expressions were proposed to predict the unrestrained thermal curvature and the effective flexural stiffness for sections subjected to both sagging (positive) and hogging (negative) moments. Designers can apply the proposed methodology using these expressions to conduct a quick assessment for the structural fire safety of RC continuous beams.

7.3 Axial Capacity of RC Columns

A rational method to predict the axial compression capacity of RC columns heated from four faces during fire events was proposed. The analyzed section was first divided into different temperature zones. Equations to evaluate the average temperature with each zone were developed. The average temperature distribution was then used to estimate the failure strain. Equations to evaluate the corresponding average concrete stress were developed by integrating the concrete stresses along the height of the cross section. The failure strain was used to evaluate the reinforcing bar stresses. The axial compressive capacity was then calculated by using the concrete average stress and the reinforcing bar stresses. The proposed method was validated by comparing its predictions with the test results of thirty three RC columns. A good agreement was found between the proposed method and the experimental results by others. The proposed method can be applied using a simple spreadsheet.

7.4 Interaction Diagrams of RC Columns

A simple technique to calculate an average one 1D temperature distribution was presented and validated in the previous chapter. Based on this temperature distribution, the heated RC column section was divided into different zones to conduct stress analysis. A number of approximations were used to allow integrating concrete stress-strain relationships with respect to mechanical strain and temperature distributions. The main assumptions included

1) using a 1D average temperature distribution instead of 2D elevated temperature contours within the RC column sections,
2) choosing an appropriate algebraic function to represent the 1D temperature variation along the section height,
3) using an integrable stress-strain constitutive relationship for concrete at elevated temperatures, and
4) identifying the envelope for concrete failure strain by plotting the variation of maximum strain along section height.

Mathematical expressions were then derived to calculate internal compression force and its location for the heated concrete. Structural engineers can use these expressions to easily construct the interaction diagrams for fire exposed RC columns using first principles. The predictions of the proposed method were in good agreement with other analytical and experimental results.

7.5 Response of RC Frames during Fire Events

The work done in Chapters 3 and 5 was extended to analyze indeterminate RC frames during fire exposure. The unrestrained thermal parameters and strength degradation were determined for each fire-exposed RC element. Self-induced strain was considered to reasonably predict the section deformation due to external loads. Due to the complexity of the problem, the concrete nonlinearity was ignored in calculating the self-induced

strain. However, the error associated with this approximation was evaluated and found to be minor. Mathematical expressions were derived to calculate internal compression force and corresponding moment for the heated concrete. Structural engineers can use these expressions to predict the free thermal deformation and the effective flexural and axial stiffnesses for individual RC elements exposed to fire temperature.

A practical approach was then proposed to analyze a RC frame during a fire event. The proposed approach was validated by comparing its results with two case studies: a RC beam-column subassemblage tested by Fang et al. (2012), and a single storey RC frame analyzed by Iding et al. (1974) using a comprehensive nonlinear FE software. A good agreement was found between the experimental data and the results of the proposed method for both case studies.

7.6 Limitations of Current Work

The work done in this thesis has a number of limitations which include:

- the presented sectional analysis method implied a simple representation of the transient creep strains.
- average one dimensional temperature distributions were used in the proposed sectional analysis method instead of the actual elevated temperature contour.
- the proposed stress-block parameters, for concrete compression stresses at elevated temperatures, in chapter 2 are only valid for the rectangular sections exposed to ASTM-E119 standard fire
- only siliceous and carbonate concrete types were considered in the thesis.
- the fire performance of RC frames was predicted based on the standard ASTM-E119 and ISO 834 standard fires due to the limited experimental work that could be found by the authors in the literature. The proposed method still needs to be validated using compartment fires.
- the proposed mathematical expressions in chapters 5 and 6, that predict the internal concrete force and its location, need to be simplified.

7.7 Recommendations for Future Work

The assigned objectives for this study were achieved. However, further experimental and analytical work is needed to

- extend the use of the proposed method to consider the effect of fire on prestressed members.
- better validate the use of the developed tools to predict the behavior of indeterminate structures during fire events.
- simplify the proposed mathematical expressions
- predict the shear capacity of fire-exposed members which can be predominant rather than the flexural capacity
- assess the residual capacity of fire-damaged structures and propose a suitable rehabilitation technique
- evaluate the seismic capacity of fire-damaged structures to judge of the structural safety of the damaged structures according to the relevant seismic codes

Curriculum Vitae

Name:	Salah El-Din Farouk El-Fitiany
Post-secondary Education and Degrees:	Alexandria University Alexandria, Egypt 1999-2004 B.Sc. Western University London, Ontario, Canada 2006-2008 M.E.Sc
Honours and Awards:	Alexander Graham Bell Canada Graduate Student (NSERC-CGS) 2009-2012 Peter A. Rosati Award for Outstanding Teaching in Civil and Environmental Engineering Department 2011
Related Work Experience	Structural EIT AMEC Americas Ltd., Calgary, AB 2012-2013 Lecturer Western University 2010

Selected Journal Publications:

El-Fitiany S.F. and Youssef M.A. (in press), “Simplified method to analyze continuous RC beams during fire exposure", ACI Struct. J., accepted Oct 2012

El-Fitiany, S.F., and Youssef, M.A. (2011), “Stress Block Parameters for Reinforced Concrete Beams During Fire Events,” ACI SP-279

El-Fitiany, S.F., and Youssef, M.A. (2009), “Assessing the Flexural and Axial Behaviour of Reinforced Concrete Members at Elevated Temperatures Using Sectional Analysis,” FSJ, Vol. 44